DEGRADATION STUDIES ON RECYCLED POLYETHYLENE TEREPHTHALATE

BY

FARAH AL-AZZAWI

SUPERVISOR

DR. MATHEW PHILIP

A THESIS SUBMITTED IN PARTIAL FULFILMENT OF THE REQUIREMENTS OF THE LONDON METROPOLITAN UNIVERSITY FOR THE DEGREE OF DOCTOR OF PHILOSOPHY

POLYMER SCIENCE AND ENGINEERING

SIR JOHN CASS FACULTY OF ART, ARCHITECTURE AND DESIGN

2010-2015

ABSTRACT

This project aims to investigate the influence of UV on the properties under natural and artificial weathering. The real-time outdoor weathering exposures provide the most accurate results but, they are very slow and manufacturers cannot afford to wait in order to see if a new or improved product formulation is really an improvement. So, accelerated testing methods are designed to simulate natural weathering with the combined action of the most weathering damaging factors; UV radiation, oxygen, temperature and water. Whatever the application, there is a concern regarding the durability of the products because if its useful lifetime can be estimated in short time, their maintenance and replacement can be planned in advance.

In this study, recycled PET samples were exposed to UV outdoors and to accelerated weathering up to 13,000 hr. The mechanical behaviour (tensile and impact), thermal behaviour (DSC), molecular structure analysis (FTIR), flow characteristics (MFI) and surface properties (colour and gloss) of the samples were investigated. The whole body of the samples was substantially unaffected by degradation for long exposure time and this is confirmed by MFI and DSC results. However, the surface of the samples is affected which is seen in FTIR analysis, colour and gloss change. This explains that the photodegradation is a surface effect.

FTIR analysis shows an increase in the gauche ratio and decrease in the trans ratio for both types of weathering indicating a less ordered structure after the UV radiation due to chain scission by Norrish Type I and II mechanism. Carboxylic acid is formed as a result of degradation and increases with the extent of UV exposure in both types of weathering, the formation of carboxylic acid by Norrish II is dominated over Norrish I. Colour and gloss measurement shows that the effect of degradation takes place strongly in the first 2000 hr of exposure in natural weathering and extended up to 5000 hr in accelerating weathering due to the formation of microcracks.

Mechanical tests show that the UV effect was not significant on bulk properties such as yield stress and elongation at yield for accelerated weathering samples up to 1000 hours, then dropped by 62% and 57% respectively up to 13000hr of exposure and remained unchanged for the whole period of exposure for

outdoors samples. The drop in the failure stress and elongation at failure for accelerated weathering samples right from the beginning indicate the formation of microcracks is from the early stages of exposure. For outdoor samples, failure stress remained unchanged for the first 1000 hr of sunlight exposure, then decreases progressively with increasing exposure in the environment. The elongation to failure is unchanged up to 13000 hours.

After 13000 hrs of exposure to sunlight, r-PET samples failed to break while those exposed to UV lamps failed in a brittle manner under impact after 250 hrs and this indicates the transition from ductile to brittle behaviour just after 10 days of accelerated UV exposure because of crack formation. For accelerated weathering samples, the impact strength remained unchanged in the first 1000 hr of exposure, then a decrease up to 5000 hr of exposure when the effects of flaws become significant and dropped sharply by 85% after 5000hr of exposure.

The correlation between both types of weathering shows that one year in natural weathering is equivalent to one and a half months in accelerated weathering according to colour measurements. The effect of accelerated weathering is much bigger than the natural weathering and this is due to higher radiation dosage, temperature and humidity during the test which accelerate chain scission rate that lead to faster crack growth.

ACKNOWLEDGEMENTS

Though only my name appears on the cover of this dissertation, a great many people have contributed to its production. I owe my gratitude to all those people who have made this dissertation possible and because of whom my graduate experience has been one that I will cherish forever.

Firstly, I sincerely appreciate my supervisor Dr. Mathew Philip. I am deeply indebted his patient guidance, profound expertise and wisdom throughout these years. He was always willing to answer my questions, provide valuable advice and support in difficulty during the study. I feel extremely honoured to work under his great guidance. Without his help and support, this work would never have been accomplished.

My co-advisor, Elena Enyshchenko, has been always there to listen and give advice. I am deeply grateful to her for the discussions that helped me through my work.

I would like to give a very special thanks to Dr. Padmasari Kankanam Gamage who was in charge of science laboratories for his technical support. His broad experience, logical way of thinking and constructive comment has been of great value for me in doing the experimental part of the research.

I am also thankful to Andy Murphy, the technician who maintained all the machines in my lab so efficiently that I never had to worry about and his support, patience and skills though my lab work.

I am grateful to Professor Shahriar Hashemi for his support and insightful comments and Professor Michel O.Brian for his practical advice that helped me sort out the technical details of my work.

I would like to acknowledge Dr. Phil Baillie in Health and Safety Office and Brian Whitening in Science Centre for discussions and advice on related topics that helped me improve my knowledge in the area.

This thesis has been made possible with the cooperation of Nick Cliffe, the marketing manager in Closed Loop Recycling who supplied recycled PET flakes and Polymer Extrusion Technology ltd who supplied the first UK grade for recycled PET – (Kudos) pellets for the study.

I am also indebted to Catherine Lee, head of Research and Postgraduate Office for her support during my research and the staff particularly, Chiara Francesconi, administrator with whom I have interacted during the course of my graduate study and kept me updated with the university research regulations.

No research is possible without the library, the centre of learning resources. I take this time to express my gratitude to Jeremy Nagle in British Library who has been very informative.

Above all, I owe it all to Almighty God for granting me the wisdom, patience, health and strength to undertake this research task and enabling me to its completion.

Thank you, Lord, for always being there for me.

This thesis is only a beginning of my journey.

DEDICATION

I would like to dedicate this Doctoral dissertation to the memory of my beloved father. His endless love and wish to complete my Ph.D degree was my inspirational force in this research.

CONTENTS

Abbreviations

PET	Polyethylene terephthalate
r-PET	Recycled polyethylene terephthalate
v-PET	Virgin polyethylene terephthalate
UV	Ultraviolet
MFI	Melt flow index
FTIR	Fourier transform infrared spectroscopy
DSC	Differential scanning calorimetry
TPA	Terephthalic acid
EG	Ethylene glycol
BHET	Bis-hydroxyethyl terephthalate
DMA	Dimethyl terephthalate
PVC	Polyvinyl chloride
HCL	Hydrochloric acid
EVA	Ethylene vinyl acetate
ABS	Acrylonitrile butadiene styrene
SSP	Solid state polymerization
SPD	Spectral power distribution
IR	Infrared
R	Alkyl group
rpm	Revolution per minute

Symbols

E	Radiation energy, J
I_o	Intensity of the incident light, W/m^2
A	Absorbance
λ	Wavelength of light, nm
υ	Frequency of radiation, s^{-1} or Hz
h	Plank's constant (6.62×10^{-34}), Js
IV	Intrinsic viscosity, dl/g
t	Time, s
wt%	Weight percentage
ρ	Density of sample, g/cm^3
Xc%	Crystallinity %
ΔHc	Heat of cold crystallization, J/g
ΔH_m	Heat of melting, J/g
ΔH_{mo}	a Reference value, represents the heat of melting if the polymer is 100% crystalline (for r-PET is 119.8 J/g)
L*	Lightness
a*	Redness
b*	Yellowness
ΔE*	Colour change
ΔG*	Colour and gloss change
σy	Yield stress, MPa
P	Load, N
P_y	Load at yield point, N
A_o	Original cross-sectional area, m^2
L_o	Gauge length, m
L_f	Final gauge length, m

U	Impact energy, J
B	Width of impact specimen, m
D	Depth of impact specimen, m

CHAPTER ONE

INTRODUCTION

1.1 INTRODUCTION

The polymer recycling became an issue during 1990s as a result of environmental pressure to improve waste management. As well as high costs, legislative pressures and public opinion of plastic waste disposal into landfills.

The amount of plastic waste generated annually in the UK is estimated to be nearly 3 million tonnes, 580,000 tonnes (19.3%) is plastic bottles waste (1 tonne = 20,000 plastic bottles).

PET & HDPE together accounted for about 95% of plastic bottles due to their widespread use, particularly PET in the beverage industry (almost all individual-sized and 2-litre bottles of carbonated soft drinks and water produced in United State are made from PET), juices, shampoo and cooking oil bottles. HDPE in milk, juice, detergent and shampoo bottles which led to large quantities of these two polymers available in plastic waste [1, 2, 3].

Polyethylene terephthalate was patented in 1941 by John Rex Whinfield and James Tennant Dickson in United Kingdom. Later DuPont in United State made new textile fibres and branded these fibers as Dacron. Today, more than half of the world's synthetic fibre is made from polyethylene terephthalate.

In 1951, researchers used the trademark Mylar in DuPont, United State after they found a way to stretch a thin extruded sheet of polyethylene terephthalate to create a film, which is used extensively as video, photographic and X-ray film, as well as for packaging film.

Polyethylene terephthalate bottle was patented in 1973 by Nathaniel Wyeth in United State and rapidly gained market acceptance and in 1977, the first PET bottle was recycled [4].

The rapid growth of polyethylene terephthalate in importance makes it today one of the world's most commonly used, versatile and trusted materials because of its toughness, strength, heat resistance, barrier to moisture and gas,

low density, transparency and excellent electrical resistant. It is most widely seen especially in the form of fibre, film and bottle.

Yarns and fabrics for clothes and heavy-duty industrial fabrics are manufactured from fibres. The orientated films of PET have found an important commercial market for graphics and recording tapes as well as in food packaging. Films and fibres are the oldest applications of PET.

Moreover, electrical instruments, electrical insulator and moulding products like automobiles products, house-wares, lighting products, power tools and material handling equipment.

In recent years, polyethylene terephthalate has increasingly been used in manufacturing fibre reinforced composites and with high strength fibres, many applications in the load-bearing reinforcement are made [5, 6, 7, 8].

Polyethylene terephthalate generally has the second highest material scrap value after aluminium. The average time taken to decompose PET products in a landfill is close to 700 years (PET molecules have a slow rate of natural decomposition), makes recycling processes the best way to economically reduce PET waste.

It is well known that post-consumer PET bottles are mostly recycled into textiles, carpets and sheets. The bottle grade PET has high performance among the various PET grades, and that presents an opportunity to develop the recycling potential of bottle grade PET.

Synthetic polymers and composites in general offer a wide range of attractive properties and in many of their applications they are exposed to the outdoor environment such as in aircraft, boat construction, building industry. Polypropylene grass and injection-moulded ABS seats in modern sports stadium highlight the revolution of outdoor applications of polymers [7, 9, 10, 11].

One problem for re-use in outdoor applications is UV degradation. The solar spectrum reaching the earth's surface is in the range from 290 nm to 3000 nm with a composition of 6%, 48% and 46% of ultraviolet, visible and infrared light respectively. The wavelength of light which has the most harmful effect on polymers is in the 290 – 400 nm range of the UV spectrum.

Although UV light makes up only about 6% of sunlight reaching the surface of earth, it is responsible for most material damage through causing photolysis of PET molecule (breaking the chemical bonds in the polymer chains) that lead to a large decrease in molecular weight due to the chain scission process which results in a serious deterioration in mechanical and other properties of PET products. The fibres tend to lose their elasticity and break easily and the films become discoloured, turn brittle and develop crazed surfaces with a reduction in strength [12, 13, 14].

Whatever the application, there is often a concern regarding the durability of polymeric materials because of their useful lifetime can be estimated in short time, their maintenance and replacement can be planned in advance.

The real-time outdoor weathering exposure tests provide the most accurate results which are realistic and inexpensive and easy to perform, but they are very slow and manufacturers and designers cannot afford to wait in order to see if a new or improved product formulation is really an improvement.

So accelerated testing methods are designed to simulate natural weathering with the combined action of the most weathering damaging factors; UV radiation, oxygen, temperature and water.

Tests are performed at reduced cycle time in order to:

1 Predict the useful life-time of the product under service conditions in a convenient short time.
2 Make comparison between chosen materials significant to specific application as a function of exposure time by measuring the retention properties (e.g. tensile strength, impact strength, gloss).
3 Study the photochemical process occurring during PET degradation [9, 15, 16].

In the current study, therefore the recycle PET bottle-grade material will be analysed for the effect of UV degradation. This material will be referred to as r-PET for brevity. This is done primarily to evaluate the potential of the material for long – term outdoor use. The aims of the project as outlined in section 1.2 are intended to evaluate this degradation.

The objectives of this programme of work are explained in detail in section 3.6.

1.2 AIM

This research aims to investigate the effects of UV on the properties of r-PET and will ask the following questions:

- What is the effect of UV exposure in the environment on the physical behaviour of PET based products that are subsequently recovered for recycling?
- How does the behaviour in the environment compare with the behaviour simulated in an accelerated weathering tester?
- In the context of two previous points, how is the physical-chemical structure of the material affected by UV radiation?
- How do UV-induced changes to properties affect the potential use of r-PET in for future applications?
- The long – term aims would be to contribute to understanding the mechanisms (combined effects of UV radiation, oxygen and moisture) of PET degradation.

CHAPTER TWO

Polyethylene Terephthalate – The Material

2.1 Virgin PET

Polyethylene terephthalate is regarded as one of the most important engineering polymers since 1970s. The patent of PET bottle attract the manufacturers to this valuable material due to its good properties especially, mechanical properties, chemical resistance and thermal stability.

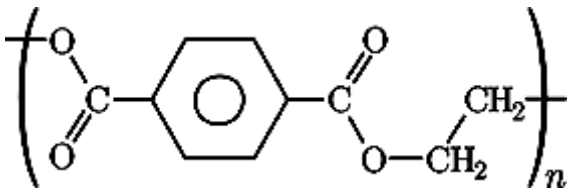

Figure2.1.1: Chemical structure of Polyethylene terephthalate (PET) with a chemical formula $(-O-CO-C_6H_4-CO-O-CH_2-CH_2-)_n$.

The bulkiness of the chain caused by phenyl group hinders the rotation of the chain and causes high stiffness of the chain. Moreover, the presence of polar groups increases the interchain forces and lead to stiff chains. The short ethylene group ($-CH_2-CH_2-$) in PET molecule reduce its flexibility [7, 17].

2.2 PET Synthesis

The synthesis of PET requires two steps:

<u>The first step:</u> Can be achieved by either these two processes:

(A) Esterification reaction where terephthalic acid (TPA) reacts with ethylene glycol (EG) at a temperature of between 240 °C and 260 °C and a pressure between 300 kPa and 500 kPa forming a so-called prepolymer (PET monomer or BHET,bis-hydroxyethyl terephthalate) and water (by-product) [7, 18].

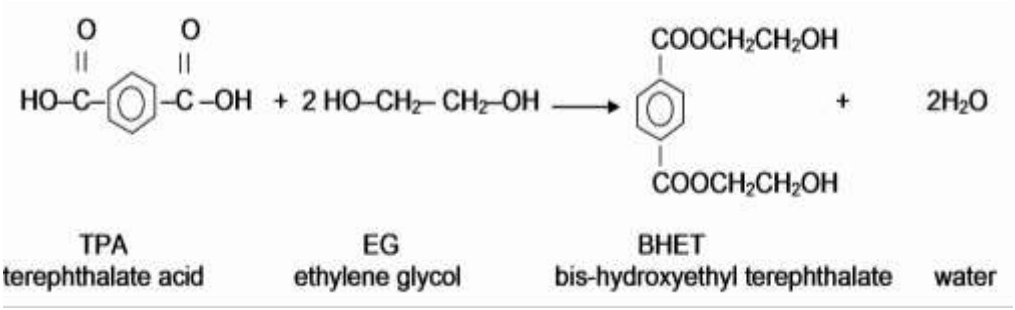

Figure2.2.1: Production of PET monomer by esterification reaction [7].

(B) The prepolymer can also be achieved by transesterification of dimethyle terephthalate (DMT) with (EG) at a temperature of between 140 °C and 220 °C and a pressure 100 kPa releasing the by-product methanol [7, 18].

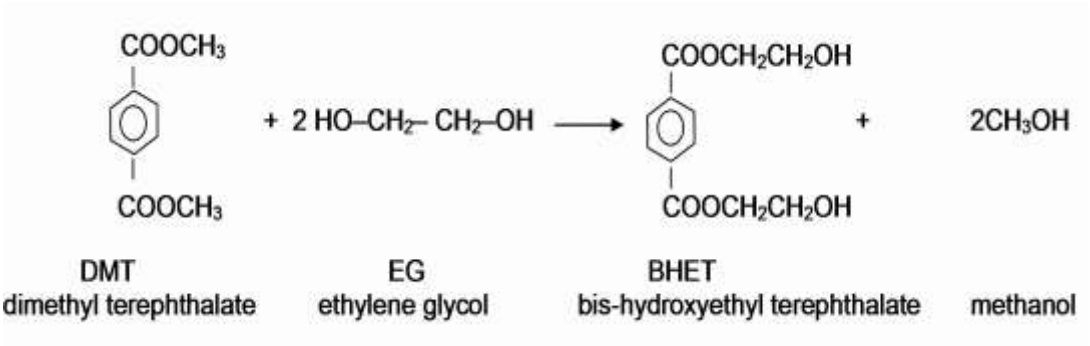

Figure2.2.2: Production of PET monomer by transesterification reaction [7].

<u>The second step:</u> Polycondensation, in which a transesterification reaction takes place in melt phase at a temperature of between 270 °C and 285 °C and a pressure between 50 to 100 Pa. The by-product, EG, is removed from the melt by using high vacuum [7, 17].

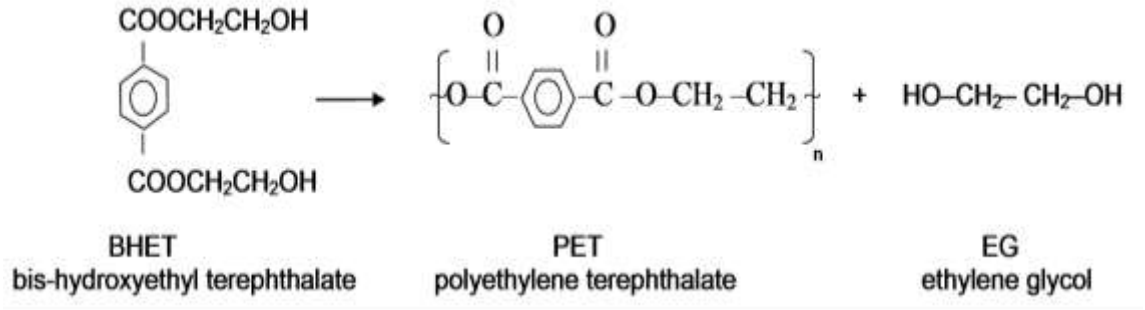

Figure2.2.3: Production of PET by polycondensation reaction [7].

2.3 PET Crystallization

The overall form of polymer structure such as crystallinity, branching and cross-linking is referred as morphology of polymer. It is generally describes the arrangement and ordering of the molecular chains.

The chemical and physical properties of the material depend on the:

A- Arrangements of molecular chains with respect to each other (crystallization)

B- Arrangement of a single molecular chain without regard to its neighbour (rotational isomerism).

Both these two factors affect the ordered (crystalline) and less ordered (amorphous) regions in semi-crystalline polymer like PET.

The crystallization process involves the transformation of the amorphous phase into a crystalline phase due to alignment of its molecular chains. It occurs in the temperature range between the glass transition temperature, Tg and the melting temperature, T_m of the polymer and that what is called cold crystallization. In this temperature range, the molecular chains are sufficiently mobile to adopt the more stable conformations for crystallization, i.e. trans conformation. Below Tg, chains are frozen, cannot move relative to one another and so cannot crystallize (the conformational motion is frozen) but becomes highly mobile above Tm.

When a material crystallizes, molecules packs more efficiently, intermolecular interactions are maximized and energy is released in the form of heat.

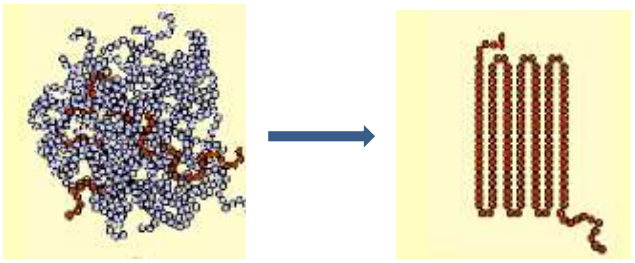

Figure2.3.1: Chain folding during crystallization [19].

When the temperature increases up to melting temperature, a condition of equilibrium exists between the crystal and melt as both phases have the same value of G and thus $\Delta G=0$.

When a molten polymer is cooled below its melting temperature, the polymer chains tend to align and form small ordered regions, called nuclei, within the disordered melt.

The crystal formation is spontaneous below the melting point. The system always tries to attempt to reach the state of the lowest energy possible which is the most stable state. From thermodynamic considerations alone, a crystal is in a lower free energy state than the melt when the temperature is below its melting temperature. Figure below illustrates the change of free energy during crystal formation which is the driving force for crystallization.

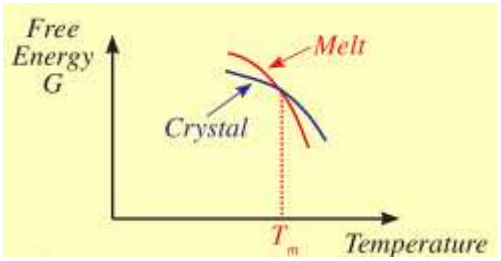

Figure2.3.2: Schematic representation of free energy as a function of temperature [19].

The crystallization does not occur at the melting point, but just below it. This is because the formed nucleus has to be stable for further growth (i. e. must not re-melt).

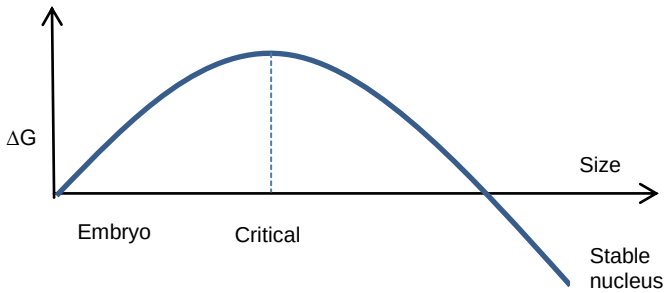

Figure2.3.3: Schematic representation of change in free energy with nucleus size.

When nucleation occurs on foreign surfaces such as dust or other solid impurities is referred to as heterogeneous nucleation. Homogeneous nucleation occurs if no foreign particles are present. A special type of nucleation called self-nucleation occurs when tiny regions of high degree of order persist in the melt for a long time.

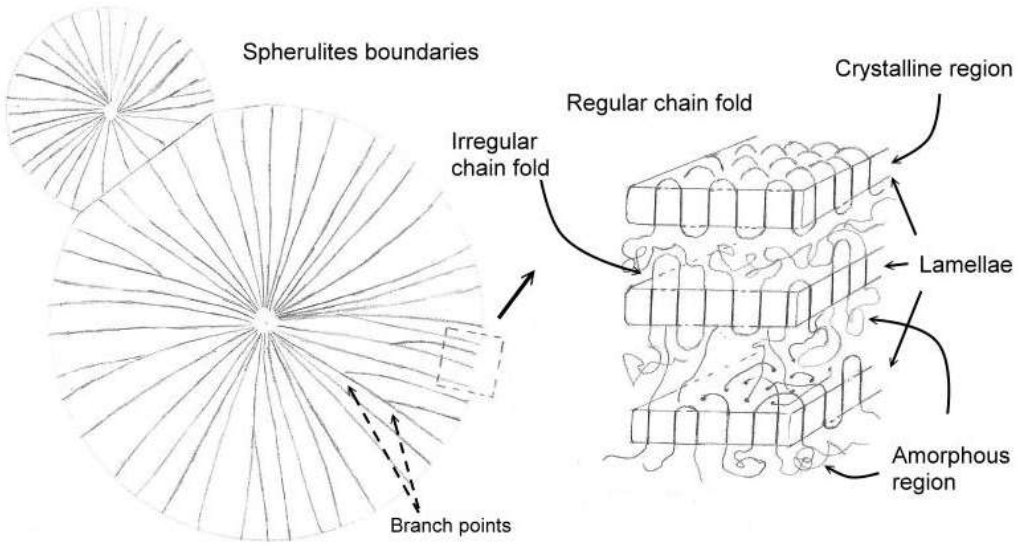

Figure2.3.4: Illustration of spherulites and lamellae [20].

The growth of nuclei in the form of lamellae radiating outward from the nucleus by molecular chain folding normal to the direction of growth as shown in figure2.3.4. These structures (spherulites) spread into the surrounding amorphous phase until surface impingement with other spherulites occurs where there is no available space which limits further growth. This first stage of crystallization is called primary crystallization, is then followed by a much slower secondary crystallization process involving the growth of existing crystals and the growth of new crystals in the amorphous regions between the lamellae. Figure2.3.5 shows the growth of spherulites from formed lamellae. The space between the arms is filled with amorphous material [17, 18, 19, 21, 22, 23, 24].

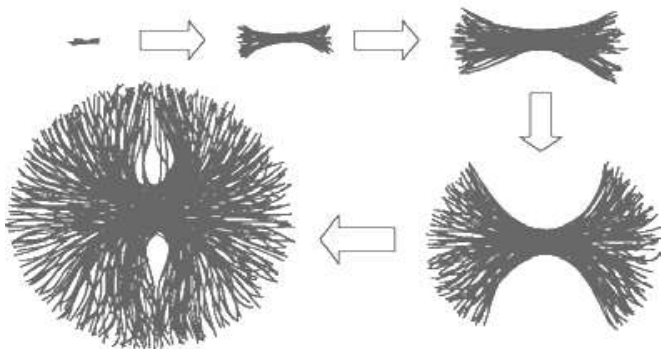

Figure2.3.5: Spherulite growth from packing of lamellae [25].

If two atoms are joined by a single carbon-carbon bond, then rotation about that bond is possible if there is enough space for rotation. Isomers are molecules with the same number of atoms i.e. same chemical formula but have different arrangement of atoms i.e different chemical structure. When isomers produced by rotation (twisting) about single bond is called conformational isomers or rotational isomers or conformers.

The structural part of the chain –O–CH_2–CH_2–O– (ethylene glycol linkage) in PET molecule can be arranged in the form of either trans or gauche conformation isomers depending on the level of energy. Figure2.3.3 illustrates the alternative trans and gauche conformations in the glycol residue of PET. The trans conformation isomers appear in the crystalline part of the polymer (only trans) whereas the gauche isomers form mainly amorphous zones (trans and gauche – primarily gauche) [7, 26, 27, 28].

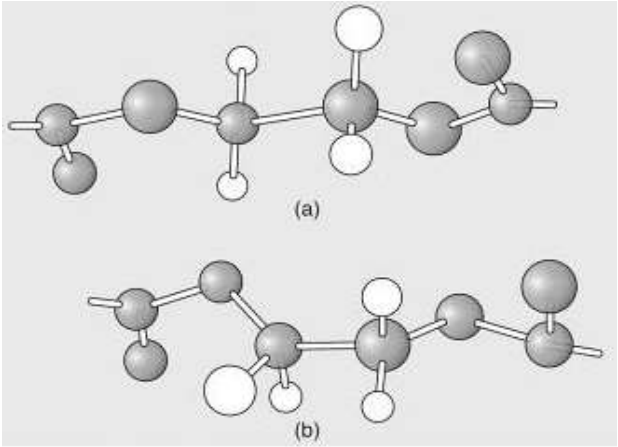

Figure2.3.6: Trans and gauche conformers in glycol residue of PET (a) PET in the crystalline trans conformation (b) PET in the gauche conformation present in amorphous regions [24].

PET conformational changes have been widely during crystallization of PET as a result of orientation and/or annealing as well as aging of PET. The amounts or concentrations of these conformers are of great importance to the PET products properties. For example, the increase or decrease of trans-conformation affects the barrier properties of the bottles as permeability occurs at higher rate in the gauche (amorphous phase) than in the trans (crystalline phase). Also crystallinity of drawn PET film increases as the trans content increases and this reflect the increase in the tensile strength of the film [7].

In order to understand better different conformations, it is convenient to use a drawing called Newman projection where we look lengthwise down a C-C bond in ~CH_2-CH_2~molecule, the front C atom is a dot and the back C atom is circle.

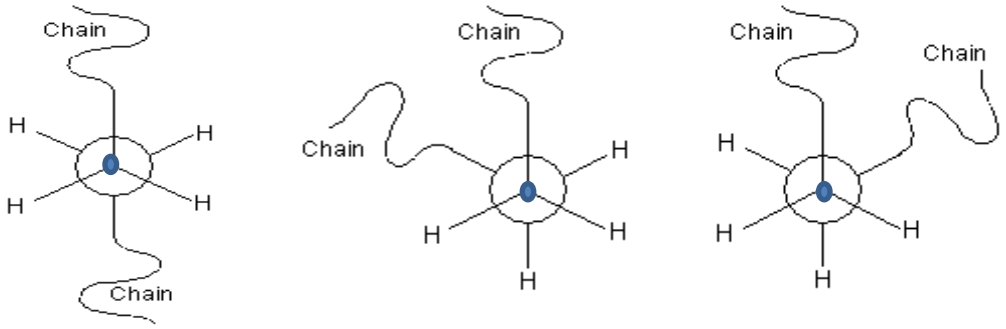

Trans + Gauche - Gauche

Figure2.3.7: Newman projection of trans and gauche conformers.

The angle of rotation away from the trans-conformation is called the torsion angle (120º gauche), and the potential energy stored in conformer can be plotted as a function of this angle.

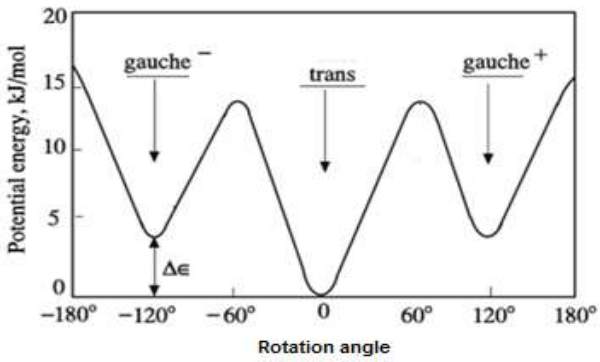

Figure2.3.8: Schematic diagram of the potential energy of trans and gauche conformer as a function of torsion angle [29].

In trans structure, the groups of atoms that are connected to carbon atoms (the dot and circle) from one side and the rest of chains from the other side are opposite to each other (180º), which minimize the interactions of their electron clouds and lower the potential energy of this type of conformation. In gauche structure, these groups of atoms are close to each other (adjacent groups), crowding and overlapping of their electron clouds which destabilizes the molecule (becoming less stable) due to the repulsion between the electron clouds of these two groups which increase the potential energy of this conformation by 3.34 kJ/mol to overcome this hindrance [17, 29].

2.4 Conversion of PET- bottles to flakes

2.4.1 The Flake Quality

The major factors affecting the suitability of post-consumer PET flakes for recycling is the amount and nature of contaminants exist in r-PET flakes. Contamination of post-consumer PET is the major cause of deterioration of its physical and chemical properties during re-processing. Minimizing the level of these contaminants leads to better recycled PET quality to be used in high-value applications. The high melting temperature of PET is the reason why most contaminants such as PVC, paper, fibers, PVA, adhesive and pigments are transformed into degradation products [7, 30].

Post-consumer PET flakes are contaminated with many substances such as:

1) Acid producing contaminants

The existence of contaminants which generate acidic compounds at high temperature during extrusion are a big problem in the re-processing of PET. The contaminants and their thermolysis products are shown below [1].

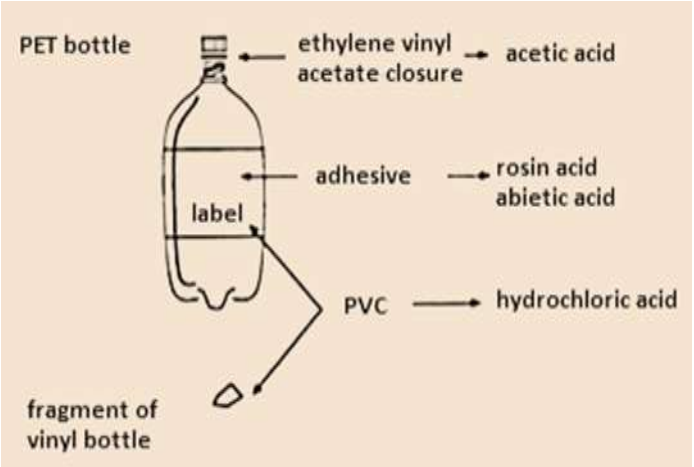

Figure2.4.1.1: Contaminants during processing [1].

The most harmful acids to the post-consumer recycling process are acetic acid, which is produced by PVA closures degradation, rosin acids (primary component abietic acid $C_{19}H_{29}COOH$) which are carboxylic acids that produced by adhesives and hydrochloric acid (HCL) that is produced by PVC (fragments of PVC bottles) [1, 7].

2) Water

Absorbed water by PET molecules reduces molecular weight during post-consumer PET recycling through a hydrolysis reaction. Moisture contamination should be below 0.02% to avoid the molecular weight reduction. Most water content comes from the flake washing process but can be reduced greatly by drying [1].

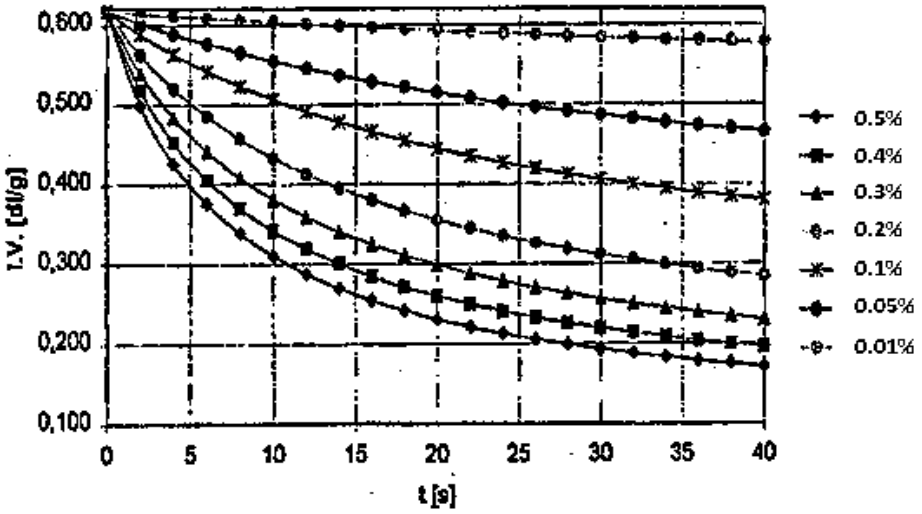

Figure2.4.1.2: Change of intrinsic viscosity as function of time for various Initial water contents [18].

3) Coloured contaminants

Fragments of coloured PET bottles (green, blue, brown and other colours) and printed ink labels cause undesirable colours during processing. Although extrusion homogenizes the melt and the colours, it takes only 1000 ppm of green PET chips to cause an observable colour shift in clear PET. Enhancement of sorting process in PET bottle recycling may greatly reduce coloured contaminants [1].

4) Acetaldehyde

Acetaldehyde is a main degradation product of PET during processing (thermal degradation). Transesterification of the vinyl ester gives vinyl alcohol which is transformed immediately to acetaldehyde. The migration of acetaldehyde into food products from PET containers is a great concern due to the flavor consideration in the early stages of developing the post-consumer PET

recycling process. Fortunately, the high volatility of acetaldehyde allows it to be extracted under vacuum degassing [1, 7].

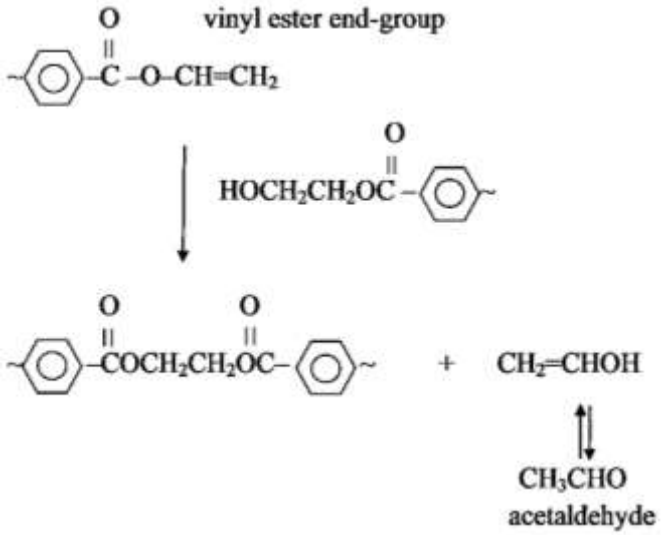

Figure2.4.1.3: Production of acetaldehyde from vinyl ester [1].

5) Labels

Paper labels can create problems in PET recycling due to the formation of cellulosic fibres that are difficult to remove from the reprocessed material. New labels comprising sleeves of ultra-thin polyethylene stretch film without any adhesive assist in separation process (can be removed by flotation) [1].

6) Particulate impurities

Foreign particles like sand, brick stone, glass fibre and metals can pass through the mechanical recycling process and cause stress concentrations that can lead to problems during fabrication such as excessive fibre breakage during fibre spinning. These contaminants affect the product quality and process productivity and can be removed easily by melt filtration [1].

7) Other contaminants

PET bottles are used by the public for non-intended storage of chemicals like detergents and fuel. If traces quantities of these chemicals remain after post-consumer PET recycling can cause great danger to human health. It can affect the colour and odour of the polymer and its suitability for food contact applications. Increase of people’s awareness of the danger of the chemicals to public health has reduced the level of these contaminants significantly [7].

2.4.2 Flake Processing

Processing of PET flakes can be either,

Method (A): involves:

- Removing moisture
- Re-pelletizing of bottle flakes
- Solid state polymerization of Flakes or pellets (depends on applications), or

Method (B): Direct conversion of bottle flakes.

Method (A):

Removing moisture:

Before removing moisture, two important factors should be carefully under control:

- ❖ The storage conditions of the material prior to processing: dry air storage.
- ❖ The humidity of the atmosphere at the inlet of the extruder: a closed-loop dehumidified air hopper dryer.

Eliminating or reducing hydrolysis is very important for reprocessing of recycled PET because it contains ester bonds which are susceptible to hydrolysis at elevated temperatures (processing temperature) in the presence of moisture which leads to chain scission and decrease molecular weight causing deterioration in the mechanical properties. The effect of hydrolysis is generally more severe for flakes than with pellets because the higher specific surface area of flakes enables it to absorb higher amount of water. The best solution to the hydroscopicity of PET is to dry the polymer before processing in a desiccant dryer before processing [1, 7, 18, 30].

Re-pelletizing of bottle flakes:

Choosing the re-pelletizing method means having an additional conversion process which is at the one side energy intensive, cost consuming and involved thermal destruction to the material. At the other side the pelletizing method is providing improvement in processing flexibility (improve r-PET flake material flow characteristics) with the use of melt filtration [1, 30].

Solid-state polymerization (SSP):

The process of increasing the molecular weight of the polymer in the solid-state (after polymerization in the melt phase) is known as solid-state polymerization (SSP). In the melt phase, a molecular weight between 16,000 and 19,000 (intrinsic viscosity IV, 0.58-0.68 dl/g) can be attained before the melt is cooled. After solid-state polymerization process, values of up to 27,000 (IV, 0.90 dl/g) for bottle grade, and as high as 38,000 (IV, 1.20 dl/g) for technical fiber applications such as seat belts and air bags can be reached.

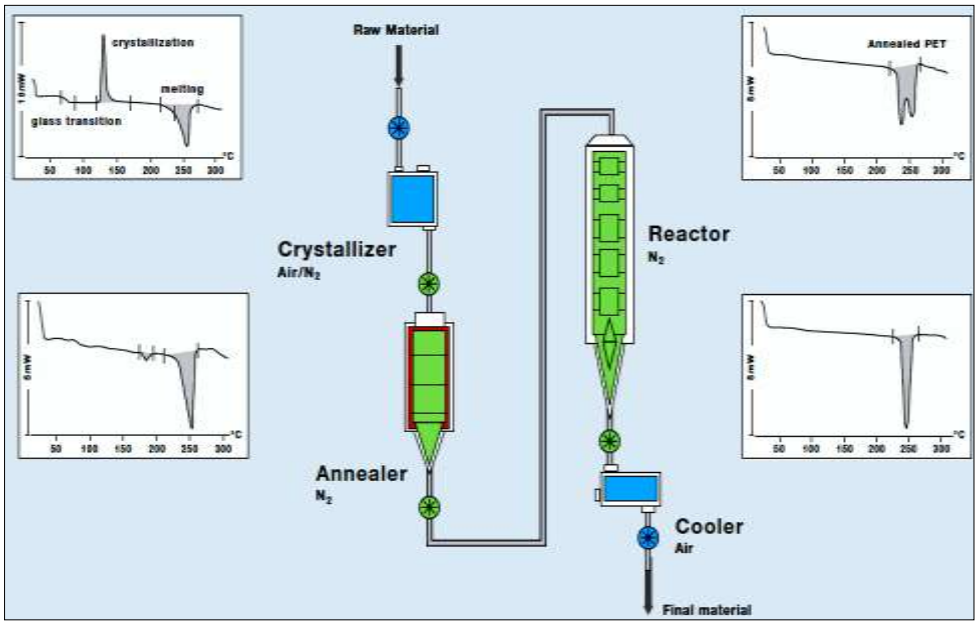

Figure2.4.2.1: Process of solid state polymerization for r-PET [31].

During solid-state polymerization process, the polymer is heated above the glass transition temperature, Tg and below the melting temperature, Tm of the polymer with a residence time of up to 12 h. The typical process stages are:

- Crystallization stage: to remove moisture from the pellets (or flakes) because the presence of moisture at high temperature in the SSP reactor can lead to hydrolysis and to increase crystallinity by crystallization of amorphous phase.
- Annealing stage: the melting temperature of the crystals formed in the crystallization stage needs to be raised to above SSP temperature to prevent sticking and agglomeration of pellets in the SSP column.

- SSP stage: typical residence time is 12hr at temperatures of 210°C. Nitrogen enters at the bottom of the reactor and flow counter currently up through the pellets in order to remove acetaldehyde and reaction by-products (water and ethylene glycol).
- Cooling stage: by fresh air [18].

Method (B):

Direct conversion of un-dried PET bottle flakes to be used directly for injection moulding with vacuum degassing is cost saving. The flakes do not need to dry before feeding and no pelletizing step is needed because the flakes is metered directly. PET reprocessed with melt-degassing (vacuum degassing) produces a polymer with a higher molecular weight (about 40%) than PET reprocessed without degassing and with increasing vacuum the molecular weight also increases.

This economic system has two features to directly process undried bottle flake. Firstly a uniquely designed hopper with a vertical feed screw conveys to carefully meter the flakes combined with a vented extruder incorporating a vacuum pump to draw off the water from the melt in the extruder. The water and other volatiles are removed from the vent port and condensed in a cooling tank [1, 30].

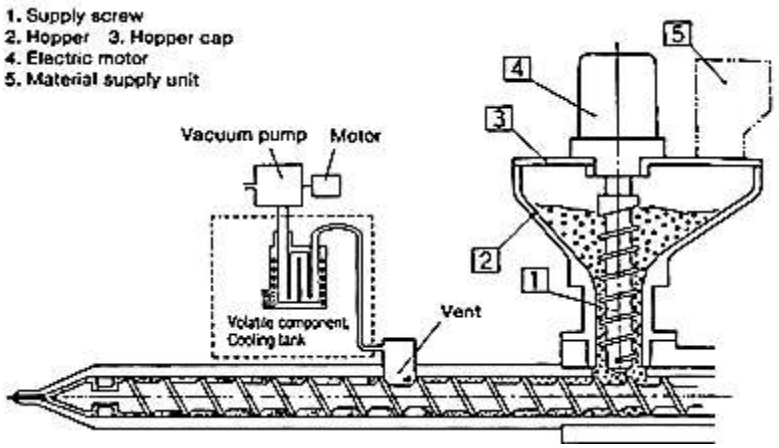

Figure2.4.2.2: Schematic of the vented extruder for reprocessing undried PET bottle flakes to use directly for injection moulding [1].

2.5 Applications for mechanically recycled PET

The main portion post-consumer PET bottle flakes is converted to fibres which are used extensively in filling (furniture) and carpets. The rest is used for containers, films, strapping, injection moulded products and a raw material for glue and coating.

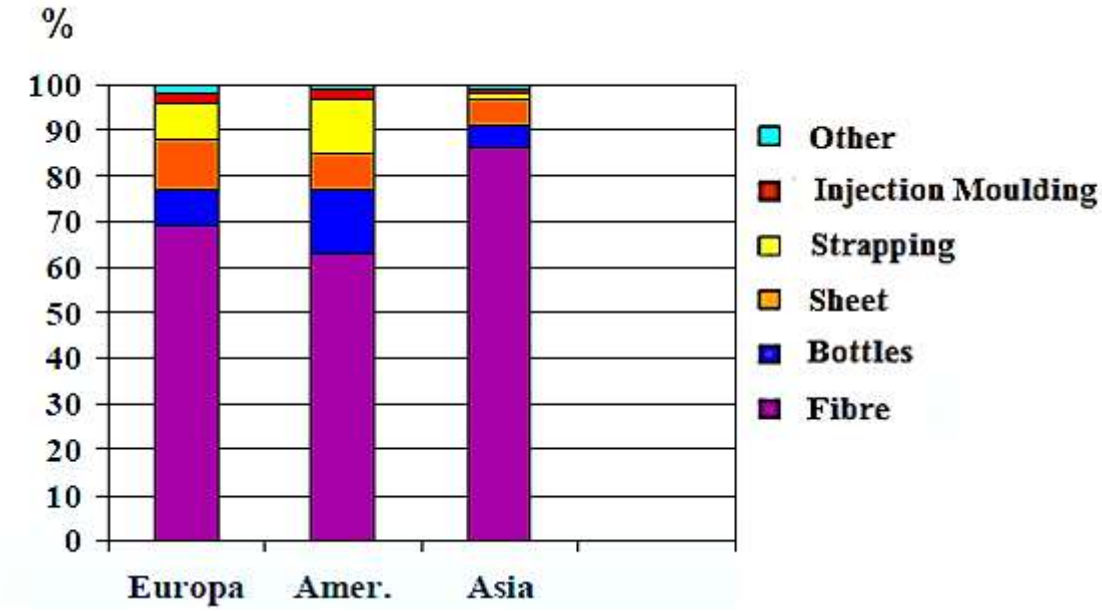

Figure2.5.1: Main application of post-consumer PET bottles [30].

The summary of post-consumer PET bottle flake processing matrix is shown below.

Table2.5.1: Post-consumer PET bottle flake processing matrix [30].

Product	Processing		
	Flakes	Extrusion + Filtration	SSP
Staple fibers	X	X	
Spun bond	X		
PET film	X	X	X
Bottles (food)	X + super clean	X	X
Bottles (non food)	X	X	X
Strapping and filament	X	X	X
polymer compounds	X	X	
Raw material for polyester production	X	X	

The applications of pot-consumer PET bottle flakes are:

1. Fiber application

1.1 Staple fibre

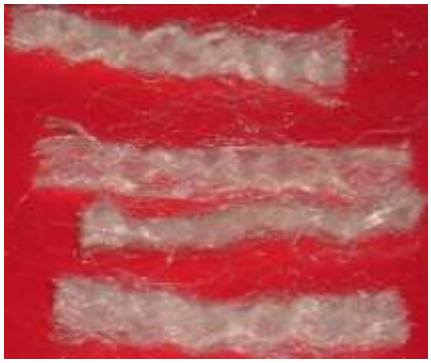

A huge quantity of the world wide collected PET bottle flakes is converted to staple fibre (about 70%) for different applications like fibre fill and carpet fibre. Standard staple fiber IV is in the range of 0.58-0.62 dl/g and melt filtration < 60 µm [30].

1.2 Filament

Filament is continuous fibre wound onto bobbins and thus attracts a higher price than staple fibre. Melt filtration of the material is very important to ensure high quality (purity) of the polymer because trace contaminants can cause breakage of the filament. IV is in a range of 0.8-1.2 dl/g. Extrusion including first coarse filtration 100-200 µm and second fine filtration 20-50 µm [30].

1.3 Spun bond:

Spun bond fabrics are produced by depositing extruded, spun filaments onto a collecting surface in a uniform manner followed by bonding the fibres by applying heated rolls to partially melt the polymer and fuse the fibres together. The fibres are separated during the web laying process by air stream without deflecting the fibres so, perforated collecting surface is used. The desired IV-range is more at the lower side between 0.58 and 0.68 dl/g and desired filter will be in a range of 25-60 µm [30, 32].

2. Strapping

Strapping is a high-tenacity tape which can be produced from r-PET flakes with a high IV (>0.80 dl/g) and low in contamination. This application can accept coloured post-consumer PET bottles. Production process and melt filtration are the same as those for filaments [1].

3. Carpets

Post-consumer PET bottle flakes are used extensively in the production of recycled PET carpets. The recycled PET is blended in a 1:8 ratio with recycled LDPE [1].

4. Film

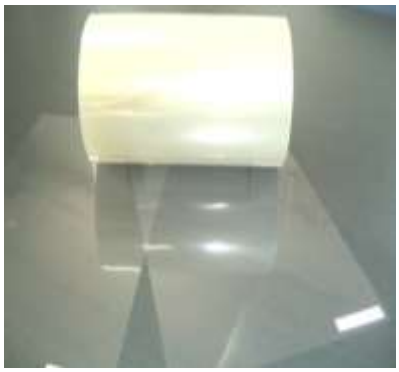

r-PET films are used to produce packing material with direct food contact like drinking cups for water, the same super cleaning process as used for r-PET bottle grade is used. The IV-range is very broad, depending on the desired mechanical properties. From r-PETflakes without SSP film of about 0.65-0.70 dl/g is possible to produce and higher IV is possible to reach with SSP. Continuous melt filtration is necessary because of the high visibility of defects (black spots) in the transparent film with filter mesh 30-37 µm [30].

5. Coextrusion – multilayer films

Thermoforming food packing trays with a layer of r- PET enclosed within two external layers of virgin PET [1].

6. Non-food contact containers (non food grade)

PET bottles use 100% r- PET flakes or it can be blended with v- PET. The IV range 0.68 to 0.80 dl/g. Impurities are to remove by melt filtration (50-100 µm) [1, 30].

7. Food contact containers (food grade)

The IV range is the same like v-PET polymer specification (0.72-0.85 dl/g). The difference to non-food application is the implementation of super cleaning and intensive vacuum degassing during extrusion and solid state polymerization.

In food grade recycling, the compliance of FDA of the whole recycling process technology is essential.

A complete filtration in a range of 35-60 µm is necessary, no black spots are allowed and continuous melt filtration is needed [30].

8. Compounds like engineering plastics

Post-consumer PET can be upgraded with fillers such as glass fibre and injection moulded to produce parts for the automotive and household (appliance housings and furniture). Allied Signal in United State has commercialized Petra^{TM}, a 100% recycled PET [1].

9. Raw material for polyester production

Polyethylene terephthalate flakes (bottle flakes) can be fed as raw material such as glue, powder coating, melt coating and paints [30].

CHAPTER THREE

WEATHERING & DEGRADATION OF PET

3.1 Introduction

The term weathering is used as a description of all possible changes (chemical and physical process) which may take place in the materials on exposure outdoors. The term degradation is any undesirable change in the properties of the material that takes place after it has been put into service.

During weathering, the most significant factors responsible for attacking polymers and cause damage are:

- Sunlight causes damage by ultraviolet radiation absorption as well as,
- Temperature
- Atmospheric oxygen and
- Moisture.

It does not only affect the mechanical behaviour such as yield strength but also aesthetically undesirable changes such as discolouration (colour fades) and loss of gloss.

Property change may be divided into:

1- Physical: reduction in molecular weight, yield strength, impact strength, elongation at break, colour and loss of gloss (paints).
2- Chemical: change in chemical structure – formation of functional group, (e. g. carbonyl) as a degradation products.

Polymer degradation takes many forms. The deterioration may be:

1- Visible: in the form of cracks or crazing and colour change.
2- Invisible: inside the material and when subjected to loads, it becomes apparent through actual breakage [33, 34, 35, 36, 37].

3.2 Natural Weathering

Most materials are subjected to weathering which is completely a natural process, but the rate of deterioration is vary depending on the nature of the material; for the hardest rocks the time scale stretches to millions of years where as for some paints only few days are enough to occur changes.

Synthetic polymers are used in everyday life because it offers a wide range of attractive properties. In many of their applications they are used outdoors, for example, polymers and composites are widely used externally and internally in aircraft, boat construction and building industry because of the weight saving they provide (high strength to weight ratio). The sports stadium with its injection-moulded ABS seats and polypropylene grass highlights the applications of the materials exposed to the outdoor environment.

Whatever the application, there is often a concern regarding the durability and the expected lifespan of the products because if the expected lifetime of these products can be predicted in short time so, their maintenance and replacement can be planned in advance [9].

3.3 Accelerated Weathering

The outdoor weathering exposures provide the most accurate results in a real time which are realistic, inexpensive and easy to perform but they are very slow (usually several months to several years). Manufacturers and designers cannot wait in order to see if a new or improved product formulation is really an improvement.

Accelerated testing methods designed to simulate natural weathering with the combined action of most weathering damaging factors; UV radiation, oxygen, temperature and water at an accelerated rate will reduce the cycle time to:

- Predict the durability (lifetime) of products under expected conditions of use.
- Compare the performance of materials or combinations of materials in a convenient short time.
- Speed up the process of deterioration in order to understand the

chemical reactions involved. The ultimate objective is the development of methods that can monitor the extent of degradation and estimate the lifetime of the products [9, 15, 38].

3.3.1 Artificial Light Sources

The determinant factor in accelerating weathering that speed up the rate of degradation is the type of radiation to which the polymeric products are exposed which is described by the wavelengths emitted and their intensities, i.e., by the spectral power distribution (SPD) of the light source [39].

There are many types of artificial light sources, but the two that are predominately used in material testing are:

1. Atlas UV-Con (QUV):

It reproduces the most damaging effects of sunlight that can occur from 300 nm to 400 nm (not the entire spectrum of sunlight). It is based on the concept that, for durable materials (like most plastics and coatings) used outdoors and exposed to sunlight, short wave in the UV region which is the most weathering damaging factor, can cause severe polymer damage (e.g. cracking, embrittlement and deterioration in the mechanical properties) [40].

2. Xenon – Arc (Q-Sun):

It does not reproduce only the short wavelength of sunlight as QUV, but the visible light (VIS) and infrared (IR) as well (the entire spectrum of sunlight). It is a good match with sunlight from 295 nm to 800 nm. For less durable material (such as pigments and dyes) longer wave in the UV region and even in the visible light region can cause significant polymer damage (e.g. colour change) [15, 41].

3.3.2 Fluorescent UV Lamps - QUV

All fluorescent lamps of QUV emit mainly ultraviolet light rather than visible light or infrared light to reproduce the damage caused by UV radiation of the sun. Fluorescent UV lamps are usually categorized as UVA or UVB lamps, depending on the region into which most of their output falls; each is used for different applications.

1. UVA Lamps

UVA-340:

It is the best possible simulation of sunlight in the critical short wavelength region from 365 nm down to the solar cut off of 295 nm. This lamp which its peak emission is at 340 nm, is specified for correlation with outdoor applications for most plastics and textiles [42].

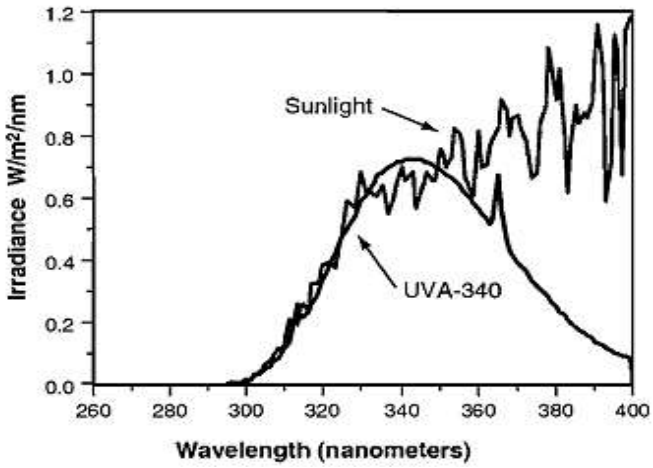

Figure3.3.2.1: SPD of UVA lamp [40].

UVA-351:

Simulate the UV region of sunlight filtered through window glass. It is specified for interior applications such as automotive interiors and for polymer damage that can occur in an environment near a window (indoors) [39, 42].

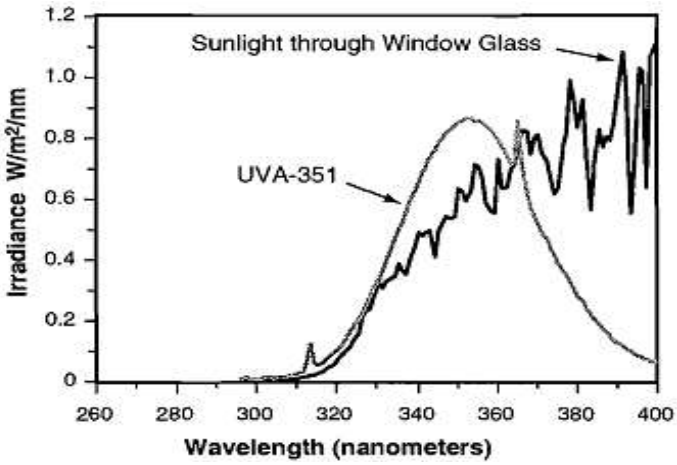

Figure3.3.2.2: SPD of UVA-351 lamp [40].

2. UVB Lamps

FS40 UVB:

Most of the lamp output is in the UV-B portion of the UV with some UV-A. It is recommended for automotive exterior coatings which demonstrated good correlation to outdoor exposures for gloss retention on automotive coatings [41].

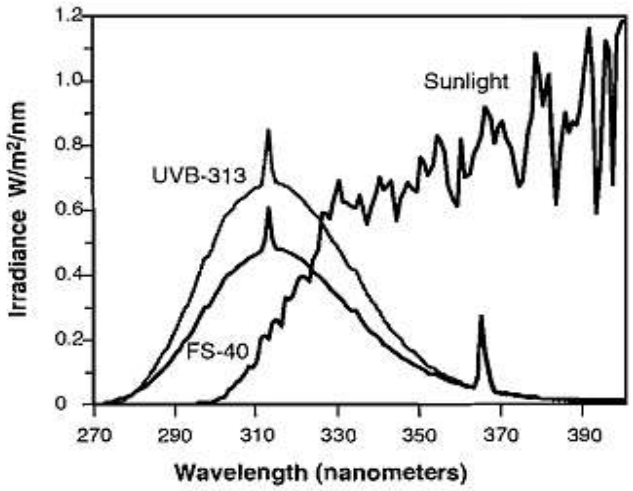

Figure 3.3.2.3: SPD of UVB-313 and FS-40 lamps [40].

UVB-313:

It is the second generation FS40 UVB, has the same SPD as the FS40 UVB, but higher output. So, the UVB-313 gives significantly greater acceleration over the FS40 UVB. Consequently, these lamps may produce unrealistically severe results for some materials. It is particularly useful for very durable materials such as building materials [43, 44].

3.4 MODES OF POLYMER DEGRADATION

The change in polymer properties depend on the type of degradation process involved. These are:

- Thermal degradation: This occurs during polymer processing (at elevated temperatures).
- Mechanical degradation: This occurs on the application of force (polymer is subjected to a stress in the solid or in solution).
- Hydrolytic degradation: This occurs in polymers containing functional groups which are sensitive to the effect of water.
- Chemical degradation: This occurs under the influence of low molecular weight compounds such as solvents brought into contact with polymers.
- Radiation degradation: This occurs on exposure to high energy radiation such as X-rays.
- Biological degradation: This occurs when microorganisms produce a great variety of enzymes which react with polymer molecule [33, 37, 45].

Degradation of polymers on exposure to weather is caused by many factors; solar radiation (ultraviolet, visible, infrared), Oxygen, water (dew, rain, humidity, snow), heat (temperature) and other atmospheric constituents such as dust, smoke, oxides of nitrogen, sulphur dioxide, carbon monoxide and dioxide.

During the PET processing, life time (use) and recycling processes, it may suffer the action of degradation agents:

- Shear stress
- water
- High temperature
- Oxygen
- UV radiation

Which act together synergistically to break bonds between atoms and degrade the polymer [12, 46, 47].

3.4.1 Shear stress

During processing, the polymer melt is under shearing forces due to screw rotation inside the barrel of extruder which cause stress at certain points in the chain high enough to disrupt bonds between atoms leading to bond scission. This process is known as mechanooxidation, results in the formation of peroxy radicals and hydroperoxides as shown below (where R-R and RH represent polymers) [48].

$$R\text{-}R \xrightarrow{shear} 2R^{\bullet} \xrightarrow{O_2} 2ROO^{\bullet} \xrightarrow{RH} 2ROOH \qquad .....3.1$$

3.4.2 Water

The amount of water vapour in atmosphere is usually expressed in terms of percentage of relative humidity (RH%), which is the ratio of the amount of water in a volume of air to that which the same volume of air would contain if fully saturated at the same temperature.

Dew, rain, humidity, frost and snow are forms of water (depends on the ambient temperature). Generally, the potential for degradation from dew exceeds that associated with rain, it lies on materials for long period allowing the water to penetrate deep within the material to cause internal oxidation. The effects of water can be:

1. Physical: destroying the bond between a polymer and filler like glass fibre resulting in fibre bloom.
2. Chemical or hydrolytic: Under ambient temperature, PET molecule is stable to hydrolytic degradation. It contains ester bonds which are susceptible to water attack at high temperatures above the glass transition temperature of the polymer. Hydrolysis begins to become significant at temperatures of 100°C and above in the presence of moisture. The hydrolysis of PET molecule involves breaking of an ester linkage by water molecule as shown in figure3.4.2.1 [16, 38, 41, 49].

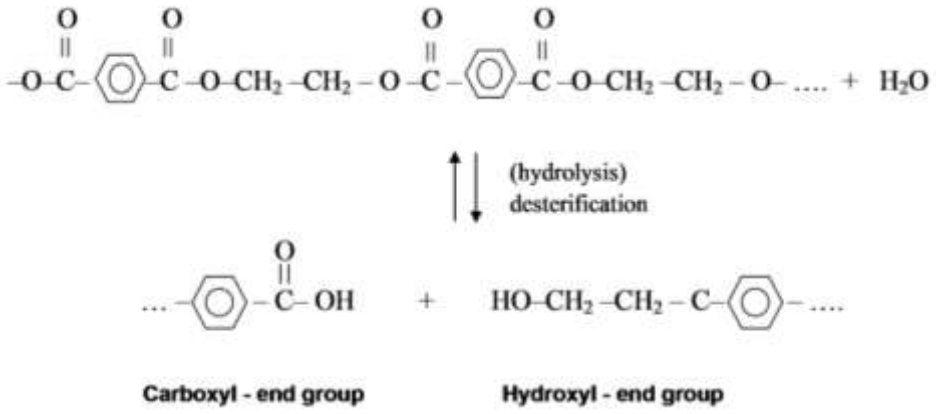

Figure3.4.2.1: Hydrolysis reaction of PET [7].

Each chain scission consume one water molecule and creates one carboxyl end group and one hydroxyl end group. With the chain scission process, polymer chain shorten (molecular weight decreases), leading to significant deterioration in mechanical properties such as tensile strength and elongation [50, 51].

3.4.3 High Temperature

During the manufacture and processing of PET into moulded products, films or fibre, the polymer is subjected to high temperature to melt and process the polymer which is sufficient to cause chain scission (thermal breakdown). The oxygen can diffuse into the molecules and cause thermal oxidation, which rapidly result in the formation of hydroperoxides. That short lived compound decomposes rapidly to alkoxy radical and hydroxyl radical [33, 52].

The initial stage of thermal degradation is a random scission of PET molecule leading to the formation of vinyl ester and carboxyl end-groups. Transesterification of the vinyl ester then occurs to give vinyl alcohol which is transformed rapidly to acetaldehyde. Hydrogen atom is removed from the molecule by impurities in the polymer and thus generating radical sites. These will be targeted by oxygen molecule producing peroxy radicals and subsequently hydroperoxides. Hydroperoxides are thermally and photolytically unstable and will cause further breakdown of the polymer molecules, producing radicals [53].

The presence of acetaldehyde in PET products (food contact applications) is an important issue in since it affects the food. Fortunately, the high volatility of acetaldehyde allows it to be readily extracted under vacuum degassing [1].

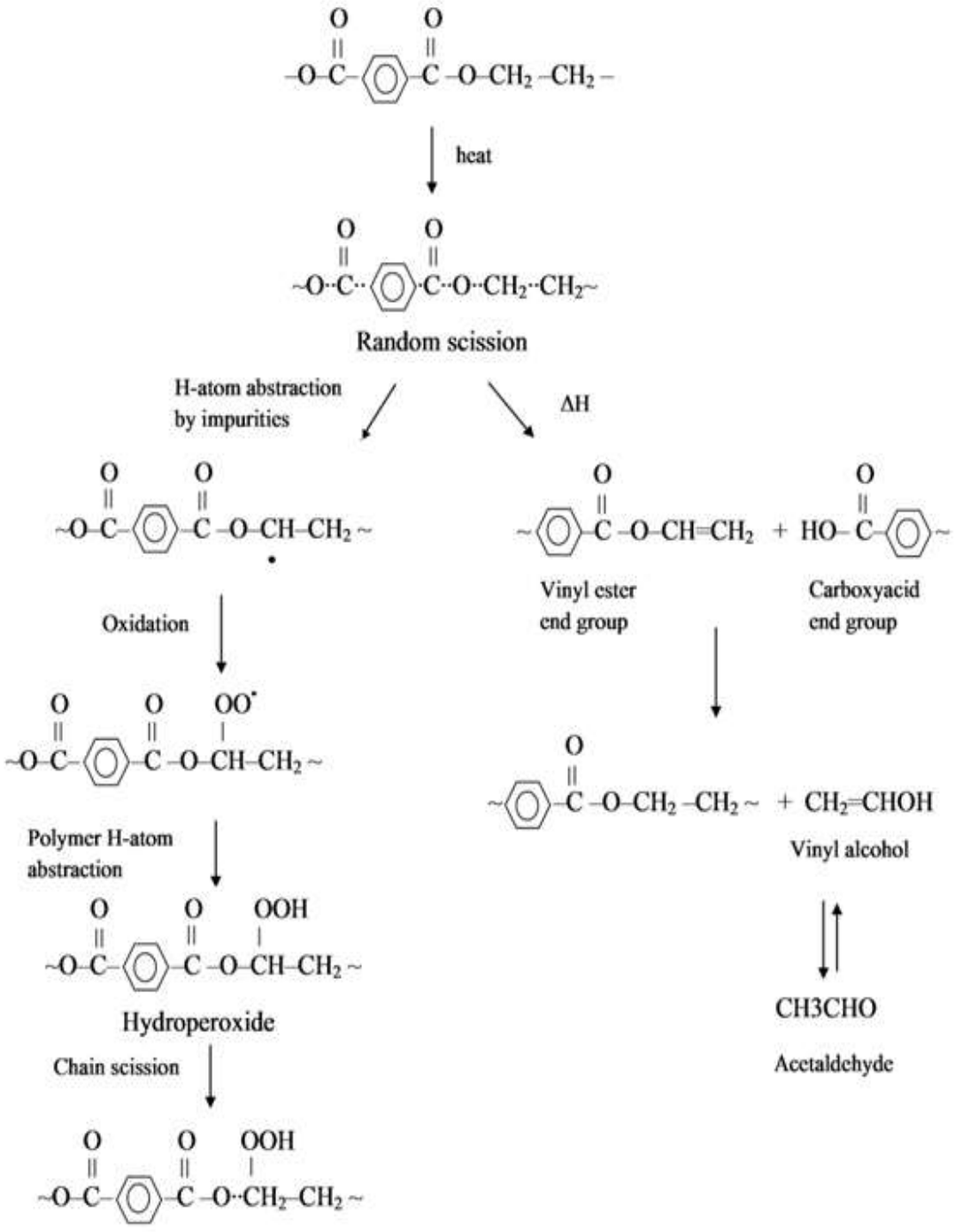

Figure3.4.3.1: Thermal degradation mechanisms of PET [53].

During PET processing, low molecular weight compound called oligomers are formed as a result of thermal degradation. Oligomers can reduce the molecular

weight of the polymer melt. Virgin, dried PET has about 0.9wt% of oligomers and this increase to 1.3-3.0 wt% after reprocessing.

Increase melt processing temperature and residence time in the extruder leads to an increase in the amount of oligomers formed. Oligomers are found to be mainly cyclic and linear oligomers as shown in figure below.

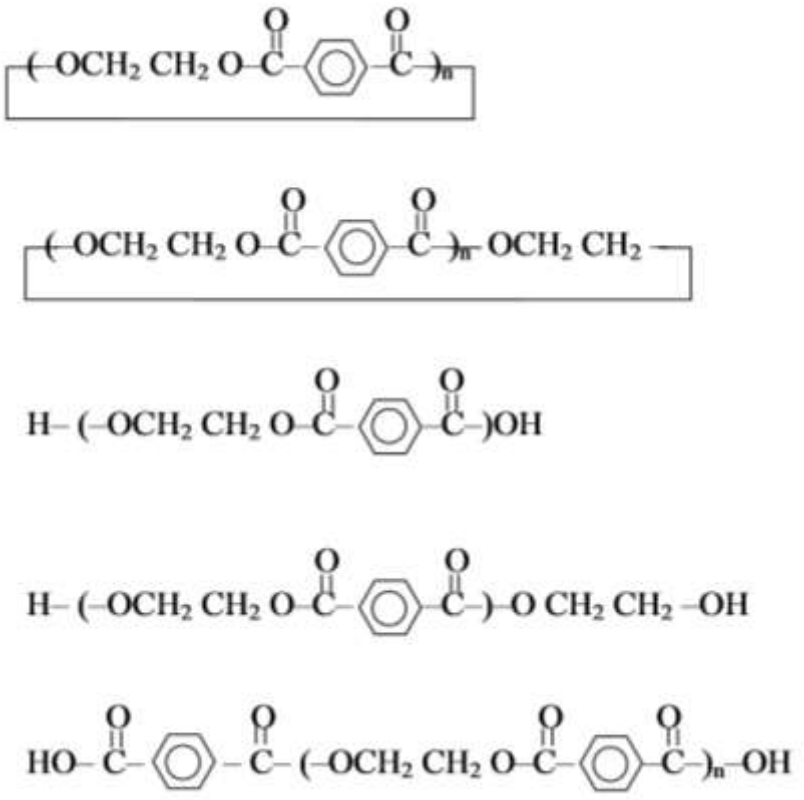

Figure3.4.3.2: Typical cyclic and linear oligomeric degradation products formed during thermal reprocessing of PET [1].

The content of cyclic and linear oligomers in reprocessed PET is important because they can affect processability and product properties. For example, they can diffuse towards the surface of PET films and fibers and affect surface properties [1].

3.4.4 UV Radiation in Sunlight

Sunlight is the total frequency spectrum of electromagnetic radiation given off by the sun.

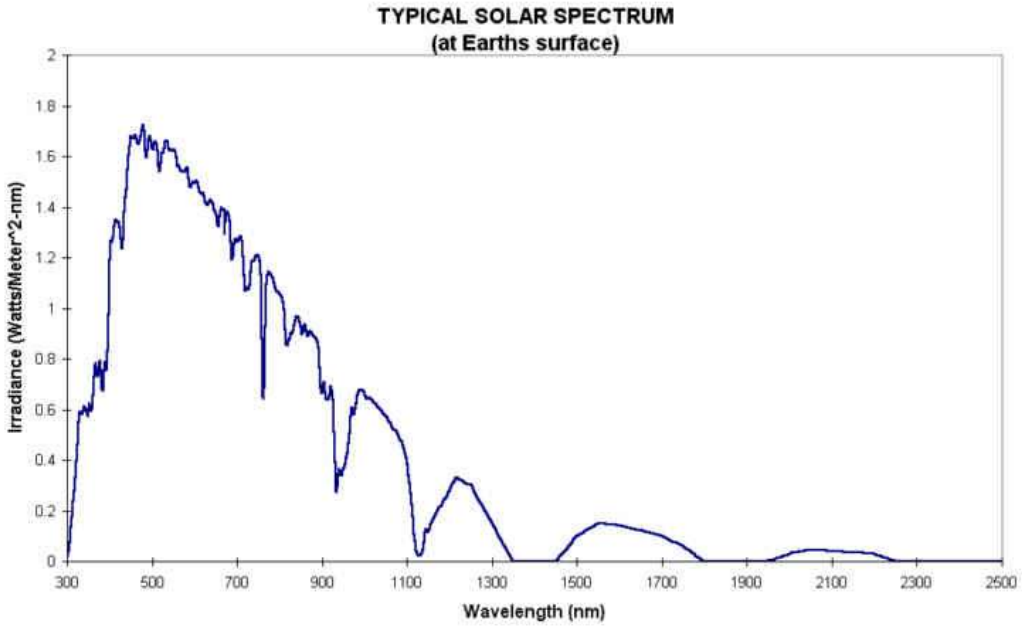

Figure3.4.4.1: Solar spectral irradiance [54].

As solar radiation penetrates the atmosphere of the earth, it is attenuated by the collision with the solid, liquid and gaseous constituents of the atmosphere (gases, water droplets, cloud, fog and dust). The solar spectrum which can reach the surface of the earth is of the range from 290 nm to 3000 nm with a composition of approximately 6% ultraviolet, 48% visible and 46% infrared [9, 38].

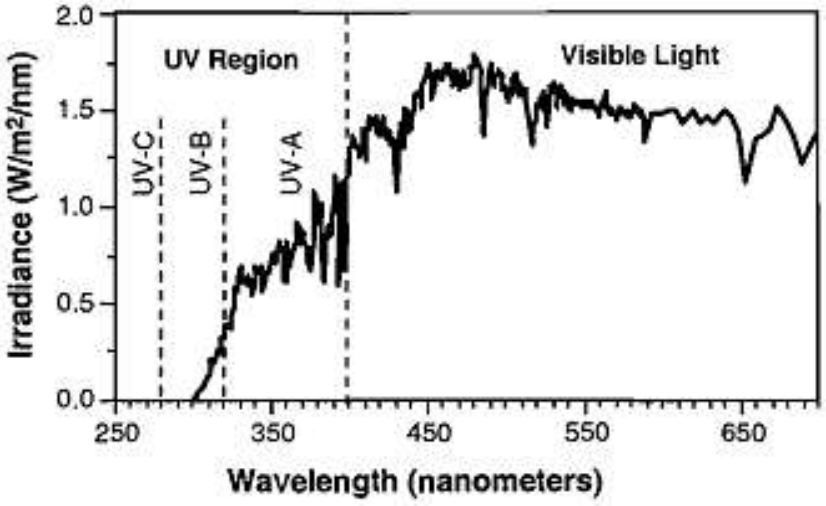

Figure3.4.4.2: Noon summer sunlight spectrum [40].

Infrared energy (IR) consists of wavelengths longer than the visible red wavelengths and starts above 700 nm Visible light (VIS) is the radiation between 400 and 700 nm. Ultraviolet light (UV) is the radiation below 400 nm. The wavelength of light available on the surface of the earth which has the most harmful effect on polymers is in the 290 – 400 nm range of the UV spectrum.

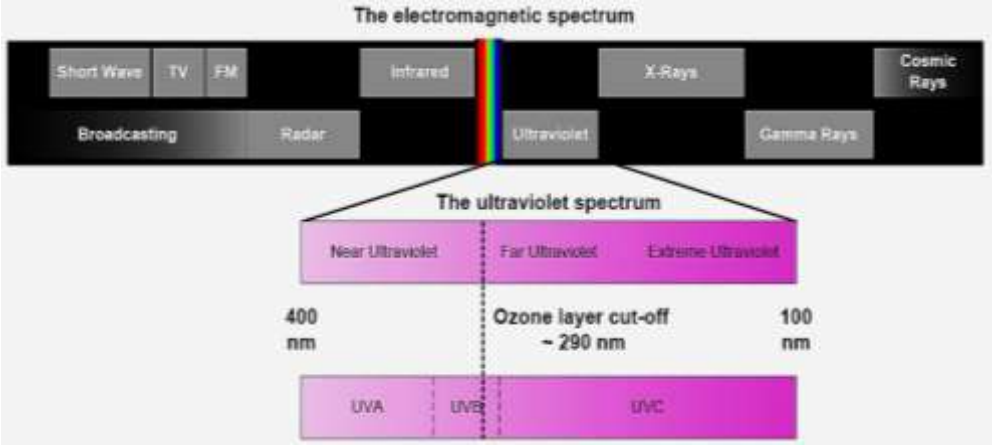

Figure3.4.4.3: The electromagnetic spectrum.

Although UV light makes up only about 6% of sunlight reaching the earth, it is responsible for most polymer damages [13, 40]. The effects of the various UV wavelength regions can be summarized as shown in the following table.

Table3.4.4.1: The effects of the various UV wavelength regions [41].

UV-A 400 – 315 nm	Causes pigmentation changes in human skin (produce bronzing not scorching) and slight polymer damage.
UV-B 315 – 280 nm	Reaches the surface of the earth with a solar cutoff at approximately 290 nm and responsible for severe polymer damage.
UV-C 280 – 100 nm	Found only in outer space (absorbed by ozone) and produce abnormal reactions and destroys microorganism.

Most pure polymers do not absorb radiation energy at wavelengths longer than 300 nm, so it should not be affected by solar radiation, but it degrades when subjected to solar radiation due to the presence of chromophoric groups such as carbonyl group [48, 55].

3.4.4.1 Absorption of Radiation

According to the quantum theory, “light arrives in discrete particles called quanta or photons”. The radiation energy of a photon (quantum) for a given wavelength, E is determined by the equation:

$$E = h\upsilon = hc/\lambda = hc\acute{\upsilon} \qquad \text{.....3.2}$$

Where, h: is Plank’s constant (6.62×10^{-34} Js)

υ : is the frequency of radiation (s^{-1} or Hz)

λ : is the wavelength of light (nm)

c : is the velocity of light (3×10^{8} m/s)

$\acute{\upsilon}$: is the wavenumber (cm^{-1}) (number of waves per unit length, inverse of wavelength).

The radiation intensity (irradiance), I_o is expressed as the amount of radiation energy per unit time (rate of radiation energy) passing through a unit surface area, A:

$$I_o = \frac{E}{t \,.\, A} \qquad \text{.....3.3}$$

When the surface of a polymer is exposed to an incident radiation with the intensity (I_o), part of radiation is reflected (I_r), another part is absorbed (I_a) and the remaining part is transmitted through the material (I_t):

$$I_o = I_r + I_a + I_t \qquad \text{.....3.4}$$

Or,

$$\frac{Ir}{Io} + \frac{Ia}{Io} + \frac{It}{Io} = 1 \qquad \text{.....3.5}$$

The value I_t/I_o=T is called the transmittance, I_r/I_o=T is called the reflectance and I_a/I_o=T is called the absorbance and usually given as a percentage [12, 56].

It is convenient to classify radiation as:

i. Exciting radiation, or

According to Grothus – Draper Law that states light must be absorbed by a molecule in order for a photochemical reaction to take place in that molecule.

When a polymer molecule absorbs radiation, its energy increases by the amount equal to the energy of the absorbed photon (E):

$$\Delta E = E_2 - E_1 \qquad \text{…..3.6}$$

Where;

E_2 and E_1 are energies of a single molecule in the final and initial states, respectively.

If the photon contains big energy (more than the bond dissociation energy of the chemical bond) which is sufficient to excite an electron (i. e. raise it to new orbit with higher energy than before), can lead to breakage of bond between atoms, but the atoms will not lose or gain electrons and hence this will produce radicals.

$$\sim A\text{-}A\text{-}A\text{-}A\text{-}A\sim \xrightarrow{h\upsilon} \sim A\text{-}A\text{-}A\bullet + \bullet A\text{-}A\text{-}A\sim$$

Where;

~A-A-A-A-A-A~ is a polymer molecule, ~A-A-A• chain radical and hυ is the absorbed photon energy.

Ultra - violet radiation from the spectrum of sun is capable of excitation only.

ii. Ionizing radiation or (high energy radiation)

If the energy of a photon is so big that it is sufficient to cause an orbital electron to move right outside the atomic nucleus attraction and thus an ion is produced [56].

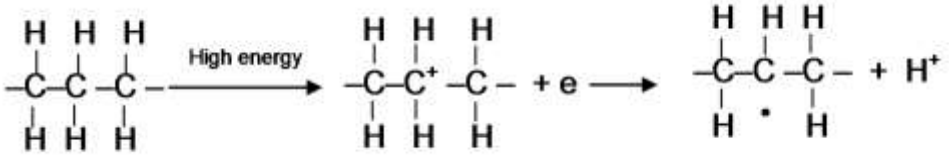

3.4.4.2 Mechanism of PET Irradiation

The most deteriorating weather's factors to polymers outdoors are the radiation of sun in the UV range and oxygen which they act together synergistically to influence the life time of polymers. The first action of an oxygen molecule on a hydrocarbon is to insert itself between carbon atom and a hydrocarbon atom attached to it, forming a hydroperoxide which rapidly decomposes producing radicals. Once radicals are formed, many other reactions will take place. Radicals themselves will add oxygen, and the overall process of oxidation becomes autocatalytic. Thus the molecular weight of the exposed surface of polymer quickly decreased due to chain scission of molecules and cracks development.

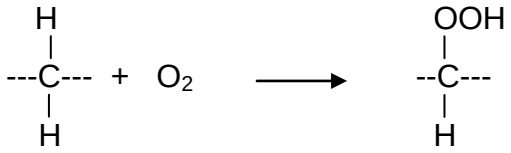

In the presence of ultraviolet radiation with oxygen, attack can be very severe as a result of chain scission of the molecules by UV attack [33].

The main product in the photo-oxidative degradation is the hydroperoxides (ROOH) which play a major role in chain scission process. Due to the weakness of the RO-OH bond (dissociation bond energy is 35 Kcal/mol), the light photons produced by solar energy are sufficiently energetic to break it and produce new free radicals ($RO^{\bullet}$ and $HO^{\bullet}$) which react with hydrogen from the same or from near polymer chain (hydrogen abstraction).

In the photo-oxidation degradation of polymers, the following steps can be considered:

1- Initiation step:
   Formation of free radicals
2- Propagation step:
   Reaction of free radicals with oxygen and production of polymer oxy and peroxy radicals. Secondary polymer radicals are resulting in chain scission.
3- Termination step:
   Reaction of different free radicals with each other [33, 55].

The most important reactions which occur during the photo-oxidative degradation are shown below:

1-Initiation

$RH \xrightarrow{h\upsilon} R^{\bullet} + H^{\bullet}$ 3.7

$H^{\bullet} + O_2 \longrightarrow HOO^{\bullet}$ 3.8

$HOO^{\bullet} + HOO^{\bullet} \longrightarrow H_2O_2 + O_2$ 3.9

$H_2O_2 \xrightarrow{h\upsilon} 2^{\bullet}OH$ 3.10

2-Propagation

$R^{\bullet} + O_2 \longrightarrow ROO^{\bullet}$ 3.11

$ROO^{\bullet} + RH \longrightarrow ROOH + R^{\bullet}$ 3.12

$ROOH \xrightarrow{h\upsilon \text{ or } \Delta} RO^{\bullet} + HO^{\bullet}$ 3.13

$ROO^{\bullet} + RH \xrightarrow{h\upsilon} R^{\bullet} + R^{\bullet} + HOO^{\bullet}$ 3.14

$HOO^{\bullet} + RH \longrightarrow HOOH + R^{\bullet}$ 3.15

$HOO^{\bullet} + RH \xrightarrow{h\upsilon} H^{\bullet} + R^{\bullet} + HOO^{\bullet}$ 3.16

$RO^{\bullet} + RH \longrightarrow ROH + R^{\bullet}$ 3.17

$HO^{\bullet} + RH \longrightarrow R^{\bullet} + H_2O$ 3.18

3-Termination

$R^{\bullet} + R^{\bullet} \longrightarrow RR$ 3.19

$ROO^{\bullet} + R^{\bullet} \longrightarrow ROOR$ 3.20

$HOO^{\bullet} + HOO^{\bullet} \longrightarrow HOOH + O_2$ 3.21

$ROO^{\bullet} + ROO^{\bullet} \longrightarrow ROOR + O_2$ 3.22

$ROO^{\bullet} + HOO^{\bullet} \longrightarrow ROOH + O_2$ 3.23

Where:

RH : Polymer

$R^{\bullet}$: Polymer alkyl radical

$RO^{\bullet}$: Polymer polymer oxy radical (alkoxy radical).

$ROO^{\bullet}$: Polymer peroxy radical

ROOH : Polymer hydroperoxide

$HO^{\bullet}$: Hydroxyl radical

H_2O_2 : Hydrogen peroxide

$HOO^{\bullet}$: Hydroperoxyl radical [12].

Absorption of UV light by PET leads to two reactions [12, 55, 57, 58]:

A) Norrish Type I :

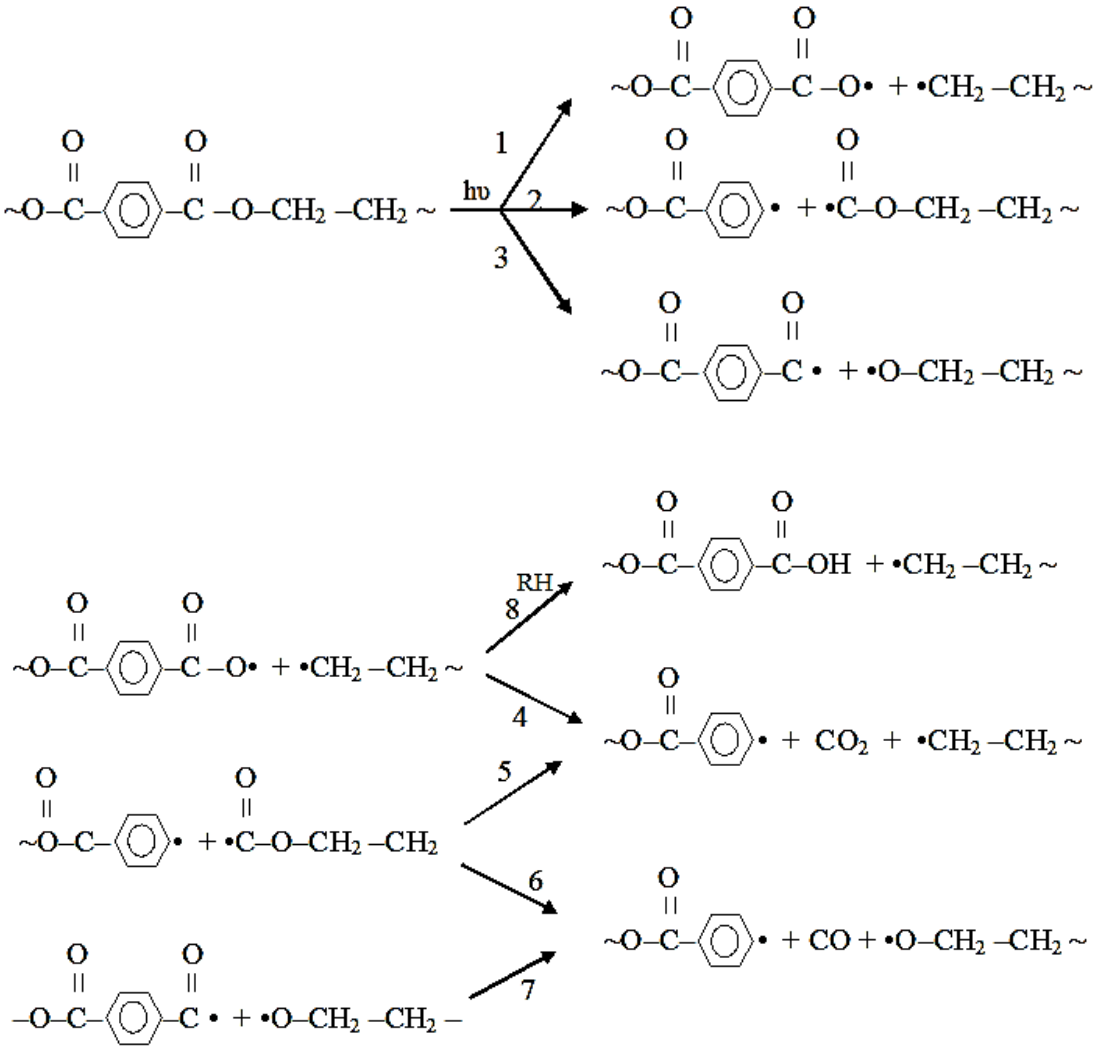

Figure3.4.4.2.1: Norrish type I mechanism [55].

B) Norrish Type II :

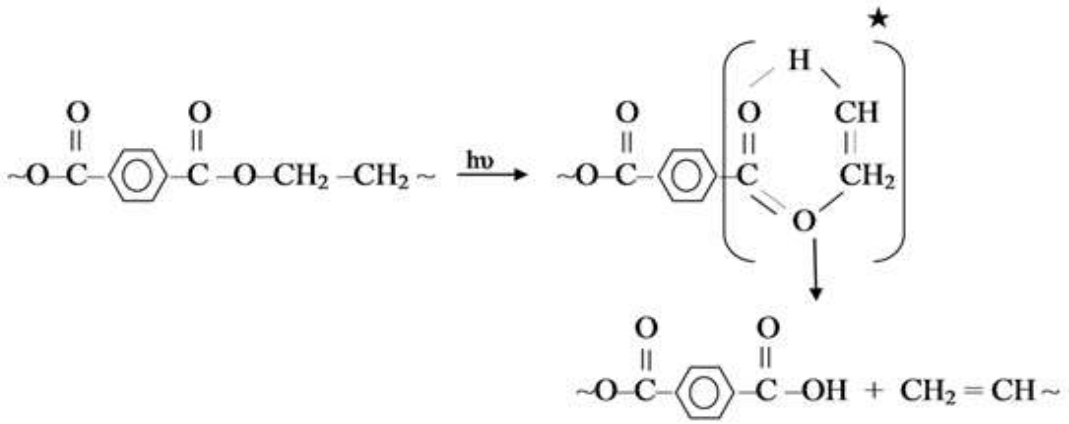

Figure3.4.4.2.2: Norrish type II mechanism [55].

3.5 Degradation Studies of PET

Investigators began to look into the problem of photodegradation of polyethylene terephthalate soon after its magnitude was appreciated. Despite the knowledge established by researchers previously, many details of the photodegradation processes are not fully understood [18, 59]. The following is a summary of some of the critical papers on the subject.

Shultz and Leahy determined that the 314nm is the most active wavelength in producing most strongly photolytic chain scission reaction in PET films. This is the result of their analysis of viscosity data [60].

Day and Wiles studied the oxidative and non – oxidative conditions using a vacuum and N_2 in artificial accelerated weathering. They found that under oxidative conditions, degradation is caused by chain scission followed by slight material discolouring. Degradation in non – oxidative conditions is caused by cross-linking and distinct material discolouring. It was also found that the rate of production of CO_2 was much higher in the presence of air, due to the participation of oxygen in the reactions responsible for its formation in air. In addition, they concluded that the slightly higher rate on the front surface in comparison to the rear surface may be accounted for by the attenuation of the light beam on passing through the film sample [43, 57, 61, 62, 63].

Blais et al. studied the changes in the surface chemical composition of irradiated PET films. They found that chemical scission reactions occurred mainly in the surface layer facing the source of irradiation. This resulted in the formation of carboxylic acid end groups at high concentration in the front surface layer and a lesser amount in the interior. The process was the result of a Norrish type II photo rearrangement reaction [64].

Krishnan et al. observed that unstabilised PET films under photooxidative conditions became brittle. They observed a decrease in molecular weight which indicated the absence of cross-linking [65].

Ilišković showed that as irradiation time was increased, tensile strength and elongation at break both decreased. In addition, the optical density of the characteristic bands and carboxylic end groups increased [66].

Norman found that upon UV irradiation, the rates of carboxyl formation is increased markedly compared with that of hydroxyl groups, confirming the

importance of an intramolecular Norrish Type II hydrogen atom abstraction mechanisms [67].

Wang et al. showed that the photodegradation process of PET takes place in two steps: a very rapid initial step (rapid decrease in molecular weight at t < 10h, which is one of the main origins causing the deterioration in the mechanical properties) followed by a normal step (a slow decrease in molecular weight at t > 10 h). The strongest degradation rate takes place at the exposure surface and decrease with increasing distance from the surface [68, 69].

Fechine and Souto showed that PET films exposed below the polymer glass temperature did not show an increase in crystallinity during exposure [70].

Zue and Kelly found that carbonyl elimination and acid creation the major photochemical results. The proposed Norrish type I and II photodegradation mechanisms accounted for the difference spectra between UV treated and untreated samples. Norrish type II process, forming acid product, dominated over Norrish type I [71].

Fechine et al. found that deterioration in mechanical properties such as tensile strength and elongation at break after UV exposure result in chain scission and the formation of carboxyl end-groups as a consequence of chemical degradation. The photodegradation takes place essentially at the sample surface due to its strong ultraviolet absorption characteristics and oxygen starvation at deeper layers. The carboxyl acid end groups are generated through Norrish type I reaction. Emission rate of CO_2 in wet oxygen was much higher than in dry air and that was significantly larger than that in dry nitrogen [59, 72, 73].

Claire and Graham showed that photodegradation process proceed through radicals formed via Norrish type I reactions, leading to a carboxylic acid and an aldehyde [74].

Fernando et al. found that under vacuum conditions, only small amounts of CO_2 are formed while in air, an increase of CO_2 formation reflects the contribution of oxidation [75].

Tuasikal et al. and Russo et al. found an increase in the carbonyl groups as a degradation product with decrease in mechanical properties (tensile strength and elongation at break) with the extent of UV exposure [76, 77].

From the literature review, there is good evidence that Norrish type II dominates over Norrish type I for the formation of carboxylic acid end groups. In particular, this agrees with Blais et al. and Norman, Zue and Kelly although disagrees with Fechine et al and Claire and Graham. No change is predicted in crystallinity during exposure. In particular, this is confirmed by Fechine and Souto. Deterioration in mechanical properties such as tensile and elongation have been confirmed by several authors including Ilišković, Fechine et al., Tuasikal et al. and Russo et al. Samples also became brittle with increasing degradation according to Krishnan et al. as a result of a decrease in molecular weight due to chain scission process.

The current study was designed to investigate the effects of UV degradation. The materials had been collected from a variety of sources and cleaned for commercial use. Impurities are likely to be present and some degradation due to additional processing is expected. However, the mechanisms of degradation impacting the polymer chain structure are likely to be similar to those to be found in thin film PET specimens that are generally studied and reported as in the current literature review. The objectives of the current study include preparation of materials, exposure to UV and testing.

3.6 OBJECTIVES

High quality bottle grade recycled PET material obtained from recycler and converted by injection moulding into test pieces. Firstly, the conditions of processing and the environment had to be understood. This involved practical experimentation with processing conditions and analysis of degradation mechanisms and test methods.

A series of tests will be done in order to characterize the material after weathering. Two sets of specimens are manufactured by injection moulding. One set of specimens is left outdoors subject to natural weathering conditions. The second set of specimens is subject to exposure in an artificial UV environment under control conditions. After a scheduled period of exposure in the natural environment and in the artificial environment, some specimens are removed and subjected to tests are described below. The periods after which the specimens were removed where 250, 500, 750, 1000, 2000, 5000, 9000

and 13,000 hr. Specimens were also tested before controlled exposure to UV. The tests were done in order to characterize bulk physical properties as well as the effects of degradation on molecular characteristics.

The density, water content and crystallinity of the material were measured at various stages of process, as flakes, extruded pellets, recycled pellets and injection moulded samples to understand the effects of degradation during processing on crystallinity, density and water content.

The changes in processability and crystallinity as a result of UV degradation were identified using the MFI and DSC tests respectively.

Chemical changes at molecular level were investigated by measuring the variations of specific bands of groups belonging to degradation products. Most commonly, using infrared spectroscopy changes in the carbonyl group resulting from the oxidation process were investigated.

Regarding aesthetic characterization or surface performance, colour and gloss changes were studied.

The effect of UV on the mechanical behaviour of PET was also studied as structure integrity is a key factor in products. Charpy impact tests were concluded on specimens at different stages of exposure to UV under accelerated condition and natural weathering. The tensile properties of the material were studied by measuring the yield stress, elongation at yield, failure stress and elongation at failure.

Yield stress is measured at various stages of UV exposure which is regarded as a failure limit in design consideration because it is a measure of the start of the permanent deformation, i.e. the material starts to yield leading to a failure.

Failure stress is a good indication of the significance of surface degradation even in the thick samples, leading to the growth of cracks.

CHAPTER FOUR

MATERIAL PREPARATION

4.1 Material and Sample Preparation

4.1.1 r-PET Flakes

Recycled polyethelene terephthalete flakes (CLR r-PET flake) were acquired from Closed Loop Recycling (CLP, UK). The composition of the flakes was tested using Fourier Transform Infrared Spectroscopy, for this 500 g samples were taken, identified by colour. r-PET flakes were kept in a closed barrel to prevent contact with air moisture because PET is a hydroscopic material.

A small amount of recycled polyethylene flakes was pelletized using twin screw co-rotating extruder (Twin Screw Extruder Micro18 Co-rotating) with two different screw speeds (60 rpm and 85 rpm to identify later which was the best to adopt for injection moulding) using the following parameters:

Table4.1.1.1: Setting parameter for the processing of r-PET in the extruder.

Setting parameter-extruder	
Temperature-zone-1	25 °C
Temperature-zone-2	267 °C
Temperature-zone-3	267 °C
Temperature-zone-4	267 °C
Temperature-zone-5	267 °C
Temperature-zone-6	262 °C
Temperature-zone-7	255 °C
Temperature-zone-8	240 °C

Tests were carried out on r-PET flakes, r-PET pellets with 60 rpm and 85 rpm: density, water content measurement, DSC analysis, FTIR analysis and MFI test.

Problems Encountered:

1- After the transfer of lab from Holloway road to the Commercial road, there was no water supply to the machines that needed water for cooling. Instead, water was supplied from a free standing tank to the machines and circulated back to the tank. In the case of extruder, this water entered warm which was less effective for cooling and caused additional problems during operations. The barrel temperature increased which increased extrudate rate that leads me to decrease screw speed from 60 rpm to 12 rpm. This caused the continuous extrudate to break up regularly and caused variable properties in the same batch of pellets. These pellets were then unsuitable for injected moulding.

2- In addition to that undried flakes which were fed to the extruder suffered extreme hydrolytic degradation that lead to big drop in the crystallinity of the pellets (from 39% to 14%) which made them unsuitable to be injected moulded.

4.1.2 r-PET Pellets

So, the new material, r-PET pellets (CLR/KUDOS r-PET pellets) were acquired from QUDAS, Scotland to be injected directly in the injection moulding machine without the step of pelletizing in the extruder and save the material from severe degradation and was tested for density, water content measurement, DSC analysis, FTIR analysis and MFI test.

Before removing moisture (drying), two important factors are carefully under control:

- The storage conditions of the material prior to processing: closed barrel.
- Use of a closed-loop air hopper dryer to prevent the pellets from contact with the humidity of the atmosphere at the inlet of the injection moulding machine (hopper).

r-PET pellets were dried at 170ºC for 2 hours and injected moulded to type 1A tensile dumbbell configuration using Klockner Ferromatik with the following settings:

Table4.1.1.2: Setting parameter for the processing of r-PET in the injection moulding machine.

Setting parameter-Injection moulding	
Temperature-zone-1	260 °C
Temperature-zone-2	265 °C
Temperature-zone-3	270 °C
Temperature-nozzle	300 °C
Temperature-mould	70 °C
Screw speed	50 rpm
Injectionpressure-zone-1	15 bar
Injectionpressure-zone-2	35 bar
Injectionpressure-zone-3	37 bar
Back pressure	50 bar
Cooling time	36 s

Problems Encountered:

1- Continuous problems associated with the operation of injection moulding machine and dealing with recycled material which makes the operation to be interrupted every regularly. As a result, only about 30% of the specimens produced for testing were defect free.

2-The same problem with the extrusion happened with the injection moulding machine. Cooling the mould (70°C) with water circulating from free standing tank to the machine and back to the tank. This water entered the injection moulding machine warm and was therefore less effective for cooling and caused problems with specimens sticking to the mould during the operation. It took time to remove the sample from the mould, clean the mould and lubricate it. During this time, the nozzle temperature would drop. The molten polymer inside the barrel degraded more because of the increase in resident time inside the barrel.

3-The water for the injection moulding machine for cooling the barrel came from a low pressure supply with low flow rate which was less effective for cooling or maintaining the barrel temperature.

4.1.3 Natural weathering

The specimens were mounted on a frame facing the south with an angle of exposure to the sun of 45º in London. They remained in position for a maximum period of 13,000 hr.

The actual peak to peak variations in temperature and relative humidity were between 32ºC (summer) and -1ºC (winter) and between 100% (winter and autumn) and 22% (summer) respectively.

The average variation in temperature and relative humidity were between 26ºC (summer) and 3ºC (winter) and between 80% (winter) and 45% (summer).

The temperature and relative humidity varied with seasons as follows:

- 0 – 1000 hr of exposure (the first 1000 hr): summer (high temperature and low relative humidity).
- 1000 – 2000 hr of exposure: autumn (low temperature and high relative humidity).
- 2000 – 5000 hr of exposure: winter (low temperature and high relative humidity).
- 5000 – 9000 hr of exposure: spring (moderate temperature and moderate relative humidity) / summer (high temperature and low relative humidity).
- 9000 – 13000 hr of exposure: autumn (low temperature and high relative humidity) / winter (low temperature and high relative humidity).

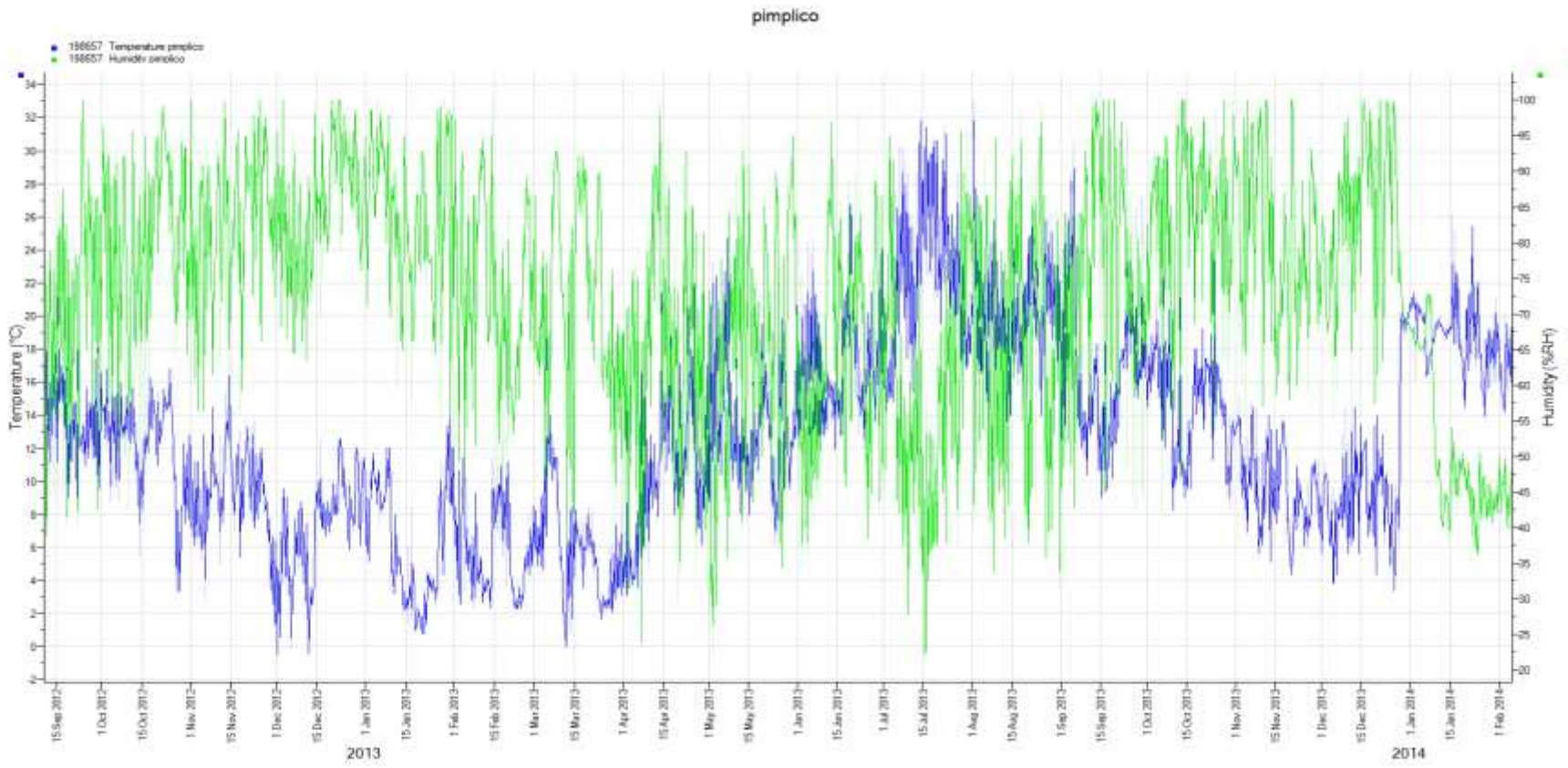

Figure6.4.1.3.1: Variation of temperature and humidity measured

by data logger facing the south in London.

4.1.4 Accelerated weathering

Tests were carried out using QUV accelerated weathering tester supplied by Q-Panel Lab Products, at an irradiance of 0.68 W/m² at 340 nm. This is considered a good match with noon summer sunlight in Northern Europe. Each 12 hr cycle compromised 8 hr of UV radiation at 60ºC and 4 hr of condensation at 40ºC. The UV exposure and condensation exposure occur separately to simulate natural weathering conditions. Test exposure times were 0, 250, 500, 750, 1000, 2000, 5000, 9000 and 13000 hour.

The QUV accelerating weathering tester is equipped with Solar Eye Irradiance Control which is a precision light control system that automatically maintains the exact level of irradiance (the rate at which light energy falls on a unit area of surface). The controller monitors UV intensity and compensates any variability by adjusting power to the lamps [44].

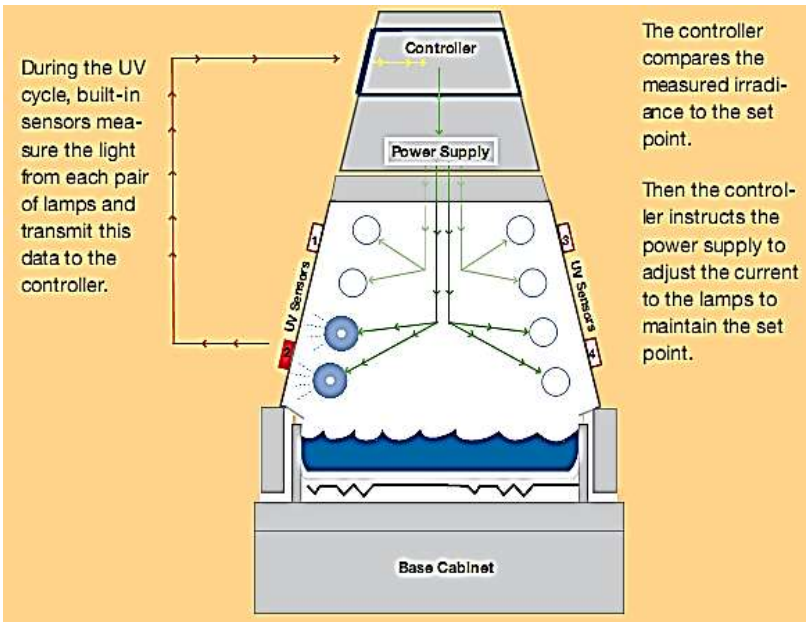

Figure 4.1.4.1: Solar Eye Irradiance Control [44].

Condensing humidity is the best way to simulate outdoor moisture attack because most of this moisture is the result of dew. QUV uses a condensation cycle for 4 hours and is conducted at an elevated temperature (typically 50°C). During the QUV condensation cycle, a water reservoir (water pan) in the bottom of the test chamber is heated to produce vapour which reaches 100% relative

humidity. Vapour continually condenses on the test panels, which are kept at a lower temperature by room air on the back surfaces of the specimens [15, 44].

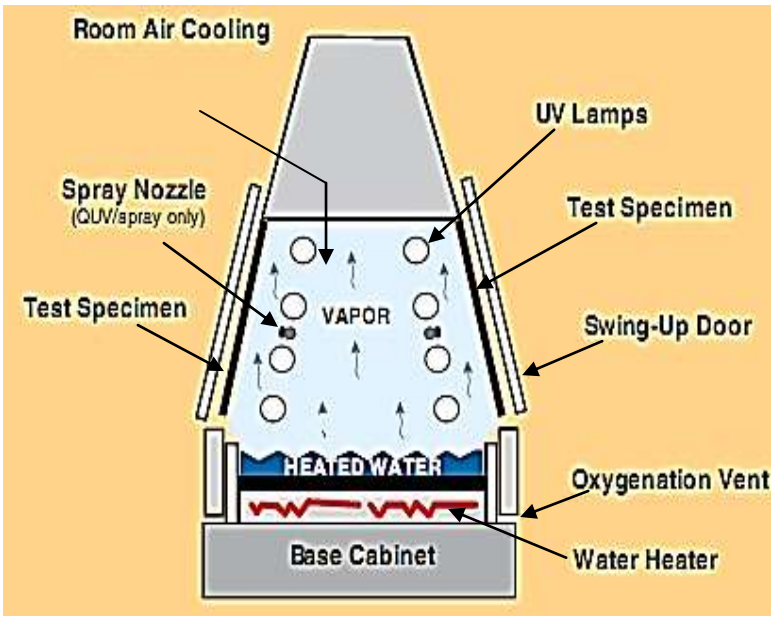

Figure 4.1.4.2: QUV cross-section during condensation period [44].

Problem Encountered:

Because of the high humidity in the lab during the condensation cycle of the QUV accelerated weathering tester, the window of the lab was opened and this caused the panel temperature of the tester to drop below 50°C so the setting temperature was reduced from 50 to 40°C.

4.2 Water Content Measurement

4.2.1 Method

PET is hydroscopic polymer and is highly susceptible to hydrolysis which causes deterioration of mechanical properties. To achieve good end – use properties, water level of PET needs to be 0.02% or less.

The evacuated container (sealed reaction vessel) of Aquatrac moisture meter is heated up to the measuring temperature. The evaporating water (absorbed by r-PET granules) reacts with the reagent calcium hydride (reagent) to generate hydrogen gas [78];

$$CaH_2 + 2H_2O \rightarrow Ca(OH)_2 + 2H_2$$

Figure4.2.1.1: Reaction of reagent with water [78].

The gas pressure is monitored and water content as a percentage is evaluated and displayed on a digital screen.

The power (1) of Aquatric moisture meter apparatus was switched on and the system was aerated (2) then, reaction chamber was opened and 10 g of sample was put in. Before closing the chamber, one small scope of reagent was put on a mesh cover at the top on the chamber.

The system was evacuated (3) and the system was adjusted on zero (5) with heating temperature of 160 ºC. After a sound was heard from instrument, water content percentage, $\%H_2O$ appeared on a digital screen. The system was aerated, the power was switched off, the reaction chamber was opened and the sample was taken out.

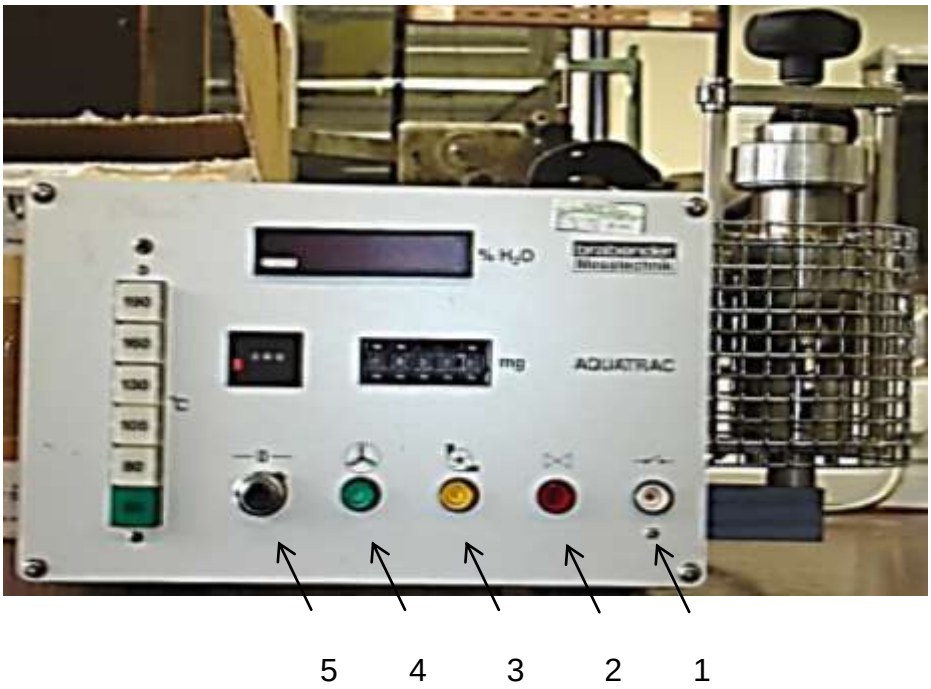

Figure4.2.1.1: Aquatrac moisture meter.

4.2.2 Results

Table4.2.2.1: Water content and crystallinity% for CLR-flakes and its pellets and CLRKodos-r-PET-pellets.

	Water Content (%)	Crystallinity (%)
CLR-r-PET-Flakes	0.337 ± 0.004	45.77 ± 1.93
Pellets-60 rpm	0.418 ± 0.003	17.16 ± 1.24
Pellets-85 rpm	0.443 ± 0.003	10.50 ± 0.73
CLRKodos-r-PET- pellets	0.165 ± 0.003	47.93 ± 1.42

4.2.3 Discussion

At ambient temperature, the PET structure is stable against water penetration. When the temperature increases especially above glass transition temperature, the energy of chains increases which makes the chains more flexible and mobile to create more free volume and this facilitate the diffusion of water molecules in this area. The water content increased as the crystallinity decreased as shown in figure 4.2.3.1.

The crystallinity percentage refers to the overall level of crystalline component in relationship to its amorphous component. During pelletizing, as mentioned before, there is a reduction chain length due to the chain scission and further chain scission as the screw speed increased from 60 rpm to 85 rpm due to increasing in shear stress.

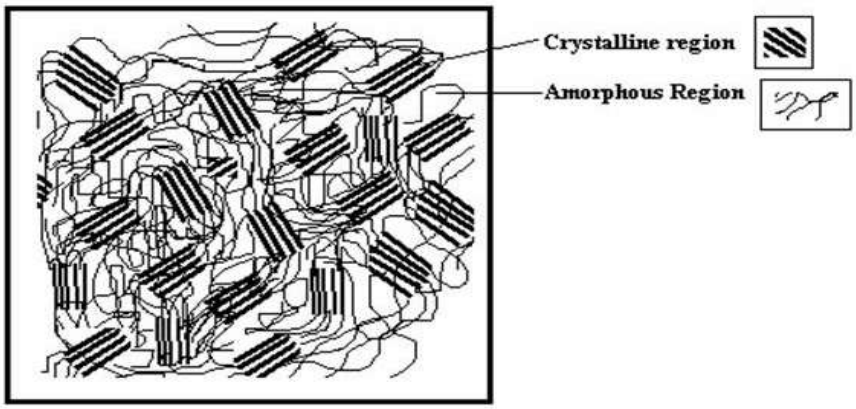

Figure4.2.3.1: Mixed a morphous-crystalline macromolecular polymer.

The process of chain scission produces shorter chains which are not enough to form enough folds to form crystalline segments, so the crystallinity decreased.

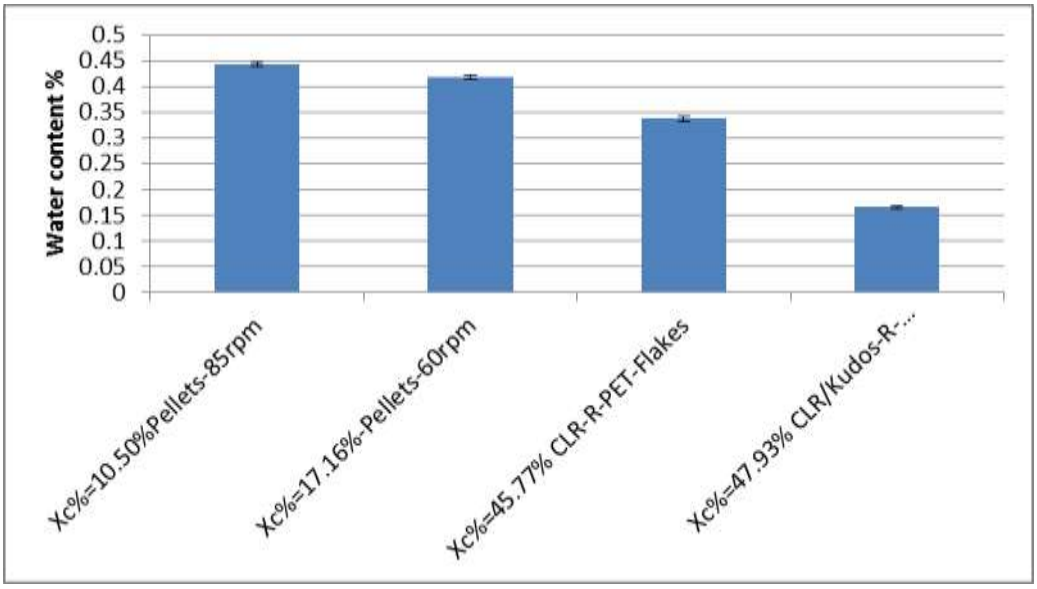

Figure4.2.3.2: Variation of water content with crystallinity percentage.

Decreasing in crystallinity means the percentage of amorphous regions increased. The water molecules are not able to easily penetrate the crystalline regions of a polymer, thus the amorphous regions are affected first and most rapidly. However, the crystalline regions are not immune to water attack. So, with increasing the amorphous component, the water content will increase [5, 79].

4.3 Density Measurement

4.3.1 Method

The density of the specimen is determined by pycnometer method, in accordance with ASTM854 standard. Density of the sample is calculated according to the following equation:

$$\rho_{sample} = \frac{W2-W1}{W2-W1+W4-W3} \quad .....4.1$$

Where;

ρ_{sample}: density of the material (g/ml) at 25°C.

W1: weight of empty bottle (g).

W2: weight of empty bottle containing sample (g).

W3: weight of bottle containing sample and filled with water (g).

W4: weight of bottle filled with water (g).

ρ_{sample} = weight of sample/volume of sample 4.2

weight of sample = W2-W1 .....4.3

volume of sample = volume of displaced water 4.4

volume of displaced water = weight of displaced water/$\rho_{water@25^oC}$ 4.5

density of water at 25ºC = $\rho_{water@25^oC}$ =1g/ml

volume of displaced water = weight of displaced water=W_{ds} 4.6

W_{ds} = [weight of sample + weight of bottle filled with water]

- [weight of bottle containing sample and filled with water] 4.7

So, W_{ds} = W2 – W1 + W4 – W3 .....4.8

By combining above equations, eq.4.1 is obtained [80].

A distilled water at 25 ºC was prepared in water bath. The weight of bottle without and with sample, W1 and W2 respectively were recorded then, the weight of bottle filled with distilled water without and with sample, W4 and W3 respectively were recorded and the density of the sample was calculated.

4.3.2 Results

Table 4.3.2.1: Density values for CLR-flakes and its pellets (at 60 and 85 rpm), CLR/Kodos-r-PET pellets and samples after injection moulding machine.

Material	Density, ρ (g/cm^3)
CLR-r-PET-Flakes	1.322 ± 0.029
Pellets-60 rpm	1.308 ± 0.016
Pellets-85 rpm	1.276 ± 0.016
CLR/Kodos-r-PET pellets	1.349 ± 0.012
Samples after injection moulding processing	1.264 ± 0.025

4.3.3 Discussion

During pelletizing and injection moulding processes, chains suffer breaking (chain scission) because of hydrolysis, thermal and oxidation degradation, and further chain scission as the screw speed increased from 60 rpm to 85 rpm due to increasing in shear stress. The process of chain scission produces shorter chains which have more ends per unit volume than long chains, hence a higher free volume, i.e. lower density as shown in figures below [81].

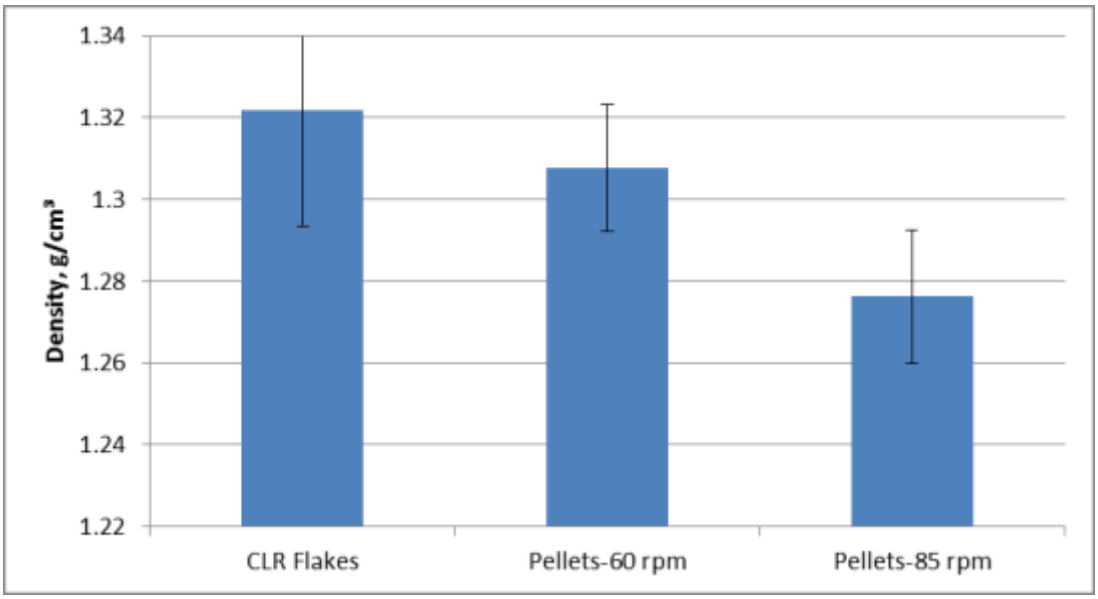

Figure4.3.3.1: Densities for CLR flakes and their pellets at different screw speeds (60 and 85 rpm).

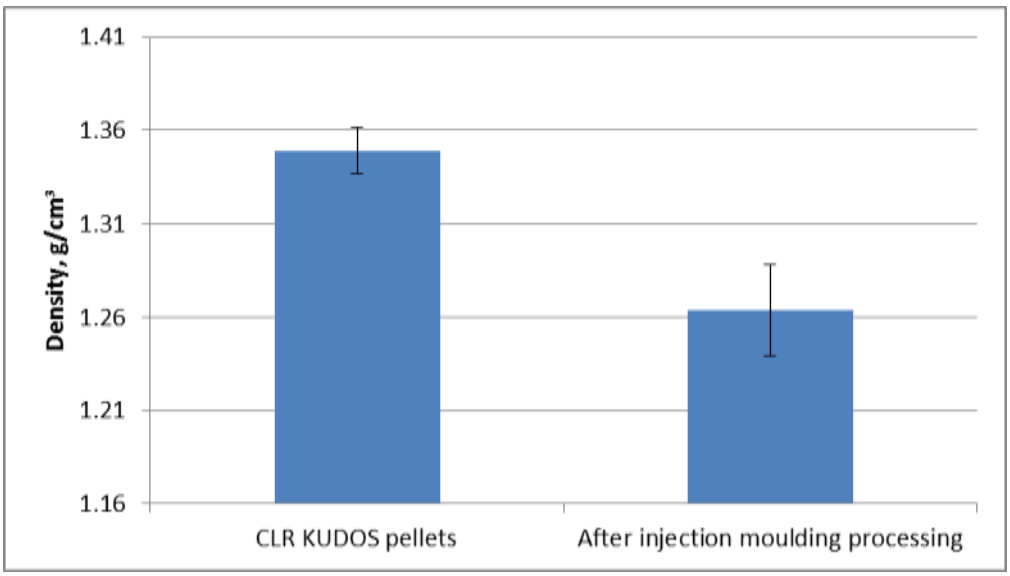

Figure4.3.3.2: Densities for CLR/KUDOS r-PET pellets and samples before processing.

CHAPTER FIVE

MATERIAL CHARACTERIZARATION

5.1 MFI

5.1.1 Method

Viscosity is a measure of the resistance of a material to flow. If a force (f) try to move a plane of area (A) relative to another plane a distance (d) from the initial plane (assuming a fluid as a stack of parallel separated plates), it takes a force such that

$$f \propto \frac{A}{d} \qquad \text{.....(5.1)}$$

$$f = \eta \frac{A}{d} \qquad \text{.....(5.2)}$$

This proportionality factor, η is called viscosity.

The ratio of the viscosity η of the polymer solution (concentration, c) to the viscosity η_o of the solvent allows calculating a reduced viscosity η_{red}:

$$\eta_{red} = \{(\eta / \eta_o) - 1\} / c \qquad \text{.....(5.3)}$$

The extrapolation of reduced viscosity to zero concentration furnishes the intrinsic viscosity [η]. This fast, reliable and simple method is the most important technique for the determination of molecular weight from [η].

Mark and Houwink correlated the intrinsic viscosity and molecular weight:

$$[\eta] = K M^a \qquad \text{.....(5.4)}$$

Where:

M is molecular weight of the polymer (g/mole).

(K) and (a) are constants for a given polymer in a given solvent [82, 83, 84].

The changes in degree of polymerization result in molecules with different molecular weights. Because of the difference in chain lengths, it is convenient to describe the molecular weight in terms of molecular weight distribution. In

order to make the best use of the experimental data, the most commonly used terms are *Mn*, *Mw* and *Mz* which are number average molecular weight, weight average molecular weight and viscosity average molecular weight respectively [85].

$$Mn = \frac{\sum ni\ Mi}{\sum ni} \qquad \text{.....(5.5)}$$

$$Mw = \frac{\sum ni\ Mi^2}{\sum ni\ Mi} \qquad \text{.....(5.6)}$$

$$Mz = \frac{\sum ni\ Mi^3}{\sum ni\ Mi^2} \qquad \text{.....(5.7)}$$

Where *ni* is the number of polymer molecules per unit volume of samples with molecular weight *Mi*. *Mz* is a function of the solvent, so a given polymer sample can be characterized only by a single value of *Mn* and *Mw*, but it may have different *Mz*'s depending on the solvent in which [η] is measured.

The ratio of *Mw* to *Mn* (*Mw/Mz*) is very important parameter and is called polydispersity index (PDI) which is an indicative of the extent of polydispersity and measure of breadth of the distribution. If PDI is equal to one that means that the sample is monodisperse (all molecules are of the same size). When *Mw/Mz* increases, the molecular weight distribution becomes broader (larger difference in the size of molecules).

The properties of the material (e.g. mechanical and thermal) and their processing behavior depend critically on the molecular weight and its distribution and this is why different grades of each polymer are available in the plastic market. For example, tensile and impact strength increase with molecular weight, also but importantly, the higher the molecular weight the better, if the highest strength is desired [83,86,87, 88].

The molecular weight measurement is complicated, time consuming and required controlled conditions. In industry therefore, it is more common to use the melt flow index measurement. This is a quick, cheap, reliable, easy to

perform and allows an assessment to be made of the effect of molecular weight and its distribution on viscosity. As an industrial technique, this allows a quick check on changes to the flow characteristics of the melt.

Melt flow index is an assessment of average molecular weight and is an inverse measure of the viscosity; in other words, the higher MFI, the more polymer flows under test conditions which means the lower viscosity or molecular weight. The flow characteristics of a polymer are important in anticipating and controlling the processing. Generally, higher MFI polymers are used in injection moulding (to be injected easily), and lower MFI polymers are used with blow oulding or extrusion processes [17, 33, 89].

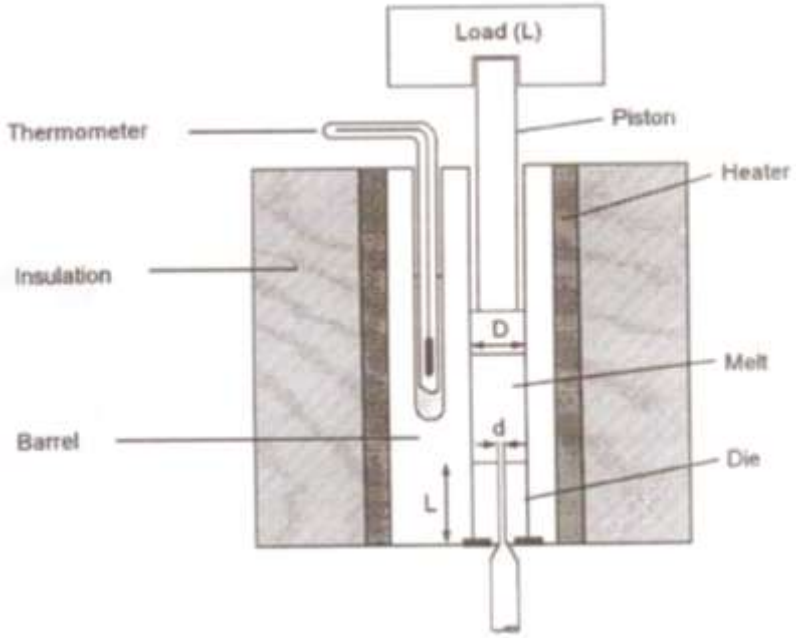

Figure5.1.1.1: Schematic diagram melt flow rate testing apparatus.

MFI was measured using Plasticode Melt Index test machine with a mass of 2.16 kg applied and a barrel temperature of 252 ºC. The barrel was filled, compacted with the material and allowed to soak for one minute. The piston was inserted after the load was located and allowed to push the material through die until first marker on piston enters the barrel. With a stopwatch, the extrudate from die was cut every 10 minutes and its weight was recorded. The average weight of extrudate per ten minutes was recorded for each specimen which is regarded as the melt flow index, MFI (or melt flow rate, MFR) for each specimen.

5.1.2 Results

Table5.1.2.1: Melt Flow Index data for r-PET flakes (CLR r-PET Flake) and their pellets using Ray-Ran advanced microprocessor system with barrel temperature = 265°C, weight of piston = 2.16 kg and drying time one hour at 100°C.

	dried r-PET flakes	Un-dried r-PET flakes	dried r-PET pellets	Un-dried r-PET pellets
Avg. MFI (g/10min)	14.94 ± 2.66	15.51 ± 1.93	15.74 ± 1.63	16.46 ± 0.84

Table5.1.2.2: Melt flow index for r-PET pellets (CLR/KUDOS PET Pellets) using Plasticode melt index test machine with barrel temperature = 252°C, weight of piston = 2.16 kg and drying time four hours at 170°C.

	Un-dried r-PET Pellets	Dried r-PET Pellets
Avg. MFI (g/10min)	12.39 ± 1.68	3.01 ± 2.53

Table5.1.2.3: Melt flow index for UV irradiation under accelerating weathering and in natural weathering.

UV exposure time, hr	MFI (accelerated weathering) g/10min	MFI (natural weathering) g/10min
0	21.48 ± 3.87	21.48 ± 3.87
250	20.76 ± 4.23	22.46 ± 4.28
500	18.97 ± 3.08	22.10 ± 4.95
750	22.04 ± 3.67	19.65 ± 3.38
1,000	18.52 ± 2.02	24.58 ± 4.38
2,000	21.03 ± 2.94	18.80 ± 5.44
5,000	20.89 ± 4.79	19.55 ± 3.82
9,000	22.00 ± 3.41	19.48 ± 3.64
13,000	22.64 ± 5.21	22.39 ± 3.93

Discussion

This is a qualitative method for comparing flow characteristics and is used universally in the processing industry for quality checks. In current study, it is used for quality check and for comparative analysis.

Pellets of CLR r-PET flakes at 60 rpm (dried and un-dried) has a melt flow index greater than CLR r-PET flakes (dried and un-dried) as shown in figure below.

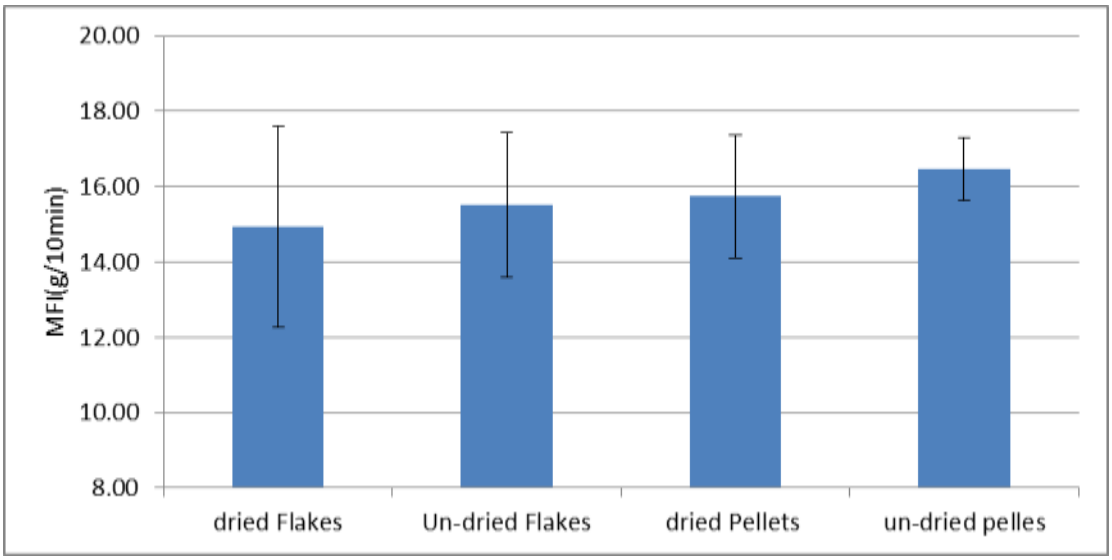

Figur5.1.3.1: Melt flow index value of r-PET flakes and pellets (dried and un-dried).

r-PET pellets suffer during processing hydrolysis, thermal and oxidation degradation which causes the chains to break, i. e. the macromolecules are converted into smaller molecules (shorter chain lengths). The hydrolytic degradation includes chain scission at ester linkages, each water molecule breaks one ester bond which leads to severe decrease in chain lengths.

The presence of oxygen with high shear rate forces in the melt leads to mecha-oxidation and the formation of hydroperoxides. Increasing the shear rate leads to increase in the formation of hyroperoxides which undergoes thermolysis when heated during processing producing radicals that attack PET chains, causing chain scission.

The shorter chain lengths, the less number of entanglements with the chains, this means it is less difficult for chains to slide pass each other and therefore it

is less difficult for the material to shear, i.e. less resistance to flow causing increasing in the melt flow rate (melt flow index). Mark and Houwink equation explained the relation between molecular weight and viscosity. Decrease in the molecular weight (chains break) leads to a reduction in viscosity i.e. reduction in the resistance to flow that cause increasing in the melt flow index.

The melt flow index for un-dried material (flakes and pellets) is greater than that of dried material. The presence of water in the material causes hydrolysis that leads to chain scission and increases in melt flow index as mentioned previously [17, 33].

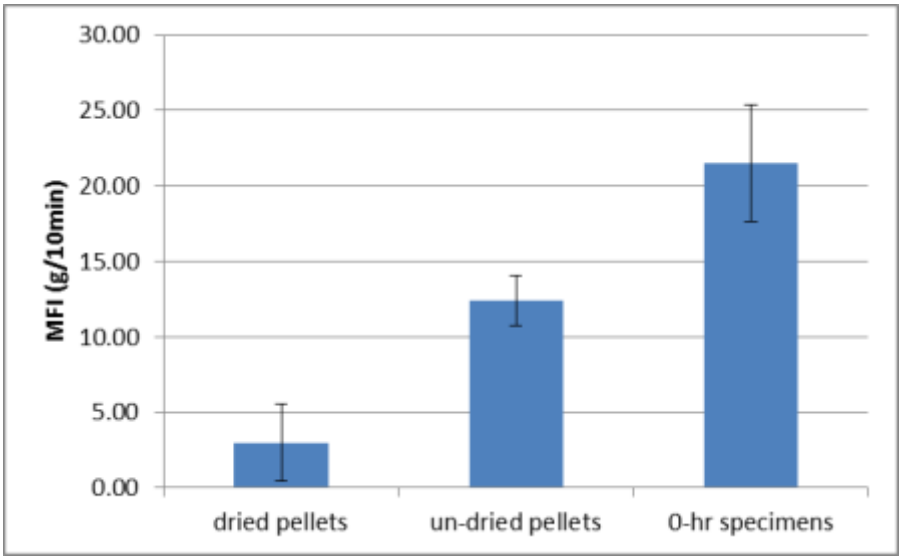

Figure 5.1.3.2: Melt flow index value of CLR/KUDOS r-PET pellets (dried and un-dried).

The melt flow index remained relatively constant after 13000 hr of UV exposure for both types of weathering (natural and accelerated) as shown in figures 5.1.3.3 and 5.1.3.4 and this explains that the degradation is a surface effect which doesn't affect the whole specimens.

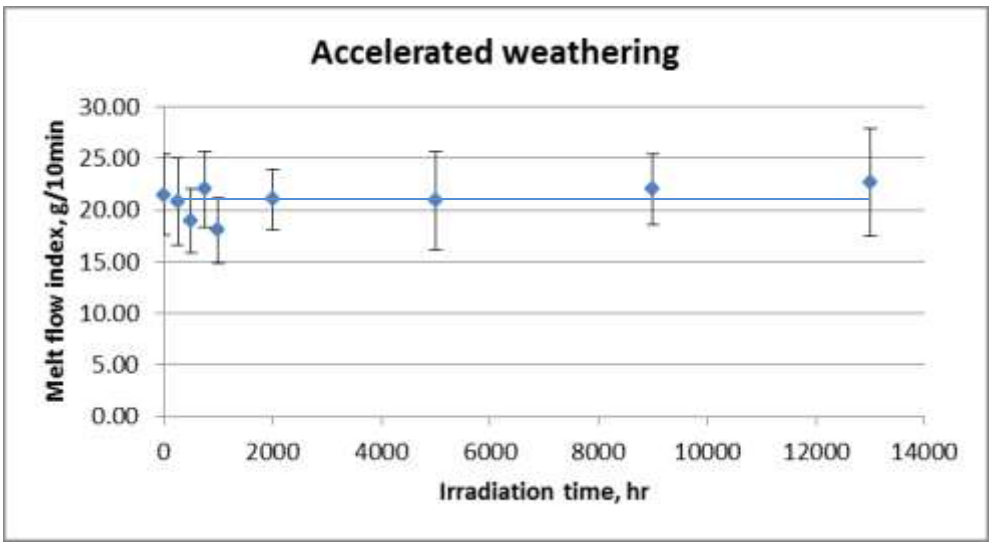

Figure 5.1.3.3: Melt flow index value of r-PET samples under accelerated weathering.

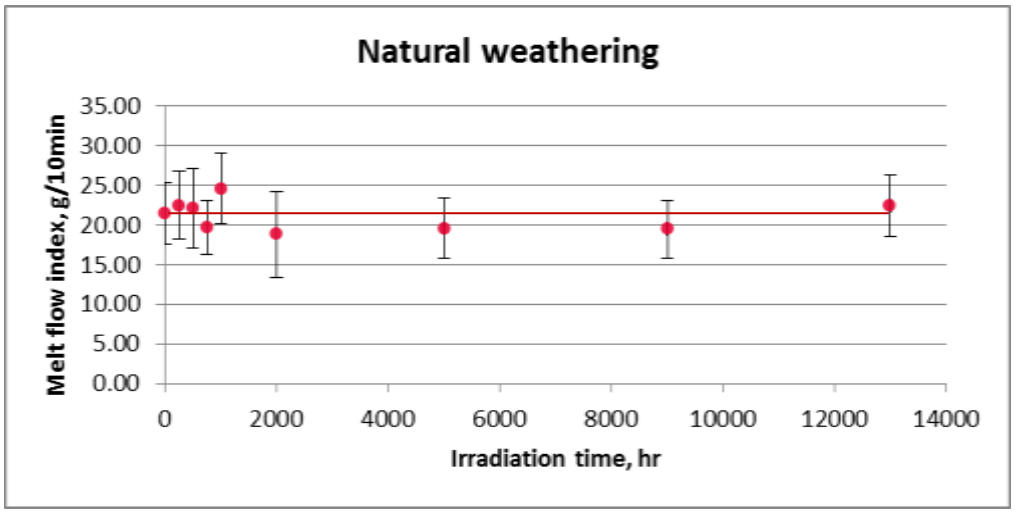

Figure 5.1.3.4: Melt flow index value of r-PET samples under natural weathering.

5.2 DSC Analysis

5.2.1 Method

Differential scanning calorimetry (DSC) is a technique which measure the difference in the quantity of heat required to increase the temperature of a polymer specimen and reference (an empty aluminium pan) at a constant heating rate (10ºC/min) as a function of temperature.

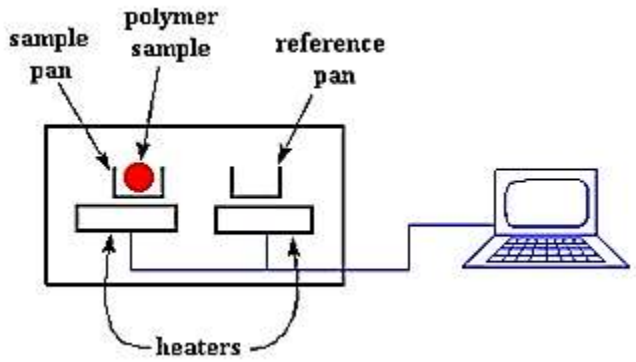

Figure5.2.1.1: Simple sketch of DSC instrument [90].

When the material undergoes a thermal transition, more or less heat will need to flow to it than the reference to maintain both at the same temperature (depend on the process if it is exothermic or endothermic).

If a solid sample melts to a liquid, it will require more heat flowing to the sample to increase its temperature at the same rate as the reference due to the absorption of heat by the sample as it undergoes the endothermic transition from solid to liquid (melting process). And if the sample undergoes exothermic processes (crystallization process), less heat is required to raise the sample temperature. Thus, by monitoring the difference in heat flow between the sample and reference, DSC can measure the amount of heat absorbed or released during such phase transitions.

TA instrument DSC 2010 apparatus was used to record DSC curves in the temperature range 30 to 300 ºC. A weight of 2-18 mg of each sample was used in an aluminium pan, encapsulated and transferred to the front cavity of the DSC heating head and the reference (an empty aluminium pan with a lid) is transferred to the back cavity of the DSC heating head and the area of the

cavity was covered. The heating rate was 10 ºC/min and the test mode was ramp. Finally the data were analysed for Tg, Tc, T_m, ΔHm and ΔH_c.

Glass transition may occur as the temperature of polymer sample increases, it appears as a step in the recorded DSC signal. This is due to the sample undergoing a change in heat capacity.

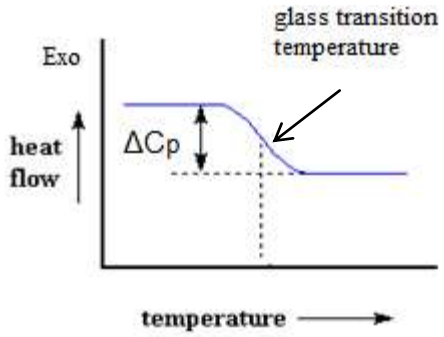

Figure5.2.1.2: Glass transition temperature [90].

As the temperature increases, the chains of amorphous region have enough energy to adopt the more stable conformation and arrange themselves into a crystalline form. This transition from amorphous solid to crystalline solid is known as crystallization and results in a peak (an exothermic peak) in the DSC signal.

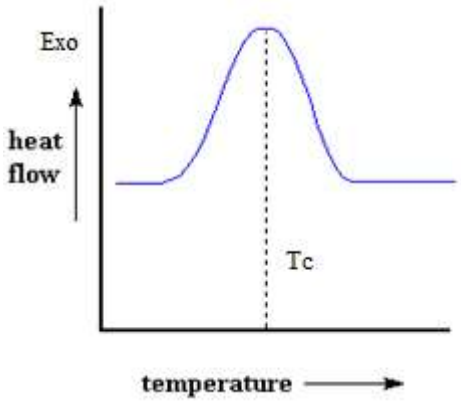

Figure5.2.1.3: crystallisation curve [90].

With increasing temperature, the sample finally reaches its melting temperature (T_m), the chains move randomly and freely (highly mobile). When the polymer crystals melt, they absorb heat, this extra heat flow during melting shows a

peak (an endothermic peak) in the DSC signal [90, 91, 92, 93].

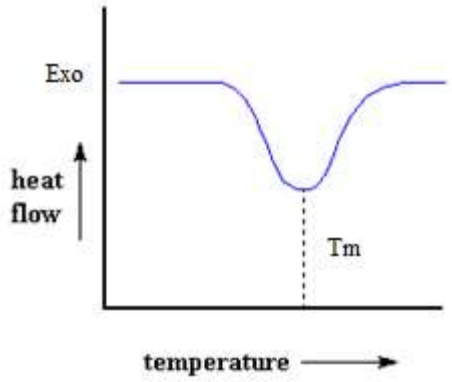

Figure5.2.1.4: melting curve [90].

DSC is widely used in industrial settings as a quality control instrument due to its applicability in evaluating sample purity and for studying polymer curing.

One of the most significant properties of semi-crystalline polymers which contain two components: a crystalline and an amorphous, is the percent crystallinity which refers to the overall amount of crystalline component in relationship to the amorphous component.

$$\% \text{ Crystallinity} = [\Delta H_m - \Delta H_c] / \Delta H_{mo} * 100\% \qquad \text{.....5.8}$$

Where ΔH_m : Heat of melting (J/g)

ΔH_c: Heat of cold crystallization (J/g)

ΔH_{mo}: A reference value represents the heat of melting if the polymer where 100% crystalline ($\Delta H_{mo}$for r-PET = 119.8 J/g) [94].

5.2.2 Results

The phase behaviour of the r-PET flakes and pellets was analysed by DSC821 differential scanning calorimeter. The percentage of crystallinity (%Xc) for CLR-r-PET-Flakes, its pellets at 60 and 85 rpm and r-PET specimens before and after UV exposure in natural and accelerated weathering are reported in tables below.

Table 5.2.2.1: Results of DSC measurements: The percentage of crystallinity (%Xc) for CLR-r-PET-Flakes and its pellets.

Material	Crystallinity, X_c (%)
CLR-r-PET-Flakes	45.77 ± 1.93
Pellets-60 rpm	17.16 ± 1.24
Pellets-85 rpm	10.50 ± 0.73

Table 5.2.2.2: The percentage of crystallinity before and after UV exposure to natural and accelerated weathering.

UV exposure time, hr	Xc% for accelerated weathering	Xc% for natural weathering
0	18.94 ± 2.39	18.94 ± 2.39
250	20.01 ± 2.94	19.73 ± 3.02
500	14.70 ± 2.58	16.93 ± 3.80
750	22.11 ± 6.21	15.68 ± 3.19
1000	18.74 ± 3.56	19.38 ± 2.37
2000	22.06 ± 3.84	22.42 ± 4.54
5000	21.96 ± 3.81	16.75 ± 4.04
9000	17.92 ± 4.89	21.66 ± 3.25
13000	18.66 ± 0.74	18.27 ± 2.52

5.2.3 Discussion

DSC thermograms for CLR-r-PET-flakes and its pellets at screw speed 60 rpm and 85 rpm are shown in figures below.

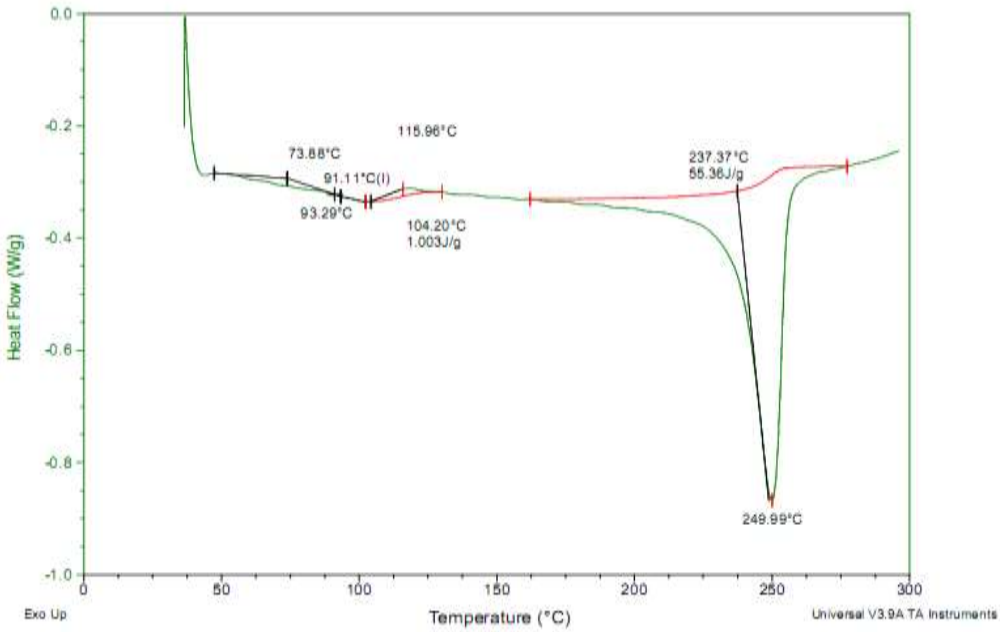

Figure5.2.3.1: DSC thermogram for CLR-r-PET flakes.

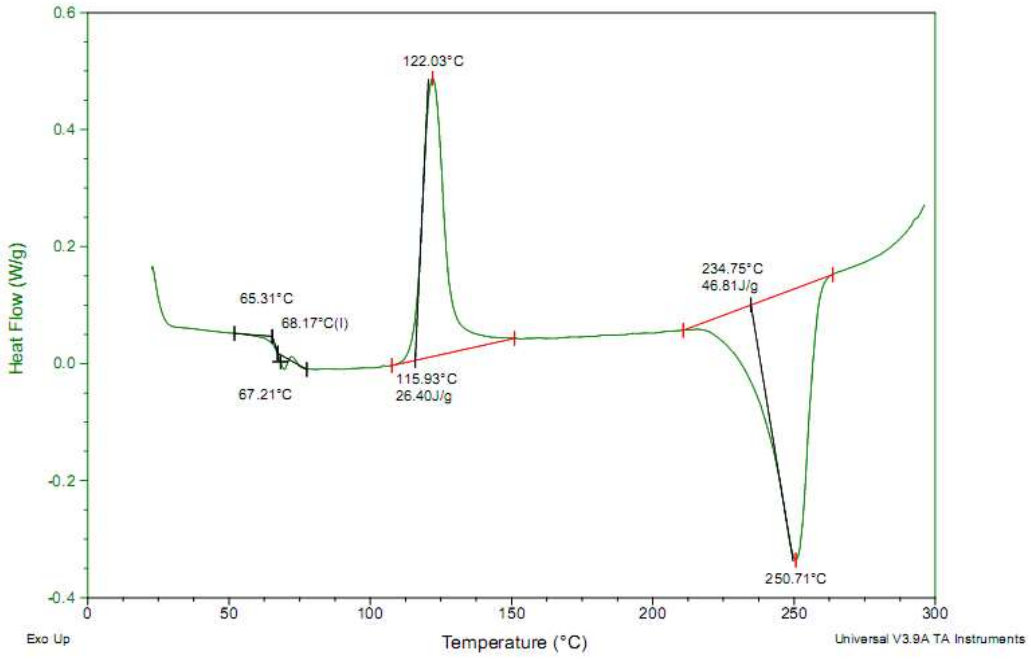

Figure5.2.3.2: DSC thermogram for r-PET pellets 60-rpm.

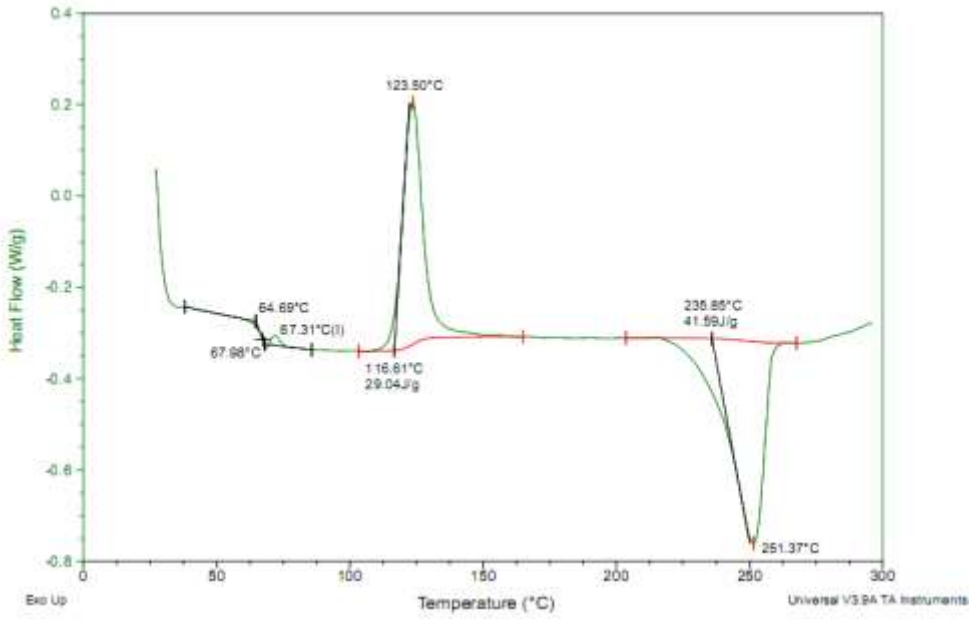

Figure5.2.3.3: DSC thermogram for r-PET pellets-85rpm

As mentioned before, during pelletizing process, there was a reduction in percentage of crystallinity 45.37%-flakes (figure5.2.3.1) to 17.04%-pellets-60rpm (figure5.2.3.2) to 10.48-pellets-85rpm (figure5.2.3.3). This drop explains the reduction in amount of crystalline region due to the chain scission and further chain scission as the screw speed increased from 60 rpm to 85 rpm due to increasing in shear stress.

The process of chain scission produces shorter chains which are not enough to form enough folds to form crystalline segments, so the crystallinity decreased though chain breaking.

Shorter chains have more ends per unit volume than long chains. The ends of a chain can move more freely than the segments in the centre of chain and thus creating more free volume (a higher free volume with shorter chains). Also the shorter the chains, the less number of entanglement which preventing or delaying the relaxation of molecular chains. Moreover, the shorter chains have less mass, so amount of absorbed energy to relax would be less resulting in earlier relaxation of these chains at lower temperature (lower temperature for transition from glassy to rubbery state) i.e. a lower Tg as shown in figures5.2.3.1, 5.2.3.2 and 5.2.3.3; reduction in Tg: 91.11ºC (flakes) to 68.17ºC (pellets-60rpm) to 67.31 ºC (pellets-85rpm).

After the injection moulding process of r-PET (CLR/KUDOS r-PET Pellets) the percentage of crystallinity decreased from 46.31% to 18.81% as shown in figure5.2.3.4 and figure5.2.3.5 respectively.

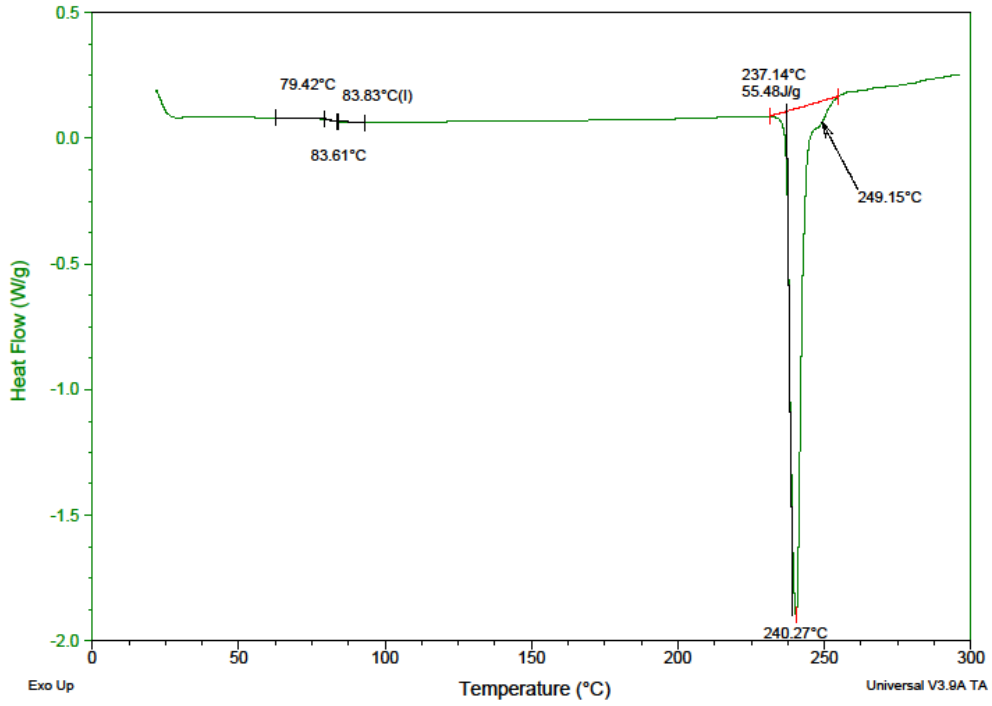

Figure5.2.3.4: DSC thermogram for CLR/KUDOS r-PET Pellets

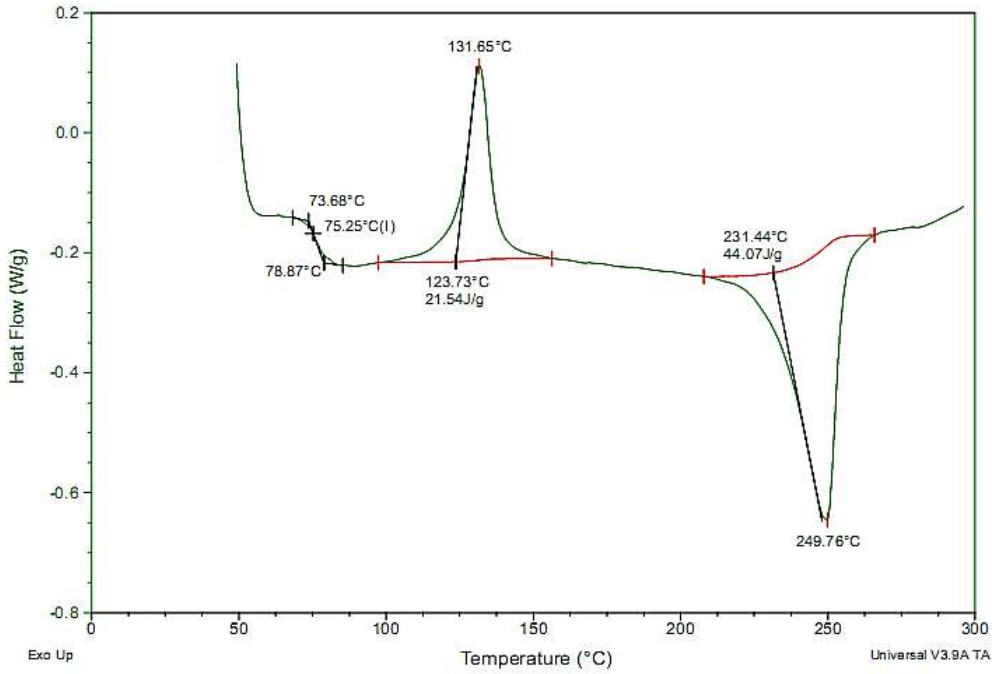

Figure5.2.3.5: DSC thermogram for r-PET before exposure.

r-PET pellets suffered hydrolysis, thermal and oxidation degradation during processing which result in breaking the molecular chains, i. e. the macromolecular chains are converted into shorter chains. Thus the crystallinity of the material decreased.

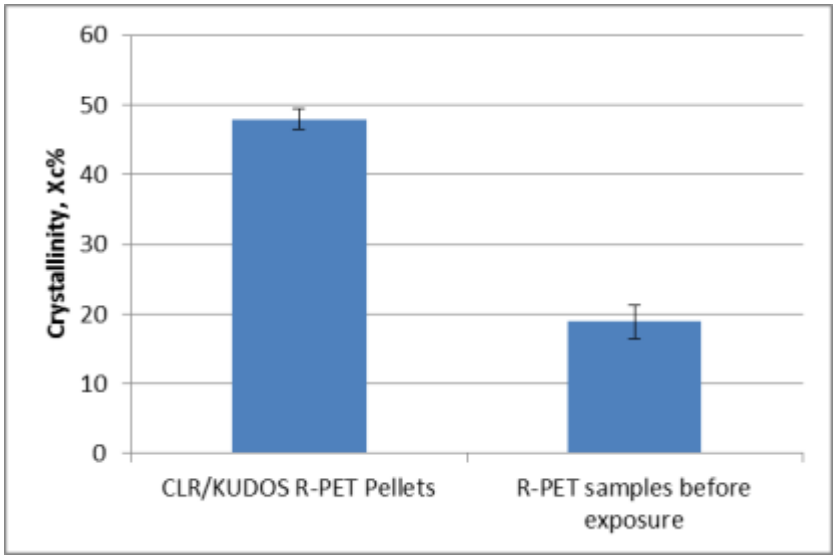

Figure5.2.3.6: Crystallinity % of CLR/KUDOS r-PET Pellets and after injection moulding processing.

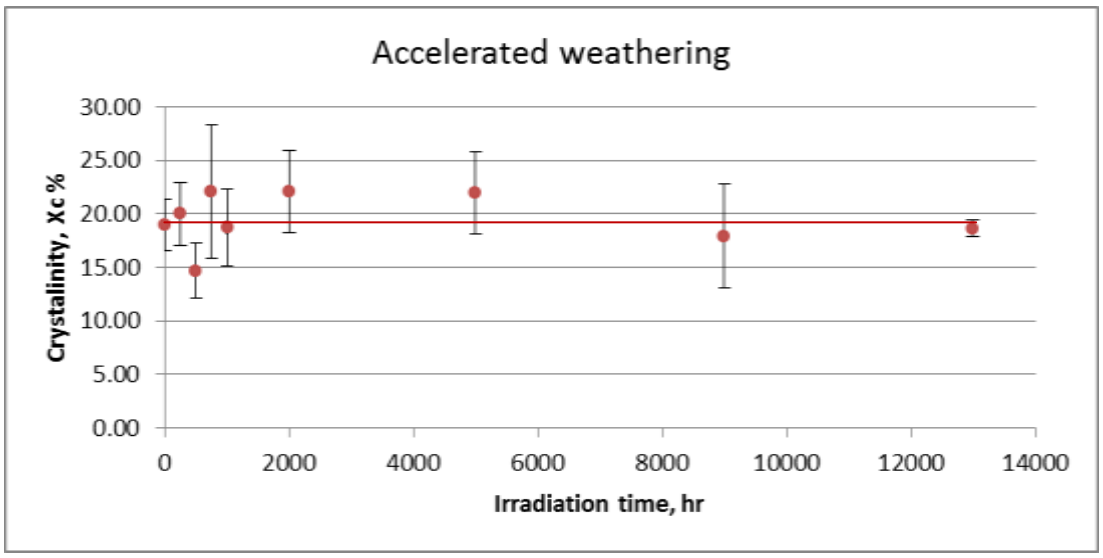

Figure5.2.3.7: Crystallinity percentage for r-PET samples in accelerated weathering.

After 13000 hours of exposure to UV outdoors and inside The QUV accelerated weathering tester, the crystallinity remained unaffected as shown in figures5.2.3.7 and 5.2.3.8, explaining that the degradation is a surface effect which does not affect the whole specimens.

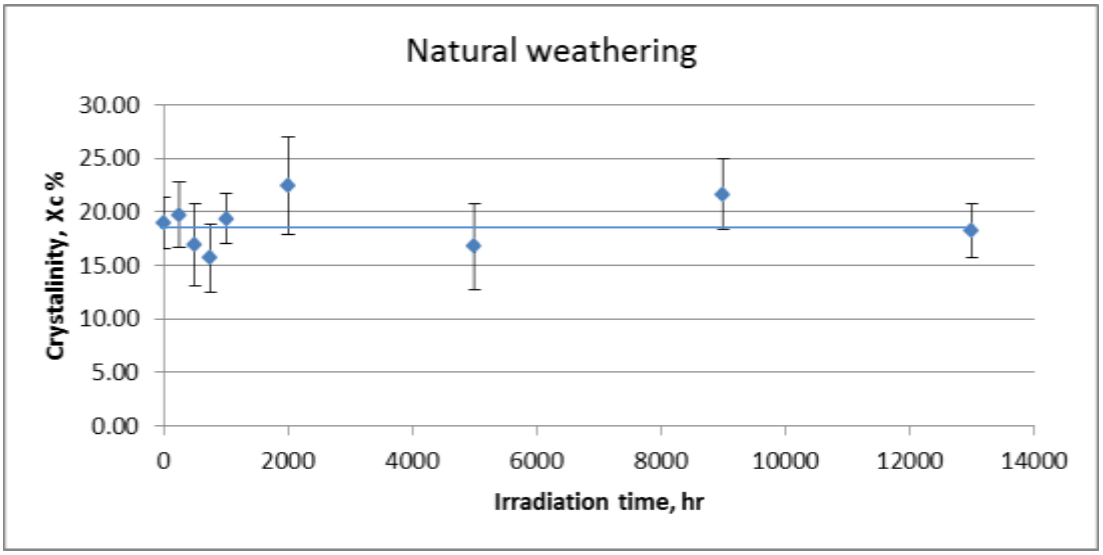

Figure5.2.3.8: Crystallinity percentage for r-PET samples in natural weathering.

5.3 FTIR Analysis

5.3.1 Method

FTIR, Fourier Transform Infrared Spectroscopy is a technique that provides information about the chemical bonding (molecular structure) and chemical composition of materials. Infrared spectrum is molecular vibrational spectrum, when a molecule exposed to infrared rays, it absorbs infrared energy at specific frequencies which are characteristic to that molecule.

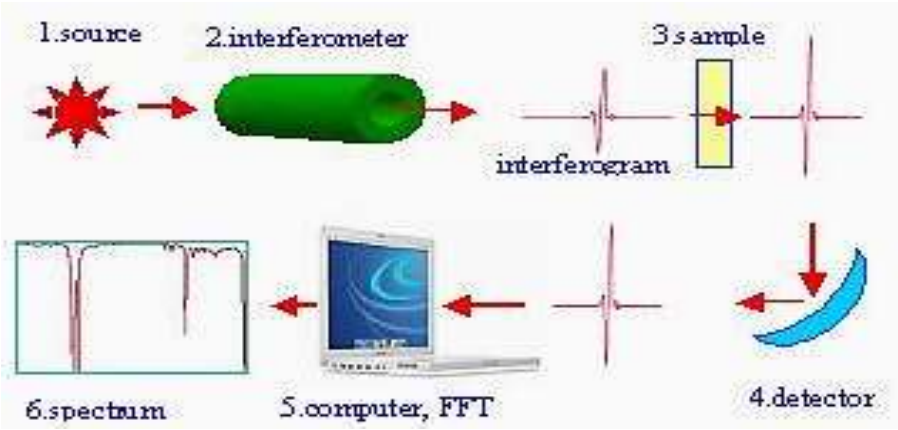

Figure5.3.1.1: Schematic illustration of FTIR system [95].

FTIR spectrometer consists of source, interferometer, sample compartment and detector. Interferometer is the core of the spectrometer, used to split the incoming infrared beam into two (their optical paths are different), one beam reflects off of a flat mirror which is fixed in place, another beam reflects off of a flat mirror which travels a very short distance (only a few millimeters). The two beams reflect off of their respective mirrors and are recombined when they finally meet back at the beamsplitter. Because the optical path that one beam travels is a fixed length and the other is changing because the mirror moves, the exit signal from the interferometer (interferogram) is the result of these two beams interfering with each other (recombined signal), has every infrared frequency comes from the source. When the interferogram signal is reflected off of the specimen surface, the specific frequencies of energy are absorbed by the sample. The infrared signal after interaction with the sample is uniquely characteristic of the specimen. The beam finally arrives at the detector to measure all of frequencies that pass though and send the information to

computer. The detected interferogram is a record of the signal (intensity) as a function of the path difference for the interferometer's two beams. To obtain an infrared spectrum, which plots absorbance versus wave number, the signal is subjected to Fourier transformation calculation by the mini-computer inside the spectrometer to give the spectrum, which depends only on frequency.

The infrared region (IR) of the electromagnetic spectrum is usually divided into three; far- infrared (< 400 cm^{-1}), mid-infrared (400–4000 cm^{-1}) and near-infrared (4000–13000 cm^{-1}), most infrared applications employ the mid-infrared region.

The positions of atoms in a molecule are not fixed; they are subject to a number of different vibrations. Vibrations can be categorised as [95, 96, 97, 98, 99]:

1-Stretching: Change in inter-atomic distance along bond axis (asymmetric stretching and symmetric stretching).

symmetrical stretching asymmetrical stretching

Figure5.3.1.2: Modes of stretching vibrations [100].

2-Bending: Change in angle between two bonds (bending in-plane and out-of-plane):

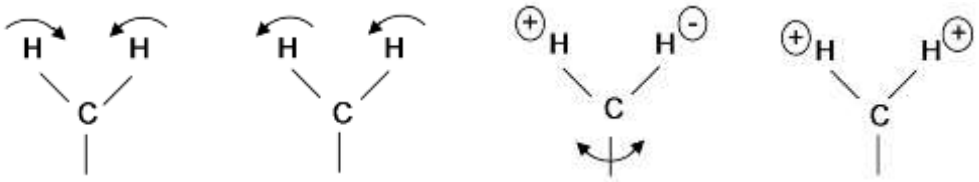

bending in-plane (scissor) bending in-plane (rocking) bending out-of-plane (twisting) bending out-of-plane (wagging)

Figure5.3.1.3: Modes of bending vibrations [100].

PET degradation (irradiation or aging) is associated with conformational changes which have been widely studied by FTIR by measuring the absorbance of specific bands representing gauche and trans conformations. The absorbance level of these bands change with the extent of degradation which are called sensitive bands. The absolute values of their absorbance do not obey any tendencies because of the differences in properties of the specimens such as dimensions and crystallinity. So, the sensitive absorbance band needs to be normalized against an insensitive absorbance band which does not change with the extent of degradation. This is done by calculating the ratio of these two bands [7, 56, 101].

The FTIR spectrum was measured using a Nicolet380 FTIR spectrophotometer coupled with Omnic software (version 7.3) with 2 cm^{-1} resolution manufactured by Thermo Scientific. Each specimen was placed on the sample compartment and secured tightly, and then the Omnic software was run to collect the spectrum of the sample. A plot of absorbance versus wave number was plotted and the absorbance peaks were indicated as absorbance values for sensitive bands. The procedure was carried out for all the samples under different periods of UV exposure.

5.3.2 Results

500 gram of flakes collected from PET bottles in United Kingdom for Closed Looped Recycling Company (CLR r-PET Flake) was separated into different groups according to their colours and each group was weighted and analyzed by FTIR to check the quality of these flakes.

Table 5.3.2.1: Flake Groups of different colours.

Group	Colour	Weight (g)	Weight (%)
1	Transparent	459.65	92.020
2	Blue	32.71	6.550
3	Green	2.48	0.496
4	Yellow	0.12	0.024
5	Light-yellow	1.11	0.222
6	White	0.88	0.176
7	Grey	0.87	0.174
8	Orange-brown	0.20	0.040
9	Dark brown	0.55	0.110
10	Dark-pink	0.56	0.112
11	Red	0.19	0.038
12	Pink	0.2	0.040

The following tables show the normalized intensity ratios of FTIR bands representing C=O & C–O of carboxylic acids, gauche and trans conformers of ethylene glycol segment and gauche and trans conformers of oxy-ethylene group in accelerated & natural weathering for various periods of UV exposure. The sensitive band absorbance should be normalized by an insensitive band because the absolute values do not obey any tendencies because of the differences in the properties of the specimens such as dimensions and crystallinity.

The carbonyl group (C=O) is located at wave number at 1711 cm^{-1} for both type of weathering is one of the strongest IR absorption and are a good indication of the formation of degradation products such as carboxylic acids.

Table5.3.2.2: Normalized intensity ratios of FTIR bands representing C=O and C–O of carboxylic acids in both type of weathering for periods of UV exposure.

UV exposure time, hr	FTIR ratio of normalized C=O & C–O bands of carboxylic acids (accelerated weathering)		FTIR ratio of normalized C=O & C–O bands of carboxylic acids (natural weathering)	
	C=O 1711/1404	C–O 1233/1404	C=O 1711/1404	C–O 1233/1404
Pellets	1.656	1.626	1.656	1.626
0	2.493	2.735	2.493	2.735
250	1.609	1.502	1.629	1.546
500	2.455	2.579	1.552	1.498
750	2.511	2.641	2.040	2.087
1000	1.421	1.599	1.379	1.577
2000	1.923	2.000	1.897	1.957
5000	2.046	2.278	2.575	2.673
9000	2.792	3.208	2.895	3.283
13000	2.659	3.156	2.341	2.776

Table5.3.2.3: Normalized intensity ratios of FTIR bands representing gauche and trans conformers of ethylene glycol segment in both type of weathering for periods of UV exposure.

UV exposure time, hr	FTIR ratio of gauche and trans of ethylene glycol segment (accelerated weathering)		FTIR ratio of gauche and trans of ethylene glycol segment (natural weathering)	
	Gauche 1376/1404	Trans 1343/1404	Gauche 1376/1404	Trans 1343/1404
Pellets	0.810	0.965	0.810	0.965
0	0.794	0.716	0.794	0.716
250	0.895	0.847	0.889	0.858
500	0.805	0.719	0.897	0.869
750	0.786	0.700	0.818	0.786
1000	0.862	0.806	0.873	0.825
2000	0.827	0.750	0.837	0.770
5000	0.810	0.723	0.786	0.711
9000	0.733	0.636	0.729	0.636
13000	0.726	0.633	0.680	0.608

Table5.3.2.4: Normalized intensity ratios of FTIR bands representing gauche and trans conformers of oxy-ethylene group in both type of weathering for periods of UV exposure.

UV exposure time, hr	FTIR ratio of gauche and trans of oxy-ethylene group (accelerated weathering)		FTIR ratio of gauche and trans of oxy-ethylene group (natural weathering)	
	Gauche 972/1404	Trans 1090/1404	Gauche 972/1404	Trans 1090/1404
Pellets	1.079	1.518	1.079	1.518
0	1.124	2.563	1.124	2.563
250	1.132	1.398	1.157	1.432
500	1.097	2.470	1.143	1.414
750	1.130	2.443	1.192	2.059
1000	1.179	1.607	1.077	1.600
2000	1.134	2.031	1.116	1.859
5000	1.168	2.232	1.069	2.477
9000	1.201	3.045	1.208	3.096
13000	1.241	3.015	1.114	2.598

5.3.3 Discussion

The FTIR spectra for the groups of coloured flakes (CLR r-PETFlake) are shown below. All groups have similar FTIR spectra which explain that all the coloured groups are polyethylene terephthalate (no other materials). It is high quality flakes due to excellent washing and sorting process.

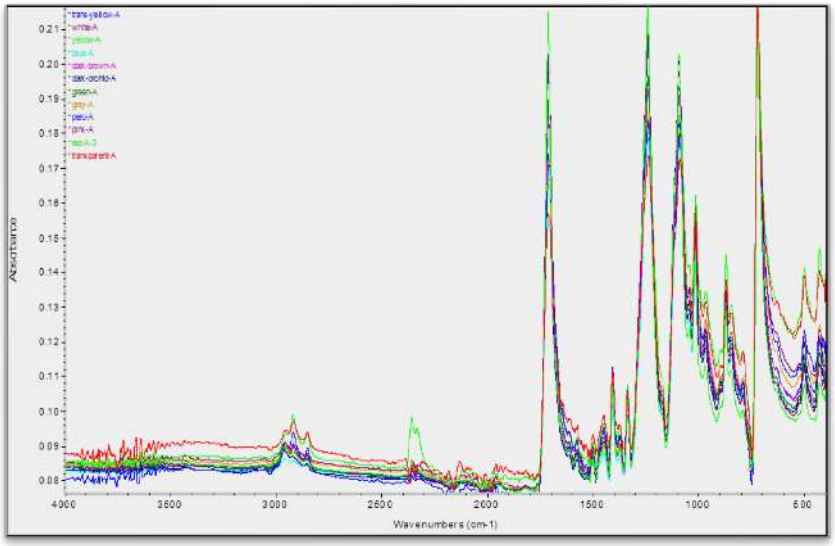

Figure5.3.3.1: FTIR spectra for the groups of coloured flakes.

The FTIR spectra for the accelerated and natural weathering samples show no differece, the type of weathering has no significant effect on the spectra.

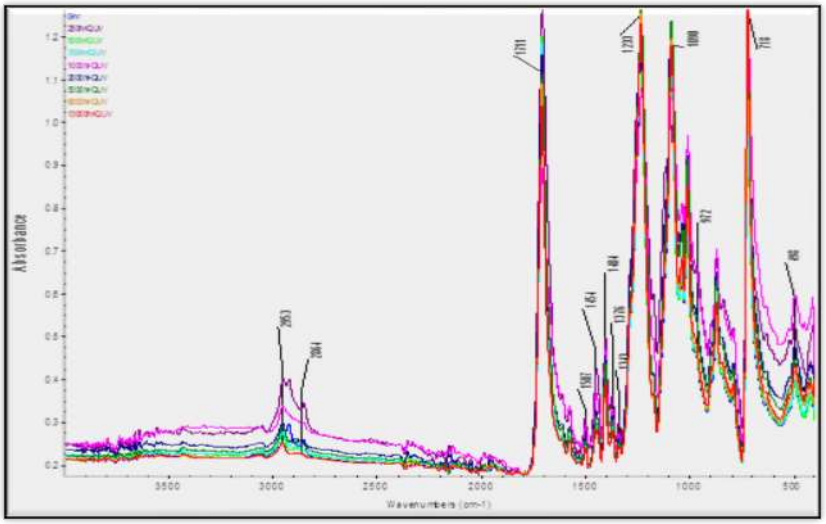

Figure5.3.3.2: FTIR spectra for the accelerating weathering samples.

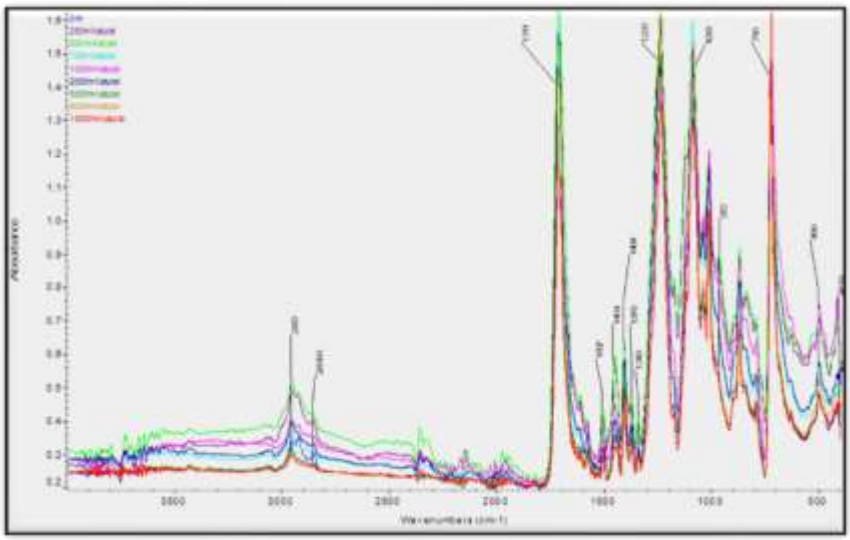

Figure5.3.3.3: FTIR spectra for natural weathering samples.

The vibrational spectrum of semi-crystalline polyethylene terephthalate, PET, seems to be complex. The absorption bands are split into two; amorpous and crystalline modes and are sensitive to chain conformation. Thus assignment of the bands has proved to be difficult and lead to differences in its interpretation [102].

The IR absorption spectrum of PET has been addressed by several researchers. By combining the information and knowledge of IR group frequencies, most of the bands observed can be assigned as follows:

- The straight line (with no peaks): no absorption occurs.
- The absorption peaks at wave number of 2953 cm^{-1}: attributed to the,
  - Asymmetry stretching aliphatic vibration of C–H of the methylene (–CH_2– in ethylene glycol segment)
  - Its stretching aliphatic vibration in the amorphous region [103, 104, 105, 106, 107, 108, 109, 110].
- The absorption peak at wave number of and 2864 cm^{-1}: attributed to the,
  - Symmetry stretching aliphatic vibration of C–H of the methylene (– CH_2 – in ethylene glycol segment)
  - Its stretching aliphatic vibration in the crystalline region [103, 104, 105, 106, 107, 108, 109, 110].

- The absorption peak at wave number of 1711 cm^{-1}: attributed to the stretching vibration of C=O (carbonyl group of carboxylic acids) [103, 105, 106, 107, 108, 109, 110, 111, 112, 113].
- The absorption peak at wave number of 1576 cm^{-1}: attributed to the
  - Stretching vibration of phenyl ring (C–C)
  - The ring stretching vibration in the amorphous region [102, 103, 104].
- The absorption peak at wave number of 1507 and 1510 cm^{-1}: attributed to the
  - Bending vibration of phenyl ring (C–H), in plane
  - Ring stretching vibration in the crystalline region [102, 103, 104].
- The absorption peak at wave number of 1454 cm^{-1}: attributed to the
  - Bending (scissoring) vibration of C–H of the methylene (–CH2– in ethylene glycol segment)
  - Bending of $–CH_2–$ in the ethylene glycol segment in the amorphous region.
  - Gauche conformer of ethylene glycol [7, 103, 104, 105, 106].
- The absorption peak at wave number of 1404 cm^{-1}: attributed to the
  - In-plane ring mode.
  - Stretching vibration of ring (C-C), in-plane.
  - Bending vibration of ring (C-C).
  - Bending vibration of ring (C-H), in-plane.
  - Aromatic skeleton stretching vibration [7, 71, 103].
- The absorption peak at wave number of 1376 cm^{-1}: attributed to the
  - Wagging vibration of C–H of the methylene ($–CH_2–$ in ethylene glycol segment).
  - Wagging vibration of $–CH_2–$ in the ethylene glycol segment in the amorphous region.
  - Gauche conformer of ethylene glycol segment [7, 71, 103, 104].
- The absorption peak at wave number of 1343 cm^{-1}: attributed to the
  - Wagging vibration of C–H of the methylene ($–CH_2–$ in ethylene glycol

segment).

- Wagging vibration of $–CH_2–$ in the ethylene glycol segment in the crystalline region.
- Trans conformer of ethylene glycol segment [7, 71, 103, 104].

- The absorption peak at wave number of 1233 cm^{-1}: attributed to the stretching vibration of C–O of carboxylic acids [105, 106, 107, 108, 109, 110, 112, 113].

- The absorption peak at wave number of 1090 cm^{-1}: attributed to the

- Symmetric stretching vibration of C–O of ethylene glycol (oxy-ethylene group, $O–CH_2$) - gauche form.
- Its gauche form in the amorphous region [71, 103].

- The absorption peak at wave number of 1012 cm^{-1}: attributed to the

- Stretching vibration of ring (C–C).
- Bending vibration of ring (C–H), in plane.
- Bending vibration of ring (C–H), in plane
- In plane ring deformation (C–H) in the amorphous phase [71, 103, 104].

- The absorption peak at wave number of 972 cm^{-1}: attributed to the

- Asymmetric stretching vibration of C–O of ethylene glycol (oxy-ethylene group, $O–CH_2$) - trans form.
- Its trans form in the crystalline region [71, 103, 104].

- The absorption peak at wave number of 898 cm^{-1}: attributed to the

- Rocking vibration of C–H of the methylene ($–CH_2–$ in ethylene glycol segment) in the amorphous region.
- Gauche form of ethylene glycol [7, 103, 104, 114].

- The absorption peak at wave number of 837 cm^{-1}: attributed to the

- Rocking vibration of C–H of the methylene ($–CH_2–$ in ethylene glycol segment) in the crystalline region.
- Trans form of ethylene glycol [7, 103, 104, 114].

- The absorption peak at wave number of 796 cm^{-1}: attributed to the

- Vibration of the phenylene ring.

- Bending vibration of ring (C–H) [108, 110, 114].

- The absorption peak at wave number of 718 cm^{-1}: attributed to the
  - Bending vibration of ring (C–H), out of plane
  - Bending vibration of benzene ring (C–C), in plane [71, 104, 105, 106, 107, 109, 111].
- The absorption peak at wave number of 498 cm^{-1}: attributed to the C–C stretching vibration in the ring-ester [103].

The insensitive band is the one that would not change in the absorbance level with the extent of degradation; the sensitive band is the one that would change in the absorbance level with the extent of degradation. The sensitive band absorbance should be normalized by an insensitive band because the absolute values (absorbance) do not obey any tendencies. This is because of the differences in properties of the specimens (compensate the differences) for example crystallinity and dimensions.

The band at wavelength 1404 cm^{-1} which is attributed to the in-plane ring mode, results from a vibration of the phenylene ring. It is generally believed to be not affected (insensitive) to molecular chain conformation, thus it a good reference to normalize spectral intensities among polymers [7, 47, 71, 104, 114].

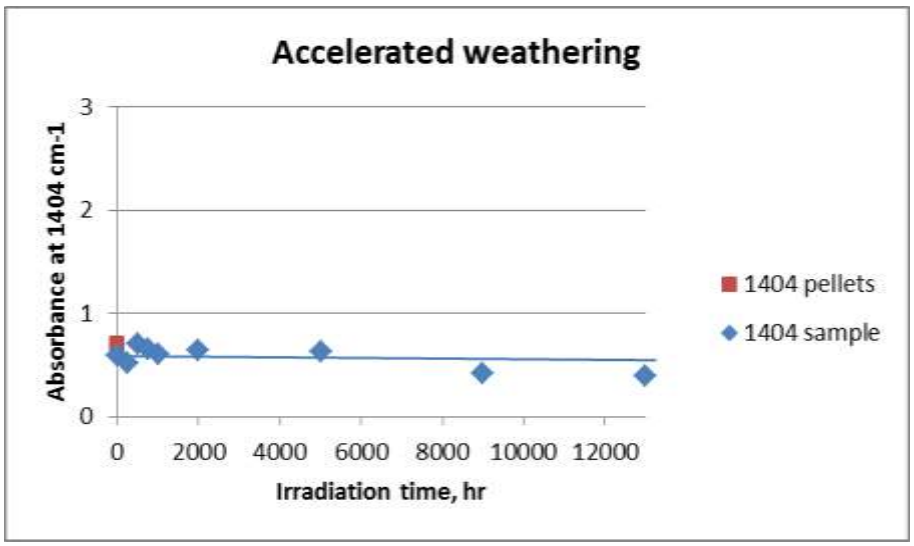

Figure5.3.3.4: Absorbance at 1404 cm^{-1} for samples in accelerated weathering.

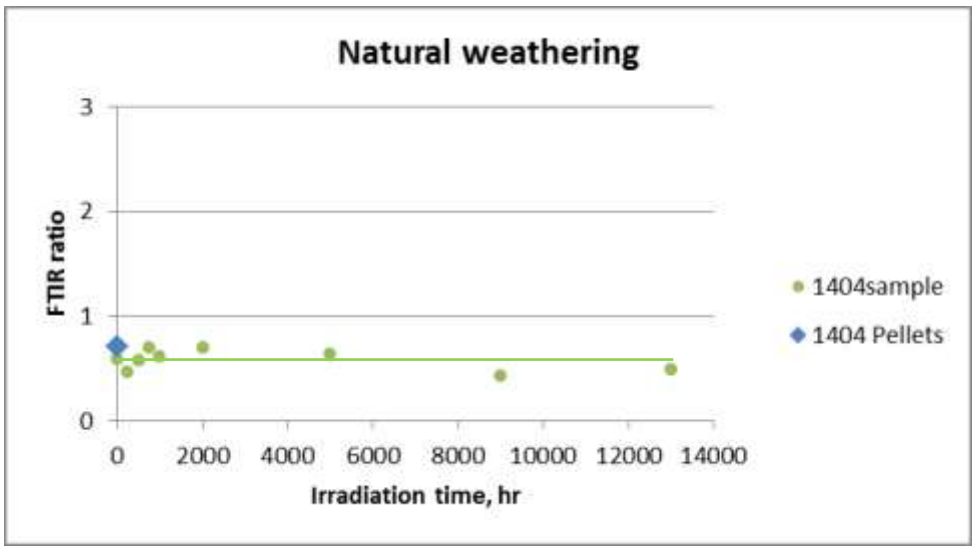

Figure5.3.3.5: Absorbance at1404 cm^{-1} for samples in natural weathering.

The intensity of asymmetry stretching aliphatic vibration of C–H of the methylene (–CH_2– in ethylene glycol segment) at 2953 cm^{-1} (for both types of weathering) and the symmetry stretching vibration of the same bond at 2864 cm^{-1} (for both types of weathering) drop with the time of exposure. As the time of exposure towards UV exposure increases, the C–H bonds suffer more damage, i.e. destruction by the attack of UV light. Thus they were unable to absorb infrared (IR) wave (decrease in absorbance) [103, 104, 105, 106, 107, 108, 109, 110, 115] as shown below.

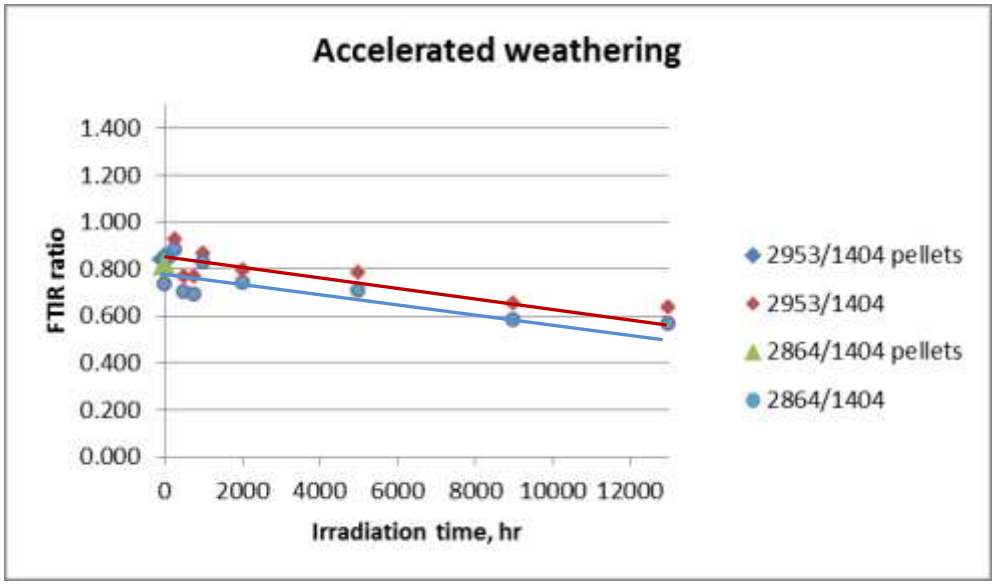

Figure5.3.3.6: FTIR ratio of C–H stretching vibration in accelerated weathering.

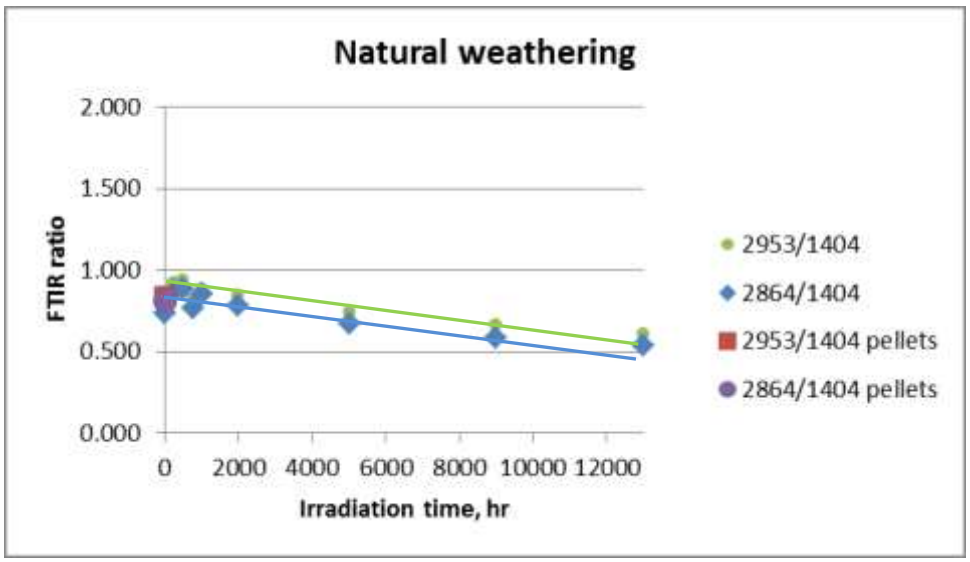

Figure5.3.3.7: FTIR ratio of C–H stretching vibration in natural weathering.

The main photodegradation products are CO, CO2, -COOH (carboxyle acid end groups).The carbonyl stretching vibration is one of the strongest IR absorption (C=O of carboxylic acid), it's peak is located at wave number at 1711 cm^{-1} (for both types of weathering), while the band at wave number at 1233 cm^{-1} (for both types of weathering) is attributed to the stretching vibration of C–O of carboxylic acids. The intensity ratios of both increase with increasing irradiation time for both types of weathering due to the formation of carboxylic acid through Norrish I and Norrish II as shown in figures 5.1.3.12 and 5.1.3.13 [103, 105, 106, 107, 108, 109, 110, 111, 112, 113, 116].

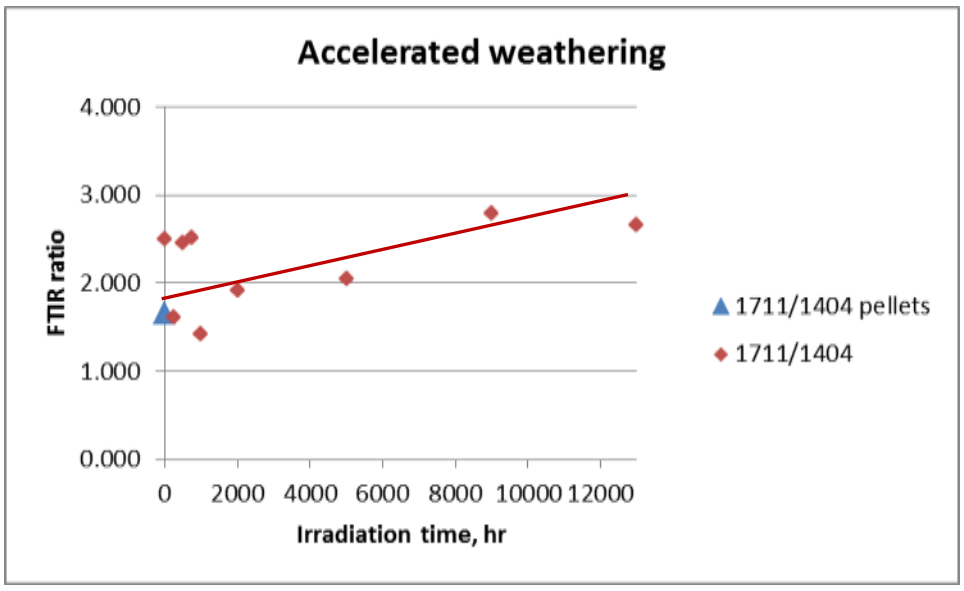

Figure5.3.3.8: FTIR ratio of 1711cm^{-1} for samples in accelerated weathering.

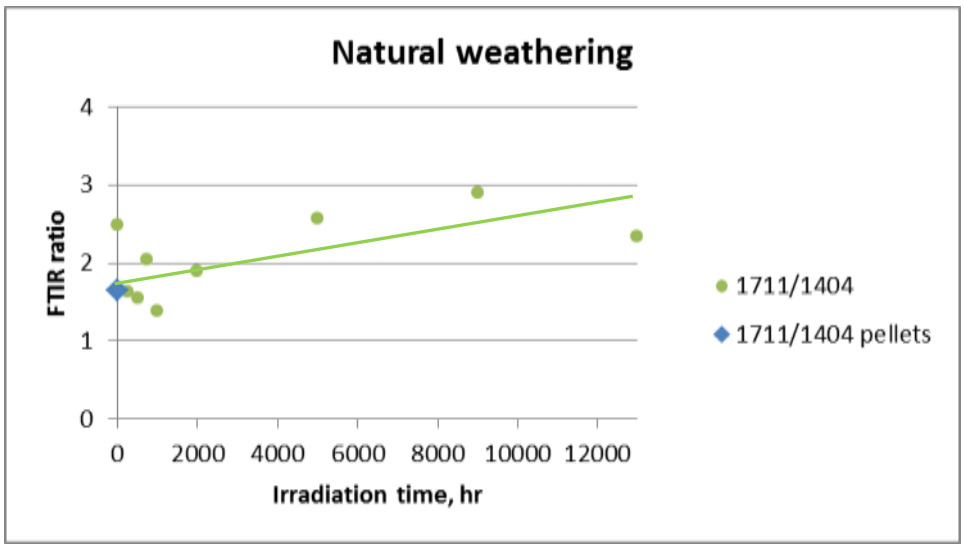

Figure5.3.3.9: FTIR ratio of 1711cm $^{-1}$ for samples in natural weathering.

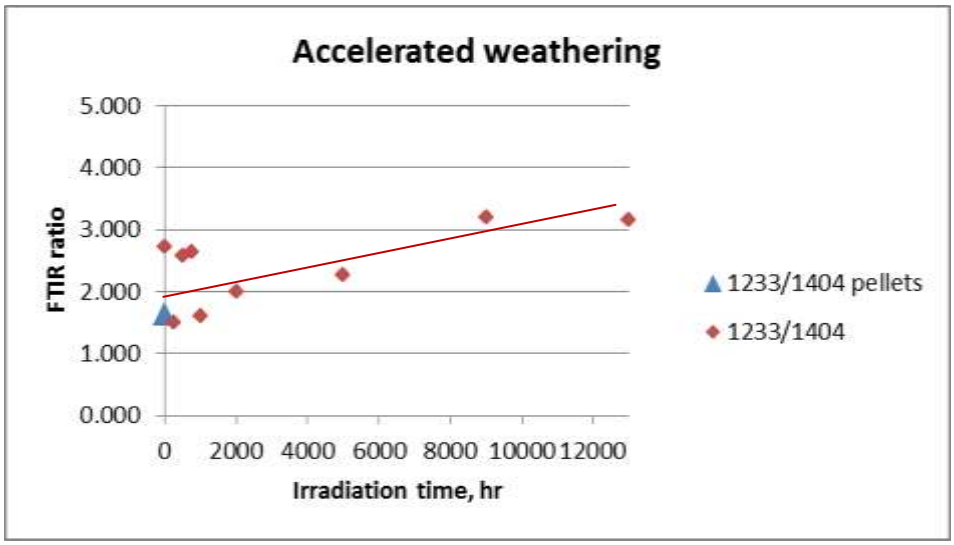

Figure5.3.3.10: FTIR ratio of 1233cm $^{-1}$ for samples in accelerated weathering.

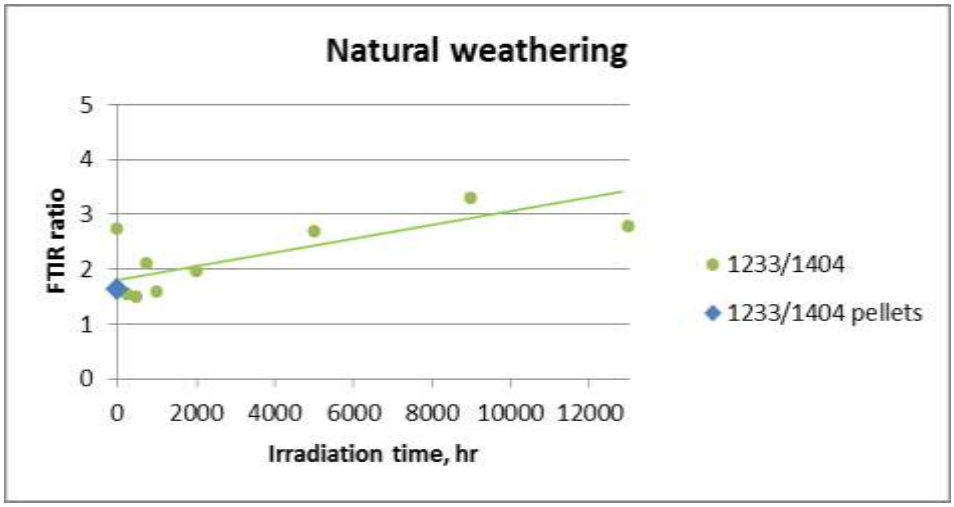

Figure5.3.3.11: FTIR ratio of 1233cm $^{-1}$ for samples in natural weathering.

Norrish I:

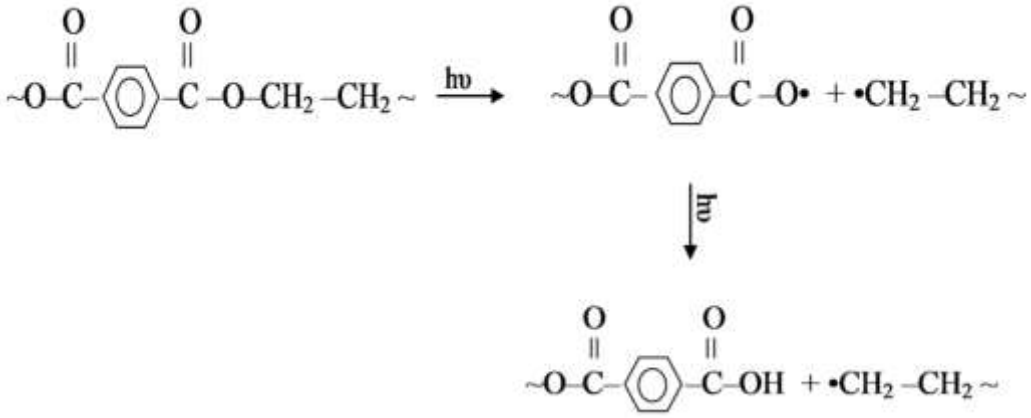

Figure5.3.3.12: Formation of carboxylic acid through Norrish I.

Norrish II:

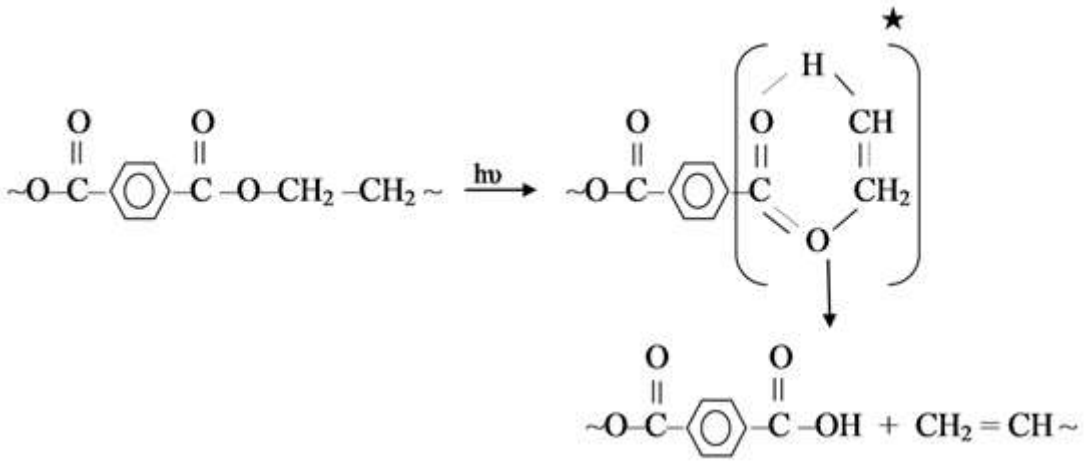

Figure5.3.3.13: Formation of carboxylic acid through Norrish II.

The aging of PET associated with conformational changes has been studied by measuring variations of specific bands representing gauche and trans conformations. The conformation of PET segments in the amorphous state is primarily gauche while crystalline is constituted only of trans conformer [56, 101].

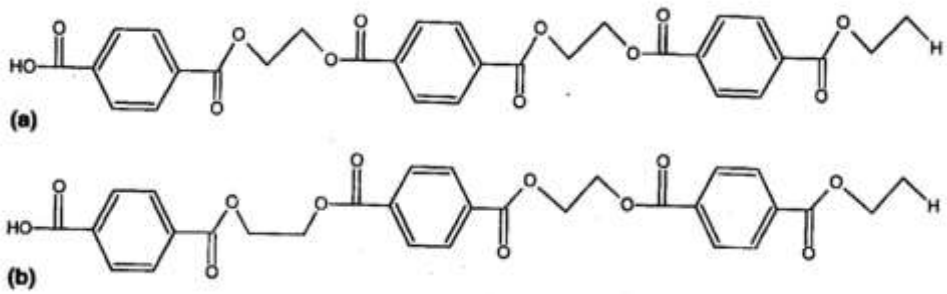

Figure5.3.3.14: Ethgylene glycol group at different conformational structures: (a) trans-crystalline structure and (b) trans/gauche-amorpmous structure [7].

The band at wave number of 1376 cm^{-1} (for both types of weathering) is attributed to the gauche conformer of ethylene glycol segment (wagging vibration of $–CH_2–$ in the ethylene glycol segment, while the band at wave number of 1343 cm^{-1} (for both types of weathering) is attributed to the trans conformer of ethylene glycol segment (wagging vibration of $–CH_2–$ in the ethylene glycol segment [7, 71, 103, 104].

Table5.3.3.1: Normalized intensity ratios of FTIR bands representing gauche and trans conformers of ethylene glycol segment in accelerated & natural weathering for various periods of UV exposure.

UV exposure time, hr	FTIR ratio of gauche and trans of ethylene glycol segment (accelerated weathering)		FTIR ratio of gauche and trans of ethylene glycol segment (natural weathering)	
	Gauche 1376/1404	Trans 1343/1404	Gauche 1376/1404	Trans 1343/1404
Pellets	0.810	0.965	0.810	0.965
0	0.794	0.716	0.794	0.716
250	0.895	0.847	0.889	0.858
500	0.805	0.719	0.897	0.869
750	0.786	0.700	0.818	0.786
1000	0.862	0.806	0.873	0.825
2000	0.827	0.750	0.837	0.770
5000	0.810	0.723	0.786	0.711
9000	0.733	0.636	0.729	0.636
13000	0.726	0.633	0.680	0.608

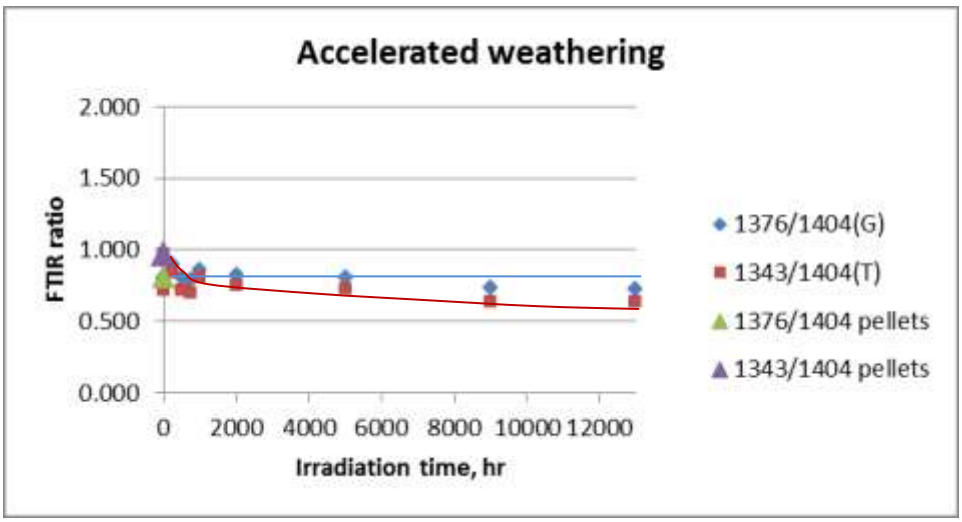

Figure5.3.3.15: FTIR ratio of representing gauche and trans conformers of ethylene glycol segment in accelerated weathering.

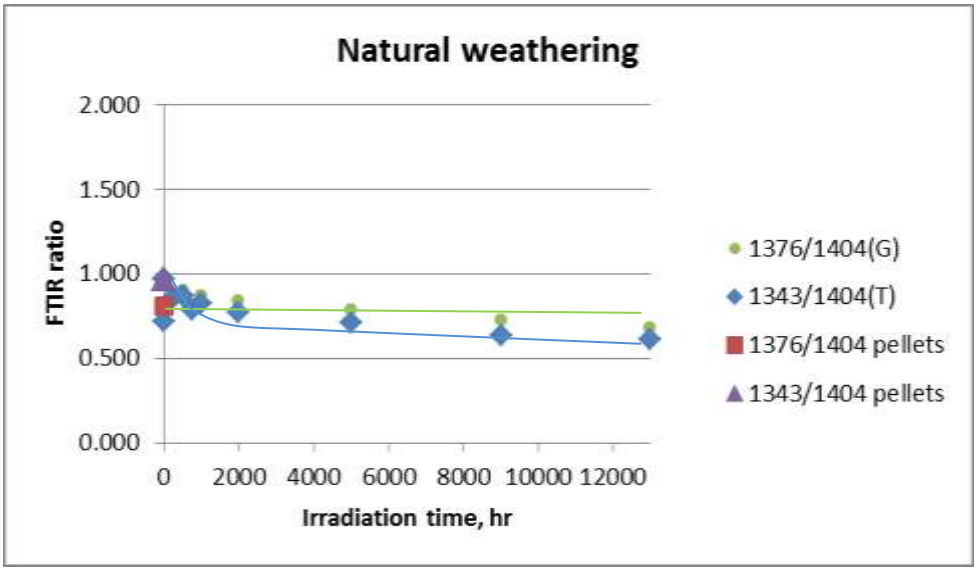

Figure5.3.3.16: FTIR ratio of representing gauche and trans conformers of ethylene glycol segment in natural weathering.

As we can see the photochemical reaction affects trans glycol conformer (consistent with the requirement of trans confirmation - Norrish II transition state).

The band at wave number at 1090 cm^{-1} (for both types of weathering) is attributed to the gauche form of oxy-ethylene group, $O–CH_2$ (symmetric stretching vibration of C–O of ethylene glycol), while the band at wave number at 972 cm^{-1} (for both types of weathering) is attributed to the trans form of oxy-

ethylene group, O–CH_2 (asymmetric stretching vibration of C–O of ethylene glycol) [7, 103, 104, 114].

Table5.3.3.2: Normalized intensity ratios of FTIR bands representing gauche and trans conformers of oxy-ethylene group in accelerated & natural weathering for various periods of UV exposure.

UV exposure time, hr	FTIR ratio of gauche and trans of oxy-ethylene group (accelerated weathering)		FTIR ratio of gauche and trans of oxy-ethylene group (natural weathering)	
	Gauche 972/1404	Trans 1090/1404	Gauche 972/1404	Trans 1090/1404
Pellets	1.079	1.518	1.079	1.518
0	1.124	2.563	1.124	2.563
250	1.132	1.398	1.157	1.432
500	1.097	2.470	1.143	1.414
750	1.130	2.443	1.192	2.059
1000	1.179	1.607	1.077	1.600
2000	1.134	2.031	1.116	1.859
5000	1.168	2.232	1.069	2.477
9000	1.201	3.045	1.208	3.096
13000	1.241	3.015	1.114	2.598

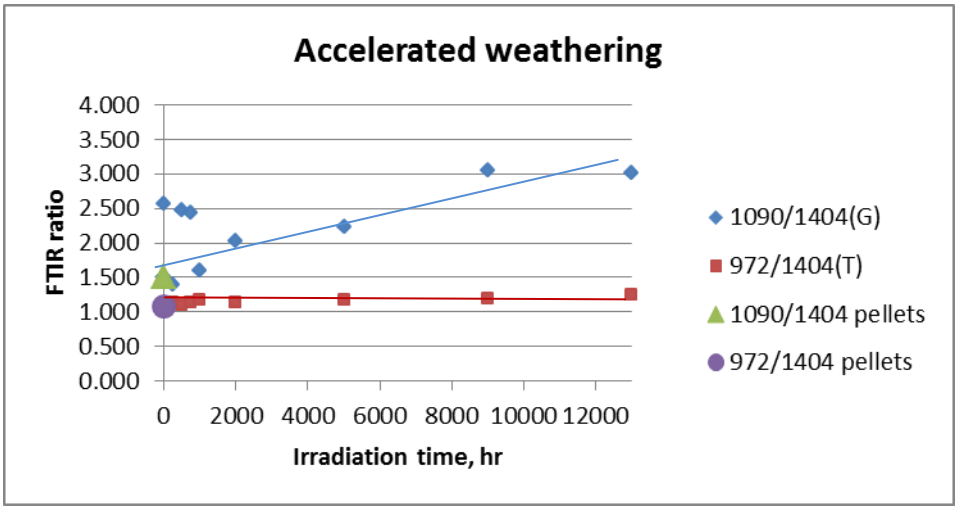

Figure5.3.3.17: FTIR ratio of representing gauche and trans conformers of oxy-ethylene group in accelerated weathering.

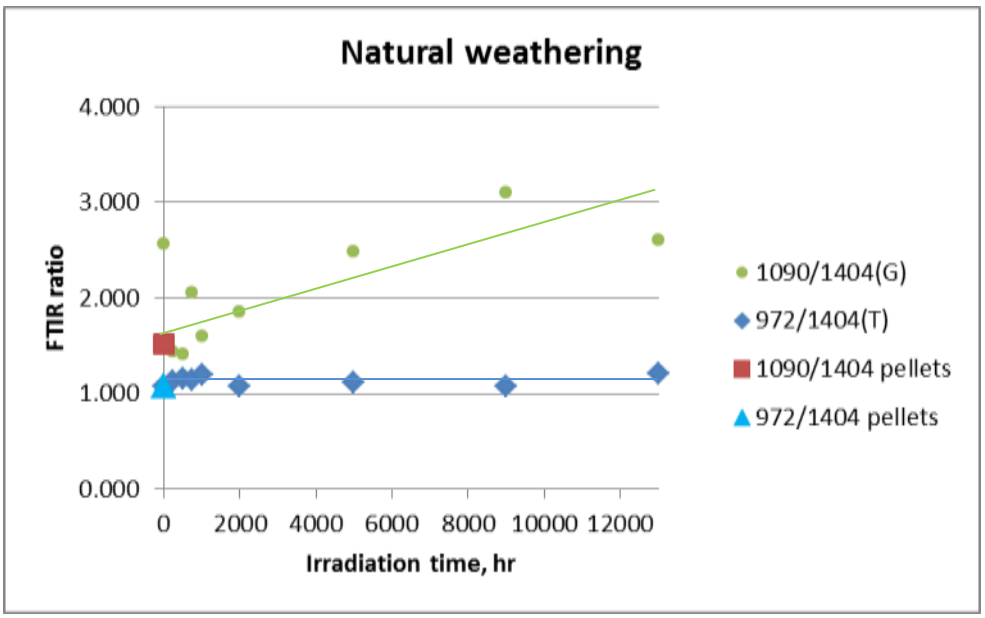

Figure5.3.3.18: FTIR ratio of representing gauche and trans conformers of oxy-ethylene group in natural weathering.

As we can see the photochemical reaction affects gauche conformer with respect to the O–CH_2 bonds of the glycol linkage (consistent with the requirement of gauche conformation - Norrish type II transition state).

The decrease in trans and increase in gauche with the extent of degradation indicating that the structure is transforming to a more random, less ordered due to the chain scission by UV attack.

Norrish type II is dominated over Norrish type I for the formation of carboxylic acid:

- Norrish type II reaction automatically proceeds through a cyclic six-membered transition state. This requires trans glycol conformation and a gauche conformation with respect to the CH_2-O bonds of the glycol linkage. As a result the hydrogen atom is removed in each molecule [71].

- The production of –COOH by Norrish type II intramolecular rearrangement reaction seems the more feasible as reported “this assumption is based on the established evidence that aliphatic and aromatic ester containing γ-hydrogen atom decomposes photochemically by an intramolecular rearrangement into an olefin and the corresponding acid” [61, 116].

CHAPTER SIX

PHYSICAL BEHAVIOUR

6.1 Colour and Gloss Measurement

6.1.1 Method

A spectrophotometer is an instrument that measures the intensity of light an object reflects by passing a beam of light through it. The reflected light is separated into spectrum uses a diffraction grating then reach the detector to measure the spectral reflectance at each wavelength. Because of this, the spectrophotometer can measure the difference in the colour which is not recognizable by the human eye.

The mini-computer inside the instrument uses the spectral reflectance data in a mathematical model called L*a*b* colour space to calculate the values of L*, a* and b* to represent the colour.

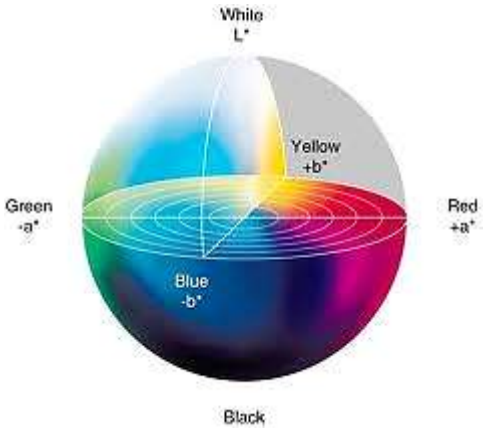

Figure6.1.1.1: Colour space L*a*b* [118].

In the L*a*b* colour space, L* represents lightness, L* axis runs from top to bottom, the maximum for L* is 100, which would be white, the minimum for L* would be zero (black). The a* and b* axes indicate colour directions, +a* is the red direction, -a* is the green direction, +b* is the yellow direction and –b* is the blue direction.

The L*a*b* colour space measurements were recorded using a calibrated hand-held CM-2600d/2500d spectrophotometer – Konica Minolta in general accordance with BS3900: Parts D8 – D10: 1986. The light of the room was turned off in order not to effect on the measurements. At the beginning of the first test (and when the setting is changed) zero calibration is required to save the setting (condition1) in the apparatus as:

- Colour space - L*a*b*, ΔE*.
- UV setting – UV 100%.
- Illuminant1 – D65.
- Observer 10º.

The instrument memory contains the calibration data of the white calibration plate supplied with the instrument. The serial number of plate should appear on screen. To confirm it is the white plate supplied by the company, the right hand button of the device is pressed once and this is called the white calibration. Then each specimen was placed on a white tile and the device was placed over it, the right hand button was pressed once to record the colour and gloss measurement.

Reflection of light from surfaces results from the incident light which has traveled through some finite thickness of a material and reflected from internal surfaces is called diffuse reflection (body reflection) which is scattered in all directions.

Specular reflection (surface reflection) is reflection as from mirror (mirror like) which is directed instead of being diffused. It is reflected from the outer surface of the object (the very first layer of the sample).

Colour measurement excluded specular reflection (the SCE system – without gloss effect) provides results similar to those observed visually and used for general purposes. While colour measurement included specular reflection (the SCI system – with gloss effect) provides results used especially for colour quality control and computer colour matching.

The total colour change, ΔE* without gloss effect (the SCE system) and with gloss affect, ΔG* (SCI system) of L*, a*, b* colour space values were calculated from the same equation:

$$\Delta E^* \,\&\, \Delta G^* = \sqrt{(\Delta L^*)^2 + (\Delta a^*)^2 + (\Delta b^*)^2} \qquad \text{.....6.1}$$

Where;

ΔE* & ΔG*: colour difference without and with gloss effect respectively between the initial (before exposure) and final values (after exposure).

ΔL*, Δa*, Δb*: difference in lightness, redness and yellowness respectively between the initial and final values [117, 118, 119, 120, 121].

6.1.2 Results

Tables below show the results of colour and gloss measurements for both samples under accelerated and natural weathering.

Table6.1.2.1: Colour Measurement in accelerated weathering.

UV exposure time, hr	Colour parameters of accelerated weathering						
	L* Whiteness	a* Red-ness	b* Yellow-ness	ΔL* White-ness change	Δa* Red-ness change	Δb* Yellw-ness change	ΔE* Colour change
0	36.43	1.82	14.69	0	0	0	0
250	38.44	0.47	16.28	2.01	-1.35	1.59	2.90
500	38.68	0.59	13.09	2.25	-1.23	-1.60	3.02
750	39.02	0.33	12.02	2.59	-1.49	-2.67	4.01
1,000	38.28	0.38	12.34	1.85	-1.44	-2.35	3.32
2,000	40.42	-0.18	13.31	3.99	-2.00	-1.38	4.67
5,000	38.96	-0.3	6.44	2.53	-2.12	-8.25	8.89
9,000	43.67	-0.23	11.27	7.24	-2.05	-3.42	8.27
13,000	41.39	-0.42	7.01	4.96	-2.24	-7.68	9.41

Table6.1.2.2: Colour and gloss measurement in accelerated weathering.

UV exposure time, hr	Colour and gloss parameters of accelerated weathering						
	L* Whiteness	a* Red-ness	b* Yellow-ness	ΔL* Whiten-ess change	Δa* Red-ness change	Δb* Yellow-ness change	ΔG* Gloss change
0	42.33	1.68	11.45	0	0	0	0
250	44.60	0.60	12.06	2.27	-1.08	0.61	2.59
500	44.14	0.64	10.57	1.81	-1.04	-0.88	2.27
750	43.93	0.53	10.41	1.60	-1.15	-1.04	2.23
1,000	44.72	0.46	9.44	2.39	-1.22	-2.01	3.35
2,000	47.45	0.13	10.30	5.12	-1.55	-1.15	5.47
5,000	39.73	-0.27	6.42	-2.60	-1.95	-5.03	5.99
9,000	47.16	0.02	10.46	4.83	-1.66	-0.99	5.20
13,000	41.57	-0.41	7.10	-0.76	-2.09	-4.35	4.89

Table6.1.2.3: Colour Measurement in natural weathering.

UV exposure time, hr	Colour parameters of natural weathering						
	L* Whiteness	a* Red-ness	b* Yellow-ness	ΔL* White-ness change	Δa* Red-ness change	Δb* Yellow-ness change	ΔE* Colour change
0	36.43	1.82	14.69	0	0	0	0
250	37.06	1.12	14.22	0.63	-0.70	-0.47	1.05
500	39.78	0.70	13.21	3.35	-1.12	-1.48	3.83
750	38.88	0.92	13.76	2.45	-0.90	-0.93	2.77
1,000	38.81	0.84	13.86	2.38	-0.98	-0.83	2.70
2,000	40.62	-0.34	12.84	4.19	-2.16	-1.85	5.06
5,000	38.41	0.60	12.15	1.98	-1.22	-2.54	3.44
9,000	40.11	0.08	11.92	3.68	-1.74	-2.77	4.92
13,000	40.73	0.23	9.51	4.30	-1.59	-5.18	6.92

Table6.1.2.4: Colour and gloss measurement in natural weathering.

UV exposure time, hr	Colour and gloss parameters of natural weathering						
	L* Whiteness	a* Red-ness	b* Yellow-ness	ΔL* White-ness change	Δa* Red-ness change	Δb* Yellow-ness change	ΔG* Gloss change
0	42.33	1.68	11.45	0	0	0	0
250	42.71	1.18	11.96	0.38	-0.50	0.51	0.81
500	44.64	0.84	11.42	2.31	-0.84	-0.03	2.46
750	44.39	0.98	11.15	2.06	-0.70	-0.30	2.20
1,000	44.61	0.91	11.09	2.28	-0.77	-0.36	2.43
2,000	46.39	-0.07	10.61	4.06	-1.75	-0.84	4.50
5,000	43.68	0.70	10.32	1.35	-0.98	-1.13	2.01
9,000	45.80	0.59	9.95	3.47	-1.09	-1.50	3.93
13,000	44.16	0.35	8.64	1.83	-1.33	-2.81	3.61

6.1.3 Discussion

Figures6.1.3.1 and 6.1.3.2 show the results of table6.1.2.1, 6.1.2.2, 6.1.2.3 and 6.1.2.4 of colour and gloss measurements for both samples under accelerated and natural weathering.

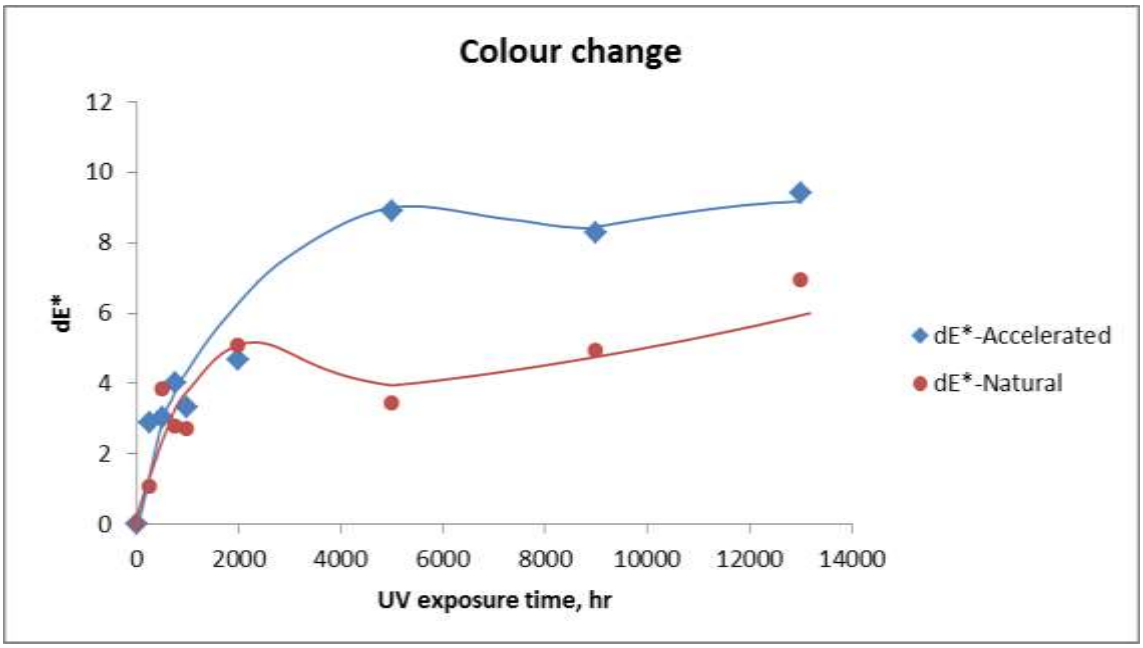

Figure6.1.3.1: Colour change for r-PET samples after 13,000 hr for natural and accelerated weathering UV exposure.

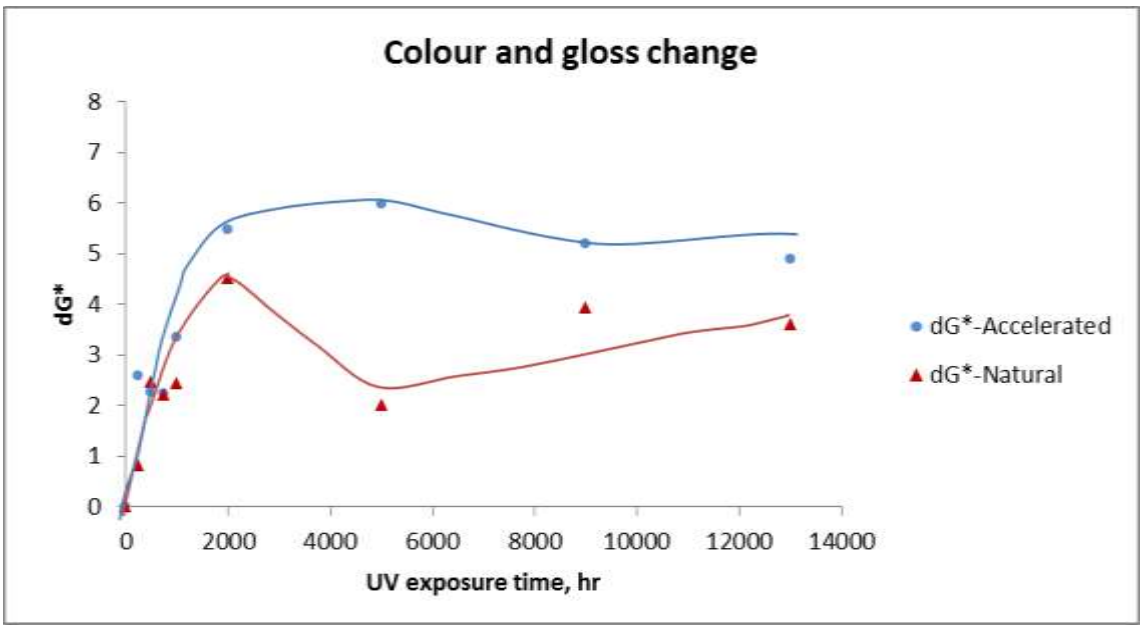

Figure6.1.3.2: Colour and gloss change for r-PET samples after 13,000 hr for natural and accelerated weathering UV exposure.

The photodegradation is known to be a surface effect, the products result from this process are concentrated at the surface of irradiated material. This phenomenon is mainly caused by UV absorption and oxygen diffusion into the surface of polymer where both at high rate.

As the UV light passes though the material, its intensity decreases according to Beer-Lambeth's law.

$$A = k * \ln(I_o/I) = \varepsilon cL \qquad \text{.....6.2}$$

Where:

A : Absorbance

k : Mathematical constant, 2.3026.

I_o : Intensity of light before it enters the material, W/m^2

I : Intensity of light which passed through the material, W/m^2

ε : Absorbance coefficient (absorptivity), $cm^2\ mole^{-1}$

c: Concentration of absorbing species, mole cm^{-3}

L: Optical path length, cm.

By rearranging this expression, we obtain a relationship for change in intensity of light as it passes through the material as shown in figure below.

$$I = (I_o\, e^{-\varepsilon/k})\, e^{-cl} \qquad \text{.....6.3}$$

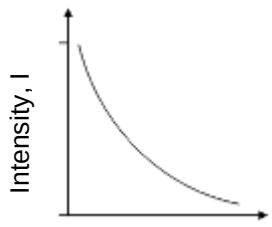

Figure6.1.3.3: Schematic representation of the depth penetration of the light through an absorbing polymer [58].

And the same phenomenon for the oxygen; as the oxygen diffuses though the material, its concentration decreases according to Fick's second law (unsteady state-concentration gradient changes) as shown in figure below.

Diffusion of oxygen into the material may restrict the photooxidation processes to a surface layer. During such process, radicals are formed at the surface of the material and react with oxygen. So, part of the oxygen is trapped at the surface which may cause oxygen starvation in the bulk of the material [58].

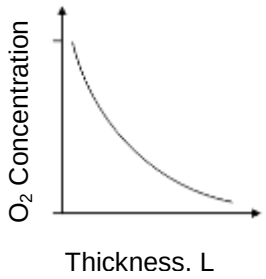

Figure6.1.3.4: Schematic representation of oxygen throughout the polymer [58].

In the first 2000 hr of UV exposure, there was maximum variation in colour and gloss for r-PET samples in natural weathering and 5000hr in accelerated weathering as shown in figures 6.1.3.1 and 6.1.3.2. This indicates that the effect of degradation takes place strongly in the early stages of UV exposure due to the high absorption rate of UV and high diffusion rate of oxygen in the surface, leading to high chain scission rate and fast crack growth. The increase in colour and gloss change become less because chain scission rate reduced with the extent of UV exposure as the material starts to consume at the surface layer with the extent of UV exposure and degradation products start to act as a barrier for further UV and oxygen attack as well as limited diffusion of UV and oxygen beyond the surface layer. Then little increase in colour and gloss change because of the effects of grown cracks and eventually colour and gloss change reached to steady state.

For accelerated weathering samples, there is a big increase in colour by 8.89 units and with effect of gloss by 5.99 units in the first 5000 hour of UV exposure and this is reflected by the wide and deep cracks as shown in the optical images in figure 6.3.3.4-C, while yield stress dropped by 37.90%, elongation at yield by 40.29%, the true stress at break by 80.01%, elongation at break by 98.43% and impact strength by 7.38%.

With the further increase of UV exposure up to 13000 hours, there is further slight increase in colour by 0.52 units and very small decrease in gloss by 1.1 units, while the yield stress dropped further by 18.16%, elongation at yield by 11.88%, the true stress at break by 5.81%, elongation at break by 0.31% and impact strength by 85.59%.

For natural weathering samples, colour change shows big increase by 5.06 units and gloss by 4.50 units up to 2000 hour of UV exposure despite there are no signs of bits on the surface as shown in the optical images in figures 6.3.3.4-A and 6.3.3.4-B, while the true stress at break dropped by 12.14% and the other mechanical properties remained unchanged.

There is then a small decrease in colour by 1.62 units and small decrease in gloss by 2.49 units with the further increase of UV exposure up to 5000 hours, while the true stress at break dropped further by 8.12% and other mechanical properties remained unchanged. With increasing UV exposure up to 13000 hr, colour and gloss increase to reach 6.92 and 3.61 units respectively with further drop in true stress at break by 21.74%.

When UV radiation reaches the surface of r-PET samples, it is absorbed by the molecules of existing chromophores and causes chain scissions leading to shorter chain lengths which have more ends per unit volume than long chains, hence a higher free volume and eventually microcracks are formed. The formation of microcracks increases the roughness of the surface, resulting in decrease in colour and gloss values.

The degradation damage results in loss of surface colour and gloss and gradually in a chalky appearance which appears as a white layer at the surface of the sample as shown in figure below.

.

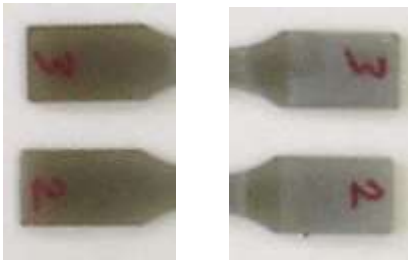

A B

Figure6.1.3.5: The surface of r-PET samples, A: unexposed samples, and B: exposed samples for 13000hr in QUV cabinet.

It started to appear after 2000hr of UV exposure in the QUV cabinet and caused by degradation of the surface layer of material (microcracks) and migration of the molecules of pigment to the surface, leaving them as a chalky layer of deposit [122]. With outdoors samples, there is no chalking even after 13000hr of exposure because weathering is less aggressive than the QUV cabinet, but in the long term of exposure, chalking is expected.

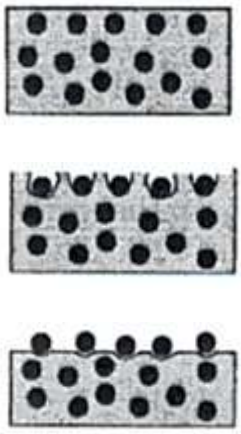

(A) Surface layer of polymer containing pigment

(B) Surface degradation causing erosion to the surface layer

(C) Pigment particles now reside on the surface giving a chalking effect

Figure6.1.3.6: Mechanism of polymer chalking [123].

The decrease in yellowness and redness (slight) causes the lightness to increase (more transparent) by 4.96 units for QUV cabinet samples and 4.30 units for outdoor samples over 13,000 hr of UV exposure as shown below.

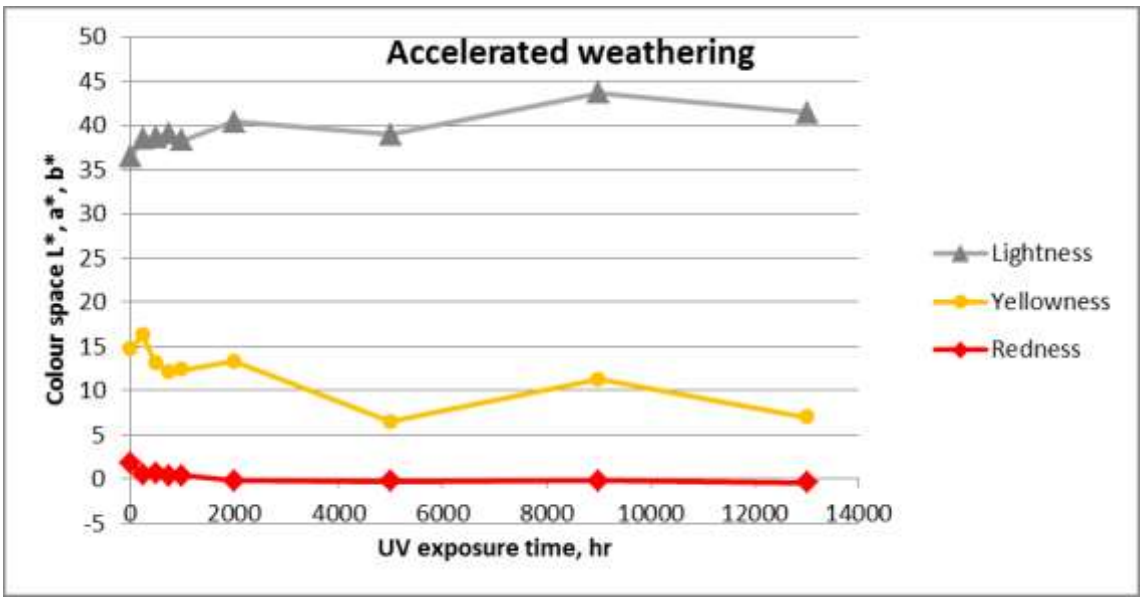

Figure6.1.3.7: Variation of colour space L*, a*, b* in accelerated weathering.

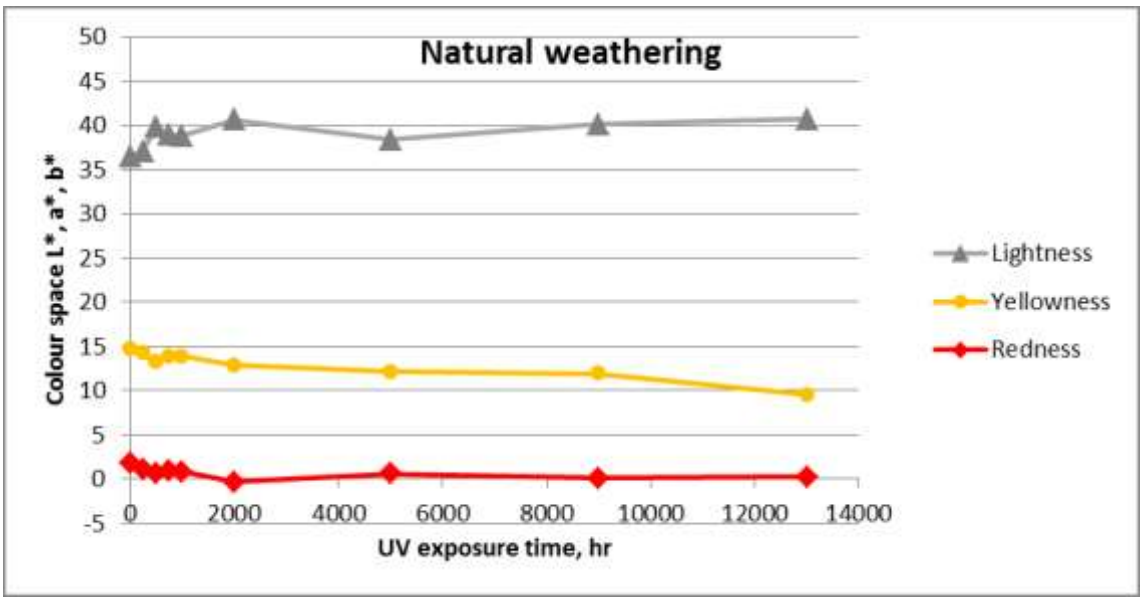

Figure6.1.3.8: Variation of colour space L*, a*, b* in natural weathering.

During the same period of exposure, the yellowness and redness decreased by 7.68 and 2.24 units respectively for QUV cabinet samples and by 5.18 and 1.59 units respectively for outdoor samples as shown in figures6.1.3.7 and 6.1.3.8. The increase in lightness, L* and decrease in yellowness, b* and redness, a* are redrawn in the following figures, so the changes can be seen more clearly.

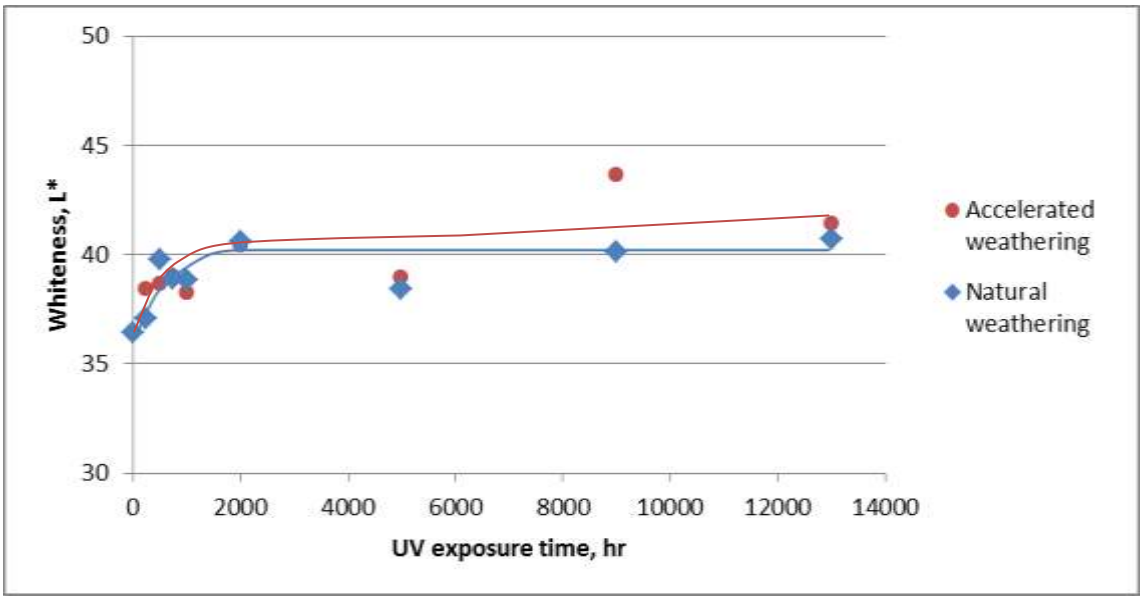

Figure6.1.3.9: Variation in whiteness for both types of weathering.

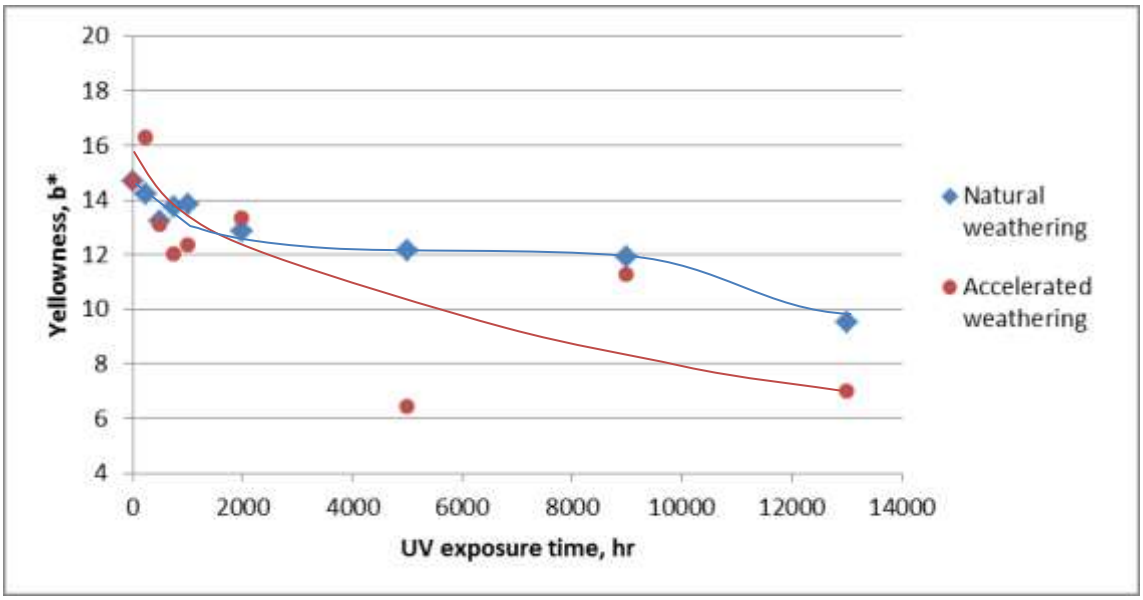

Figure6.1.3.10: Variation in yellowness for both types of weathering.

The presence microcracks in the degraded surface increases the roughness of the surface which causes more scattering to the measured reflected light from the surface of the specimen during testing, resulting in decrease in colour and gloss values i.e. decrease in yellowness and redness.

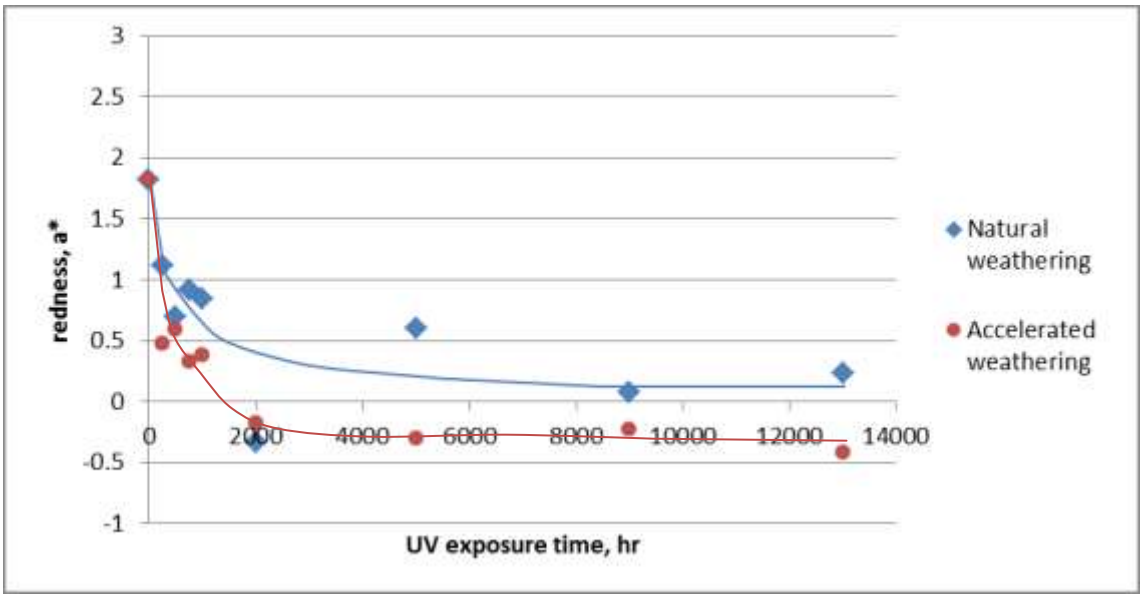

Figure6.1.3.11: Variation in redness for both types of weathering.

Moreover, when pigment molecules absorb UV radiation, chain scission takes place and thus dissociates (pigment molecules exhaustion) and loses their original light absorption properties, so the amount of reflected light reduces. Over time, the pigment concentration will decrease and will cause the colour to fade as seen in decrease in yellowness, redness and increase in lightness (whiteness) [124].

An example of pigment molecule is shown below.

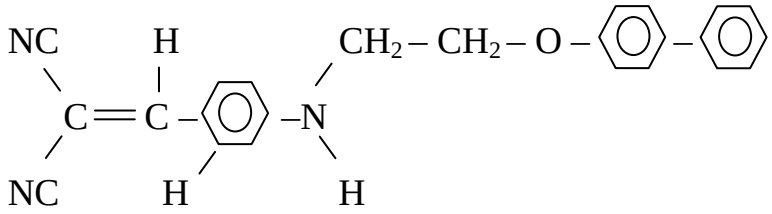

Figure6.1.3.12: Dye formula for polyester [125].

At the end of the experiments, I confirm visually that both QUV cabinet and outdoors samples after 13,000 hr of UV exposure lost their colour to less yellowish and more lightness (more transparent) than the unexposed samples. This is indicative of the gradual effect of the UV radiation on the dye molecules.

Colour and gloss measurements are used for testing the quality of the products. As a guide, if ΔE^* is less than 0.8, the sample is a colour match (acceptable match) to the standard. Values between 0.8 and 1.2 are a possible match (can be acceptable match) and values exceeding 1.2 are not a colour match (not acceptable match).

The results has shown that the values of colour and gloss changes exceeded 1.2, so r-PET products are not suitable for outdoors applications where colour and gloss properties are essential requirements without additives to slow the degradation rate and extent the useful lifetime of the polymer [52].

6.2 Tensile Test

6.2.1 Method

Tensile test is one the most fundamental type of mechanical test showing in details, the reaction of material to the applied force (in tension) through clamping the specimen at both ends as shown in figure below and pulled slowly at one of the clamped ends at a constant extension rate until it breaks.

During stretching the specimen, the force-extension curve is plotted. The mechanical properties are then determined such as yield stress, elongation of the material at yield, stress at break and elongation at break to characterize the material under the applied load.

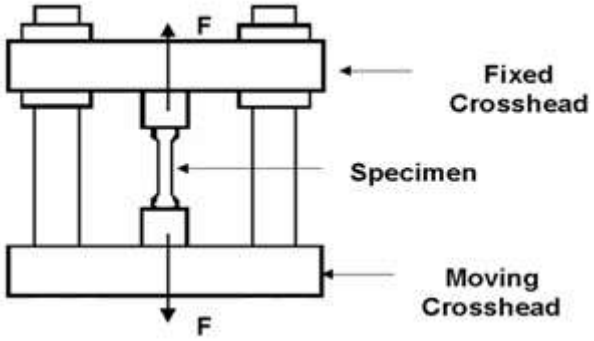

Figure6.2.1.1: Schematic diagram of tensile test machine.

The tensile specimens was placed in the Tinius Olsen testing machine after measuring the width, B and the thickness, D of each specimen at three different points along the gauge length and their mean value was determined. The setting parameters were:

- Load range = 8500 N.
- Extension range = 500 mm.
- Gauge length = 100 mm.
- Speed = 10 mm/min.
- Preload = 0

The sample was pulled at a constant crosshead speed (10 mm/min) and the stress – strain curve was recorded by an attached computer. From the curve,

yield stress, elongation at yield, stress at break and elongation at break were calculated on an average of six test specimens.

Stress: stress σ_t is defined as load per unit area.

$$\sigma_t = p / A_o \qquad \text{.....6.4}$$

where p is the applied load and A_o is the original cross-sectional area.

Strain: The extension on the specimen is measured over a gauge length, L_o. Strain, ε_t is defined as the change in length ΔL divided by the original length, L_o.

$$\varepsilon_t = \Delta L / L_o = (L - L_o) / L_o = (L / L_o) - 1 \qquad \text{.....6.5}$$

Elongation at break: (failure strain) is often expressed as a percentage called the percentage elongation at break.

$$\text{Elongation\%} = ((L_f - L_o) / L_o) * 100\% \qquad \text{.....6.6}$$

Where L_f is the final gauge length.

Yield stress: Yield stress σ_y is the stress at which the slope of stress-strain curve is zero (i.e. $d\sigma/de=0$). If load-extension curve is plotted rather than stress-strain curve, then yield stress is calculated from the load at which the slope of curve is zero, i.e. $dp/de=0$.

$$\sigma_y = P_y / A_o \qquad \text{.....6.7}$$

where P_y is load at which load-extension curve has a zero slope $(dp/de)=0$

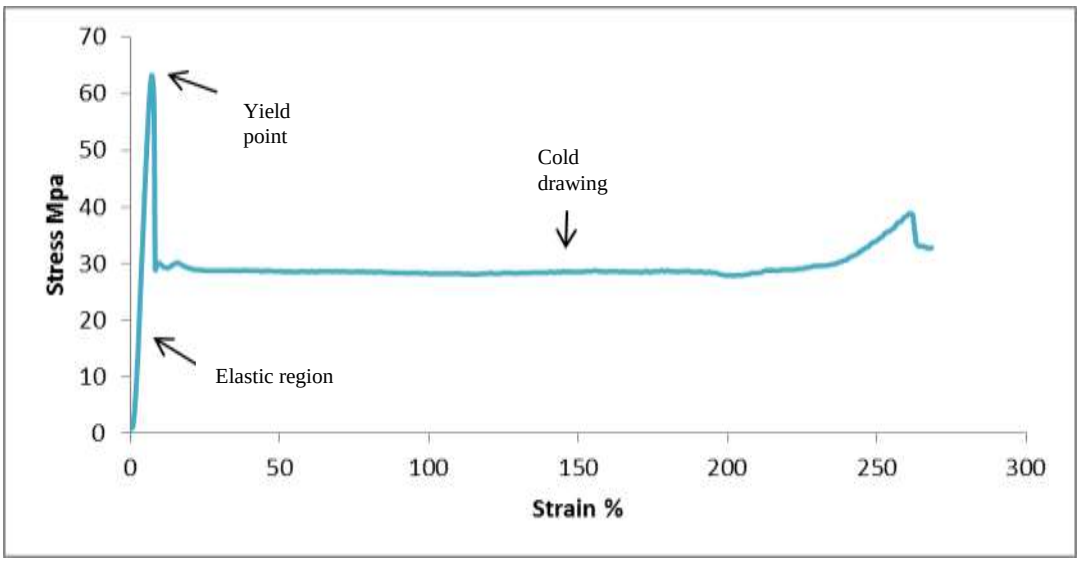

Figure6.2.1.2: Stress-strain curves for r-PET at 10mm/min and 20°C before UV exposure.

As the strain is increased, the material passes through a recoverable elastic region (reversible deformation), due to the elongation of the molecular chains by bond stretching and bond rotation (amorphous region) along the direction of the applied stress as shown schematically in the following figure.

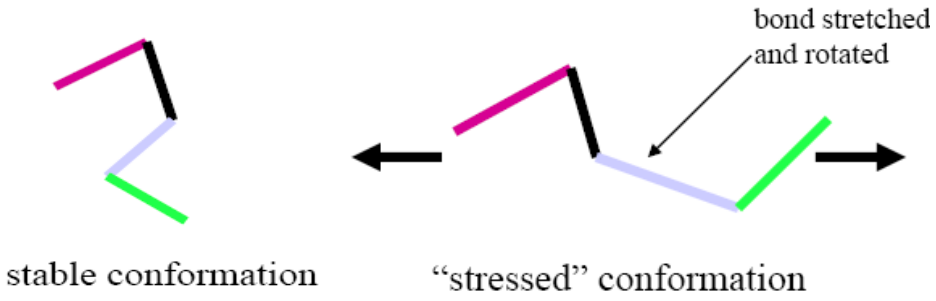

Figure6.2.1.3: Elastic deformation.

And as the strain continues to increase, chains cannot stretch anymore, so they start to slip past each other and bonds break (in the crystalline region). This is the start of permanent irreversible plastic deformation, i.e the material start to yield. Plastic deformation in semi-crystalline polymers can be explained in main four stages as shown in figure6.2.1.4; The Initial structure: Two regions, crystalline (chain-folded chains) and amorphous region before deformation.

(1) Reversible elastic deformation: Elongation of amorphous tie during first stage of deformation.

(2 & 3) Irreversible plastic deformation: Crystalline regions begin to slip past each other (shear deformation) towards the direction of the applied stress. Also the separation of crystalline blocks into segments. The crystalline regions start to break apart, but their segments remain attached to each another by the tie chains within the amorphous structure.

(4) Stretching (orientation) (4): of crystallites (block segments) and tie chains (amorphous regions) along tensile axis.

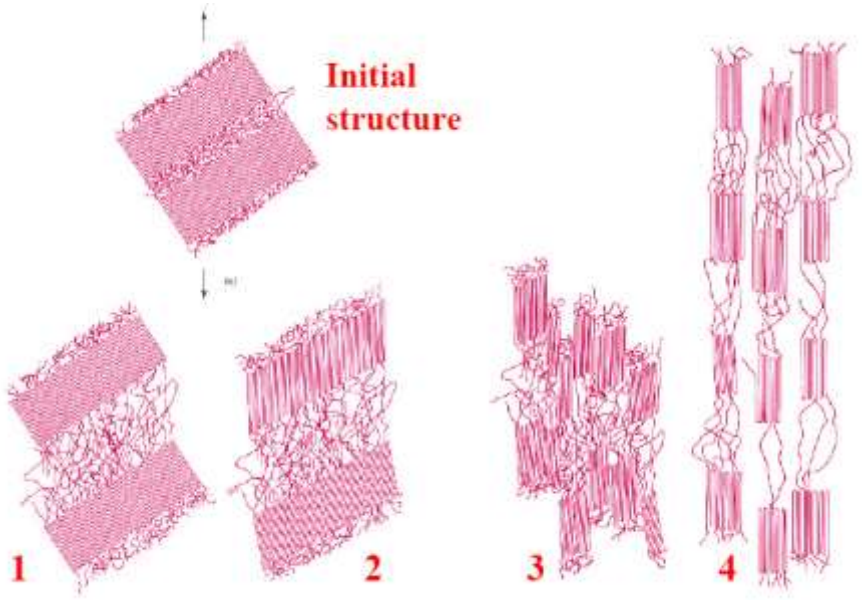

Figure6.2.1.4: Typical tensile deformation of a semi-crystalline polymers [141].

When the permanent irreversible plastic deformation starts (the material yields), the cross-sectional area of the specimen begins to decrease (onset of necking). This results in extensive deformation of the polymer material (crystalline regions) in the vicinity of the necked region and the polymer chains in the amorphous regions become oriented (stretched) in the direction of the applied tensile stress. The extended chains resist further deformation. If this orientation-induced hardening (resistance) is sufficiently high to overcome the increased stress due to the reduction in the cross-sectional area, then further deformation (extension) of the specimen will occur only through the propagation of the neck along the sample (cold drawing). If the resistance of extended chains to further deformation is less than the increased stress (the increased stress at the neck region increases faster than orientation hardening), then the necked region deepens continuously, leading to local failure at that region [126, 127, 128, 129, 130, 131].

6.2.2 Results

The tables below describe the tensile properties generated under accelerated and natural weathering over time periods up to 13000 hour of UV exposure.

Table6.2.2.1: Tensile properties for UV exposed samples under accelerated weathering.

UV exposure time, hr (Acc.)	Yield stress (MPa)	Elongation at yield (%)	True stress at break (MPa)	Elongation at break, %
0	59.60 ± 2.63	6.90 ± 0.17	186.13 ± 19.13	262.50 ± 27.68
250	67.75 ± 0.59	7.37 ± 0.18	100.01 ± 35.55	41.89 ± 50.59
500	69.65 ± 7.67	7.45 ± 0.77	93.10 ± 32.43	11.03 ± 5.50
750	67.48 ± 2.02	7.37 ± 0.25	77.58 ± 24.84	24.45 ± 22.02
1000	68.82 ± 1.68	7.67 ± 0.28	67.40 ± 24.96	11.90 ± 4.70
2000	50.15 ± 15.75	5.93 ± 1.70	50.10 ± 15.67	5.97 ± 1.78
5000	37.01 ± 9.17	4.12 ± 0.68	37.01 ± 9.17	4.12 ± 0.68
9000	32.09 ± 2.20	3.87 ± 0.24	32.09 ± 2.20	3.87 ± 0.24
13000	26.19 ± 2.97	3.30 ± 0.11	26.19 ± 2.97	3.30 ± 0.11

Table6.2.2.2: Tensile properties for UV exposed samples under natural weathering.

UV exposure time, hr (Nat.)	Yield stress (MPa)	Elongation at yield (%)	True stress at break (MPa)	Elongation at break, %
0	59.60 ± 2.63	6.90 ± 0.17	186.13 ± 19.13	262.50 ± 27.68
250	59.52 ± 0.46	6.70 ± 0.15	185.24 ± 37.01	251.33 ± 13.31
500	58.55 ± 0.37	6.87 ± 0.12	183.32 ± 8.85	241.13 ± 8.24
750	60.18 ± 0.48	7.09 ± 0.58	195.02 ± 10.49	249.50 ± 40.99
1000	57.10 ± 1.10	6.81 ± 0.27	191.07 ± 15.57	253.30 ± 6.65
2000	59.83 ± 0.84	6.79 ± 0.02	163.54 ± 24.62	255.73 ± 20.59
5000	61.65 ± 0.99	6.78 ± 0.27	148.42 ± 3.19	242.53 ± 12.06
9000	61.88 ± 0.95	6.42 ± 0.29	118.91 ± 30.39	257.00 ± 81.71
13000	63.05 ± 1.28	6.56 ± 0.28	107.96 ± 32.56	246.73 ± 61.91

6.2.3 Discussion

The general behaviour of r-PET under tensile tension before UV exposure is shown in figure6.2.3.1, ductile behaviour and it remains the same after 13000 hr of exposure outdoors as shown in figure below.

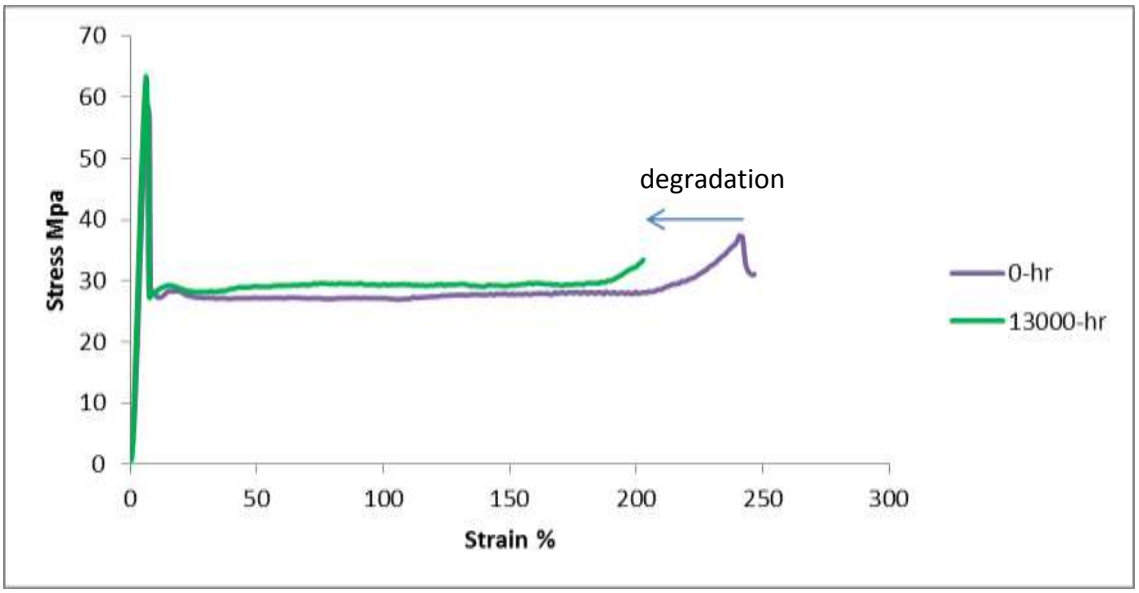

Figure6.2.3.1: Stress-strain curves for r-PET at 10mm/min and 20°C after 13000hr of UV exposure outdoors.

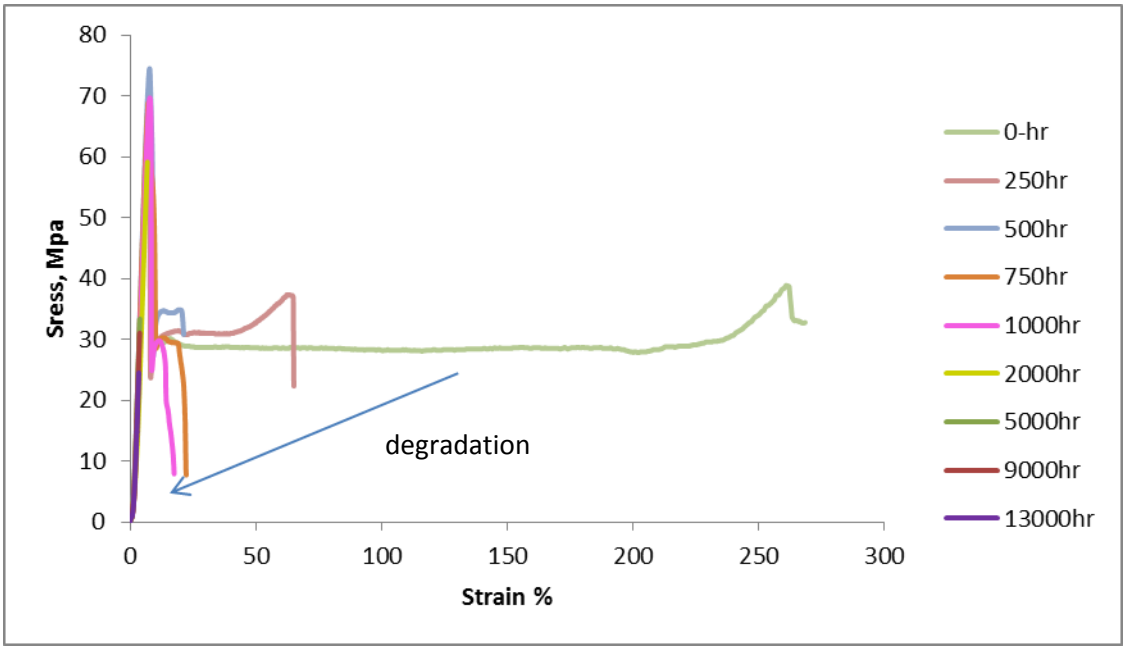

Figure6.2.3.2: Stress-strain curves for r-PET at 10mm/min and 20°C after 13000hr of accelerated UV exposure.

Ductility (ductile behavior) is the ability of the material to deform plastically (extensive plastic deformation) under tensile stress before fracture as shown below, deformation in the neck region of samples before exposure and after 13,000 hr of outdoor exposure A and B respectively, while the behaviour of the material changed to brittle after the same period of UV exposure under accelerated weathering as shown in figure6.2.3.3-C (no apparent plastic deformation taken place before fracture). The optical images in figure6.3.3.4-C do reflect the mode of fracture, no signs of visible pits on the surface of oudoor samples while wide and deep cracks do exist on the surface of accelerated weathering samples after 13,000 hr of exposure.

A

B

C

Figure6.2.3.3: r-PET specimens after tensile test: A: before exposure (ductile behavior), B: after 13000hr outdoors (ductile behavior) and C: after 13000hr in QUV cabinet (brittle behavior).

When tensile stress applied on these specimens, the chains stretch and orientate in a very localized area forming a craze. The oriented chains break creating voids which become elongated normal to the direction of the applied stress as shown below. These voids grow and form cracks which propagate leading to failure.

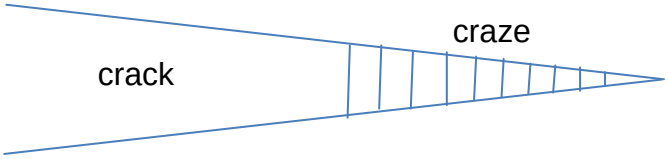

Figure6.2.3.4: Craze and crack.

When UV radiation reaches the surface of r-PET samples, it is absorbed by the molecules of existing chromophores, its energy increases by the amount equal to the energy of the absorbed photon. If this energy reaches the magnitude of the energy for bond disruption, can lead to breakage of bond between atoms (chain scission) and give rise to radicals. These radicals attack neighboring groups and abstract hydrogen atom creating more radicals and with the presence of oxygen and water, the situation becomes more complicated due to oxidation and hydrolysis reactions.

Chain scission leads to shorter chain lengths which have more ends per unit volume than long chains, hence a higher free volume which provides a good medium for easily penetration of water molecules and diffusion of oxygen molecules in the available spaces converting them to local stress raisers (high stressed locations) that lead to the formation of microvoids. During weathering, if the stress in these locations increased due to the accumulated of diffused molecules will cause the microvoids (under tension) to grow (open wider) forming microcracks.

The formations of microcracks in r-PET samples happened from early stages of exposure in both types of weathering as indicated from the sharp increase in colour and gloss changes during this period. Under the tension of tensile test machine, these microcracks at the degraded surface extended and propagate to the undegraded regions inside the specimens leading to failure.

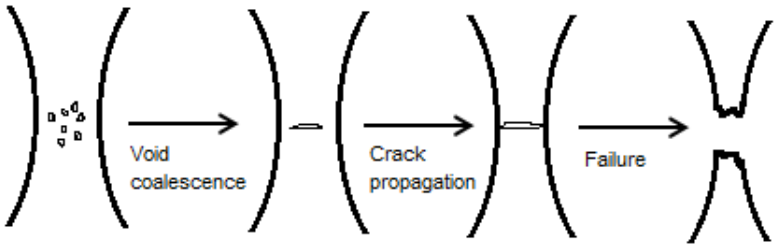

Figure6.2.3.5: Failure due to voids formation.

Chain scission happens at high rate during the early stages of exposure as seen in the sharp increase in colour and gloss changes. It occurs mostly in the amorphous regions and has no significant effect in the crystalline region as the yield stress and elongation at yield remain unchanged for outdoors samples during this period as shown below (on normal and logarithmic scale, so the change can be seen more clearly). This does not mean that the crystalline region is immune to the attack of UV, but the chain scission is much less than that in the amorphous region which has more free volume between chains providing easy medium for the penetration of water and oxygen diffusion which accelerate the chain scission process.

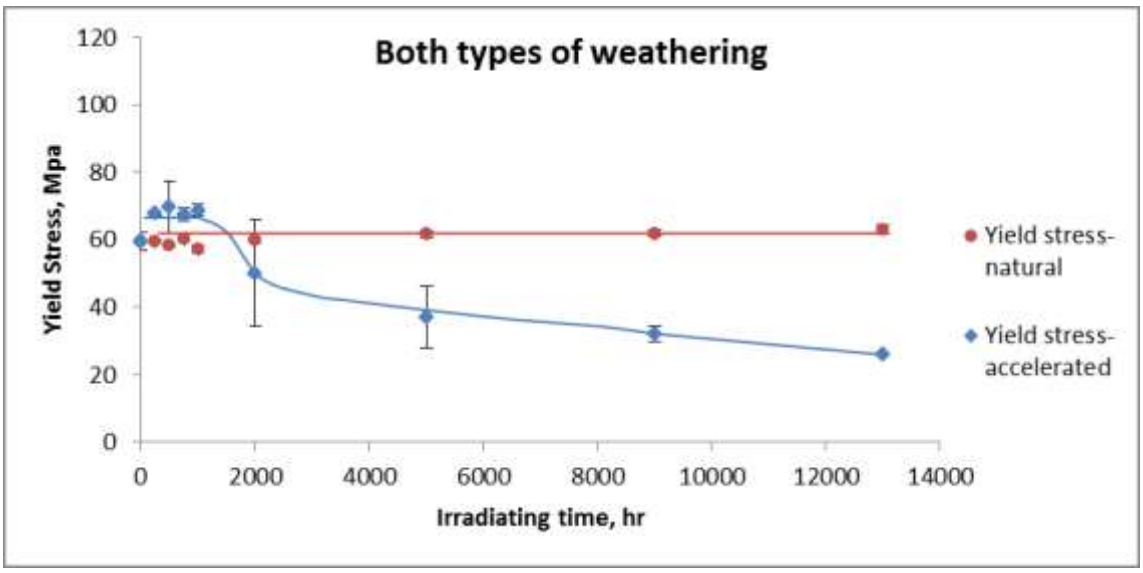

Figure6.2.3.6: Yield stress of samples in accelerated and natural weathering.

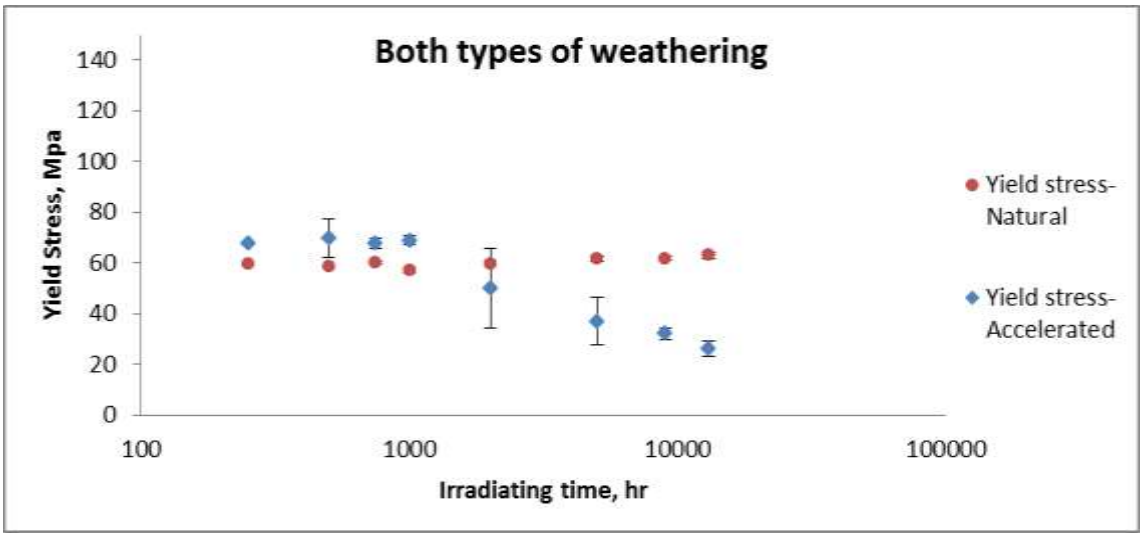

Figure6.2.3.7: Yield stress of samples in accelerated and natural weathering (x-axis-logarithmic scale).

Yield stress is defined as the minimum stress at which permanent deformation produced in the material after the stress is removed. Permanent deformation is irreversible plastic deformation occurs in the crystalline regions when the chains breaks due to the chain scission which reflects the effects on the elongation at yield (deformation or stretching of the sample at yield) as shown below.

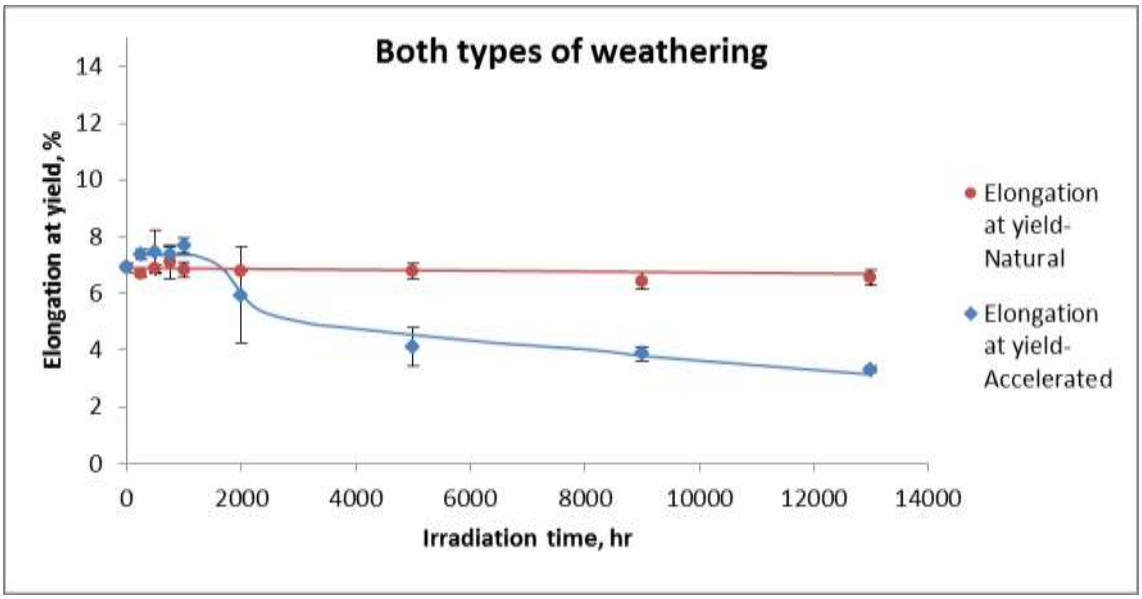

Figure6.2.3.8: Elongation at yield of samples in accelerated and natural weathering.

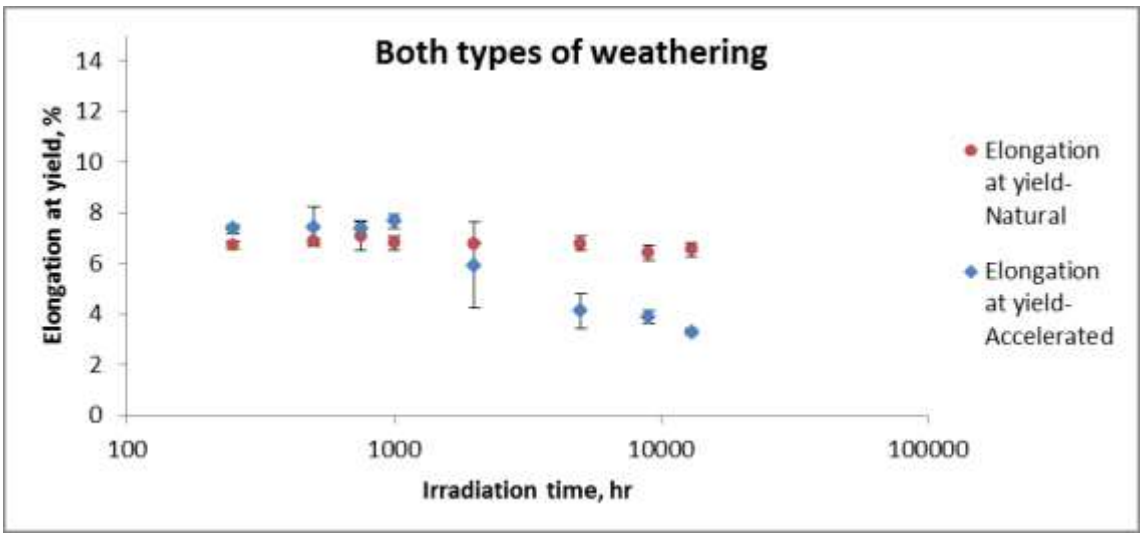

Figure6.2.3.9: Elongation at yield of samples in accelerated and natural weathering (x-axis-logarithmic scale).

After 1000hr of accelerated UV exposure, yield stress and elongation at yield dropped significantly by 61.94% and 56.98% respectively up to 13000 hr of exposure indicating that there is a significant effect for the chain scission in crystalline region in this period. Yield stress is decreasing with the extent of exposure means the material starts to yield earlier (early start of plastic deformation because of the effect of degradation). Elongation at yield is decreasing means the stretching of the sample under tension stress is decreasing because the material can elongate less as the long chains are converted to shorter chains during the chain scission process.

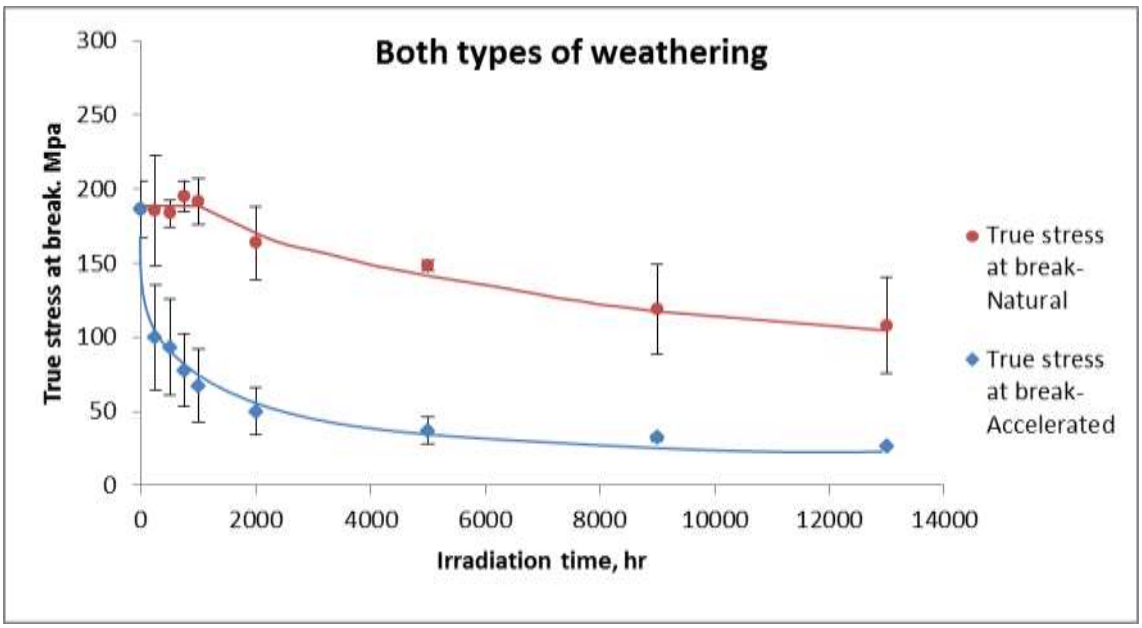

Figure6.2.3.10: True stress at break of samples in accelerated and natural weathering.

Failure stress is a measure of true stress required to fail (break) the material, it is calculated by the division of the final force fail the material to the cross sectional area after break. The initiation of failure is due to surface degradation through the microcracks which reflects the sharp drop in the failure stress and elongation at failure for r-PET samples. The optical images show clear cracks lines in figures 6.3.3.4-B and 6.3.3.4-C.

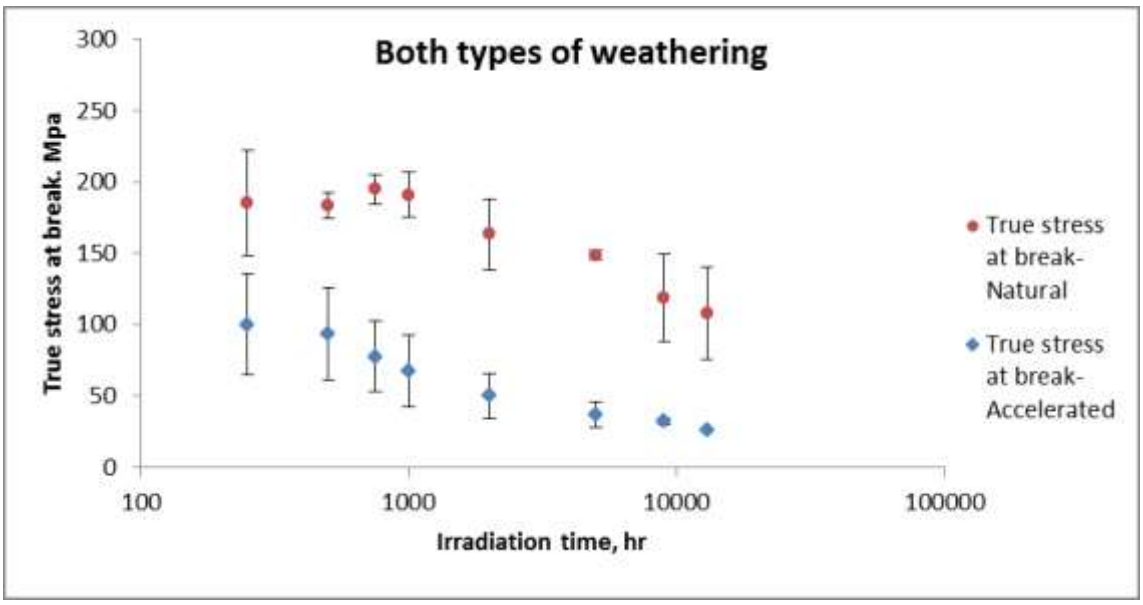

Figure6.2.3.11: True stress at break of samples in accelerated and natural weathering (x-axis-logarithmic scale).

Failure stress and elongation at failure of the samples irradiated in the QUV chamber decreased sharply by 63.79% and 95.46% respectively right from the beginning of exposure up to 1000 hr of exposure as shown in figures 6.2.3.10 and 6.2.3.11, indicating the rapid formation of microcracks during this period due to high chain scission rate.

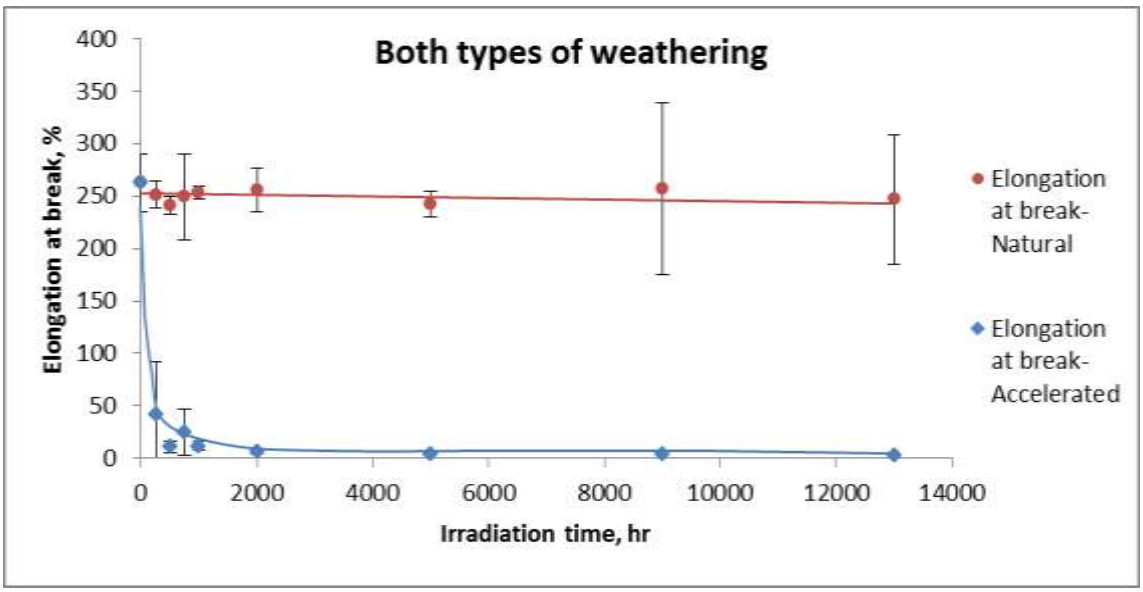

Figure6.2.3.12: Elongation at break of samples in accelerated and natural weathering.

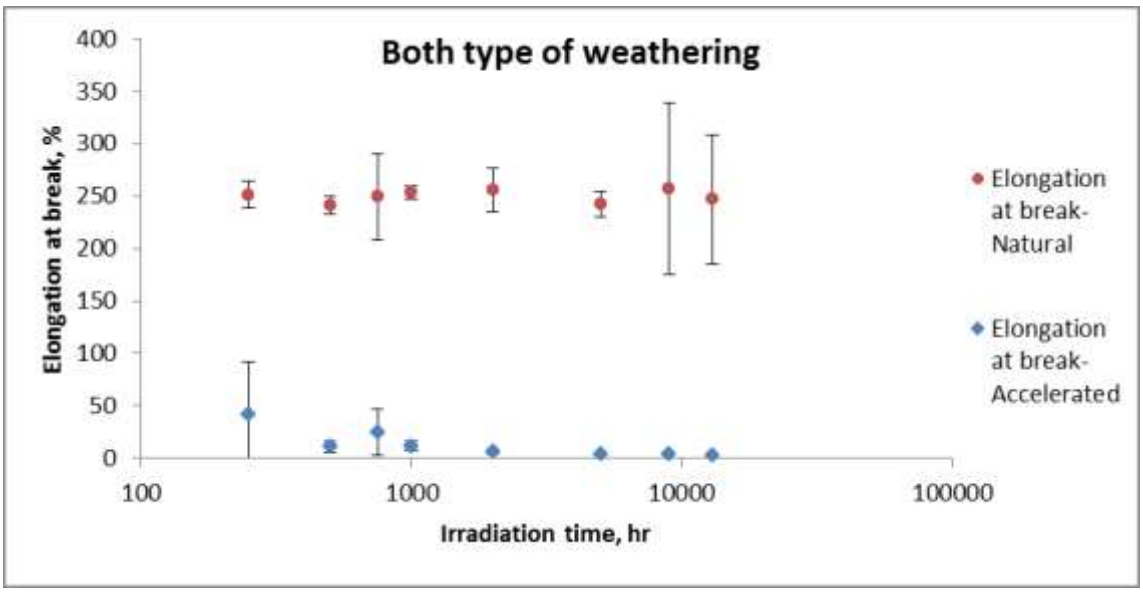

Figure6.2.3.13: Elongation at break of samples in accelerated and natural weathering (x-axis-logarithmic scale).

Then further slight drop in failure stress and elongation at failure by 22.14% and 3.28% respectively after 13000 hr of exposure because chain scission reduced with the extent of UV exposure because the material consumed at the surface layer due to chain scission and degradation products act as a barrier for further UV and oxygen attack as well as limited diffusion of UV and oxygen, thus the total drop in failure stress and elongation at failure was 85.93% and 98.74% respectively.

For outdoor samples, failure stress remained unchanged for the first 1000 hr of sunlight exposure because the microcracks in the degraded surface are shorter than the critical crack length for propagation, i.e. unable to propagate under the tension forces of tensile test machine. Then failure stress dropped by 43.50% after 13000hr as shown in figures 6.2.3.10 and 6.2.3.11 indicating that these microcracks becomes bigger and able to propagate, although photo images show no signs of any visible pits. While elongation at failure seems to be unchanged as shown in figures 6.2.3.12 and 6.2.3.13 although the calculations shows very slight decreased (2.59%) after 13,000 hr of outdoor exposure.

6.3 Impact Test

6.3.1 Method

Polymers may fail in service due to the effects of rapid stress loading (impact load). Various test methods are used but the most common method is Charpy impact test. It is high speed fracture test measuring the energy required to break a specimen under bending conditions through the transfer the energy of impact to deflect in the structure.

Accidental occurrence of impact makes resistance of material to this type of abuse a very important in specific applications involving sudden loading. Impact strength is the typical parameter for characterizing resistance of material to impact which is a measure of its toughness to assure safety against fracture.

The impact strength (J/m^2) is defined as the energy (impact energy) divided by the cross-sectional area of the sample, which has undergone fracture.

$$\text{Impact strength} = U/BD \qquad \text{.....6.8}$$

Where,

B : width of sample, mm

D : thickness of sample, mm

Charpy impact test is not only used to polymers, but also to metals, ceramics and composites as a quality control test and comparative test for chosen the best shocking – absorbing material for specific applications. It is simple, cheap, fast and reliable which has been used for many years.

Impact test is not only used to measure the ability of the material to absorb energy when subjected to sudden load; but also to determine the minimum service temperature for a material by determining the ductile-brittle transition temperature (from ductile to brittle behaviour or brittle fracture) from the plot of impact energy as a function of temperature [132, 133, 134, 135, 136].

Ray-Ran impact tester – set for the Charpy mode was used with a pendulum hammer of weight 1.189 kg and velocity of 2.9 m/s. The width, B and thickness, D of each specimen at three different positions were measured and the mean values were recorded. The specimen was placed on the support as a simple beam and impacted by at the central part by the released pendulum hammer

and the impact strength was recorded on the digital display. The procedure was repeated for all the specimens and the average impact strength was evaluated.

6.3.2 Results

The table below describes the impact strength for un-notched samples under accelerated and natural weathering over time periods from 250 to 13000 hour of UV exposure. The specimens outdoors did not break (failed to break) and have bending failure, while the specimens in accelerated weathering have brittle failure.

Table6.3.2.1: Impact strength values (kJ/m^2) for accelerated and natural weathering samples.

UV exposure time, hr	Impact strength (kJ/m^2) (Accelerated)	Impact strength (kJ/m^2) (Natural)
250	46.35 ± 3.79	Failed to break
500	46.17 ± 1.47	Failed to break
750	46.19 ± 5.83	Failed to break
1000	40.04 ± 1.25	Failed to break
2000	41.92 ± 0.39	Failed to break
5000	42.93 ± 5.79	Failed to break
9000	3.61 ± 3.35	Failed to break
13000	3.26 ± 0.79	Failed to break

6.3.3 Discussion

In order to assess whether a plastic is brittle or tough is to carry out an impact test to determine the capacity of the plastic to absorb energy when subjected to sudden load. Toughness is a measure of the energy absorbed during an impact test up to the point of failure of the material; the higher the impact energy, the higher toughness and vice versa.

r-PET samples before UV exposure and after exposure outdoors up to 13000 hr failed to break (buckled) due to its high toughness, while the samples in accelerated weathering broke completely in a brittle manner after 250 hr of UV exposure as shown in figures6.3.3.1-A and 6.3.3.2-B; this indicates the transition from ductile to brittle failure, i.e. the material transform from brittle to

ductile just after 250 hr of accelerated UV exposure.

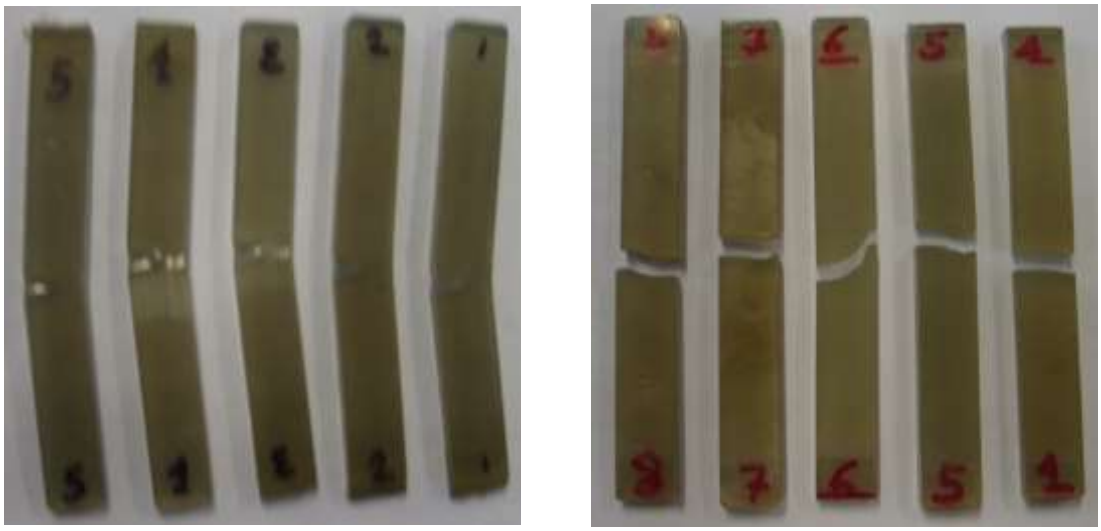

(A) (B)

Figure6.3.3.1: r-PET specimens after 13000 hr in A- natural weathering and B- accelerated weathering.

For accelerated weathering samples, the impact strength remained unchanged in the first 1000 hr of exposure then decreased slightly by 7.38% up to 5000 hr of exposure. As the time of UV exposure increases up to 9000 hr, it sharply dropped further by 84.83% and remained unchanged afterwards up to 13000 hr of UV exposure as shown below.

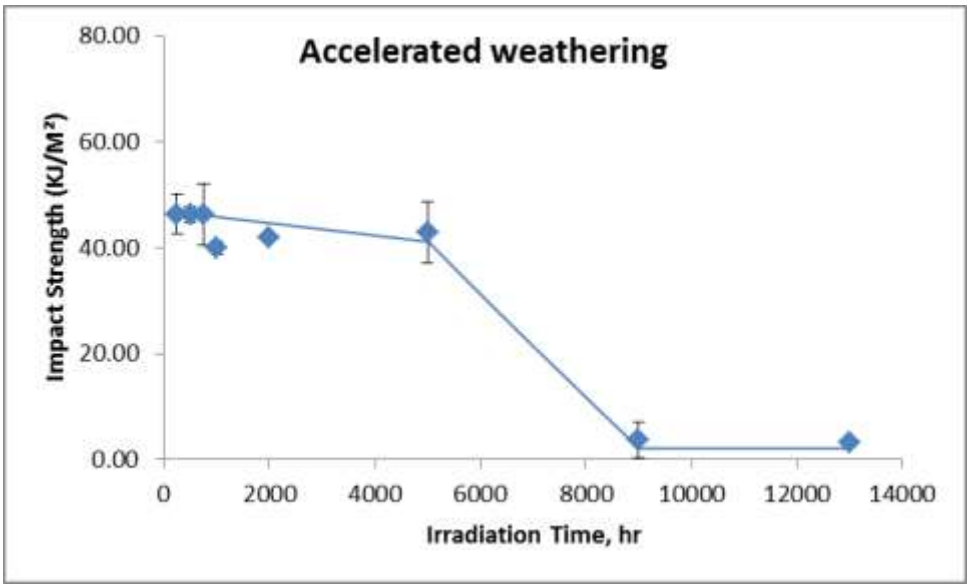

Figure6.3.3.2: Impact strength values for accelerated weathering samples (x-axis-normal scale).

Figure6.3.3.2 can be redrawn on logarithmic scale (x-axis), so the change can be seen more clearly especially after 5000 hr of UV exposure.

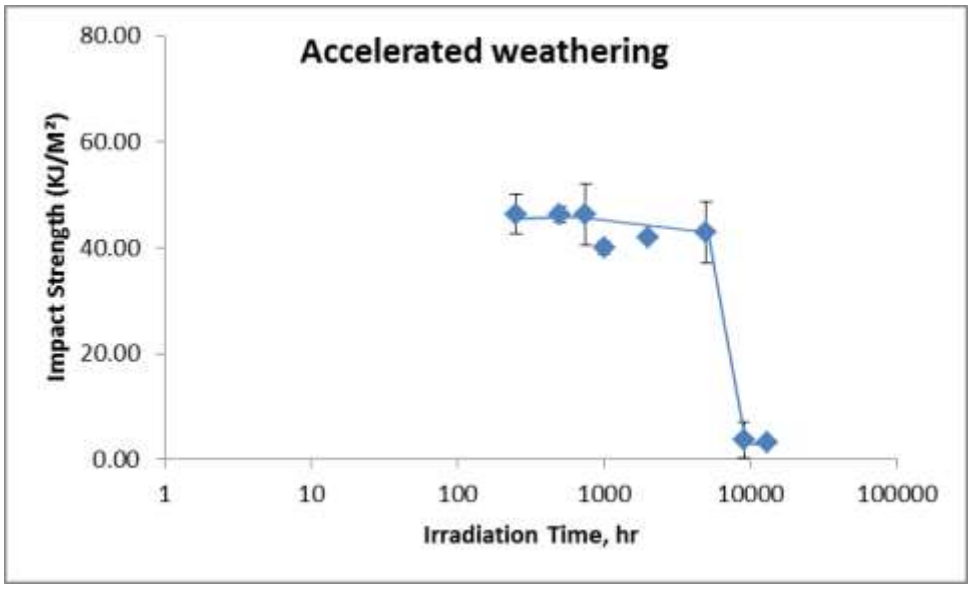

Figure6.3.3.3: Impact strength values for accelerated weathering samples (x-axis-logarithmic scale).

When UV radiation reaches the surface of r-PET samples, it is absorbed by the molecules of existing chromophores and causes chain scissions that produce free radicals able to react with the diffused oxygen or water molecule or abstracting hydrogen from the nearby chains. This process continues, shorter chain lengths are formed, low molecular weight chains have more ends per unit volume than long chains and hence a higher free volume and eventually microcracks are formed.

In the first 1000 hr, the microcracks started to form in r-PET samples under accelerated weathering, but there is no effect for it on impact strength, because these flaws are small and able to absorb and transmit the applied energy, but the increase in colour by 3.32 units and gloss by 3.35 units reflect the existence of these flaws as well as the decrease in true stress at break by 63.79% and elongation at break by 95.46% because stress at failure and elongation at failure are related to surface degradation and the initiation of failure is through the existing cracks on the surface layer. With the extent of UV exposure up to 5000 hr, its effects started to appear on impact strength but not significant with slight decrease by 7.38%, decrease in yield stress by 37.90% and elongation at yield by 40.29%. Also further increase in colour by 5.57 units,

gloss by 2.64 units, failure stress by 16.33% and elongation at failure by 2.97%. These flaws also speed up the process of deterioration through the diffusion of oxygen molecules and penetration of water molecules.

After 5000 hr of UV exposure, the formation and growing of microcracks continues very fast, the surface layer becomes full of flaws and more pronounced as shown in figure6.3.3.5-C photo of the surface cracks. These are unable to absorb and transmit the energy applied by the hammer of the pendulum to the whole specimen. The cracks has exceeded critical crack length, so it progressed uncontrollably (independent on material properties) and this reflects further sharp drop in impact strength by 84.83%, further decrease in yield stress by 8.26%, elongation at yield by 3.62%, failure stress by 2.64% and elongation at failure unchanged (by 0.1%) up to 9000 hr, while colour and gloss fluctuated around steady state value.

As the surface layer continues to deteriorate by the weathering after 9000 hr, the impact strength remained nearly unchanged means that the impact strength reached to its lowest level after 9000 hr of exposure, but the tensile properties continue to drop.

The deterioration cannot go deeper into the specimens as shown in the results of crystallinity and MFI because of the limited diffusion of oxygen and UV radiation in the samples and the degradation products act as a barrier towards further weathering effects.

While r-PET samples in natural weathering are tough and strong, it can withstand the weathering factors. Chain scission process is very slowly compared to that in accelerated weathering because these factors are much less than that in the QUV chamber. The photo of surface cracks does not show the cracks, but the microcracks do exist and this is proven by the decrease in colour, gloss and true stress at break of the samples.

In the long term weathering which is not seen in natural weathering will involve moisture absorption into the cracks as example in winter freezing causing tension at the crack tip which cause the crack to grow further and by this mechanism, the critical crack length can be reached.

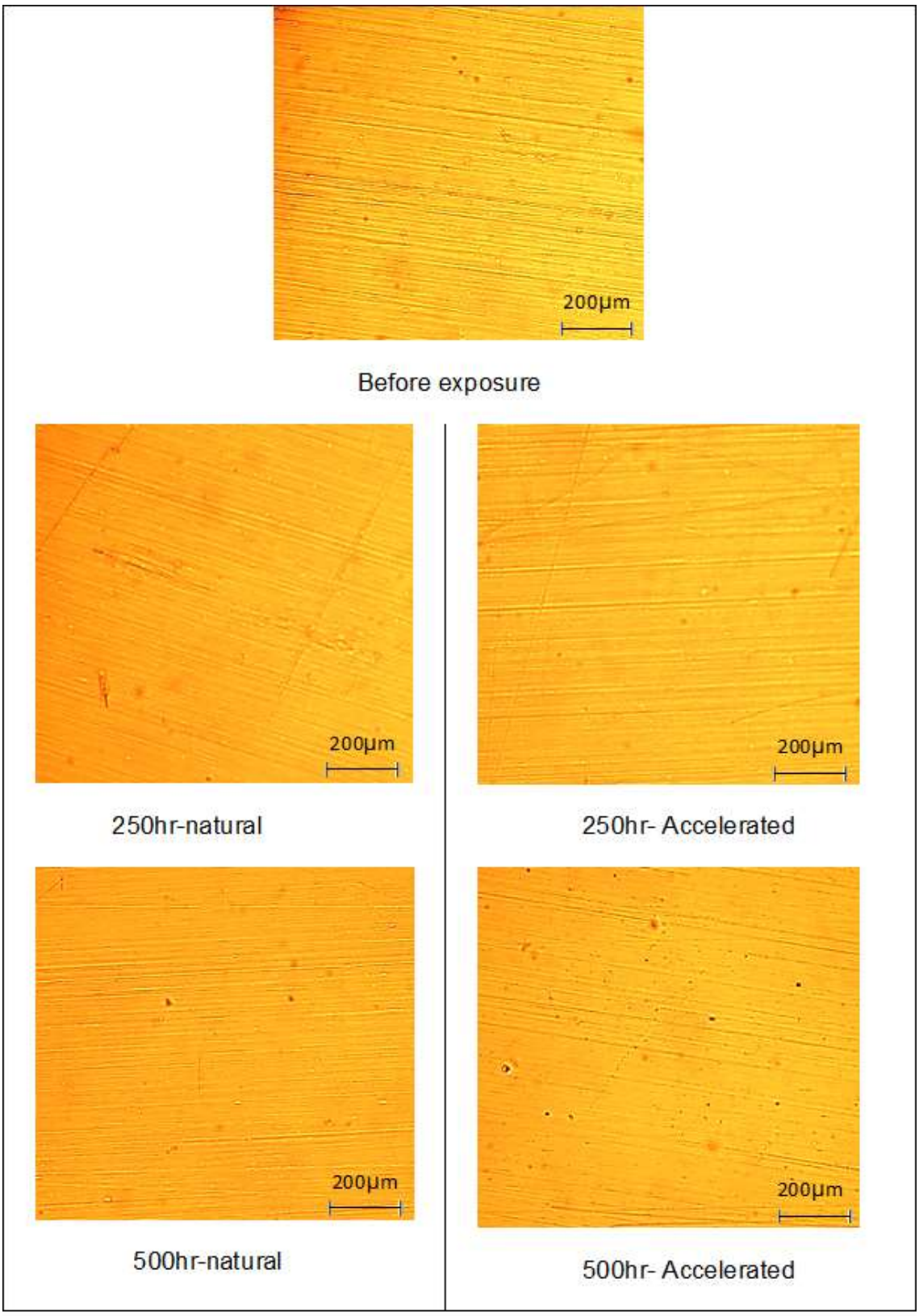

Figure6.3.3.4-A: Surface photos using "Nikon Eclipse50i-magnification10"

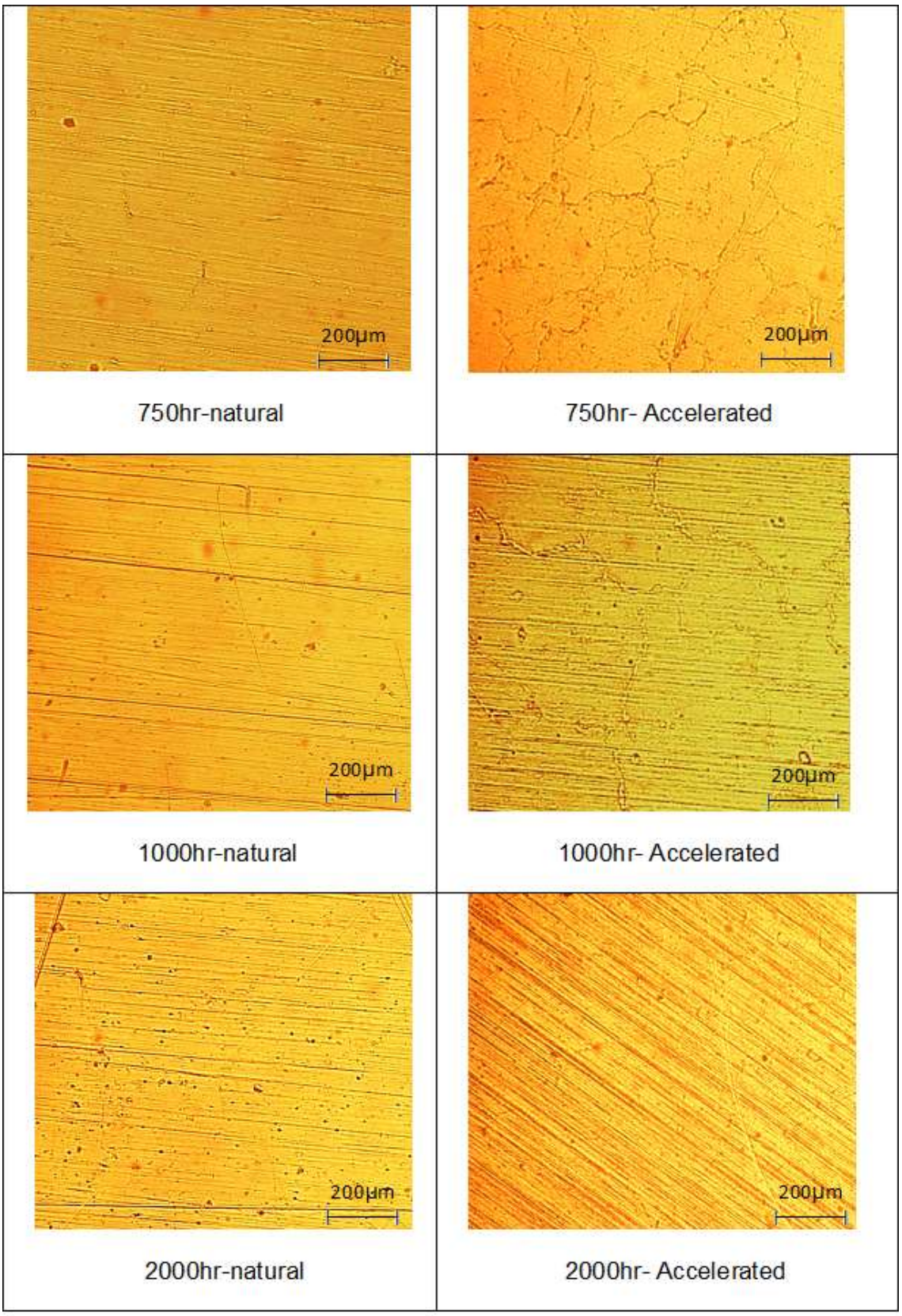

Figure6.3.3.4-B: Surface photos using "Nikon Eclipse50i-magnification10"

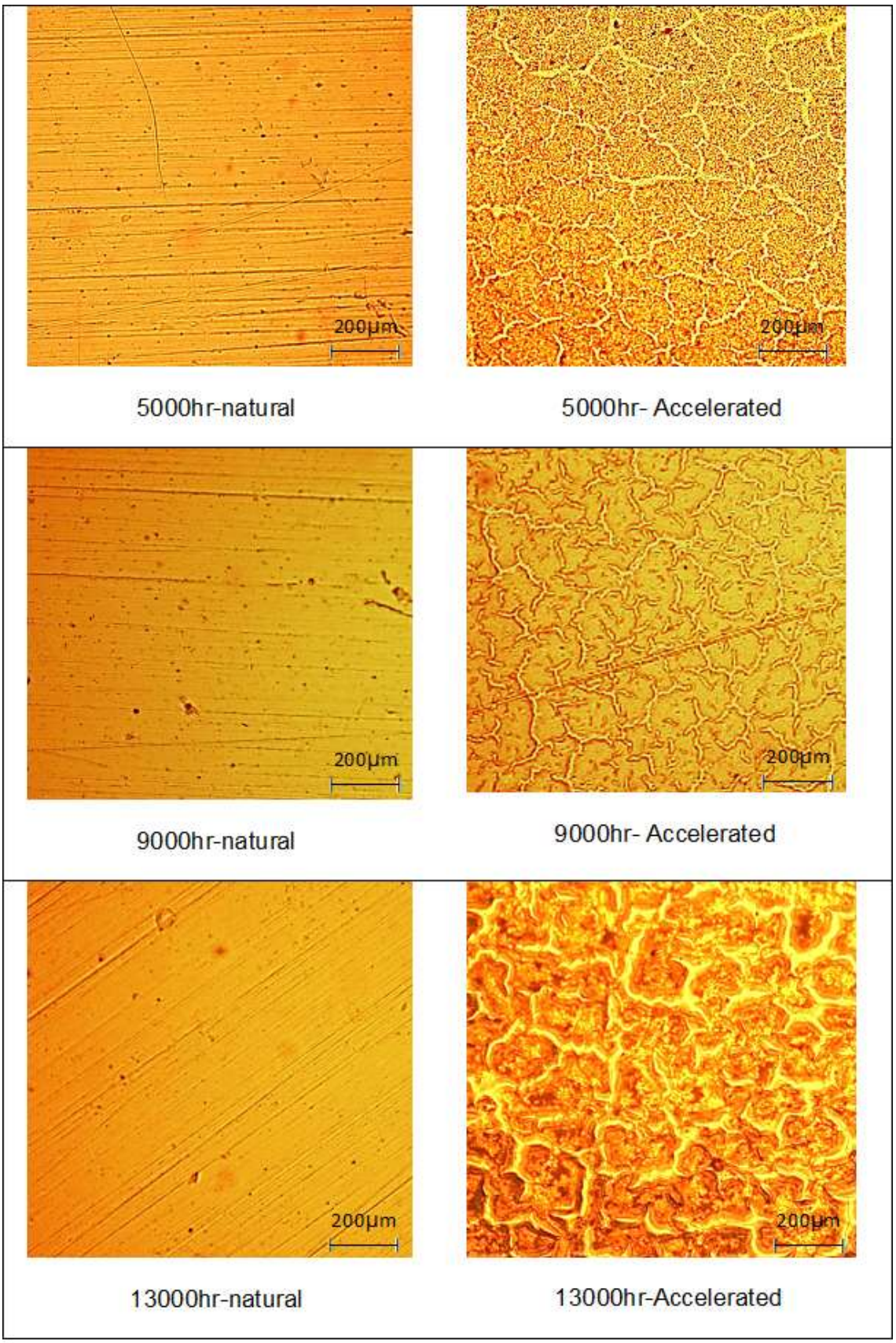

Figure6.3.3.4-C: Surface photos using "Nikon Eclipse50i-magnification10"

The concept of crack propagation i.e. growth is that every crack causes stress concentration where the local stress in the vicinity of the crack tip is higher than that applied to the body as a whole) and each crack grows (absorbing energy) randomly and some will join and lead to catastrophic failure.

By looking at the optical images of outdoors r-PET samples, there are no signs of any visible and clear pits for all periods of UV exposure and this reflects the failure to break during impact test. However colour and gloss change increased sharply in the early stages of exposure indicating that the microcracks do exist right from the beginning of exposure; after 1000hr of exposure, it grew to initiate failure under tensile force.

While the optical images of the accelerated weathering r-PET samples shows significant and visible crack lines on the surface after 750 hr of UV exposure, although the transition from ductile to brittle failure during the impact test started after 250 hr of exposure. The microcracks do exist right from the beginning of exposure as indicated by colour, gloss and failure stress values. After 5000hr of exposure, they became wide and more pronounced leading to a sharp increase in colour and gloss change, a sharp drop in impact strength and in stress at break. After 13,000 of exposure, these cracks became wider and deeper and colour cause gloss, impact strength, stress at failure and elongation at failure reaching to their lowest steady state values.

CHAPTER SEVEN

OVERALL DISCUSSION

7.1 Inter-relationship between Tests

The relation between artificial and natural weathering according to true stress at break shows clearly how this property changes with the extent of degradation. In the QUV chamber, the failure stress dropped sharply right from the beginning of exposure while it remained unchanged for outdoor samples. As mentioned before, the initiation of failure is due to surface degradation through the formation of microcracks. The depth of these microcracks is bigger then the critical crack length due to very high rate of chain scission in artificial weathering that lead to rapid failure while it is smaller than the critical values in natural weathering due to a lower chain scission rate.

After 2000 hr of exposure to UV, samples kept outdoors showed a slight drop in failure stress while under artificial weathering, the failure stress became the same as yield stress and therefore all the ductility lost.

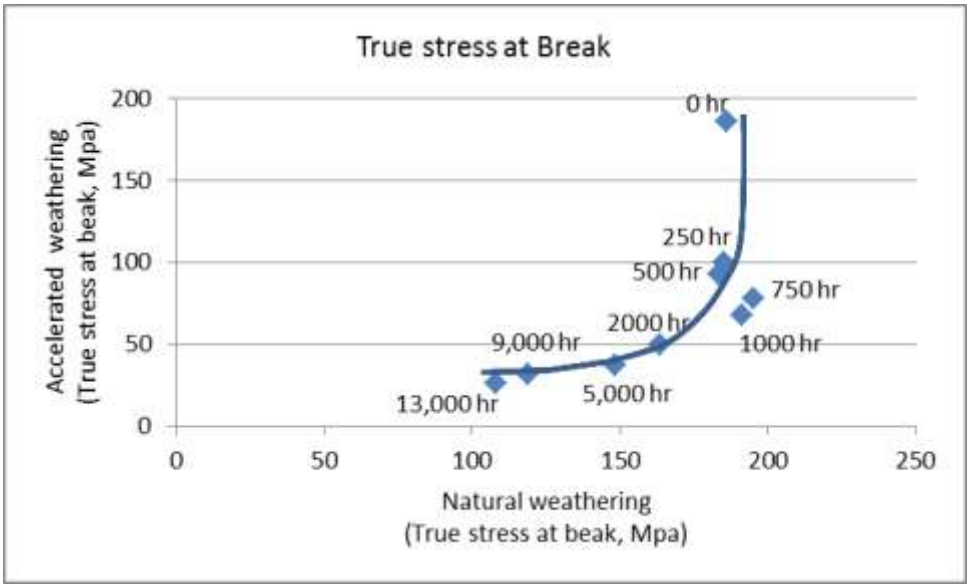

Figure7.1.1: Correlation between natural and accelerated weathering according to true stress at break changes.

This relationship between failure stress and weathering is reflected in the changes seen with colour and gloss in figures7.1.2, 7.1.3, 7.1.4 and 7.1.5. The colour and gloss changes reflected increase in surface degradation in the form of surface flaws. These flaws lead to a reduction in the failure stress indicating the initiation of failure from these flaws. In the case of natural weathering, the flaws caused by surface degradation are appear to be shorter than the critical crack length and so do not lead to crack propagation and reduction in failure stress.

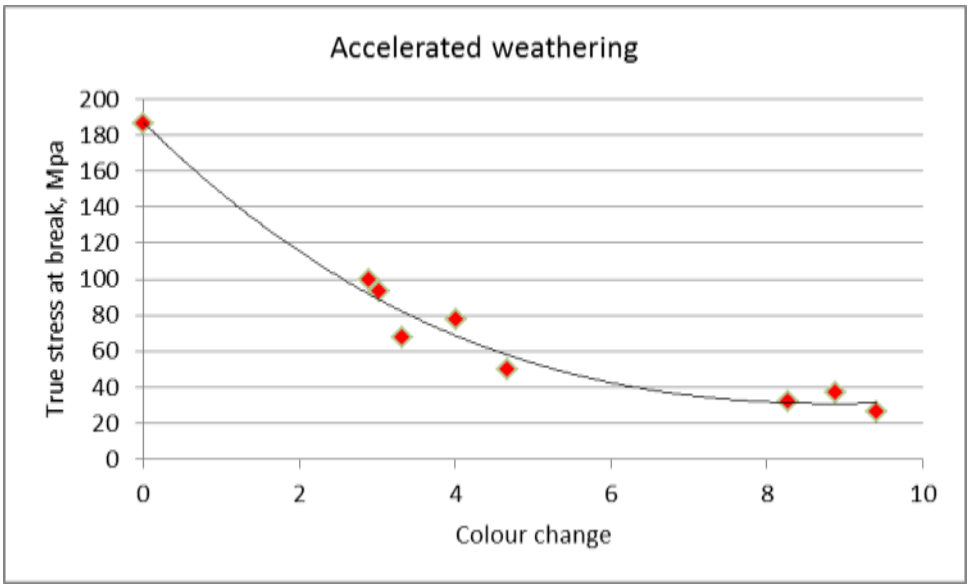

Figure7.1.2: Relationship between colour changes and true stress at break in accelerated weathering.

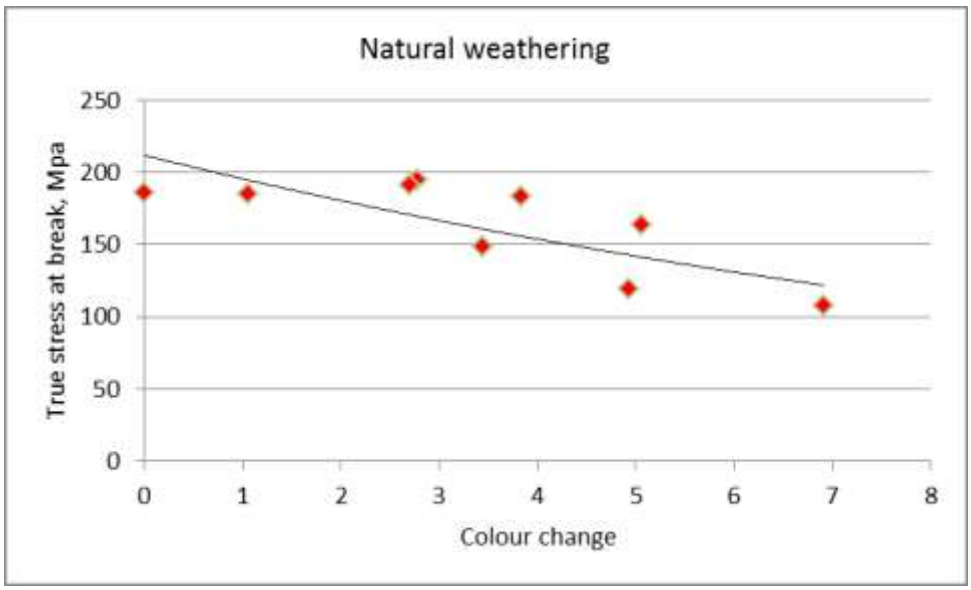

Figure7.1.3: Relationship between colour changes and true stress at break in natural weathering.

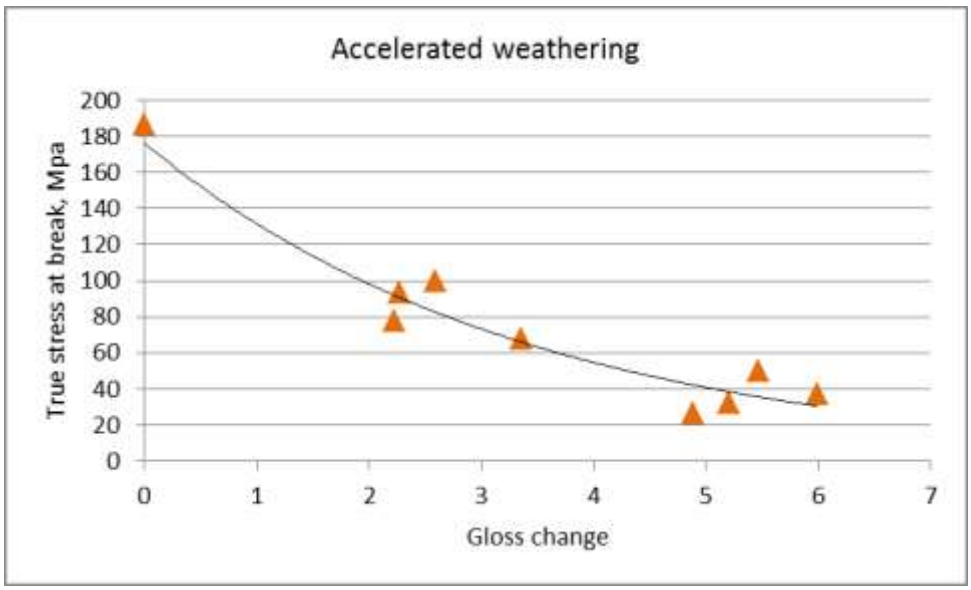

Figure7.1.4: Relationship between gloss changes and true stress at break in accelerated weathering.

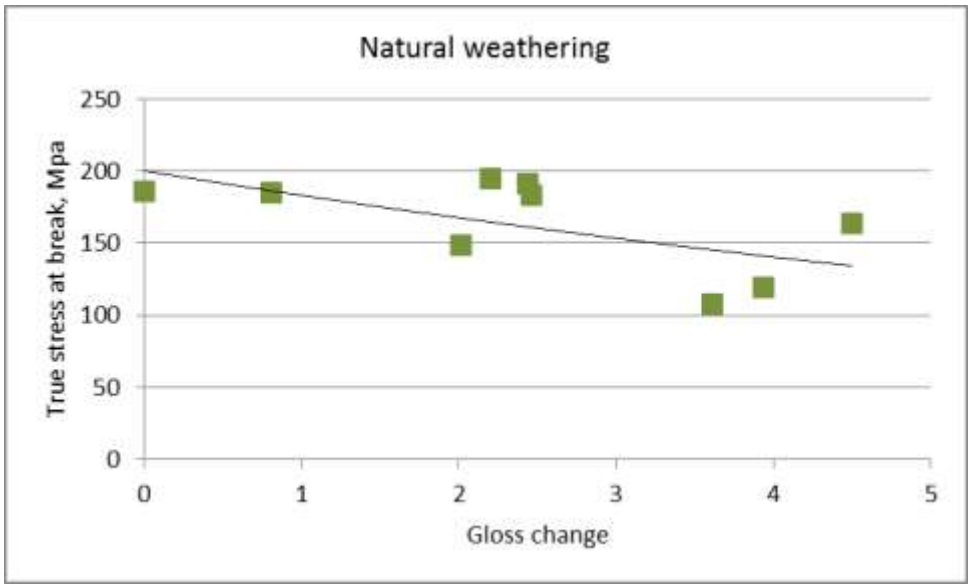

Figure7.1.5: Relationship between gloss changes and true stress at break in natural weathering.

Colour and gloss changes occurred right from the beginning of exposure as indicated by a decrease in these properties. The rate of surface degradation occurred at a higher rate in artificial weathering than that in natural weathering as reflected by the higher values of these two properties in the y-axes as shown in figure7.1.6 and 7.1.7.

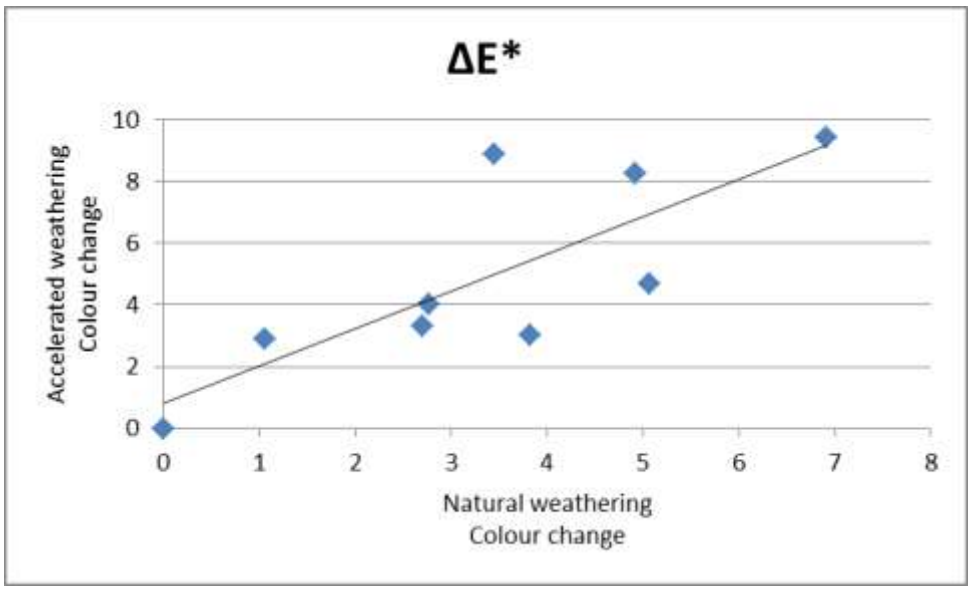

Figure7.1.6: Correlation between natural and accelerated weathering according to colour changes.

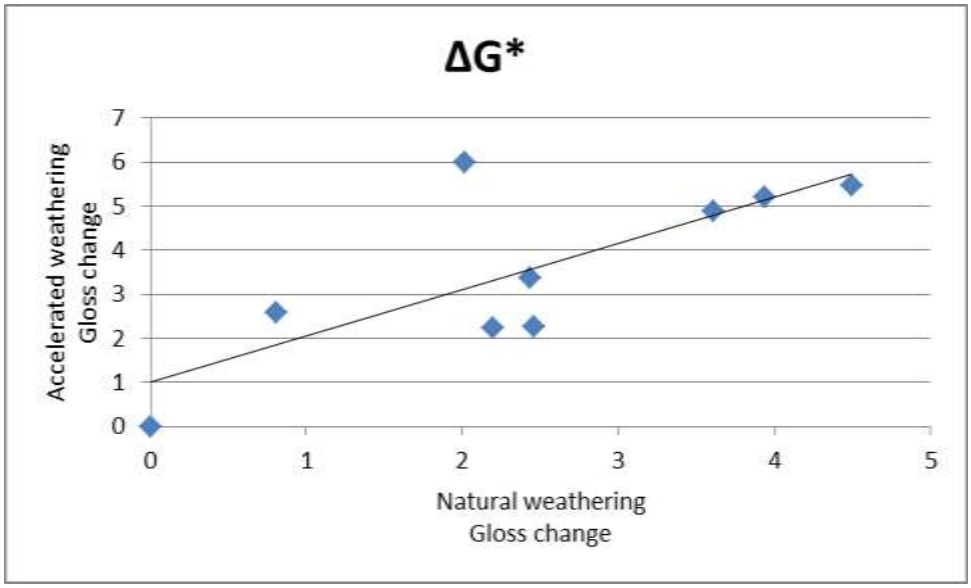

Figure7.1.7: Correlation between natural and accelerated weathering according to gloss changes.

As mentioned before, the initiation of failure is due to surface degradation through the formation of microcracks. The first step of the formation of microcracks is due to the chain scission process. For example C-H bond (asymmetry stretching vibration at 2953 cm^{-1} in the ethylene glycol segment) suffers chain scission with the extent of degradation which leads to the formation of microvoids and finally microcracks. So, it is appropriate to draw the

relation between these two variables to see clearly how they changed synergistically.

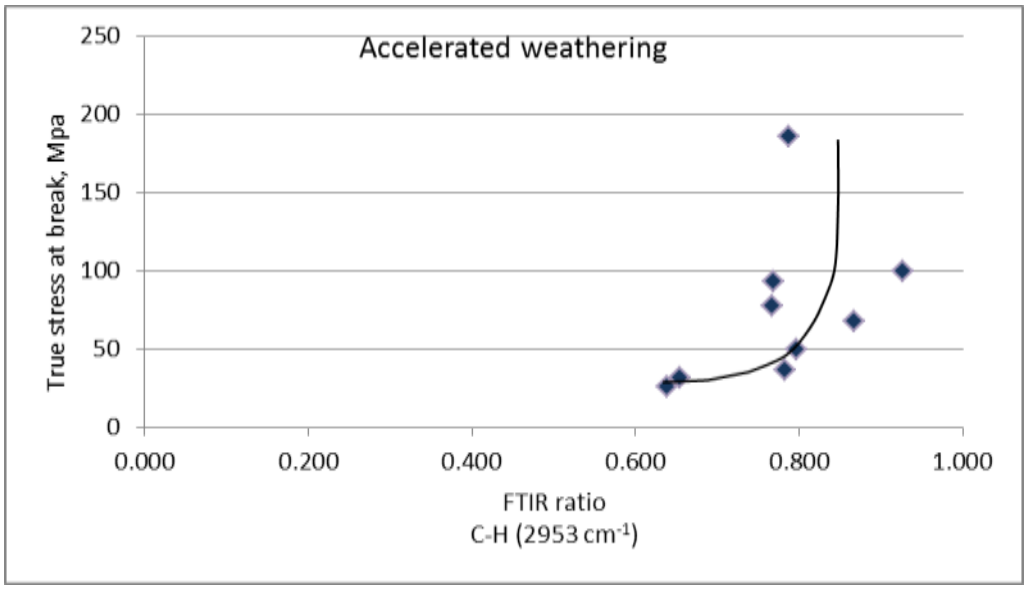

Figure7.1.8: Relationship between FTIR ratio of C-H bond and true stress at break in accelerated weathering.

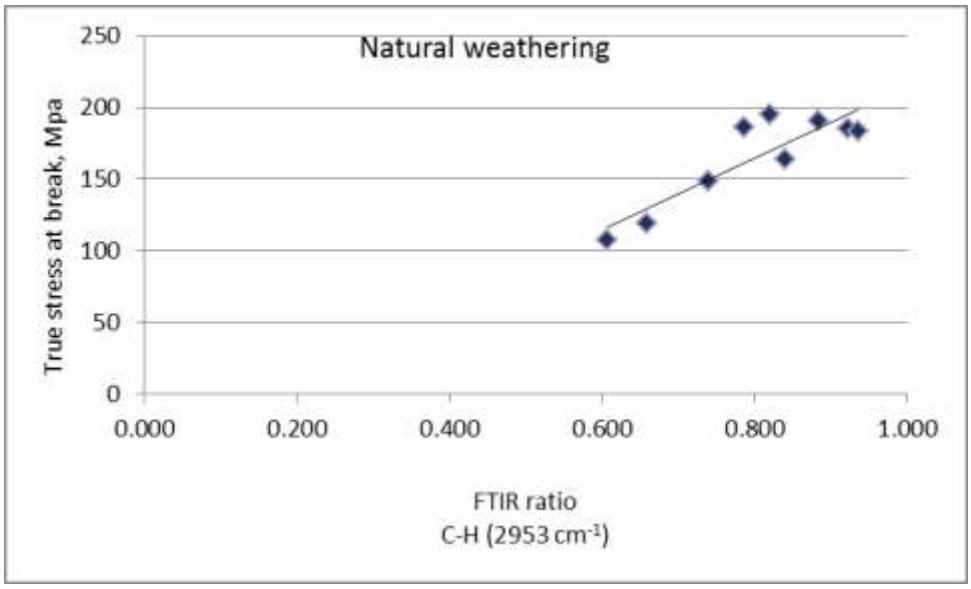

Figure7.1.9: Relationship between FTIR ratio of C-H bond and true stress at break in natural weathering.

Both accelerated and natural weathering seems to show a reduction in C-H bonds with increasing degradation which correlates with the decrease in true stress at break.

7.2 Correlation between Both Types of Weathering

The radiant dosage (radiant exposure) is the radiant energy incident over a specific area for a given period of time. Comparing the annual radiant dosage of UVA-340 lamp to the annual average solar radiation in UK-London in the UV range to get a theoretical relation between the UV dosage in these two types of environment.

Theoretical correlation between both type of weathering

Irradiance of UVA-340 at 340 nm = 0.68 W/m^2 = 0.68 J/sm^2

Annual radiant dosage = 0.68*3600*24*365 = 21444.5 kJ/m^2 of UVA-340 at 340 nm

Hence, the annual radiant dosage of UVA-340 in the UV range is determined to be $2144.45*10^3$ kJ/m^2

The annual average solar radiation received in London per square metre [137] has been shown to be 1100kWh/m^2, which is equal to $3.96*10^6$ kJ/m^2.

Now, converting this to UV range, using American ratio (avg.) = 0.0423

Table7.2.1: Annual solar radiant exposure in Arizona and Florida [138].

	Annual solar radiant exposure, MJ/m^2		
	Total (295-3000 nm)	UV (295-385 nm)	Total/UV
Arizona	8004	333	0.0416
Florida	6500	280	0.0431

So, annual UV radiant dosage in London = $0.0423*3.96*10^6$ = 167508 kJ/m^2

$$\therefore \quad \frac{\text{UV lab intensity}}{\text{Natural weathering intensity}} = \frac{2144.45 * 10^3}{167508} = 12.8$$

1 year of natural weathering = 365/12.8 = 28.5 days in accelerated weathering

1 year of accelerated weathering = 365/12.8 = 12.8 years in natural weathering

Practical correlation between both types of weathering:

According to colour change, figure6.1.3.1:

13000hr of oudoor exposure is equivalent to 1600hr of accelerated exposure, (1year of natural weathering = 45 days in accelerated weathering)

By drawing 13000hr v. 45 days and for all data, we get figure below.

According to colour and gloss change, figure6.1.3.2:

13000hr of oudoor exposure is equivalent to 820hr of accelerated exposure (1year of natural weathering = 23 days in accelerated weathering)

By drawing 13000hr v. 23 days and for all the data, we get figure below:

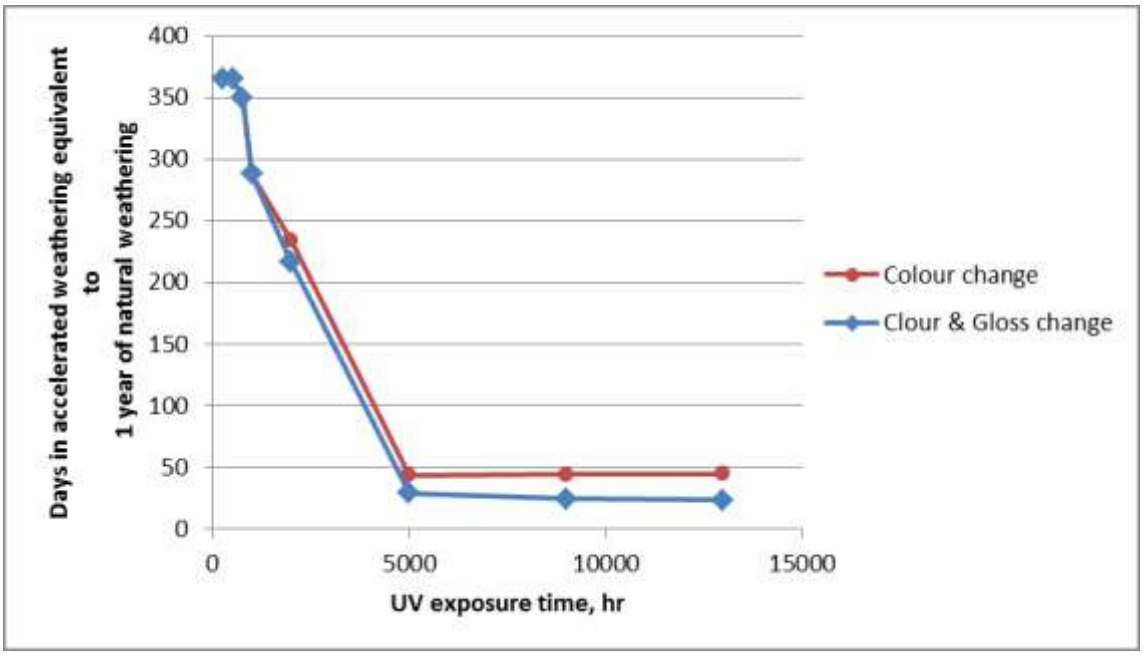

Figure7.2.1: Correlation between natural and accelerated weathering according to colour and gloss changes.

So, according to colour changes:

1year of natural weathering = 45 days (1080hr- in accelerated weathering)

And, according to colour and gloss changes:

1year of natural weathering = 26 days (624hr- in accelerated weathering)

According to failure stress, figure6.2.3.10:-

1year of natural weathering = 8 days in accelerated weathering

Theoretical correlation:

The theoretical correlation between both type of weathering shows that the annual UV radiant dosage of UVA-340 lamp is higher than the annual UV radiant dosage in London by a factor 12.8.

1 year of natural weathering ≈ 1 month in accelerated weathering

This theoretical correlation regarded the UV radiant dosage as the key factor for degradation ignoring the other effects such as temperature and humidity. That means that one year of natural weathering could be equivalent to more than one month in accelerated weathering.

Practical correlation:

Practical correlation between both types of weathering shows that;

According to colour changes:

1year of natural weathering = 1.5 months in accelerated weathering

According to colour and gloss changes:

1year of natural weathering ≈ 1 month in accelerated weathering

According to failure stress:

1year of natural weathering ≈ 1/4 month in accelerated weathering

Although, failure stress measure the actual stress at break, but the test need to be conducted with higher UV exposure period to cause further crack grow in outdoors r-PET samples so that the critical crack length can be reached to get to get better and closer correlation.

When a person looks at a green plastic object with a shiny glossy surface at the specular angle, the object does not appear to be as green because the mirror-like reflection from the light source is added to the colour of the object (the colour appears different). Usually, a person looks at the colour of a sample and ignores the specular reflection of the light source. To measure the colour of the sample in the same manner that is viewed (similar to those observed visually), the specular reflection must be excluded to get better correlation. Thus; according to colour changes:

1year of natural weathering = 1.5 months in accelerated weathering

The effect of accelerated weathering is much bigger than the natural weathering and this is due to higher radiation dosage, temperature and humidity during the test which accelerate chain scission rate that lead to faster crack grow and increase the exposed area to weathering.
Table below shows the difference between the natural UV light in London and the artificial UV light for UVA-340 lamp.

Table7.2.2: Annual radiant dosage and irradiance of sunlight and QUV radiation.

Accelerated weathering	Natural weathering (London)
Annual radiant dosage of UVA-340 in the UV range = 2144 MJ/m^2	Annual mean radiant dosage of sun light in the UV range = 167 MJ/m^2
Irradiance of UVA-340 in the UV range = 68 W/m^2	Irradiance of sunlight in the UV range = 5.31 W/m^2
Irradiance of UVA-340 at 340 nm = 0.68 W/m^2	Irradiance of sunlight at 340 nm = 0.0531 W/m^2

The radiation energy of a photon for a given wavelength, E is determined by the equation 3.19; E = hu = hc/λ

$$E = \frac{1.19 * 10^8}{\lambda} \qquad \text{.....7.1}$$

Table7.2.3: Energy of sunlight and QUV accelerated weathering radiation.

Bond	Bond dissociation energy [139]		Wavelength limit – below these values the bond breaks nm (from eq. 7.1)	Photon energy kJ/mol	
	kcal/mol	kJ/mol		sunlight	QUV (*12.8)
C – C	83	346.94	345 (UVA)	346.94	4440.83
O – O	35	146.30	818 (IR)	146.30	1872.64
C – O	85	355.30	337 (UVA)	355.30	4547.84
C – H	99	413.82	289 (UVB)	413.82	5296.896

The radiation from the sun is sufficiently energetic to break weak bonds such as O – O, C – C, C – O and none is available to break strong bond such as C – H or very strong bonds such as C = C, and C = O, which have dissociation bond energies greater than 100 kcal/mol (418 kJ/mol). However the energy of UVA-340 lamp is more than energy of the sun by a factor equal to 12.8. This can accelerate chain scission and lead to earlier crack growth.

7.3 Aspects that can Influence Prediction of Life Time

In addition to radiant dosage effect, the fluctuations in test results, temperature and humidity as well.

7.3.1 Fluctuations in results are due to the following factors:

1- Material source:

r-PET pellets are produced by pelletizing post-consumer PET flakes which are collected from wide range bottle products (water, fizzy drink, juices and oil bottles). These flakes are made from different v-PET manufacturers and therefore have different properties such as intrinsic viscosity and additives. Post-consumer bottles may be exposed to different weathering conditions such as temperature, humidity and UV dosage which vary during the day and seasons, all these factors influence and modify the physical properties of the material.

2- Processing:

During the injection moulding operation, melt temperature drops from 260°C to 70°C in the mould in 36 seconds (cooling time). During clearing of the frozen nozzle, mould temperature decreased to about 40°C, so melt temperature drops from 260 to about 40°C in 36 seconds in the mould which results in higher cooling rate and thus lower crystallinity which led to some variation in the properties of r-PET samples.

3- Environmental conditions:

Accelerated weathering conditions in QUV chambers are as follows:

8 hours UV radiation at 60°C with UVA-340 lamps at 340nm with irradiance 0.68 W/m^2 which is equivalent to $2144*10^3$ kJ/m^2 annual UV radiant dosage

followed by 4 hours condensation at 40°C with relative humidity = 100%. Both UV dosage and moisture content remain constant.

The outdoors weathering conditions cannot be controlled due to variation of temperature from a maximum of 32°C to a minimum of -1°C and a variation of humidity from a minimum of 22% to a maximum of 100%. The radiation dosage during the day and seasons also varies but the estimated annual UV radiant dosage in UK is 167 MJ/m^2. This is much lower than that dosage recommended for the QUV chamber which is designed to accelerate the process of degradation.

4- Test conditions:

Variation of temperature and humidity in the laboratory effect the mechanical properties. Therefore care was taken to ensure that temperature variation was limited to ± 2°C. There was little humidity control in the laboratory. However, this would be typical of tests conducted in laboratories.

Measurement errors can be minimized by controlling test conditions and by careful documenting of test conditions.

7.3.2 Fluctuations of temperature and humidity

1- Temperature:

Temperature in QUV chamber was 60 ºC for 8 hr and 40ºC for 4 hr a day, while annual variation of temperature outdoors between 32ºC and -1ºC

A general rule of thumb assumes that 10ºC rise in material temperature doubles the rate of reaction.

According to Arrhenius equation for a chemical reaction is given by:

$$K = A \exp(-E/RT) \quad \ldots. (7.2)$$

Where:

K = Reaction rate (s^{-1})

A = Constant

E = Activation energy of the reaction (J/mol)

R = Gas constant (8.314 J/mol K)

T = temperature, K [140].

If the temperature is 32ºC, so the difference between 60 and 32ºC is ≈ 30ºC that means the rate of reaction in accelerated weathering is 6 times more than that in natural weathering for 8 hr and 2 times more for 4 hr.
If the temperature is -1ºC, so the difference between 60 and -1ºC is ≈ 60ºC that means the rate of reaction in accelerated weathering is 12 times more than that in natural weathering for 8 hr and 8 times more for 4 hr.
So, the rate of reaction in accelerated weathering varies annually between 12 to 2 times more than that in natural weathering leading to accelerate the rate of deterioration.

2- Humidity:

Relative humidity in QUV chamber was 100% for 24 hr a day, while annual variation of relative humidity 22% to 100% outdoors (London-UK). Water absorption of PET depends on the temperature, degree of crystallinity, shape of the sample and relative humidity. Water content greater than 0.02% can result in a considerable decrease in molecular weight by hydrolytic chain scission.
PET molecule contains ester bonds which are sensitive to water attack at high temperatures especially above the glass transition temperature of the polymer and begins to become significant at temperatures of 100°C and above in the presence of moisture.

7.4 General Overview

During pelletizing process by extrusion and the injection moulding process, material degradation occurs at the high temperature and under the severe mechanical deformation between screw and barrel and in the die. Changes in the material will occur due to oxidation, hydrolysis, thermal degradation and less significantly by mechanical shear. This leads to chain scission that produces shorter chains. This leads to increasing number of chain ends. Glass transition temperature will therefore decrease and so will the degree of crystallinity as the shorter chains will not form sufficient free folds for crystal formation. As the amorphous volume increases, the greater free volume allows greater absorption of moisture and other aqueous solutions. Moreover, the shorter chain lengths, will lead to a reduction in the number of entanglements

between chains, making it is less difficult for chains to slide past each other and therefore there is less resistance to flow. The melt flow rate will be seen to increase.

In the current test, r-PET samples, 4mm thick were exposed to natural and accelerated weathering. The internal body of specimens were substantially unaffected by degradation for long exposure time and this is confirmed by MFI and DSC results. However, the surface of the specimens is affected by degradation which is seen in FTIR analysis, colour and gloss change.

The carboxylic acid degradation products produced on the surface can be detected by FTIR spectroscopy by measuring the absorbance of the carbonyl bond, C=O which increases with increasing irradiation time for both types of weathering. They are produced due to chain scission by Norrish I and Norrish II mechanisms. Of these, Norrish II appears to dominate over Norrish I as Day and Wiles (1971) reported “this assumption is based on the established evidence that aliphatic and aromatic ester containing γ-hydrogen atom decomposes photochemically by an intramolecular rearrangement into an olefin and the corresponding acid”. Moreover, Norrish type II reaction automatically proceeds through a cyclic six-membered transition state. This requires trans glycol conformation and a gauche conformation with respect to the CH_2-O bonds of the glycol linkage. As a result the hydrogen atom is removed in each molecule.

The decrease in trans conformers and increase in gauche conformers indicates that there is a transformation in the molecular changes to a more random, less ordered structure due to the chain scission by UV attack.

In natural weathering, both colour and gloss measurements increase to a peak value at about 2000 hr after which the value drops and levels off. In the case of accelerated weathering, there is a greater increase in colour and gloss variation which continues up to 5000 hr when it peaks. The level drops slightly and then levels off.

This indicates that the effect of degradation takes place strongly during this period of exposure due to the rapid formation of flaws as a result of a high rate of chain scission caused by high rate of UV absorption and high oxygen diffusion in the surface layer in the early stages of exposure in both types of weathering.

The rate of increase in colour and gloss change then reduces because the material consumed at the surface layer with the extent of UV exposure and degradation products act as a barrier for further UV and oxygen attack as well as limited diffusion of UV and oxygen beyond the surface layer. Eventually colour and gloss changes reaches steady state.

Chain scission leads to shorter chain lengths and therefore lower molecular weight. This increases the number of ends per unit volume and hence the free volume. Oxygen and water molecules diffuse more easily into the available spaces converting them to high stressed locations that lead to the formation of microvoids. During weathering, if the stress in these locations increases due to the accumulation of diffused water molecules, the microvoids will grow into microcracks. The formation of microcracks will increase the roughness of the surface and cause more scattering to the measured reflected light from the surface of the specimen during testing. This will result in decrease in colour and gloss values.

After 2000hr of UV exposure in the QUV cabinet, the surface of the sample appears chalky. This is caused by migration of pigment molecules to the surface.

The exhaustion of pigment molecules results in losing their original light absorption properties and thus the amount of reflected light reduces. With the extent of UV exposue, the pigment concentration will decrease and will cause the colour to fade as seen in the decrease in yellowness, redness and whiteness.

Tensile tests were conducted at temperature at 19 ^{o}C ± 1 and test speed of 10 mm/s. The general behaviour of r-PET under tension before UV exposure is ductile behaviour and it remains the same after 13000 hr of exposure outdoors. In accelerated weathering, it changed to brittle behavior after 2000 hr of exposure in accelerated weathering.

The yield stress and elongation at yield remain unchanged for outdoor samples during the period of UV exposure because chain scission occurs mostly in the amorphous regions and only on the surface and has no significant effect in the crystalline region. The amorphous regions have more free volume between chains, facilitate oxygen diffusion and water penetration and accelerate chain scission process.

After 1000hr of accelerated UV exposure, yield stress and elongation at yield dropped significantly indicating that there is a significant effect for chain scission. Surface flaws are sufficiently large to exceed the crack value for crack propagation. Yield stress is decreasing with the extent of exposure and the material start to yield earlier due to chain pull out from entanglement.

Under tension, the microcracks at the degraded surface extend and propagate to the undegraded regions inside the specimens leading to failure. The sharp drop in the failure stress and elongation at failure for r-PET samples indicates that the formation of microcracks is from the early stages of exposure. Then slight drop in failure stress and elongation at failure because chain scission becomes less with the extent of UV exposure because the material consumed at the surface layer as mentioned before.

For outdoor samples, failure stress remained unchanged for the first 1000 hr of sunlight exposure because the microcracks in the degraded surface are shorter than critical crack length for propagation. Failure stress dropped less significantly indicating that these microcracks became bigger and able to propagate under the tensile stress. While elongation at failure remained constant as seen in the graphs, calculation showed very slight decrease after 13000 hr of outdoor exposure.

After 13000 hrs of exposure to sunlight, r-PET samples failed in a ductile manner due to its high toughness, while those exposed to UV lamps at 340 nm wavelength failed in a brittle manner after 250 hrs. This indicates the transition from ductile to brittle failure just after 10 days of accelerated UV exposure as surface cracks reached critical length for propagation to failure.

For accelerated weathering samples, the impact strength remained unchanged in the first 1000 hr of exposure. There was no effect of cracks on impact strength, because flaws are small and able to absorb and transmit the applied energy. The impact strength then decreased slightly up to 5000 hr of exposure during which the effects of flaws started but was not significant. As the time of UV exposure increased up to 9000 hr, the impact strength sharply dropped and remained unchanged afterwards up to 13000 hr of UV exposure.

After 5000 hr of UV exposure, optical images show that the surface layer has a high density of flaws. This explains the sharp drop in impact strength. These

flaws have the effect of causing a stress concentration; the local stress in the vicinity of the crack tip is higher than that applied to the body as a whole, so it absorbs the energy, grows and joins leading to catastrophic failure.

While, r-PET samples in natural weathering are tough and strong, they can withstand the weathering factors because chain scission proceeds much more slowly compared to that in accelerated weathering.

After 13000 hrs, the melt flow characteristics and crystallinity remained unaffected by the length of UV exposure for both natural and accelerated weathering. This confirms that the photodegradation is a surface effect.

CHAPTER EIGHT

CONCLUSION AND FURTHER WORK

8.1 Conclusion

Recycled PET pellets were exposed to UV light outdoors and accelerated weathering up to 13,000 hr. The mechanical behaviour (tensile and impact), thermal behaviour (DSC), molecular structure analysis (FTIR), flow characteristics (MFI) and surface properties (colour and gloss) were characterized.

Although the weathering factors in QUV accelerated weathering chamber are controlled and the outdoors weathering factors are variable through the day and seasons, the correlation between both types of weathering is generally accepted by industry.

The estimated typical 1 year of natural weathering equivalent to accelerated weathering gives a good indication for a life time assessment of recycled polyethylene terephthalate. According to colour measurement:

1year of natural weathering = 1.5 months in accelerated weathering

From the prospective of the user of the material, what is important, is the appearance of the material in use, therefore the loss of colour is a very important factor in deciding when the material fails. Colour change measures directly the effect of surface degradation due to UV radiation.

The whole body of the specimens was substantially unaffected by degradation for long exposure time and this is confirmed by MFI and DSC results. However, the surface of the specimens is affected by degradation which is seen in FTIR analysis, colour and gloss change. This explains that the photodegradation is a surface effect.

In the first 3 months which equates to about 2000hr of UV exposure there was maximum variation in colour and gloss for r-PET samples in natural weathering and 7 months (5000hr) in accelerated weathering. This indicates that the effect of degradation takes place strongly in the early stages of UV exposure due to high rate of chain scission. This results in high rate of crack formation which increased the roughness of the surface and causes more scattering to the

measured reflected light from the surface of the specimen. The pigment concentration also decreased with the extent of UV exposure due exhaustion of pigment molecules which means losing their original light absorption properties, and with that the colour of the light that they reflect fades.

As a result, colour changes exceeded 1.2, so r-PET products are not suitable for colour properties as an essential outdoors requirement. Also the chalky appearance at the surface of the sample after 3 months of UV exposure in the QUV cabinet due to migrating of pigment molecules to the surface makes the material unsuitable for outdoor use from a point of view.

FTIR analysis shows that increase in the gauche ratio related to amorphous content and decrease in the trans ratio relating to crystalline content for both types of weathering. This indicates that the structure is transformed to a less ordered, more random. The crystalline regions are converted to amorphous after the UV radiation due to chain scission by Norrish Type I and II mechanism. The photo degradation of PET strongly influences the spectral changes of the carbonyl bonds (C=O) which appear at wavelength of 1711 cm^{-1}. Carboxylic acid is formed as a result of degradation and increases with the extent of UV exposure in both types of weathering; the formation of carboxylic acid by Norrish II is dominated over Norrish I.

The decrease in mechanical properties during UV exposure is because of the molecular changes due to chain scission process, which might be seen in FTIR analysis.

After 18 months (13,000hr) of exposure to sunlight, the yield stress and elongation at yield remained constant compared to exposure under UV lamp of wavelength 340 nm which shows a decrease in both values after 41 days (1000hr) of exposure.

There is a sharp decrease in the failure stress and elongation at failure for the QUV cabinet samples from the beginning of exposure, while for the outdoor samples, failure stress dropped significantly after 1000hr of UV exposure and elongation at failure remained unchanged although calculations showed very slight decrease.

The drop in elongation at failure and failure stress is related to surface degradation which is seen in the form of microcracks on the surface. It takes about 1000 hr of UV exposure outdoors for surface degradation to cause effective microcracks reaching critical crack length, leading to failure and in the

accelerated weathering, effective microcracks start right from the beginning. In outdoor weathering, the crack lengths are shorter than the critical value and reached that value well after 1000 hr of exposure.

The transition from ductile to brittle failure occurs just after 10 days (250hr) of accelerated UV exposure. The samples in natural weathering are tough and strong and so can withstand the sudden loading. After 7 months (5000hr) of accelerated UV exposure, the impact strength dropped sharply, so r-PET is not recommended for high toughness applications without the addition of UV absorber.

8.2 Further Work

The current study should be expanded to consider the effect of temperature and humidity on other environments.

For thick samples such as the one which is used in this study, extend the period of UV exposure so the critical crack length for outdoor samples can be reached thus giving better and closer correlation with respect to failure stress.

A study using very thin samples may allow a better understanding of the effects of surface degradation in short UV exposure period.

UV absorbers may be added to improve stability against degradation and thus extending the life time of the polymer for outdoor applications.

Further study of multiple recycling to analyse degradation would be useful, so that some correlation can be made for a better understanding.

REFERENCES

1. John Scheir, Polymer Recycling: Science, Technology and Applications, John Wiley and sons Ltd, England, 2001.
2. http://www.Wasteonline.org.uk/resources/InformationSheets/Plastics.htm (15/10/2010).
3. Brandrup, Bittner, Menges, Michaeli, Recycling and Recovery of Plastics, Hanser Gardner publishers, New York, (1995).
4. http://www.petresin.org/ (15/3/2015).
5. Donald E. Duvall, Environmental Degradation of PET and Its Potential Effect on Long-Term Mechanical Properties of Oriented PET Products, Polymer – Plastics Technology and Engineering, 34 (1995) 2, p: 227-242.
6. http://www.earthodyssey.com/symbols.html (6/11/2010).
7. F. Awaja and D. Pavel, Recycling of PET, European Polymer Journal 41 (2005) 7, p: 1453-1477.
8. http://www.goodfellow.com (15/11/2012).
9. A. Davis and D. Sims, Weathering of Polymers, Applied Science Publishers Ltd, England, (1983).
10. K. Regel, W. Michaeli, Processing of PET Without Pre-drying, ANTEC 1996, p: 3104.
11. PET-Recycling Forum; "Current Technological Trends in Polyester Recycling"; 9th International Polyester Recycling Forum Washington, 2006, Sao Paulo.
12. B. Ranby and J. F. Rabek, Photodegradation, Photo-oxidation and Photostabilisation of Polymers: Principles and Applications, John Wiley and Sons Ltd, 1975.
13. Mascia, The Role of Additives in Plastics, Edward Arnold Publishers Ltd, London, 1974.
14. S. P. Pappas and F. H. Winslow, Photodegradation and Photostabilization of Caotings, American Chemical Society, ACS Symposia Series, 151, USA, 1981.
15. http://www.q-lab.com/EN_Weblit/QUV-Q-SUN-LU-8009_1_pdf (7/12/2010).

16. C. Capanescu and Corneliu, Paint and Coatings Industry, 18 (2002)9, p:50.
17. P. Painter and M. Coleman, Fundamentals of Polymer Science: An Introductory Text, 2nd edition, CRC Press, USA, 1997.
18. John Scheirs, Modern Polyesters: Chemistry and Technology of Polyesters and Copolyesters, John Wiley and Sons Ltd, England, 2003.
19. P. Painter and M. Coleman, Essentials of Polymer Science and Engineering, Destech publications, Inc, UK, 2008.
20. Z. Chen, The Crystallization of Poly(ethylene terephthalate) Studied by Thermal Analysis and FTIR Spectroscopy, Ph.D Thesis, University of Birmingham, 2012.
21. D. C. Bassett, Principle of Polymer Morphology, Cambridge University Press, UK, 1981.
22. B. Wunderlich, Macromolecular Physics: Crystal Nucleation Growth, Volume 2, Anealing Academic Press, London, 1976.
23. E. Charles, J. Carraher, Seymour/Carraher's Polymer Chemistry, 6th edition, CRC Press, New York, 2003.
24. I. Ward, J. Sweeney, Mechanical Properties of Solid Polymers, 3rd edition, John Wiley Publisher Ltd., UK, 2013.
25. M. Asanishi, T. Takaki and Y. Tomita, AES – ATEMA' 2007 International Conference, Montreal, Canada, August 06 -10, 2007, pp. 195 – 203.
26. A. Ravve, Principles of Polymer Science, Springer Science and Business Media LLC, New York, 1995.
27. L. H. Sperling, Introduction to Physical Polymer Science, John Wiley and Sons Inc., Canada, 2006.
28. V. Machoviè, J. Andertová, L. Kopecký, M. Èerný, L. Borecká, O. Pøibyl, F. Koláø and J. Svítilová, Effect of Aging of PET fibre on the Mechanical Properties of PET Fibre reinforced cement Composite, Ceramics-Silikáty, 52 (2008) 3, p:172-182.
29. M. Chanda, Introduction to Polymer Science and Chemistry: A Problem-Solving Approach, 2nd edition, CRC Press., USA, 2013.
30. http://www.polyester-technology.com/ (1/11/2011).

31. N. J. Mills, Plastics Microstructure and Engineering Applications, 3rd edition, Butterworth – Heinemann, UK, 2005.

32. http://www.pharosproject.net/uploads/files/sources/1828/1406921711.pdf (24/11/2015).

33. D. B. V. Parker, Polymer Chemistry, Applied Science Publishers Ltd, London, 1974.

34. Ferdinand Rodrigues, Principles of Polymer System, 2nd edition, Hemisphere Publishing Corporation, London, 1982.

35. Norman Grassie and Gerald Scott, Polymer Degradation and Stabilisation, Cambridge University Press, London, 1985.

36. http://www.iupac.org/publications/pac/pdf/1972/pdf/3001x0135.pdf (30/12/2010).

37. Norman S. Allen and Michele Edge, Fundamentals of Polymer Degradation and Stabilisation, Elsevier Science Publishers Ltd, England, 1992.

38. Robert L. Feller, Accelerated Aging: Photochemical and Thermal Aspects, J. Pual Getty Trust, USA, 1994.

39. G. Li, Y. Chen and X. Tang, Geosynthetics in Civil and Environmental Engineering, Proceedings of the 4th Asian Regional Conference on Geosynthetics in Shanghai, China, 2008.

40. http://www.q-lab.com/EN_Weblit/Weathering-LU-0822.pdf (20/12/2010).

41. Plastic Design Library, The Effect of UV Light and Weather on Plastics and Elastomers, William Andrew Inc., USA, 1994.

42. http://www.q-lab.com/EN_Weblit/QUV-LU-8160_web.pdf (7/12/2010).

43. M. Day and D. M. Wiles, Photochemical Degradation of Poly(ethylene terephthalate). I. Irradiation Experiments with the Xenon and Carbon Arc, Journal of applied Polymer Science 16 (1972) 1, p: 175-189.

44. www.labmat.eu/document/docGB/06DA_QUV_B.pdf (9/12/2010).

45. W. Schnabel, Polymer Degradation: principles and Practical Applications, Macmillan Publishing Co., Inc., New York, 1981.

46. http://handle.dtic.mil/100.2/ADA301675 (22/11/2010).

47. S. Mancini and M. Zanin, Degradation of Post-Consumer PET During Recycling by Injection Moulding, Polymer Recycling 3 (1997/98) 3, p: 239-245.

48. Gerald Scott, Polymers and The Environment, The Royal Society of Chemistry, UK, 1999.

49. Stuart Fairgrieve, Degradation and Stabilisation of Aromatic Polyesters, Smithers Rapra, 2009.

50. N. Grassie, Development in Polymer Degradation, volume 5, Applied Science Publishers Ltd, England, 1984.

51. J. Campanelli, M. Kamal and D. Cooper, A kinetic Study of the Hydrolytic Degradation of Polyethylene Terephthalate at High Temperatures, Journal of Applied Polymer Science 48 (1993) 3, P: 443-451.

52. J. Attwood, M. Philip, A. Hulume, G. Williams and P. Shipton, The Effects by Ultraviolet Radiation of Recycled Polyolefin Blends, Polymer Degradation and stability 91 (2006) 12, p: 3407-3415.

53. E. Edge, M. Hayes, M. Mohammadian, N. S. Allen and T. S. Jewitt, Aspects of Poly(ethylene terephthalate) Degradation for Archival Life and Environmental Degradation, Polymer Degradation and Stability 32 (1991) 2, p: 131-153.

54. http://www.cropscan.com/response.html (11-11-2015).

55. J. F. Rabek, Polymer Photodegradation: Mechanisms and Experimental Methods, 1st Edition, Chapman and Hall, London, 1995.

56. Douglas M. Grossman, Ultraviolet Light for Accelerated Weathering, Pitture E Vernici Europe 3 (1991).

57. M. Day and D. M. Wiles, Photochemical Degradation of Poly(ethylene terephthalate). III. Determination of Decomposition Products and Reaction Mechanism, Journal of applied Polymer Science 16 (1972) 1, p: 203-215.

58. http://alexandria.tue.nl/extra2/200910369.pdf (20/10/2013).

59. G. Fechine, M. Rabello and R. Souto, Surface Characterization of Photodegraded Poly(ethylene terephthalate). The Effect of Ultraviolet Absorbers, Polymer 45 (2004) 7, p: 2303-2308.

60. A. Shultz and S. Leahy, Random Chain Scission of Polyethylene Terephthalate by Light Determination of Active Wavelength V (1961) 13, P: 64-66.

61. M. Day and D. M. Wiles, Photochemical Decomposition Mechanism of Poly(ethylene terephthalate), Journal of Polymer Science 9 (1971) B9, p: 665-669.

62. M. Day and D. M. Wiles, Photochemical Degradation of Poly(ethylene terephthalate). II. Effect of Wavelength and Environment on the Decomposition Process, Journal of applied Polymer Science 16 (1972) 1, p: 191-202.

63. D. M. Wiles, The Effect of Light on Some Commercially Important Polymers, Polymer Engineering and Science 13 (1973) 1, p: 74-77.

64. P. Blais, M. Day and D. Wiles, Photochemical Degradation of Poly(ethylene terephthalate). IV. Surface Changes, Journal of applied Polymer Science 17 (1973) 6, p: 1895-1907.

65. S.Krishnan, S. B. Mitra, P. M. Russell and G. Benz, Quantitative of Non Volatile Components from the Photochemical Decomposition of Poly(ethylene terephthalate), American Chemical Society 1985, p: 389-401.

66. N.Ilišković and M. Bravar, Correlation of Physico-chemical, Mechanical and Electrical Properties of Ultraviolet-degraded Poly(ethylene terephthalate), Polymer Degradation and Stability 15 (1986) 2, p: 173-182.

67. S. Norman, M. Edge, M. Mohammadian and K. Jones, Physicochemical Aspects of the Environmental Degradation of Poly(ethylene terephthalate), Polymer Degradation and Stability 43 (1994) 2, p: 229-237.

68. W. Wang, A. Taniguchi, M. Fukuhara and T. Okada, Surface Nature of UV Deterioration in Properties of Solid Poly(ethylene terephthalate), Journal of Applied Polymer Science 67 (1998) 4, p: 705-714.

69. W. Wang, A. Taniguchi, M. Fukuhara and T. Okada, Two-Step Process of Poly(ethylene terephthalate), Journal of Applied Polymer Science 74 (1999) 2, p: 306-310.

70. G. Fechine and R. Souto, Structural Changes During Photodegradation of Poly(ethylene terephthalate), Journal of Materials Science 37 (2002) 23, p: 4979-4984.

71. Z. Zhu and M. Kelley, IR Spectroscopic Investigation of the Effect of Deep UV Irradiation on PET Films, Polymer 46 (2005) 20, p: 8883-8891.

72. G. Fechine, M. Rabello and R. Souto, The Effect of Ultraviolet stabilizers on the

Photodegradation of Poly(ethylene terephthalate), Polymer Degradation and Stability 75 (2002) 1, p: 153-159.

73. G. Fechine, P. Christensen, T. Egerton and J. White, Evaluation of Poly(ethylene terephthalate) Photostabilisation using FTIR Spectrometry of Evolved Carbon Dioxide, Polymer Degradation and Stability 94 (2009) 3, p: 234-239.

74. C. Hurley and G. Leggett, Quantitative Investigation of the Photodegradation of Polyethylene Terephthalate Film by Friction Force Microscopy, Contact-Angle Goniometry and X-ray Photoelectroscopy, ACS Applied Materials and Interfaces 1 (2009) 8, p: 1688-1697.

75. S. Fernando, P. Christensen, T. Egerton and R. Eveson, Carbon Dioxide Formation During Initial Stages of Photodegradation of Poly(ethylene terephthalate) (PET) Films, Materials Science and Technology 25 (2009) 4, p: 549-555.

76. P. Russo, D. Acierno, L. Marinucci, A. Greco and M. Frigione, Influence of Natural and Accelerated Weathering on Performance of Photoselective Greenhouse Films, Journal of Applied Polymer Science, 127 (2013) 3, p:2213-2219.

77. M. Tuasikal, O. Alothman, M. Luqman, S. Al-Zahrani and M. Jawad, Influence of Natural and Accelerated Weathering on the Mechanical Properties of Low-Density Polyethylene Films, International Journal of Polymer Analysis and Characterization, 19 (2014) 3, p:189-203.

78. http://www.brabender-mt.de/index.php?id=2116&type=101 [7/7/2014].

79. S. Hosseini, S. Taheri, A. Zadhoush and A. Zeinabad, Hydrolytic Degradation of Poly(ethylene terephthalate), Journal of Applied Polymer Science 103 (2007) 4, p: 2304-2309.

80. http://blog.cencophysics.com/2009/07/density-liquids-solids-pycnometer-method/ (5/6/2013).

81. J. Cowie and V. Arrighi, Polymers: Chemistry and Physics of Modern Materials, 3rd edition, CRC Press, USA, 1997.

82. S. F. Sun, Physical Chemistry of Macromolecules, Basic Principles and Issues, John Wiley and Sons Inc, New York, USA, 1994.

83. C. E. Carraher, Introduction to Polymer Chemistry, Taylor and Francis CRS, U.S.A, 2007.

84. H. G. Ellias, An Introduction to Polymer Chemistry, VCH publication, U.S.A, 1997.

85. P. E. Slade, Polymer Molecular Weights, Part I, Marcel Dekker Inc, New York, 1975.

86. R. H. Boyd and P. J. Phillips, The Science of Polymer Molecules, Cambridge University Press, New York, 1993.

87. A. Rudin, The Elements of Polymer Science and Engineering, 2nd edition, Academic Press, U.S.A, 1999.

88. V. R. Growariker, N. V. Viswanathan and J. Sreedhar, Polymer Science, John Wiley and Sons, New York, 1986.

89. http://investigadores.ciqa.mx/maestria/docs/reologia3a.pdf (4/4/2015).

90. http://pslc.ws/macrog/dsc.htm (13/12/2010).

91. J. Dean, Analytical Chemistry Handbook, McGraw-Hill, New York, 1995.

92. E. Punjor, a Practical Guide to Instrumental Analysis, CRC Press, USA, 1995.

93. D. Skoog, F. James and T. Nieman, Principles of Instrumental Analysis, 5th edition, Saunders College Publisher, New York, 1998.

94. M. Pluta, Z. Bartczak, A. Pawlak, A. Galeski and M. Prac#ella, Phase Structure and Viscoelastic Properties of Compatibilized Blends of PET and HDPE Recyclates, Journal of Applied Polymer Science, 82(2001) 1423-1436.

95. P. R. Griffiths and J. A. De Haseth, Fourier Transform Infrared Spectroscopy, 2nd edition, John Wiley and Sons Inc., U.S.A, 2007.

96. http://www.siliconfareast.com/FTIR.htm (1/12/2010).

97. B. K. Sharma, Spectroscopy, Krishna Prakashan Media Ltd., India, 1981.

98. M. R. Derrick, D. Stulik and J. M. Landry, Infrared Spectroscopy in Conservation Science, Getty Publications, U.S.A, 2000.

99. B. C. Smith, Fundamentals of Fourier Transform Infrared Spectroscopy, 2nd edition, CRC Press, U.S.A, 2011.

100. D. Campbll, R. A. Pethrick and J. R. White Arrighi, Polymers Characterization:

Physical Techniques, 2nd edition, Stanley Thornes Publishers, UK, 2000.

101. A. Ajji, J. Guevremont, K. C. Cole and M. M. Dumoulin, Orientation and Structure of Drawn Poly (ethylene terephhalate), Polymer 37 (1996) 16, p: 3707-3714.

102. C. O. Lee, B. Chae, S. B. Kim, Y. M. Jung and S. W. Le, Two-Dimentional Correlation Analysis Study of the Photo-Degradation of Poly (ethylene terephthalate) Film, Vibrational Spectroscopy 60 (2012), p:142-145.

103. E.Pearce, B. Bulkin and M. Yeen , Fourier Transform IR Spectroscopy for the Study of Polymer Degradation – Thermal and Thermooxidative Degradation of Polyethylene Terephthalate, American Chemical Society 1983, p: 571-593.

104. Z. Chen, J. Hay and M. Jenkins, FTIR Spectroscopic Analysis of poly(ethylene terephthalate) on Crystallization , European Polymer Journal 48 (2012) 9, p: 1586-1610.

105. http://infrared.als.lbl.gov/BLManual/IR_Interpretation.pdf (22/10/2013).

106. B. C. Smith, Infrared Spectral Interpretation: A Systematic Approach, CRC Press, U.S.A, 1999.

107. B. H. Stuart, Infrared Spectroscopy: Fundamentals and Applications, John Wiley and Sons Ltd, England, 2004.

108. J. Coates, Interpretation of Infrared Spectra: A Practical Approach in Encyclopedia of Analytical Chemistry, John Wiley and Sons Ltd, Chichester, 2000.

109. D. W. Mayo, F. A. Miller, R. W. Hannah, Course Notes on the Interpretation of Infrared and Raman Spectra, John Wiley and Sons Publication, U.S.A, 2003.

110. J. R. Ferraro and L. J. Basile, Fourier Transform Infrared Spectroscopy: Applications to Chemical Systems: Tables and Charts, Volume4, academic Press Inc., U.S.A, 1985.

111. N. P. G. Roeges, A Guide to the Complete Interpretation of Infrared Spectral of Organic Structures, John Wiley and Sons Ltd, UK, 1994.

112. G. Socrates, Infrared and Raman Characteristic Group Frequencies:Tables and Charts, 3rd edition, John Wiley and Sons Ltd, UK, 2001.

113. http://www.rsc.org/learn-chemistry/resource/res00001299/infrared-

spectroscopy (22/10/2013).

114. S. A. Jabarin and E. A. Lofgren, Environmental Aging and Stress-Cracking of Poly (ethylene terephthalate), Polymer Engineering and Science 32 (1992) 2, p:146-156.

115. M. F. Aziz and W. N. A Ngeline, Characteristics Study of Polyethylene Terephthalate (PET) used for Commercial Drinking Bottles under Ultaviolet (UV) Radiation, Journal of Sustainability Science and Management 5 (2010)1, p:47-56.

116. H. Fashandi, A. Zadhoush and M. Haghighat, Effect of Orientation and Crystallinity on the photodegradation of Poly(ethylene terephthalate), polymer Engineering and Science, 48 (2008) 5, P:949-956.

117. http://www.konicaminolta.com/instruments/download/catalog/color/pdf/cm2500d_catalog_eng.p (20/11/2014).

118. http://www.konicaminolta.com/instruments/knowledge/color/pdf/color_communication.pdf (9/7/2014).

119. J. L. Koenig, Spectroscopy of Polymers, 2nd edition, Elsevier Science Inc., U.S.A, 1999.

120. R, S. Hunter and R. W. Harold, The Measurement of Appearance, 2nd edition, John Wiley and Sons Inc., Canada, 1987.

121. K. Nishikida, E. Nishio and R. W. Hannah, Selected Applications of Modern FT-IR Techniques, Kodansha Ltd., Japan, 1995.

122. www.drb-mattech.co.uk/uv%20degradation.html (22/11/2010).

123. John Scheir, Compositional and Failure Analysis of Polymers: A practical Approach, John Wiley and sons Ltd, England, 2002.

124. M. Wijdekop, J. C. Arnold, M. Evans, V. John and A. Alloyd, Monitoring the Reflectance Spectroscopy the Colour Change of PVC Plastisol Coated Strip Steel Due to Weathering, Materials Science and Technology, 21 (2005) 7, p:791-797.

125. http://www.google.co.uk/patents/US7193001 (15/7/2014).

126. R. Brown, Handbook of Polymers Testing: Physical Method, Marcel Dekker Inc., U.S.A., 1999.

127. W. D. Callister, D. G. Rethwisch, Fundamentals of Materials Science and Engineering: An Integrated Approach, 4th edition, John Wiley and Sons Inc., U.S.A., 2012.

128. A. K. Rakhit, The Essentials of Material Science and Technology for Engineers, Xlibris LLC, U.S.A., 2013.

129. C. A. Daniel, Polymers: Structure and Properties, Technomic Publishing Company Inc., U.S.A., 1989.

130. R. W. Messler, The Essence of Materials for Engineers, Jones and Bartlett Learning LLC, U.S.A., 2011.

131. Y. W. Chung, Introduction to Materials for Engineering, CRC Press, U.S.A., 2007.

132. M. Kutz, Handbook of Materials Selection, John Wiley and Sons Inc., U.S.A., 2002.

133. http://www.wmtr.com/en.charpy.html (1/4/2015)

134. D. Francois and A. Pineau, From Charpy tp Present Impact Testing, Elsevier Science Ltd., UK, 2000.

135. K. Friedrich, S. Fakirov and Z. Zhang, Polymer Composites from Nano- to Mcrio-Scale, Springer Science and Business Media Inc., U.S.A, 2005.

136. R. O. Ebewele, Polymer Science and Technology, CRC Press, U.S.A, 2000.

137. http://www.dardni.gov.uk (11/11/2015).

138. www.strenometer.dk/files/downloads/**guidebook**.pdf (1/7/2014).

139. H. Yasuda, Magneto Luminous Chemical Vapor Deposition, CRC Press, U.S.A, 2011.

140. M. Clugston and R. Flemming, Advanced Chemistry, Oxford University Press, UK, 2000.

APPENDIX A

Density Data

Table A1: Density data for CLR-r-PET flakes and its pellets at screw speed 60 rpm.

	Flakes	Flakes	Flakes	Pellets-60rpm	Pellets-60rpm	Pellets-60rpm
W1	26.8579	26.8579	26.8579	26.8579	26.8579	26.8579
W2	27.2632	27.2611	27.2743	27.4100	27.2621	27.2623
W3	76.2603	76.2504	76.2667	76.2950	76.2512	76.2547
W4	76.1588	76.1588	76.1588	76.1588	76.1588	76.1588
Density (g/ml)	1.3302	1.2901	1.3458	1.3236	1.2925	1.3070
Avg.	1.3220			1.3077		
S.D.	0.0287			0.0155		

Table A2: Density data for pellets of CLR-r-PET flakes at screw speed 85 rpm and CLR/KUDOS R-PET pellet.

	Pellets-85-rpm	Pellets-85rpm	Pellets-85rpm	KUDOS Pellets	KUDOS Pellets	KUDOS Pellets
W1	26.8579	26.8579	26.8579	23.2886	23.2886	23.2886
W2	27.2738	27.2701	27.2778	23.5471	23.7581	23.8081
W3	76.2478	76.2536	76.2478	72.6259	72.6778	72.6895
W4	76.1588	76.1588	76.1588	72.5565	72.5565	72.5565
Density (g/ml)	1.2724	1.2948	1.2652	1.3630	1.3444	1.3401
Avg.	1.2762			1.3492		
S.D.	0.0162			0.0121		

Table A3: Density data for r-PET samples before UV exposure.

	r-PET before UV exposure	r-PET before UV exposure	r-PET before UV exposure
W1	23.2886	23.2886	23.2886
W2	23.5377	23.4501	23.6867
W3	72.6134	72.5893	72.6365
W4	72.5565	72.5565	72.5565
Density (g/ml)	1.2922	1.2512	1.2478
Avg.	1.2637		
S.D.	0.0247		

Water Content Measurements

Table A4: Water content measurements for CLR-r-PET flakes and its pellets at screw speed 60 and 85 rpm and CLR/KUDOS-r-PET pellets.

	Water Content (%)	Water Content (%)	Water Content (%)	Avg.	S.d.
CLR-r-PET-Flakes	0.338	0.340	0.333	0.337	0.004
Pellets-60 rpm	0.417	0.421	0.415	0.418	0.003
Pellets-85 rpm	0.443	0.446	0.441	0.443	0.003
CLRKodos-r-PET-pellets	0.168	0.164	0.162	0.165	0.003

Health and Safety:

- There are no specific requirements for handling r-PET.
- Calcium hydride is flammable solid and water reactive and should be handled as a potential health hazard. Inhalation produces damaging effects on the mucous membranes and upper respiratory tract (symptoms – irritation of the nose and throat and labored breathing). Contact with eye and skin causes redness, pain and burn can occur to body and eye tissues. Protective clothing, including boots, gloves and lab coat, as appropriate should be wear to prevent skin contact, chemical safety goggles should be used.
- The UV light may cause painful sunburn or eye inflammation (symptoms – pain, redness and hot sensation) and premature aging of the skin with repeated exposure. UV absorbing goggles should be used.

APPENDIX B

MFI Data

TableB1: Setting parameters for the CLR r-PET Flakes and their pellets.

Ray-Ran Advanced Microprocessor System	
Parameters	Value
Test weight (Kg)	2.16
Temperature of the barrel, ºC	265

TableB2: Melt Flow Index data for CLR r-PET Flakes and their pellets.

Sample No.	Un-dried r-PET Flakes	Un-dried r-PET pellets	dried r-PET Flakes (1 hr at 100 °C)	dried r-PET pelles (1 hr at 100 °C)
1	16.24	16.24	13.92	13.92
2	16.24	16.24	16.24	16.24
3	16.24	16.24	12.18	13.92
4	16.24	16.24	18.49	13.92
5	16.24	16.24	8.85	13.92
6	16.24	16.24	16.24	16.24
7	16.24	16.24	16.24	16.24
8	16.24	16.24	12.18	16.24
9	9.74	19.49	16.24	19.49
10	16.24	16.24	16.24	16.24
11	13.92	16.24	16.24	16.24
12	16.24	16.24	16.24	16.24
Avg. MFI (g/10min)	15.51	16.46	14.94	15.74
S.d.	1.93	0.84	2.66	1.63

TableB3: Setting parameters for the CLR/KUDOS-r-PET pellets.

Plasticode Melt Index Test Machine	
Parameters	Value
Test weight (kg)	2.16
Temperature of the barrel, ºC	252

TableB4: MFI for un-dried r-PET pellets.

Sample No.	Time for cut (s)	Weight (g)	MFI (g/10min)
1	10	0.189	11.34
2	10	0.222	13.32
3	10	0.168	10.08
4	10	0.224	13.44
5	10	0.230	13.80
6	10	0.228	13.68
7	10	0.208	12.48
8	10	0.256	15.36
9	10	0.214	12.84
10	10	0.221	13.26
11	10	0.212	12.72
12	10	0.169	10.14
13	10	0.157	9.42
14	10	0.212	12.72
15	10	0.236	14.16
16	10	0.198	11.88
17	10	0.166	9.96
Avg.			12.39
S.d.			1.68

TableB5: MFI for dried r-PET pellets (4hr at 170 °C).

Sample No.	Time for cut (s)	Weight (g)	MFI (g/10min)
1	30	0.108	2.16
2	30	0.061	1.22
3	30	0.097	1.94
4	30	0.085	1.70
5	30	0.104	2.08
6	30	0.14	2.80
7	30	0.093	1.86
8	30	0.062	1.24
9	30	0.141	2.82
10	30	0.139	2.78
11	30	0.149	2.98
12	30	0.049	0.98
13	30	0.456	9.12
14	30	0.423	8.45
Avg.			3.01
S.d.			2.53

TableB6: MFI for r-PET specimens before UV irradiation.

Sample No.	Time for cut (s)	Weight (g)	MFI (g/10min)
1	10	0.291	17.46
2	10	0.313	18.78
3	10	0.352	21.12
4	10	0.371	22.26
5	10	0.321	19.26
6	10	0.311	18.66
7	10	0.400	24.00
8	10	0.292	17.52
9	10	0.318	19.08
10	10	0.392	23.52
11	10	0.431	25.86
12	10	0.504	30.23
Avg.			21.48
S.d.			3.87

TableB7: MFI for r-PET specimens after 250 hr of UV irradiation under accelerated weathering.

Sample No.	Time for cut (s)	Weight (g)	MFI (g/10min)
1	10	0.293	17.58
2	10	0.345	20.70
3	10	0.350	21.00
4	10	0.306	18.36
5	10	0.367	22.02
6	10	0.378	22.68
7	10	0.340	20.04
8	10	0.256	15.36
9	10	0.295	17.70
10	10	0.358	21.48
11	10	0.218	15.36
12	10	0.500	28.26
13	10	0.504	29.04
Avg.			20.76
S.d.			4.23

TableB8: MFI for r-PET specimens after 500 hr of UV irradiation under accelerated weathering.

Sample No.	Time for cut (s)	Weight (g)	MFI (g/10min)
1	10	0.290	17.40
2	10	0.270	16.20
3	10	0.380	22.80
4	10	0.370	22.20
5	10	0.399	23.94
6	10	0.300	18.00
7	10	0.334	20.04
8	10	0.337	20.22
9	10	0.309	18.54
10	10	0.315	18.90
11	10	0.367	22.02
12	10	0.221	13.26
13	10	0.260	15.60
14	10	0.274	16.44
Avg.			18.97
S.d.			3.08

TableB9: MFI for r-PET specimens after 750 hr of UV irradiation under accelerated weathering.

Sample No.	Time for cut (s)	Weight (g)	MFI (g/10min)
1	10	0.272	16.32
2	10	0.316	18.96
3	10	0.351	21.06
4	10	0.319	19.14
5	10	0.362	21.72
6	10	0.353	21.18
7	10	0.361	21.66
8	10	0.335	20.10
9	10	0.317	19.02
10	10	0.462	21.72
11	10	0.405	24.30
12	10	0.430	25.80
13	10	0.483	28.98
14	10	0.476	28.56
Avg.			22.04
S.d.			3.67

TableB10: MFI for r-PET specimens after 1000 hr of UV irradiation under accelerated weathering.

Sample No.	Time for cut (s)	Weight (g)	MFI (g/10min)
1	10	0.293	17.58
2	10	0.317	19.02
3	10	0.343	20.58
4	10	0.308	18.48
5	10	0.337	20.22
6	10	0.353	21.18
7	10	0.307	18.42
8	10	0.353	21.18
9	10	0.291	17.46
10	10	0.254	15.24
11	10	0.291	17.46
12	10	0.161	9.66
Avg.			18.52
S.d.			2.02

TableB11: MFI for r-PET specimens after 2000 hr of UV irradiation under accelerated weathering.

Sample No.	Time for cut (s)	Weight (g)	MFI (g/10min)
1	10	0.274	16.44
2	10	0.344	20.64
3	10	0.252	15.12
4	10	0.379	22.74
5	10	0.309	18.00
6	10	0.382	22.92
7	10	0.358	21.48
8	10	0.369	22.14
9	10	0.400	24.00
10	10	0.377	22.62
11	10	0.400	24.00
12	10	0.370	22.20
Avg.			21.03
S.d.			2.94

TableB12: MFI for r-PET specimens after 5000 hr of UV irradiation under accelerated weathering.

Sample No.	Time for cut (s)	Weight (g)	MFI (g/10min)
1	10	0.347	20.82
2	10	0.375	22.50
3	10	0.367	22.02
4	10	0.323	19.38
5	10	0.423	25.38
6	10	0.457	27.42
7	10	0.299	17.94
8	10	0.293	17.58
9	10	0.251	15.06
10	10	0.469	28.14
11	10	0.225	13.50
Avg.			20.89
S.d.			4.79

TableB13: MFI for r-PET specimens after 9000 hr of UV irradiation under accelerated weathering.

Sample No.	Time for cut (s)	Weight (g)	MFI (g/10min)
1	10	0.268	16.08
2	10	0.300	18.00
3	10	0.330	19.80
4	10	0.324	19.44
5	10	0.367	22.02
6	10	0.377	22.62
7	10	0.348	20.88
8	10	0.397	23.83
9	10	0.407	24.42
10	10	0.437	26.22
11	10	0.378	22.68
12	10	0.467	28.02
Avg.			22.00
S.d.			3.41

TableB14: MFI for r-PET specimens after 13000 hr of UV irradiation under accelerated weathering.

Sample No.	Time for cut (s)	Weight (g)	MFI (g/10min)
1	10	0.405	24.30
2	10	0.410	24.60
3	10	0.393	23.58
4	10	0.281	16.86
5	10	0.481	28.86
6	10	0.306	18.36
7	10	0.473	28.38
8	10	0.386	23.16
9	10	0.263	15.78
10	10	0.262	15.72
11	10	0.490	29.40
Avg.			22.64
S.d.			5.21

TableB15: MFI for r-PET specimens after 250 hr of UV irradiation under natural weathering.

Sample No.	Time for cut (s)	Weight (g)	MFI (g/10min)
1	10	0.292	17.52
2	10	0.323	19.38
3	10	0.344	20.64
4	10	0.359	21.54
5	10	0.352	21.12
6	10	0.359	21.54
7	10	0.345	20.70
8	10	0.337	20.22
9	10	0.322	19.32
10	10	0.514	30.84
11	10	0.451	27.06
12	10	0.494	29.64
Avg.			22.46
S.d.			4.28

TableB16: MFI for r-PET specimens after 500 hr of UV irradiation under natural weathering.

Sample No.	Time for cut (s)	Weight (g)	MFI (g/10min)
1	10	0.317	19.02
2	10	0.315	18.90
3	10	0.366	21.96
4	10	0.364	21.84
5	10	0.399	23.94
6	10	0.402	24.12
7	10	0.258	15.48
8	10	0.236	14.16
9	10	0.481	28.86
10	10	0.422	25.32
11	10	0.492	29.52
Avg.			22.10
S.d.			4.95

TableB17: MFI for r-PET specimens after 750 hr of UV irradiation under natural weathering.

Sample No.	Time for cut (s)	Weight (g)	MFI (g/10min)
1	10	0.283	16.98
2	10	0.352	21.12
3	10	0.348	20.88
4	10	0.306	18.36
5	10	0.272	16.32
6	10	0.346	20.76
7	10	0.364	21.84
8	10	0.381	22.86
9	10	0.354	21.24
10	10	0.394	23.64
11	10	0.203	12.18
Avg.			19.65
S.d.			3.38

TableB18: MFI for r-PET specimens after 1000 hr of UV irradiation under natural weathering.

Sample No.	Time for cut (s)	Weight (g)	MFI (g/10min)
1	10	0.328	19.68
2	10	0.350	21.00
3	10	0.393	23.58
4	10	0.409	24.54
5	10	0.344	20.64
6	10	0.438	26.28
7	10	0.378	22.68
8	10	0.516	30.96
9	10	0.531	31.86
Avg.			24.58
S.d.			4.38

TableB19: MFI for r-PET specimens after 2000 hr of UV irradiation under natural weathering.

Sample No.	Time for cut (s)	Weight (g)	MFI (g/10min)
1	10	0.275	16.50
2	10	0.288	17.28
3	10	0.405	24.30
4	10	0.287	17.22
5	10	0.445	26.70
6	10	0.248	14.88
7	10	0.173	10.38
8	10	0.385	23.10
Avg.			18.80
S.d.			5.44

TableB20: MFI for r-PET specimens after 5000 hr of UV irradiation under natural weathering.

Sample No.	Time for cut (s)	Weight (g)	MFI (g/10min)
1	10	0.280	16.8
2	10	0.318	19.08
3	10	0.345	20.70
4	10	0.388	23.28
5	10	0.386	23.16
6	10	0.429	25.74
7	10	0.328	19.68
8	10	0.329	19.74
9	10	0.326	19.56
10	10	0.345	20.70
11	10	0.233	13.89
12	10	0.205	12.30
Avg.			19.55
S.d.			3.82

TableB21: MFI for r-PET specimens after 9000 hr of UV irradiation under natural weathering.

Sample No.	Time for cut (s)	Weight (g)	MFI (g/10min)
1	10	0.30	18.00
2	10	0.346	20.76
3	10	0.345	20.70
4	10	0.306	18.36
5	10	0.283	16.98
6	10	0.274	16.44
7	10	0.326	19.56
8	10	0.442	26.52
9	10	0.336	20.16
10	10	0.397	23.82
11	10	0.217	13.20
Avg.			19.48
S.d.			3.64

TableB22: MFI for r-PET specimens after 13000 hr of UV irradiation under natural weathering.

Sample No.	Time for cut (s)	Weight (g)	MFI (g/10min)
1	10	0.30	18.00
2	10	0.403	24.18
3	10	0.338	20.28
4	10	0.332	19.92
5	10	0.402	24.12
6	10	0.348	20.89
7	10	0.292	17.52
8	10	0.347	20.82
9	10	0.386	23.16
10	10	0.346	20.76
		0.499	29.94
		0.485	29.10
Avg.			22.39
S.d.			3.93

APPENDIX C

FTIR Spectra

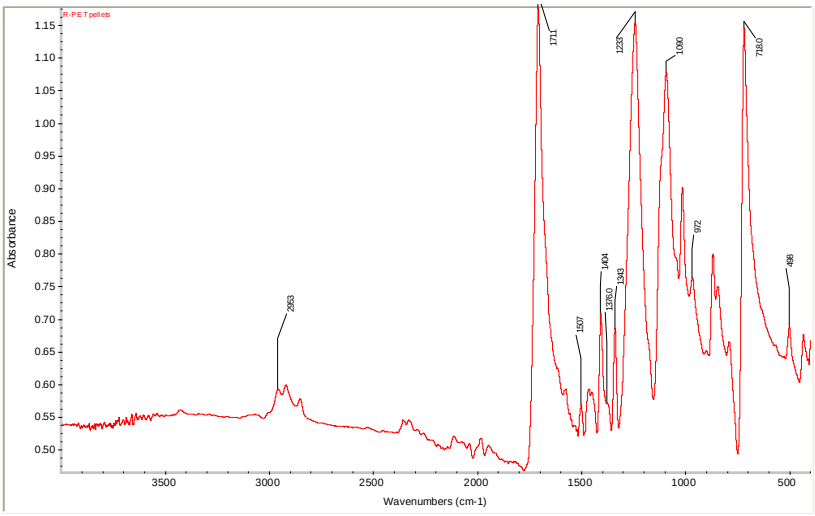

Figure C1:FTIR spectrum of CLR/KUDOS-r-PET pellets.

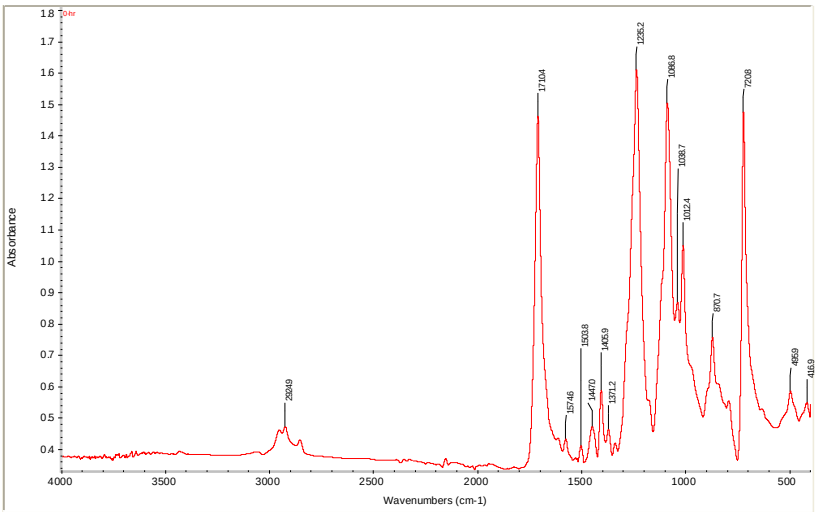

Figure C2:FTIR spectrum for r-PET specimens before UV exposure.

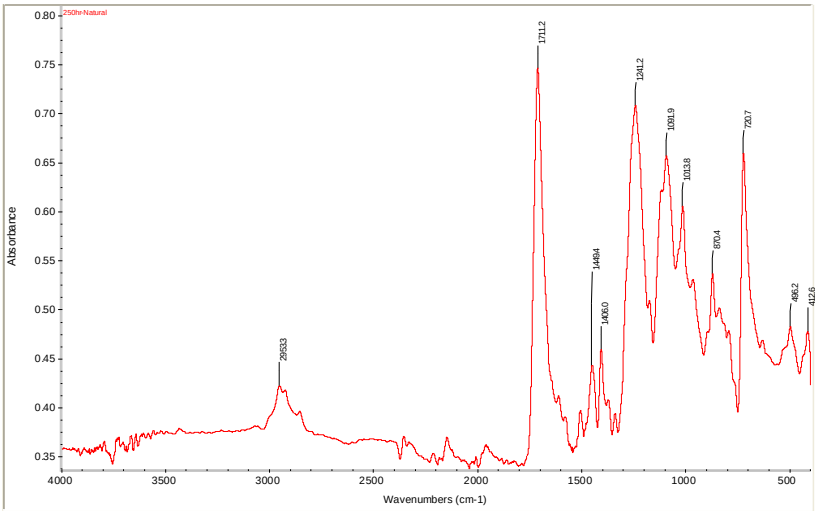

Figure C3:FTIR spectrum for r-PET specimens after 250hr outdoor exposure.

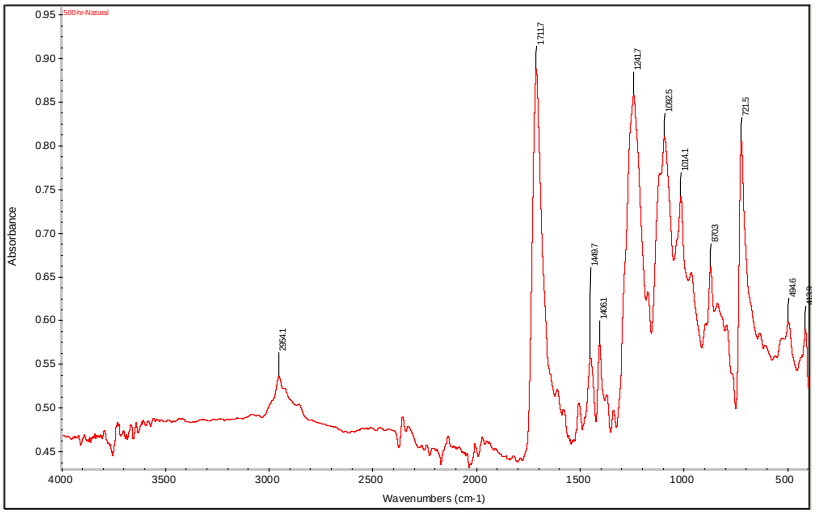

Figure C4:FTIR spectrum for r-PET specimens after 500hr outdoor exposure.

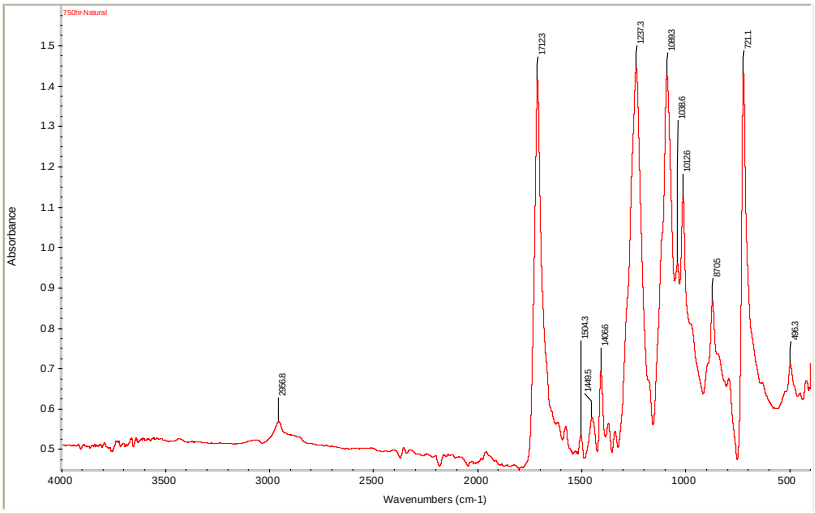

Figure C5:FTIR spectrum for r-PET specimens after 750hr outdoor exposure.

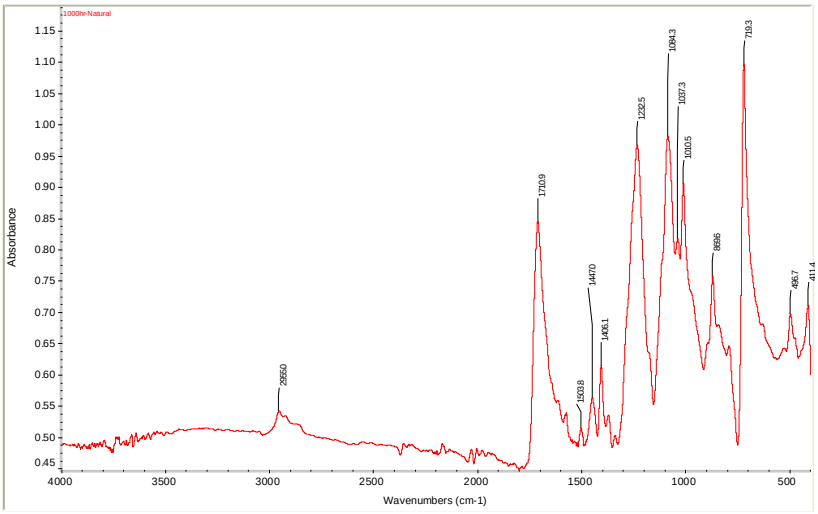

Figure C6:FTIR spectrum for r-PET specimens after 1000hr outdoor exposure.

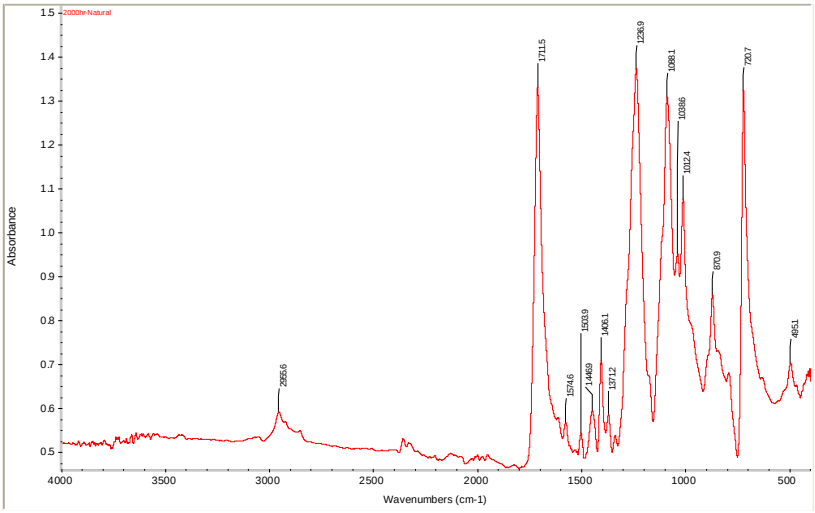

Figure C7:FTIR spectrum for r-PET specimens after 2000hr outdoor exposure.

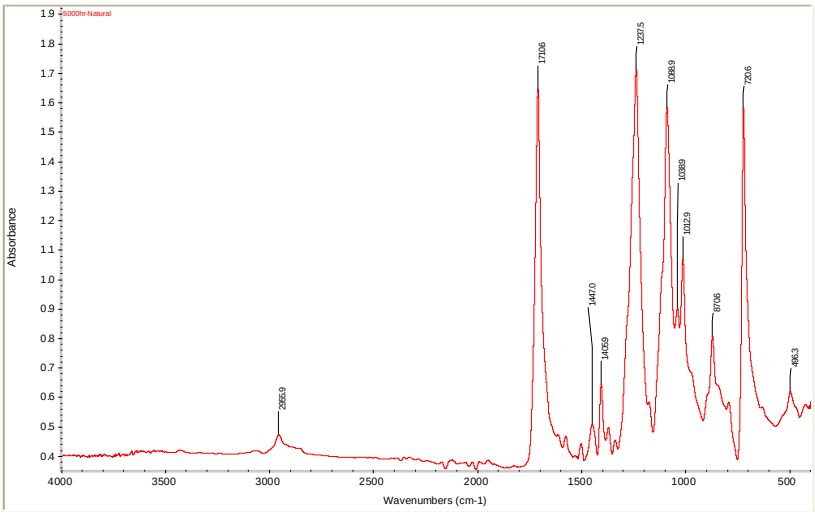

Figure C8:FTIR spectrum for r-PET specimens after 5000hr outdoor exposure.

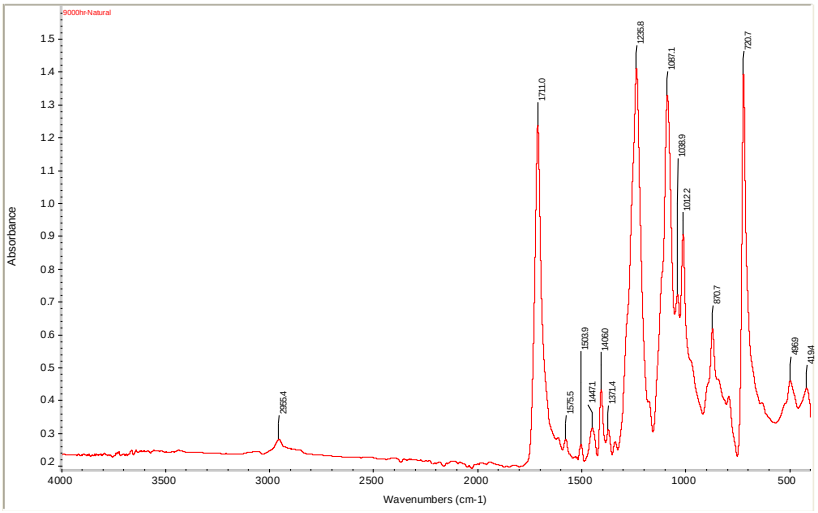

Figure C9:FTIR spectrum for r-PET specimens after 9000hr outdoor exposure.

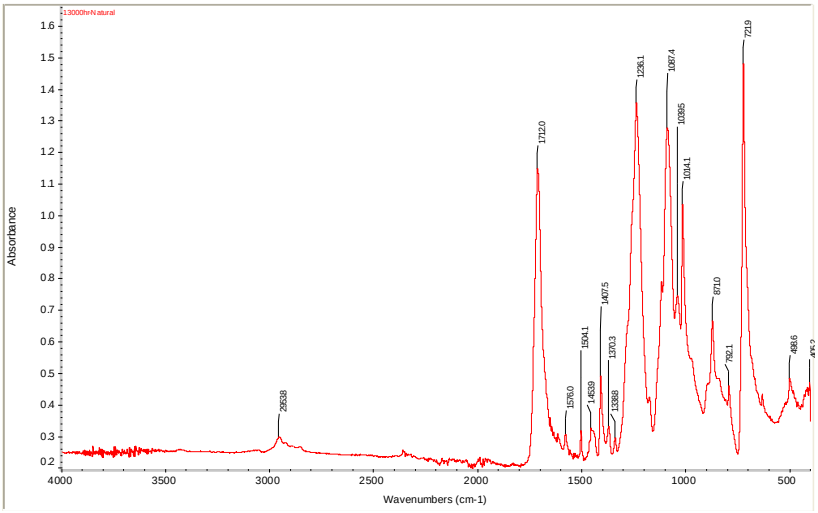

Figure C10:FTIR spectrum for r-PET specimens after 13000hr outdoor exposure.

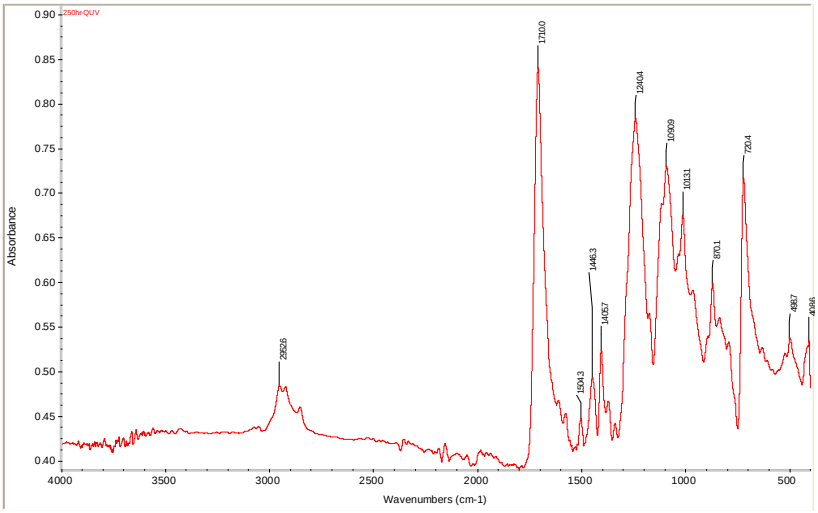

Figure C11:FTIR spectrum for r-PET specimens after 250hr of UV irradiation under accelerated weathering.

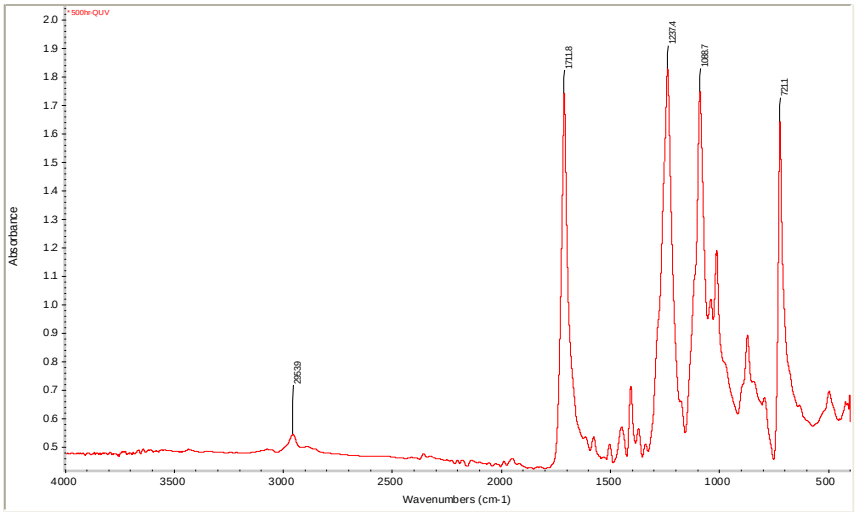

Figure C12:FTIR spectrum for r-PET specimens after 500hr of UV irradiation under accelerated weathering.

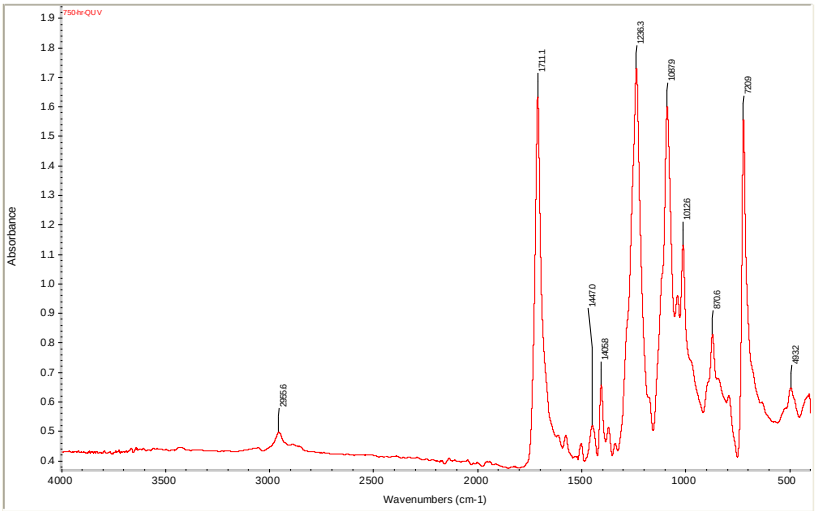

Figure C13:FTIR spectrum for r-PET specimens after 750hr of UV irradiation under accelerated weathering.

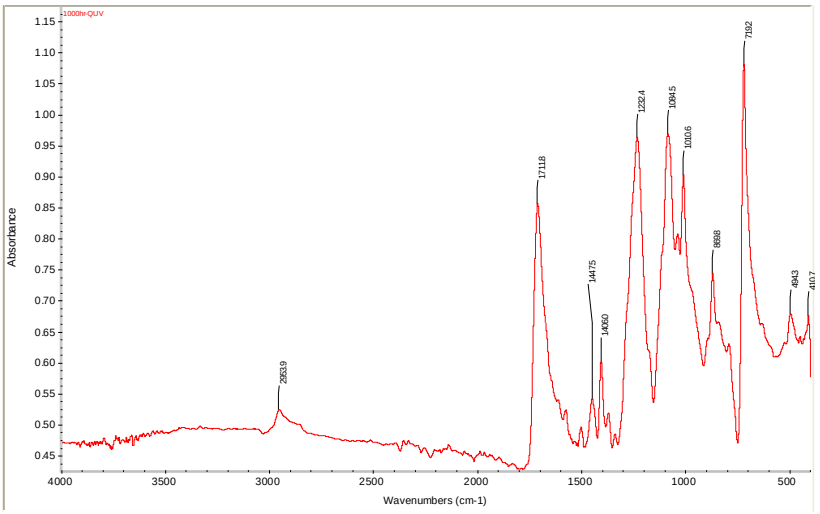

Figure C14:FTIR spectrum for r-PET specimens after 1000hr of UV irradiation under accelerated weathering.

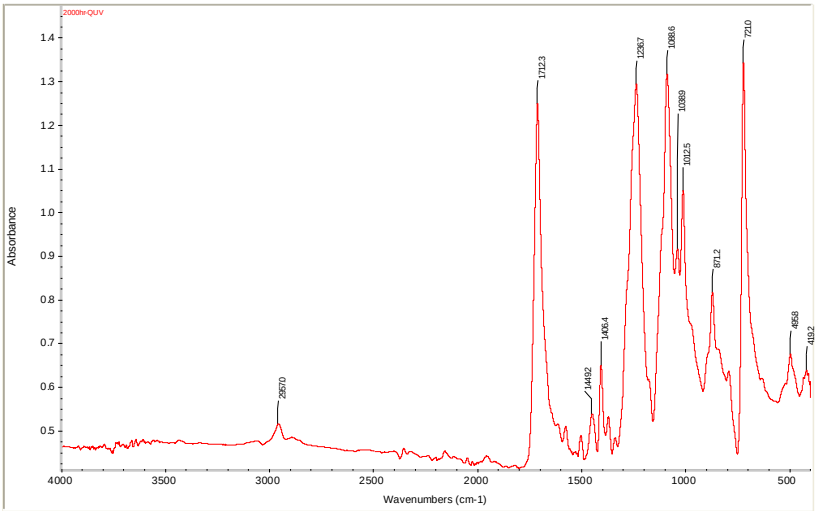

Figure C15:FTIR spectrum for r-PET specimens after 2000hr of UV irradiation under accelerated weathering.

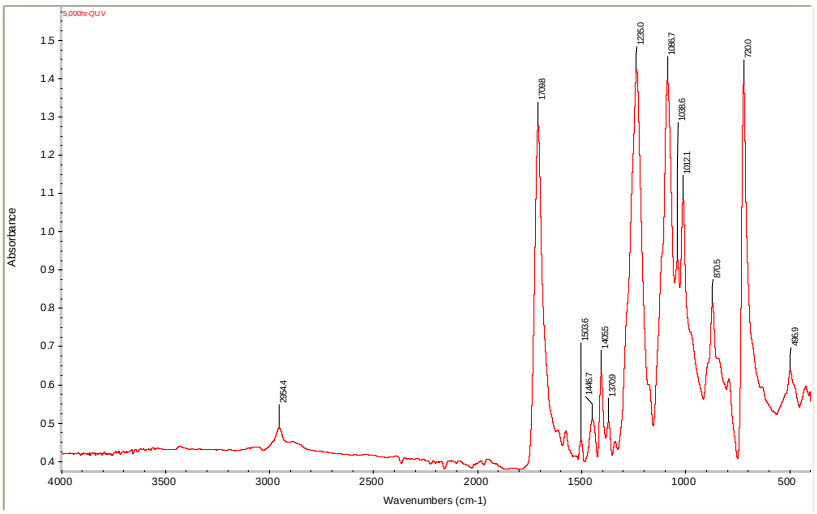

Figure C16:FTIR spectrum for r-PET specimens after 5000hr of UV irradiation under accelerated weathering.

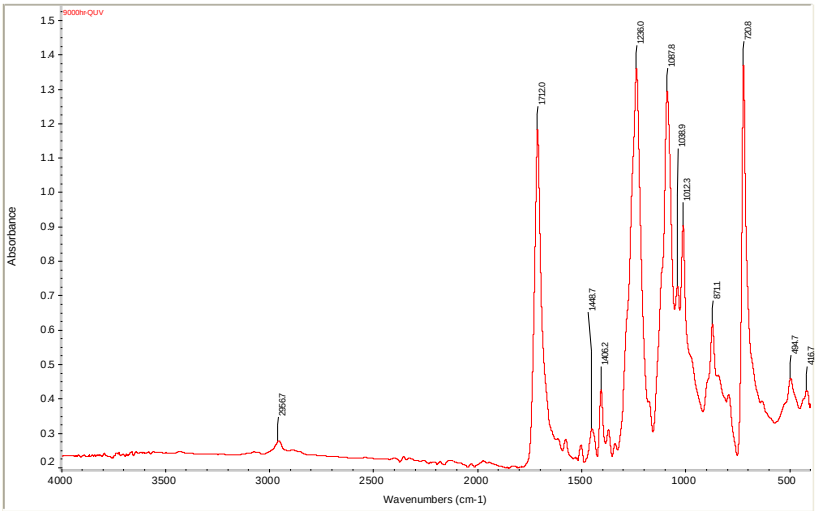

Figure C17:FTIR spectrum for r-PET specimens after 9000hr of UV irradiation under accelerated weathering.

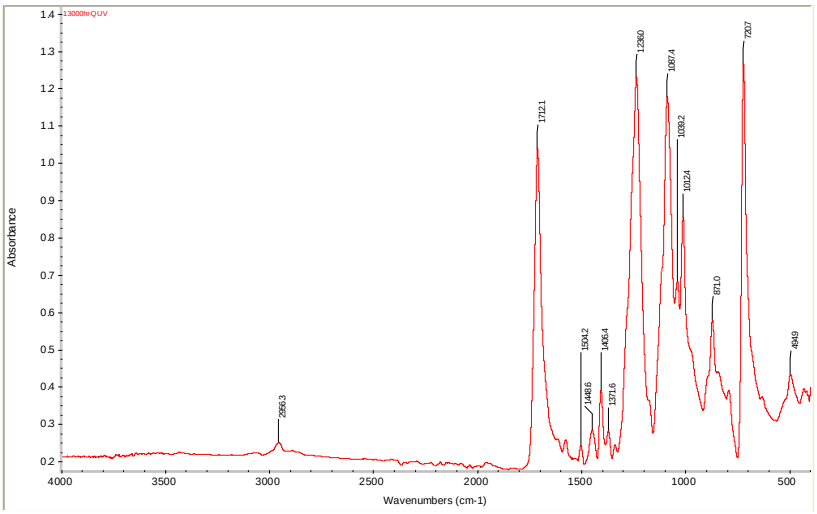

Figure C18:FTIR spectrum for r-PET specimens after 13000hr of UV irradiation under accelerated weathering.

APPENDIX D

DSC Results

Table D1: The percentage of crystallinity (%Xc) for CLR-r-PET-Flakes and its pellets for at screw speed 60 and 85 rpm and CLR/KUDOS-r-PET pellets.

	X_c (%)	X_c (%)	X_c (%)	Avg.	S.d.
CLR-r-PET-Flakes	45.37	44.07	47.87	45.77	1.93
Pellets-60 rpm	17.04	15.98	18.45	17.16	1.24
Pellets-85 rpm	10.48	9.78	11.23	10.50	0.73
CLRKodos-r-PET-pellets	46.31	48.51	48.96	47.93	1.42

TableD2: The percentage of crystallinity before and after UV exposure in accelerated weathering.

UV exposure time, hr	Xc% for accelerated weathering					Avg. Xc%	S.d
0	21.4	16.62	18.81			18.94	2.39
250	17.25	18.19	23.82	20.76		20.01	2.94
500	12.1	14.74	17.26			14.70	2.58
750	20.07	14.41	25.41	28.54		22.11	6.21
1000	19.3	18.86	20.7	22.05	12.78	18.74	3.56
2000	26.34	18.91	20.92			22.06	3.84
5000	20.18	26.34	19.37			21.96	3.81
9000	20.23	21.23	12.31			17.92	4.89
13000	19.45	17.98	18.54			18.66	0.74

TableD3: The percentage of crystallinity before and after UV exposure in natural weathering.

UV exposure time, hr	Xc% for natural weathering			Avg. Xc%	S.d
0	21.4	16.62	18.81	18.94	2.39
250	18.78	17.3	23.11	19.73	3.02
500	19.13	19.13	12.54	16.93	3.80
750	19.12	15.11	12.82	15.68	3.19
1000	19.05	17.2	21.9	19.38	2.37
2000	18.41	21.5	27.34	22.42	4.54
5000	19.42	18.73	12.1	16.75	4.04
9000	20.08	19.5	25.4	21.66	3.25
13000	20.54	18.71	15.56	18.27	2.52

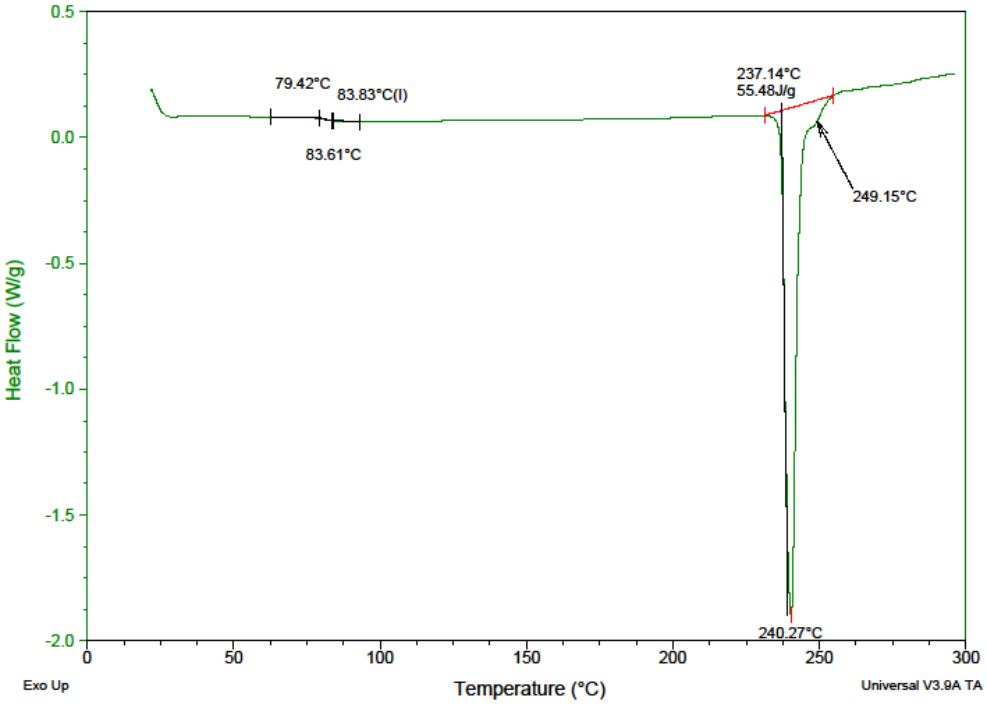

FigureD1: DSC thermogram for CLR/KUDOS-r-PET Pellets.

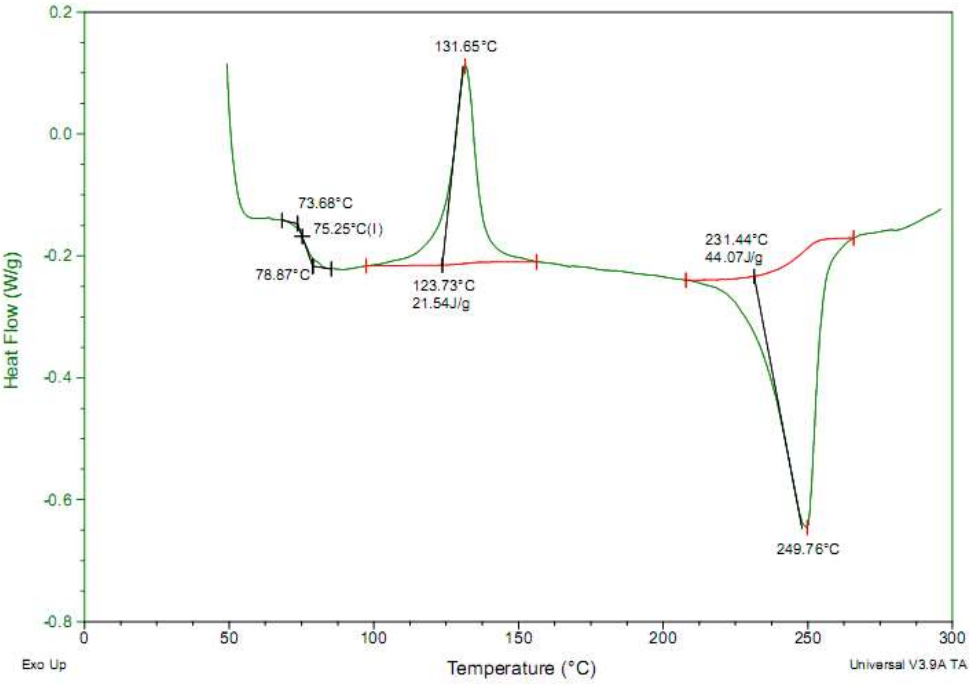

FigureD2: DSC thermogram for r-PET before exposure.

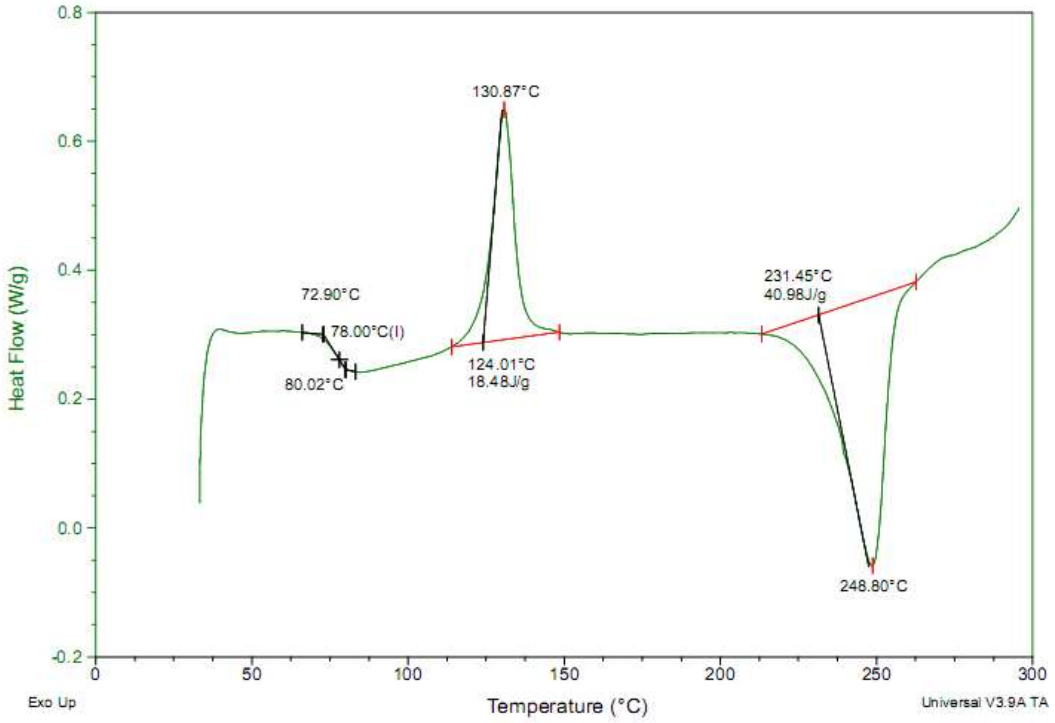

Figure D3: DSC thermogram after 250 hr of UV exposure in nature weather.

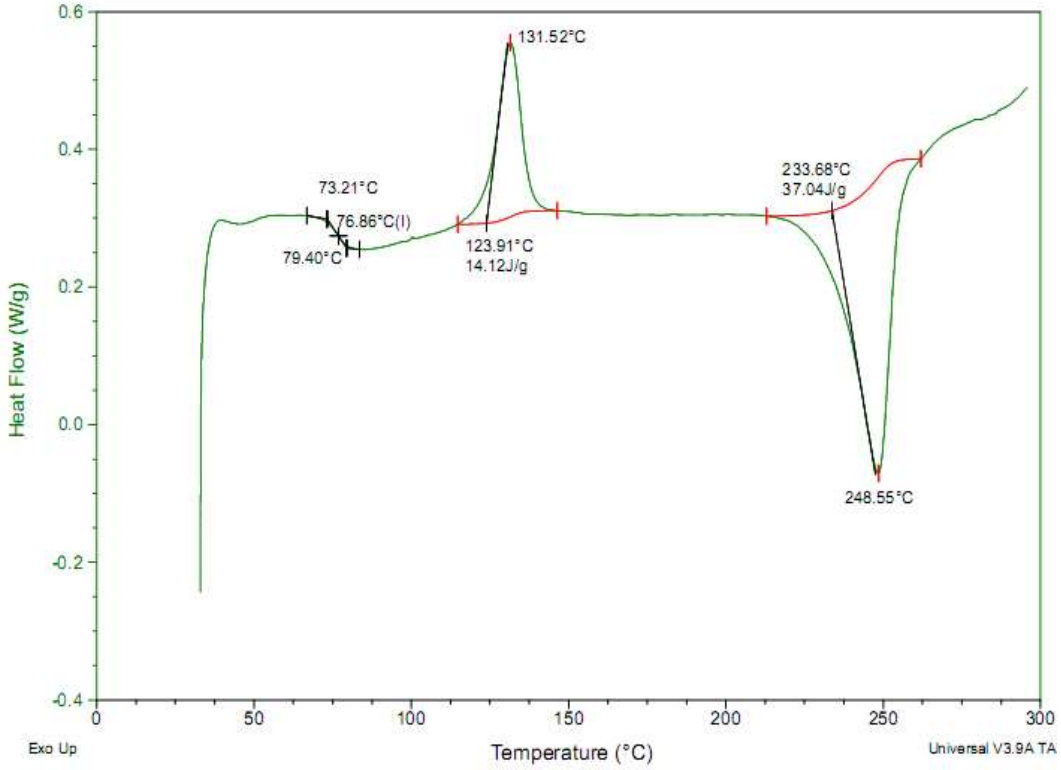

Figure D4: DSC thermogram after 500 hr of UV exposure in nature weather.

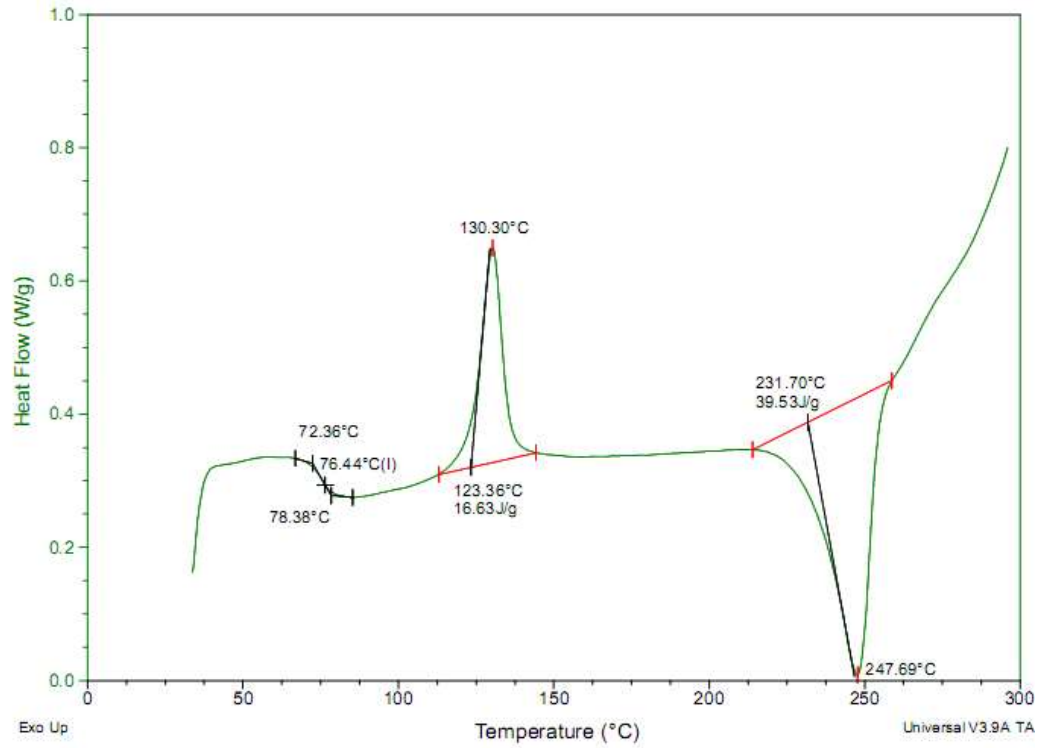

Figure D5: DSC thermogram after 750 hr of UV exposure in nature weather.

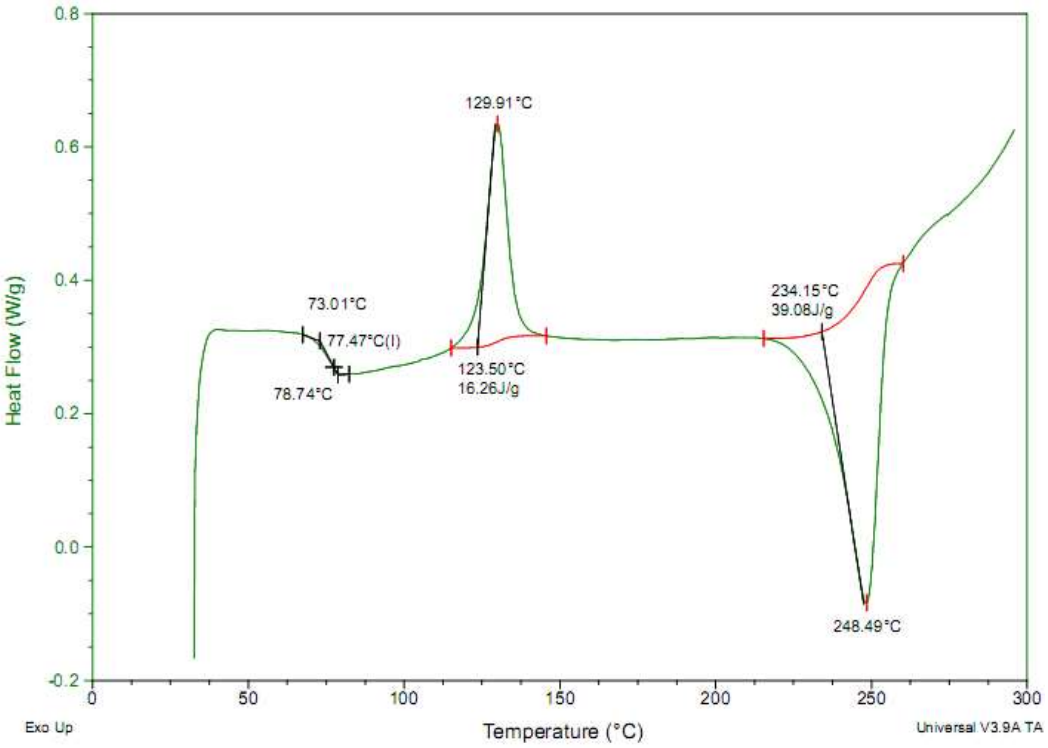

Figure D6: DSC thermogram after 1000 hr of UV exposure in nature weather.

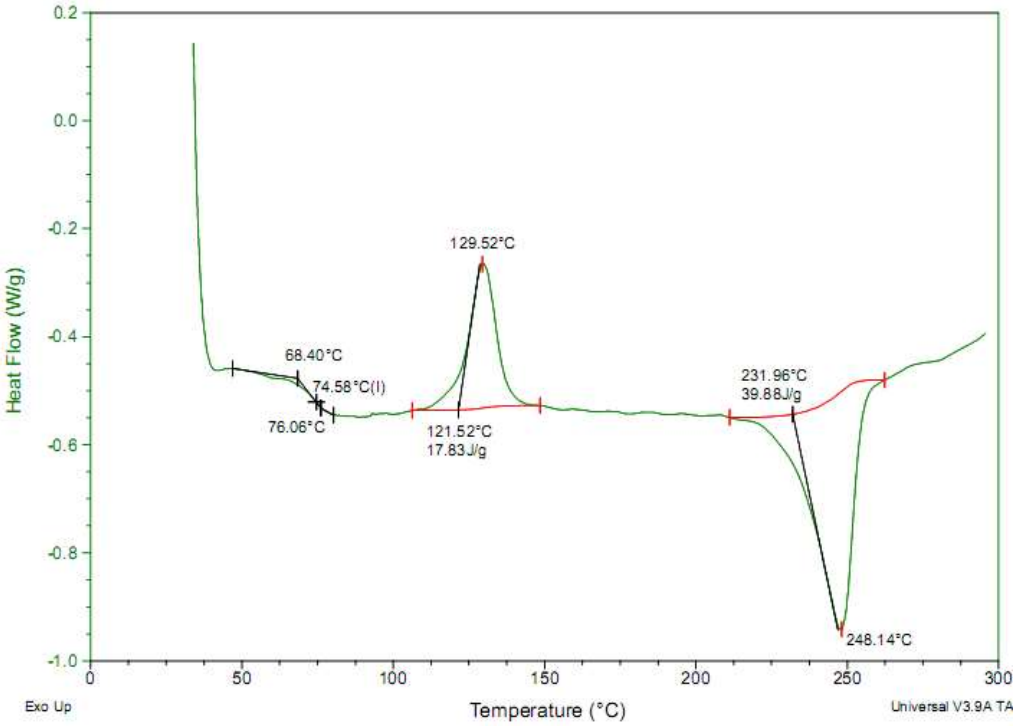

Figure D7: DSC thermogram after 2000 hr of UV exposure in nature weather.

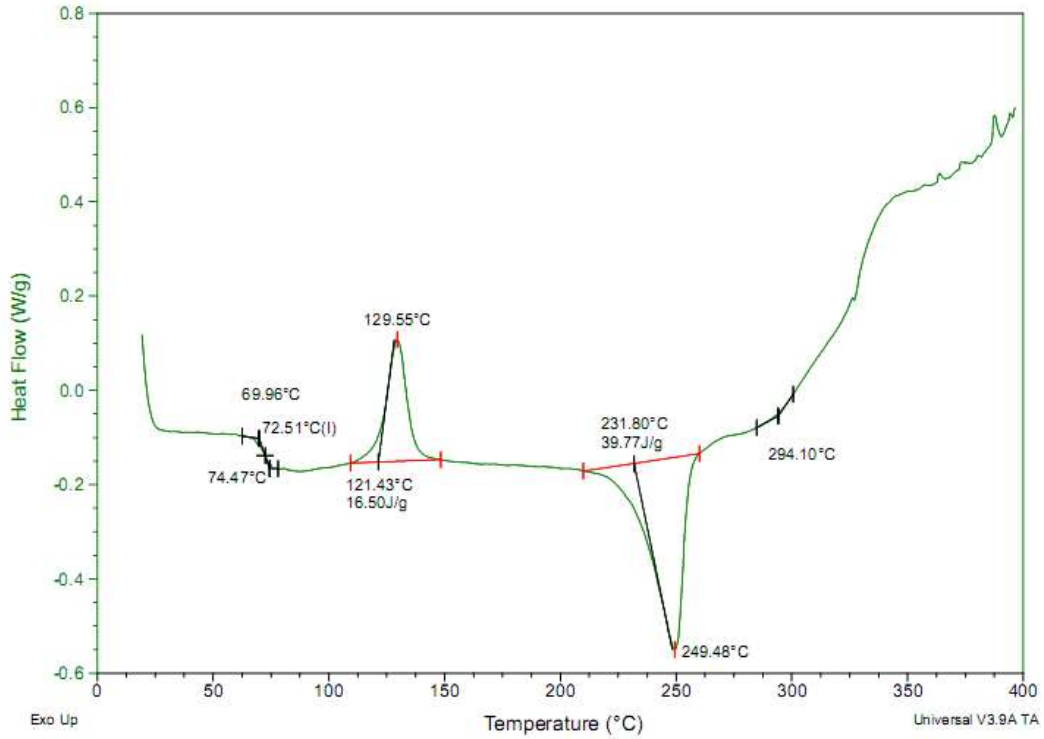

Figure D8: DSC thermogram after 5000 hr of UV exposure in nature weather.

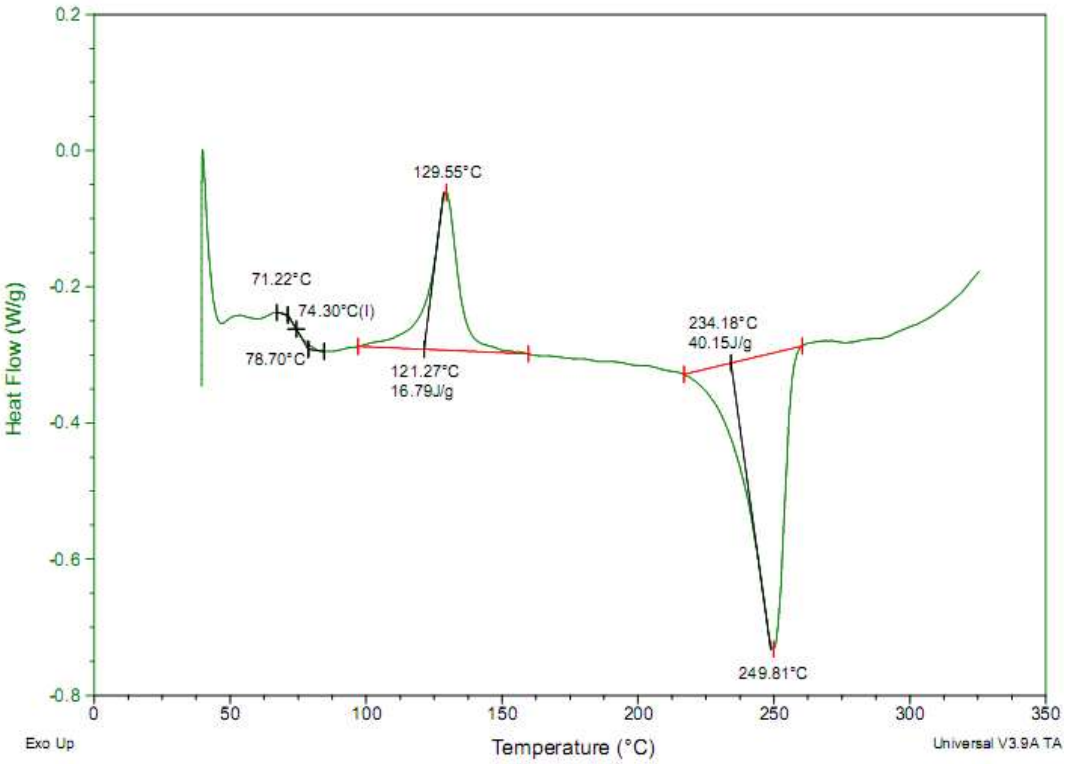

Figure D9: DSC thermogram after 9000 hr of UV exposure in nature weather.

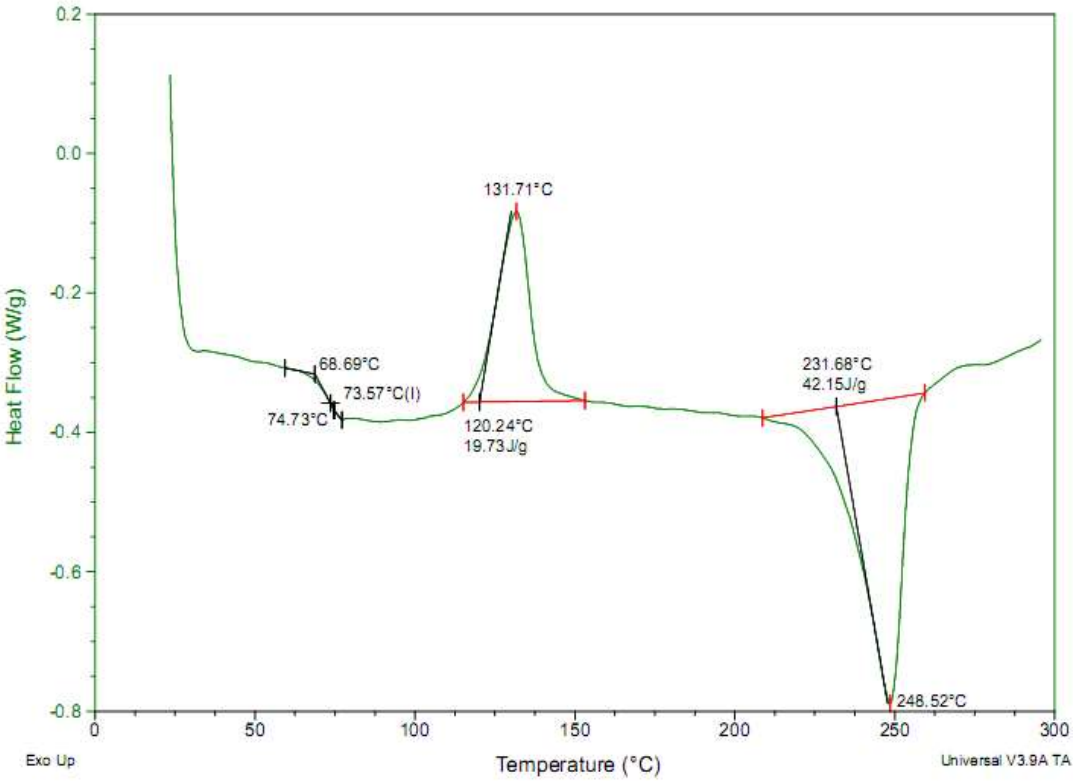

Figure D10: DSC thermogram after 13000 hr of UV exposure in nature weather.

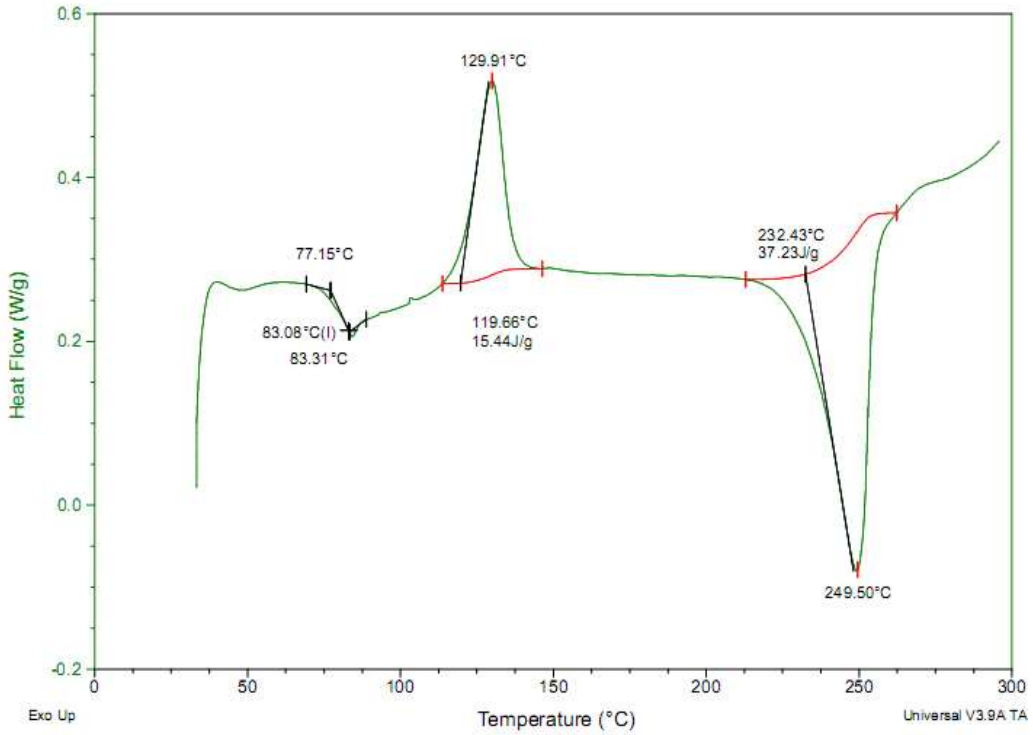

Figure D11: DSC thermogram after 250 hr of UV exposure in accelerated weather.

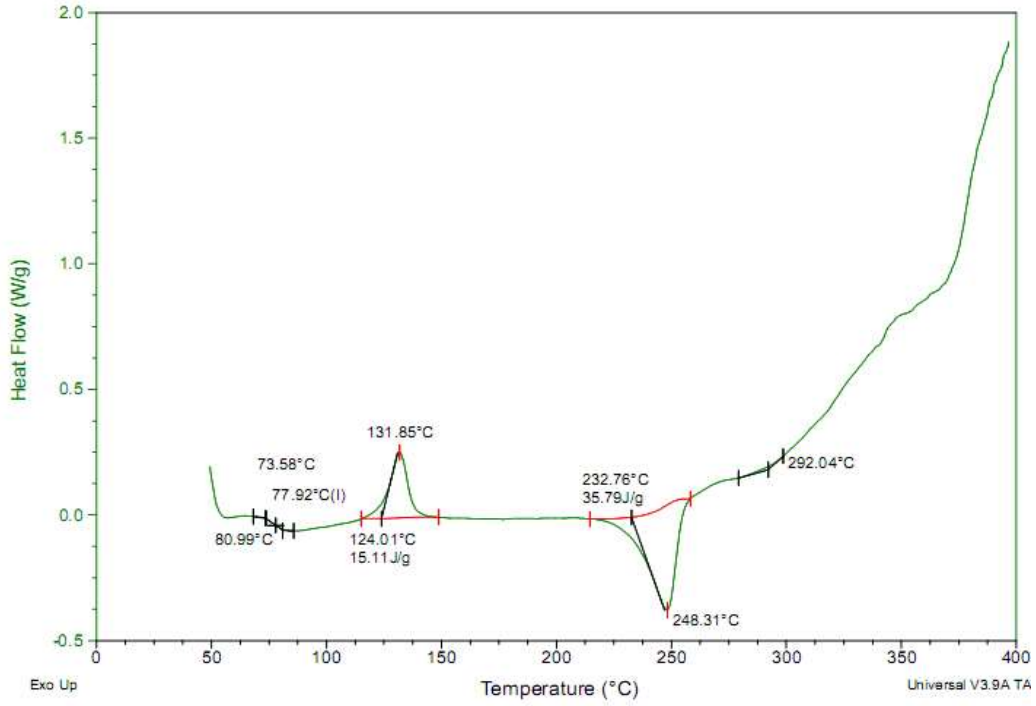

Figure D12: DSC thermogram after 500 hr of UV exposure in accelerated weather.

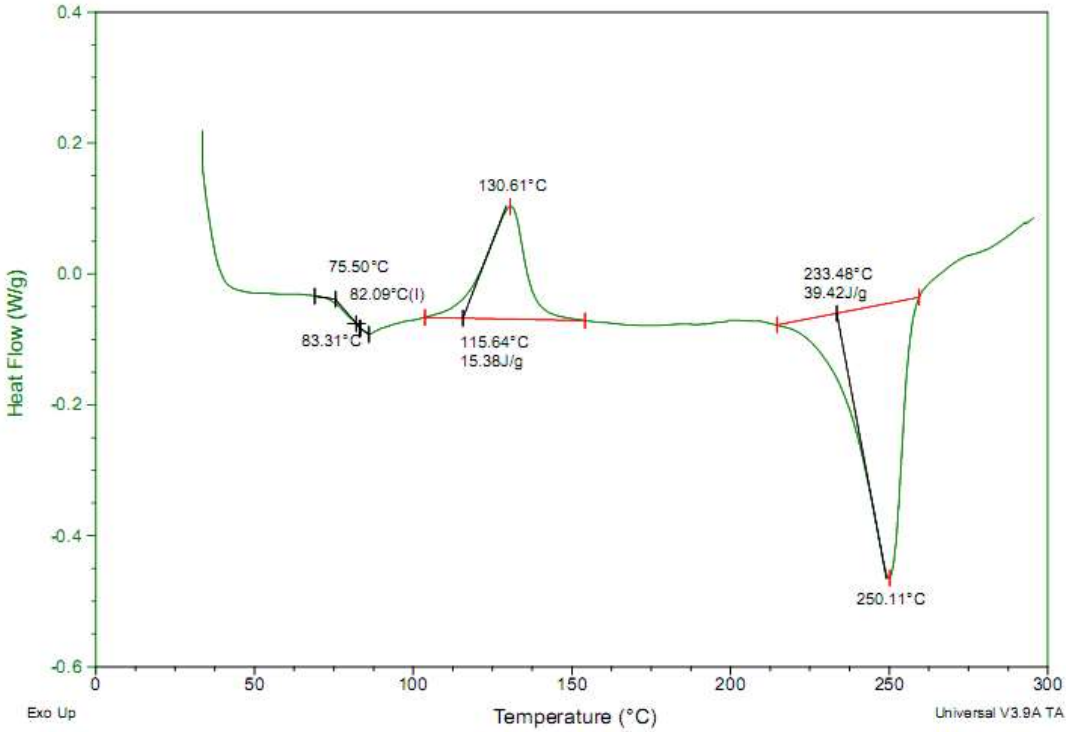

Figure D13: DSC thermogram after 750 hr of UV exposure in accelerated weather.

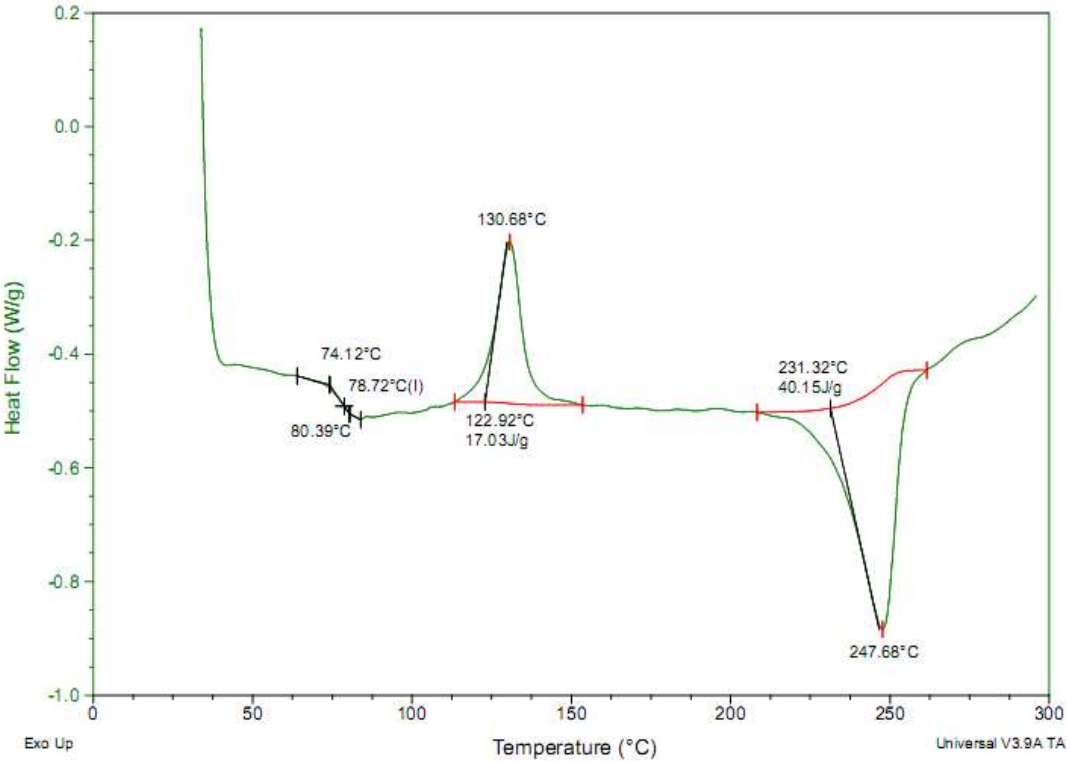

Figure D14: DSC thermogram after 1000 hr of UV exposure in accelerated weather.

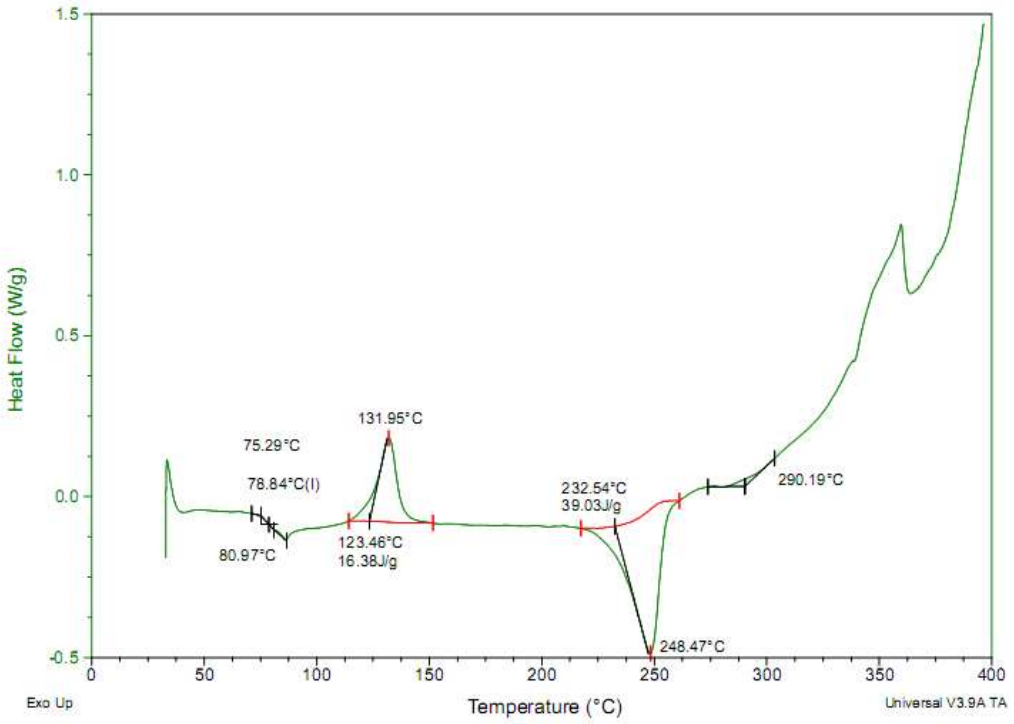

Figure D15: DSC thermogram after 2000 hr of UV exposure in accelerated weather.

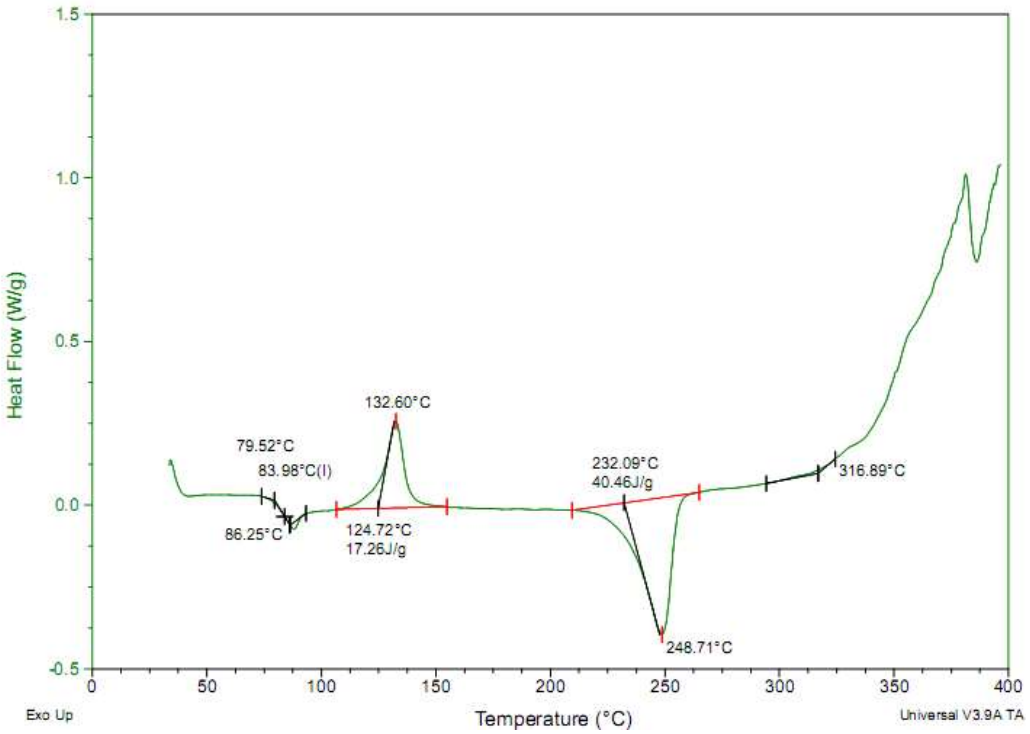

Figure D16: DSC thermogram after 5000 hr of UV exposure in accelerated weather.

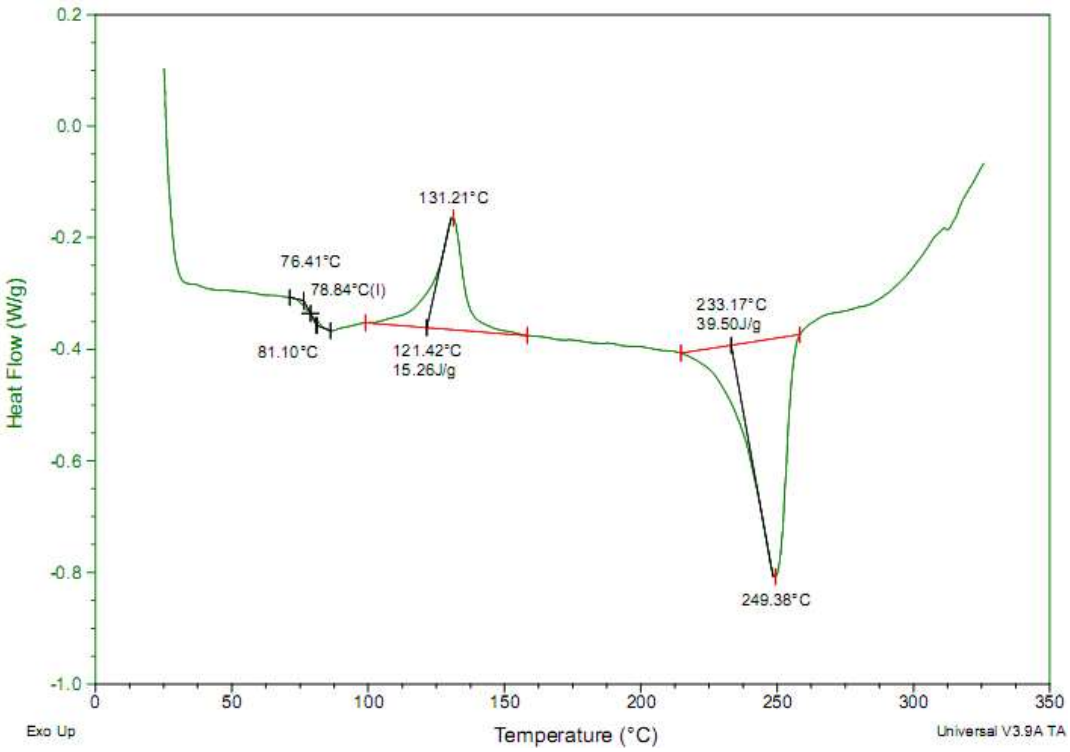

Figure D17: DSC thermogram after 9000 hr of UV exposure in accelerated weather.

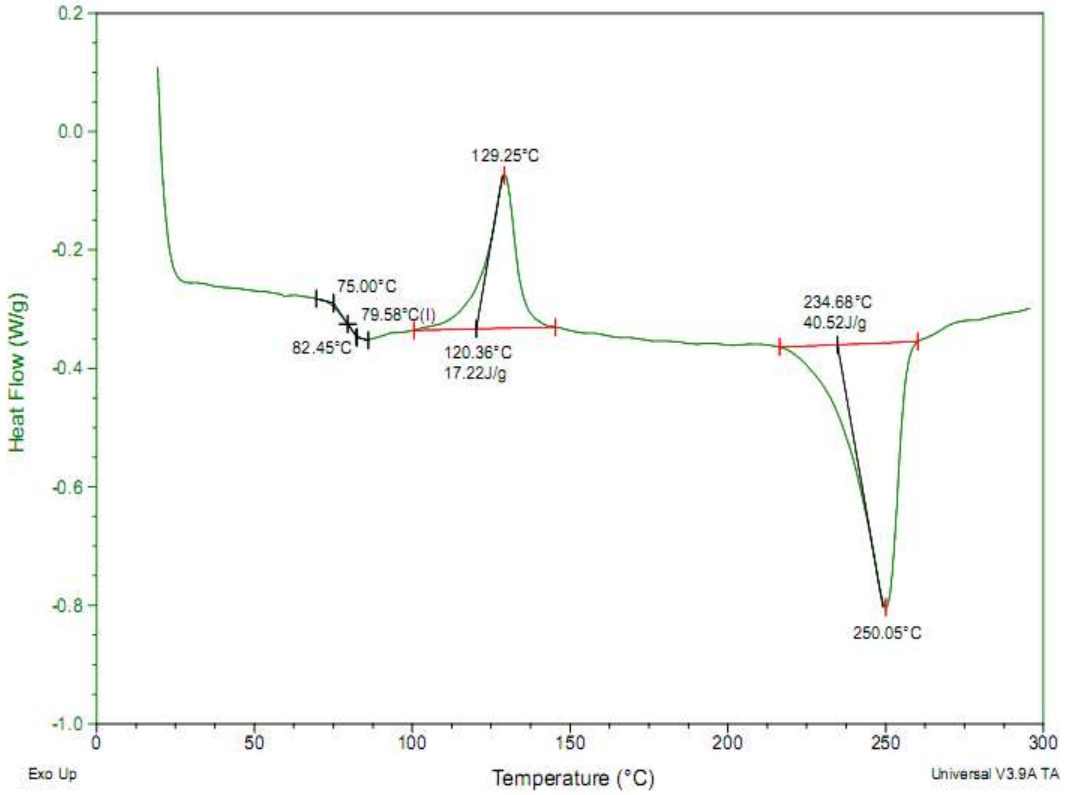

Figure D18: DSC thermogram after 13000 hr of UV exposure in accelerated weather.

APPENDIX E

Colour and Gloss Measurements

Table E1: Colour components (CC) for r-PET specimens before UV exposure.

Position of test	CC	SCI	SCE
upper	L*	42.17	36.76
	a*	1.69	1.84
	b*	11.50	14.45
middle	L*	42.76	36.38
	a*	1.71	1.86
	b*	11.85	15.65
lower	L*	42.05	36.14
	a*	1.65	1.77
	b*	10.99	13.96

Table E2: Colour components (CC) for r-PET specimens after 250 hr of UV exposure for both accelerated and natural weathering.

		Accelerated weathering		Natural weathering	
Position of test	CC	SCI	SCE	SCI	SCE
Upper	L*	42.57	38.92	43.40	37.62
	a*	0.57	0.46	1.07	1.04
	b*	12.06	15.89	10.71	13.08
Middle	L*	45.99	38.34	42.34	36.43
	a*	0.58	0.43	1.22	1.16
	b*	12.34	16.93	12.53	14.96
Lower	L*	45.44	38.07	42.40	37.14
	a*	0.64	0.52	1.25	1.16
	b*	11.80	16.02	12.63	14.62

Table E3: Colour components (CC) for r-PET specimens after 500 hr of UV exposure for both accelerated and natural weathering.

		Accelerated weathering		Natural weathering	
Position of test	CC	SCI	SCE	SCI	SCE
Upper	L*	43.75	36.93	44.83	39.39
	a*	0.67	0.62	0.86	0.74
	b*	9.99	13.35	11.72	13.95
Middle	L*	44.36	39.59	44.71	39.88
	a*	0.64	0.60	0.83	0.68
	b*	10.86	13.08	11.42	13.20
Lower	L*	44.31	39.52	44.37	40.08
	a*	0.62	0.56	0.82	0.67
	b*	10.87	12.83	11.12	12.48

Table E4: Colour components (CC) for r-PET specimens after 750 hr of UV exposure for both accelerated and natural weathering.

		Accelerated weathering		Natural weathering	
Position of test	CC	SCI	SCE	SCI	SCE
Upper	L*	44.02	39.14	44.53	38.79
	a*	0.49	0.26	0.94	0.91
	b*	10.40	11.97	11.33	14.27
Middle	L*	43.87	38.98	44.18	38.29
	a*	0.55	0.35	1.02	0.97
	b*	10.43	12.01	11.05	13.90
Lower	L*	43.90	38.95	44.46	39.56
	a*	0.55	0.37	0.99	0.89
	b*	10.41	12.07	11.06	13.10

Table E5: Colour components (CC) for r-PET specimens after 1000 hr of UV exposure for both accelerated and natural weathering.

		Accelerated weathering		Natural weathering	
Position of test	CC	SCI	SCE	SCI	SCE
upper	L*	44.94	38.85	44.70	39.04
	a*	0.43	0.33	0.90	0.85
	b*	9.28	11.70	11.10	13.84
middle	L*	44.81	37.84	44.85	39.03
	a*	0.48	0.39	0.95	0.90
	b*	9.51	12.93	11.17	13.95
lower	L*	44.41	38.14	44.28	38.35
	a*	0.47	0.42	0.87	0.78
	b*	9.52	12.40	10.99	13.81

Table E6: Colour components (CC) for r-PET specimens after 2000 hr of UV exposure for both accelerated and natural weathering.

		Accelerated weathering		Natural weathering	
Position of test	CC	SCI	SCE	SCI	SCE
Upper	L*	47.81	40.07	46.44	40.63
	a*	0.06	- 0.23	- 0.08	- 0.34
	b*	10.18	13.55	10.66	12.98
Middle	L*	47.29	40.24	46.37	40.88
	a*	0.18	- 0.11	- 0.06	- 0.33
	b*	10.31	13.33	10.58	12.64
Lower	L*	47.25	40.96	46.36	40.36
	a*	0.14	- 0.20	- 0.08	- 0.35
	b*	10.42	13.05	10.59	12.90

Table E7: Colour components (CC) for r-PET specimens after 5000 hr of UV exposure for both accelerated and natural weathering.

		Accelerated weathering		Natural weathering	
Position of test	CC	SCI	SCE	SCI	SCE
Upper	L*	40.05	39.17	43.68	38.67
	a*	- 0.27	- 0.30	0.71	0.59
	b*	6.48	6.52	10.54	12.19
Middle	L*	39.78	38.76	43.56	38.45
	a*	- 0.27	- 0.30	0.71	0.60
	b*	6.34	6.32	10.17	11.89
Lower	L*	39.73	38.96	43.80	38.11
	a*	- 0.26	- 0.30	0.69	0.61
	b*	6.45	6.49	10.26	12.38

Table E8: Colour components (CC) for r-PET specimens after 9000 hr of UV exposure for both accelerated and natural weathering.

		Accelerated weathering		Natural weathering	
Position of test	CC	SCI	SCE	SCI	SCE
Upper	L*	46.31	42.40	45.60	39.87
	a*	-0.06	- 0.15	0.28	0.05
	b*	9.80	10.80	9.91	12.04
Middle	L*	47.70	44.45	45.57	39.93
	a*	- 0.05	- 0.30	0.23	0.02
	b*	10.79	11.38	10.18	12.10
Lower	L*	47.48	44.16	46.22	40.52
	a*	0.01	- 0.23	0.08	- 0.15
	b*	10.79	11.62	9.76	11.63

Table E9: Colour components (CC) for r-PET specimens after 13000 hr of UV exposure for both accelerated and natural weathering.

		Accelerated weathering		Natural weathering	
Position of test	CC	SCI	SCE	SCI	SCE
Upper	L*	41.07	40.90	43.49	41.54
	a*	- 0.33	- 0.34	0.35	0.36
	b*	7.24	7.17	8.37	9.07
Middle	L*	42.13	41.98	44.93	40.52
	a*	- 0.54	- 0.55	0.32	0.10
	b*	7.63	7.53	8.96	9.98
Lower	L*	41.50	41.28	44.07	40.13
	a*	- 0.36	- 0.37	0.38	0.24
	b*	6.43	6.34	8.60	9.48

APPENDIX F

TENSILE TEST RESULTS

Natural tensile test results

Table F1: Tensile test data of r-PET specimens before UV irradiation.

No.	Yield stress	Elong. at yield	Elong. at break	stress at break	True stress at break	Thick	Width	Thick after break	Width after break
	MPa	%	%	MPa	MPa	mm	mm	mm	mm
1	55.60	7.00	243.00	31.52	179.6	4.13	10.12	1.06	6.92
2	59.90	6.80	251.20	30.76	174.22	4.12	10.12	1.07	6.88
3	58.70	6.80	248.80	30.14	186.39	4.11	10.13	0.98	6.87
4	58.70	6.80	247.20	31.12	189.47	4.14	10.13	1.01	6.82
5	63.30	7.20	268.80	32.87	165.97	4.16	10.12	1.25	6.67
6	61.40	6.80	316.00	45.18	221.15	4.12	10.10	1.51	5.63
Avg.	59.60	6.90	262.50	33.6	186.13				
S.d.	2.63	0.17	27.68	5.75	19.13				

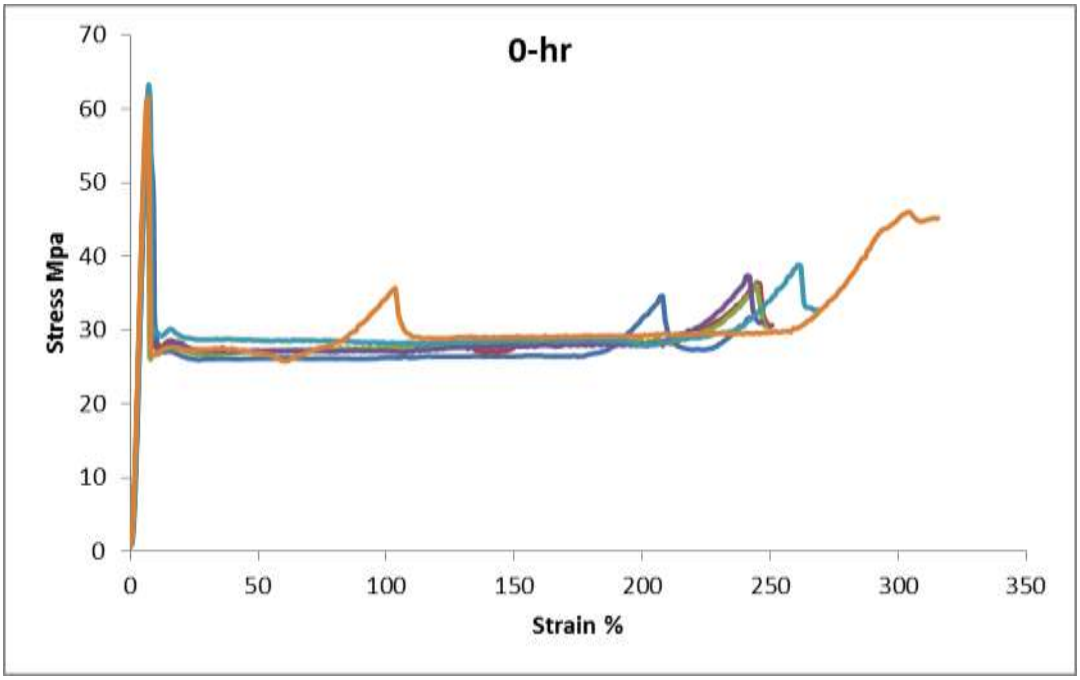

FigureF1: Stress-strain curve for r-PET samples before UV exposure.

Table F2: Tensile test data of r-PET specimens after 250 hour of UV irradiation under natural weathering.

No.	Yield stress	Elong. at yield	Elong. at break	stress at break	True stress at break	Thick	Width	Thick after break	Width after break
	MPa	%	%	MPa	MPa	mm	mm	mm	mm
1	59.10	6.75	246.00	29.09	174.78	4.11	10.10	1.05	6.58
2	59.60	6.75	242.00	30.01	179.78	4.14	10.12	1.03	6.79
3	59.70	6.75	248.00	27.13	161.69	4.11	10.11	1.05	6.64
4	58.90	6.40	256.00	30.50	173.42	4.11	10.11	1.05	6.96
5	60.20	6.80	276.00	42.03	259.36	4.11	10.12	1.23	5.48
6	59.60	6.75	240.00	29.16	162.41	4.14	10.14	1.13	6.67
Avg.	59.40	6.70	251.33	31.32	185.24				
S.d.	0.46	0.15	13.31	5.37	37.01				

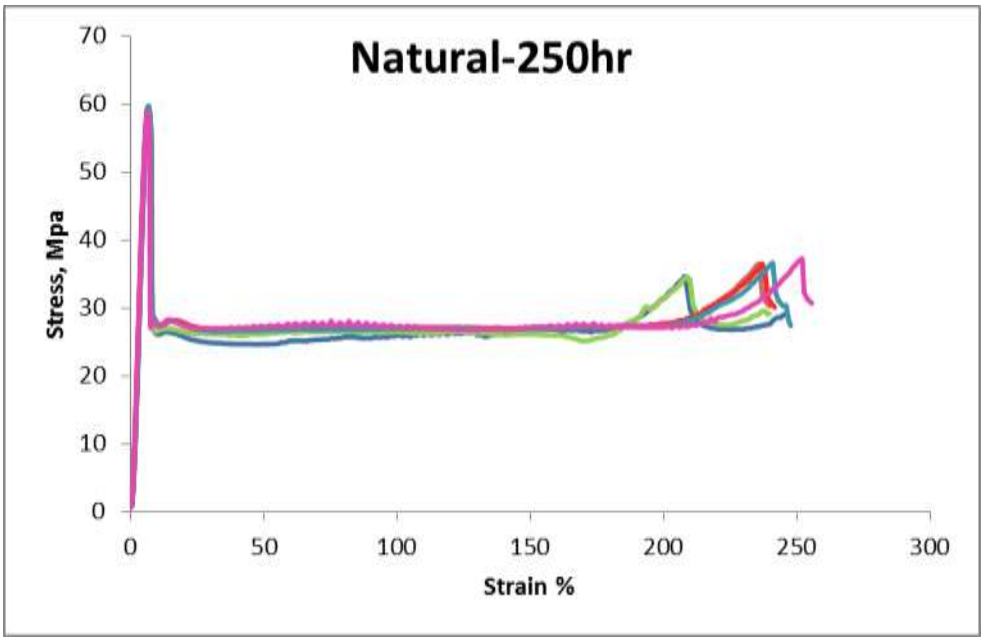

FigureF2: Stress-strain curve for r-PET samples after 250 hour of UV irradiation under natural weathering.

.

Table F3: Tensile test data of r-PET specimens after 500 hour of UV irradiation under natural weathering.

No.	Yield stress	Elong. at yield	Elong. at break	stress at break	True stress at break	Thick	Width	Thick after break	Width after break
	MPa	%	%	MPa	MPa	mm	mm	mm	mm
1	58.70	7.00	235.00	28.37	187.63	4.11	10.12	0.95	6.62
2	58.40	6.80	252.00	31.52	193.32	4.15	10.13	1.02	6.72
3	58.40	6.80	248.80	29.89	188.10	4.10	10.12	0.99	6.66
4	59.00	6.80	262.00	31.17	211.06	4.11	10.11	0.92	6.67
5	58.50	7.00	241.00	29.63	167.72	4.11	10.12	1.10	6.68
6	59.20	6.75	24000	28.27	182.01	4.12	10.11	0.95	6.81
Avg.	58.55	6.87	241.13	29.21	183.32				
S.d.	0.37	0.12	8.24	1.43	8.85				

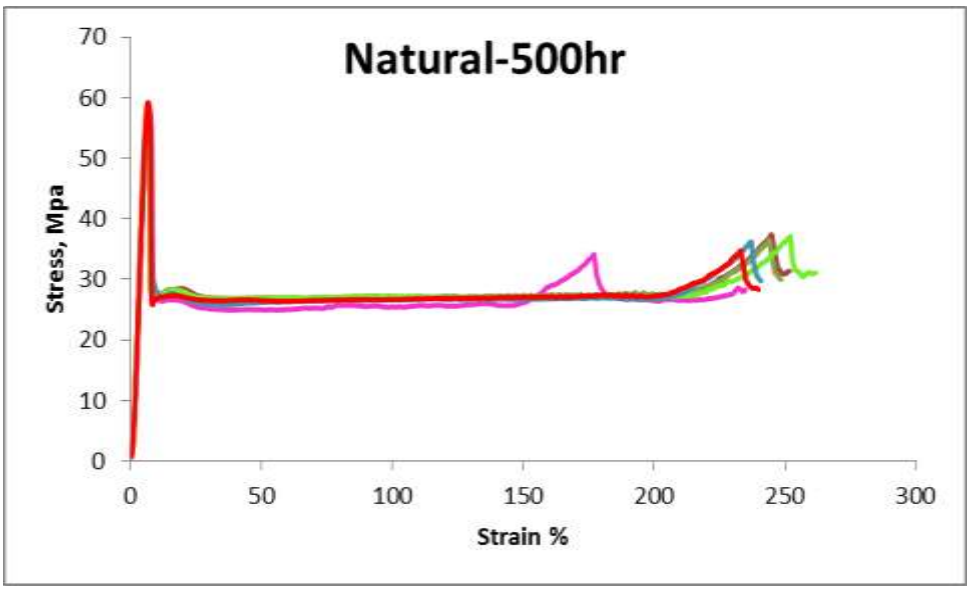

FigureF3: Stress-strain curve for r-PET samples after 500 hour of UV irradiation under natural weathering.

Table F4: Tensile test data of r-PET specimens after 750 hour of UV irradiation under natural weathering.

No.	Yield stress	Elong. at yield	Elong. at break	stress at break	True stress at break	Thick	Width	Thick after break	Width after break
	MPa	%	%	MPa	MPa	mm	mm	mm	mm
1	60.70	6.80	330.00	40.30	206.02	4.11	10.12	0.90	9.04
2	59.70	7.00	244.00	30.93	192.97	4.11	10.11	1.00	6.66
3	59.60	6.75	235.00	28.77	176.41	4.1	10.11	1.00	6.76
4	60.10	8.25	212.00	30.62	192.91	4.09	10.1	0.96	6.83
5	60.30	7.00	236.00	29.25	202.42	4.1	10.11	0.89	6.73
6	60.70	6.75	240.00	29.24	199.39	4.11	10.12	0.92	6.63
Avg.	60.18	7.09	249.50	31.52	195.02				
S.d.	0.48	0.58	40.99	4.39	10.49				

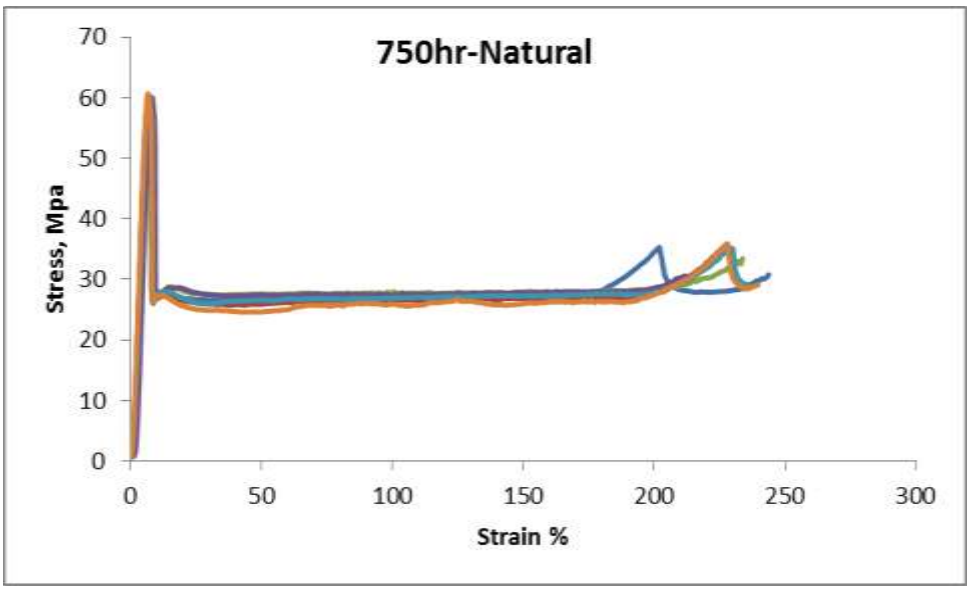

FigureF4: Stress-strain curve for r-PET samples after 750 hour of UV irradiation under natural weathering.

Table F5: Tensile test data of r-PET specimens after 1000 hour of UV irradiation under natural weathering.

No.	Yield stress	Elong. at yield	Elong. at break	stress at break	True stress at break	Thick	Width	Thick after break	Width after break
	MPa	%	%	MPa	MPa	mm	mm	mm	mm
1	59.2	6.80	251.20	31.16	204.14	4.15	10.13	0.9	7.13
2	57.40	7.25	245.00	29.29	177.01	4.12	10.13	1.02	6.75
3	56.60	6.80	263.20	32.76	216.04	4.11	10.12	0.85	7.42
4	56.30	6.80	250.00	29.51	185.83	4.11	10.12	0.98	6.74
5	56.70	6.80	251.20	28.34	184.66	4.11	10.13	0.98	6.52
6	56.40	6.40	259.20	29.47	178.76	4.12	10.13	1.03	6.68
Avg.	57.10	6.81	253.30	30.09	191.07				
S.d.	1.10	0.27	6.65	1.59	15.57				

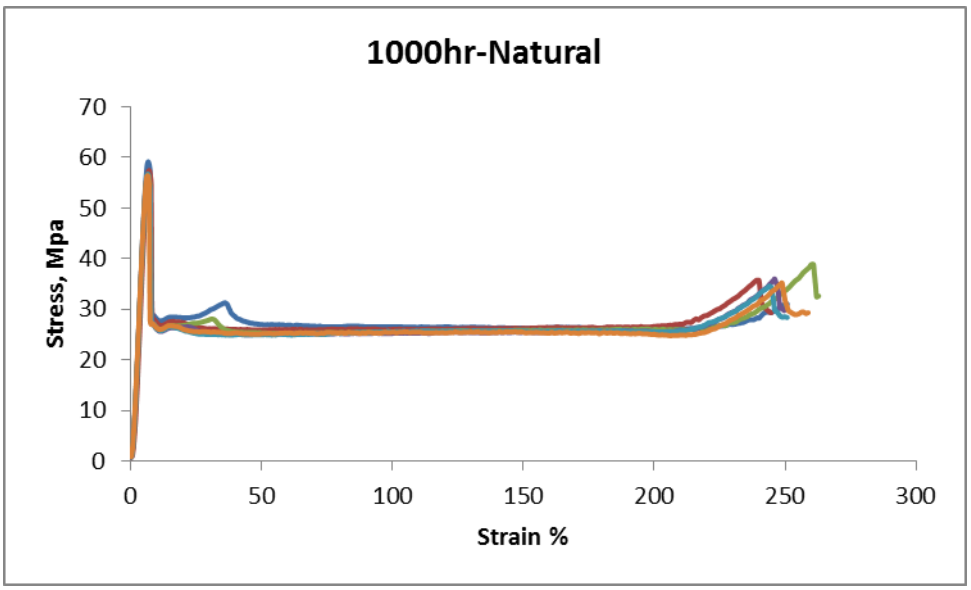

FigureF5: Stress-strain curve for r-PET samples after 1000 hour of UV irradiation under natural weathering.

Table F6: Tensile test data of r-PET specimens after 2000 hour of UV irradiation under natural weathering.

No.	Yield stress	Elong. at yield	Elong. at break	stress at break	True stress at break	Thick	Width	Thick after break	Width after break
	MPa	%	%	MPa	MPa	mm	mm	mm	mm
1	59.30	6.80	247.20	29.85	178.84	4.13	10.12	1.09	6.4
2	59.30	6.80	279.20	42.99	180.51	4.13	10.11	1.76	5.65
3	58.70	6.75	224.00	19.37	115.96	4.11	10.11	0.96	7.23
4	60.40	6.80	276.00	34.27	163.55	4.11	10.11	1.26	6.91
5	60.60	6.80	248.00	30.88	179.15	4.10	10.11	1.04	6.87
6	60.70	6.80	260.00	31.61	163.24	4.11	10.1	1.17	6.87
Avg.	59.83	6.79	255.73	31.50	163.54				
S.d.	0.84	0.02	20.59	7.62	24.62				

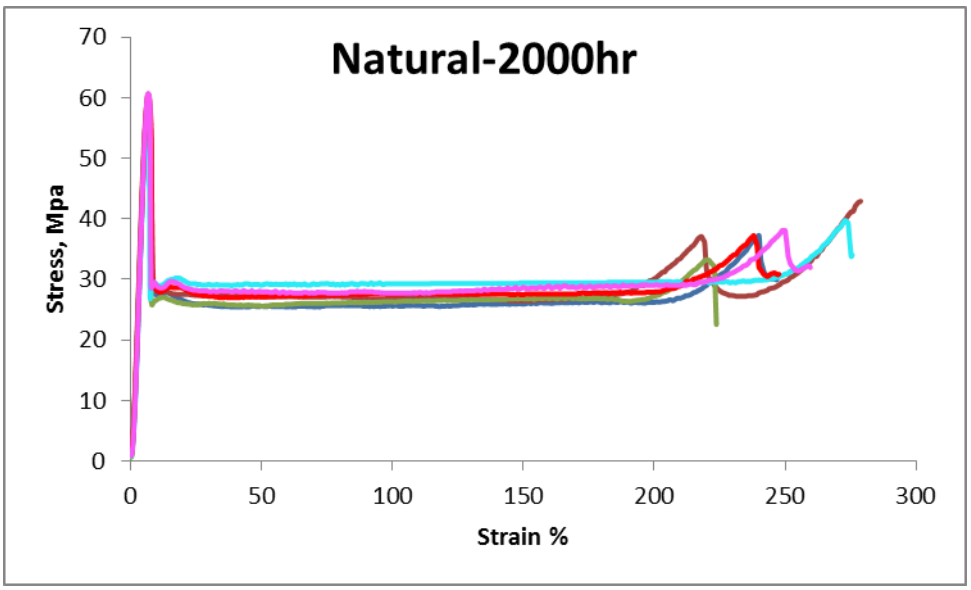

FigureF6: Stress-strain curve for r-PET samples after 2000 hour of UV irradiation under natural weathering.

Table F7: Tensile test data of r-PET specimens after 5000 hour of UV irradiation under natural weathering.

No.	Yield stress	Elong. at yield	Elong. at break	stress at break	True stress at break	Thick	Width	Thick after break	Width after break
	MPa	%	%	MPa	MPa	mm	mm	mm	mm
1	61.90	6.75	238.00	30.3	153.88	4.10	10.11	1.22	6.69
2	62.20	6.75	233.00	29.78	146.30	4.11	10.10	1.29	6.55
3	60.10	6.40	264.00	40.65	148.74	4.10	10.11	1.2	9.44
4	60.80	7.25	231.00	29.01	144.53	4.16	10.11	1.26	6.7
5	62.70	6.75	242.00	31.77	149.33	4.11	10.11	1.36	6.5
6	62.20	6.8	247.20	30.57	147.73	4.12	10.10	1.27	6.78
Avg.	61.65	6.78	242.53	32.01	148.42				
S.d.	0.99	0.27	12.06	4.33	3.19				

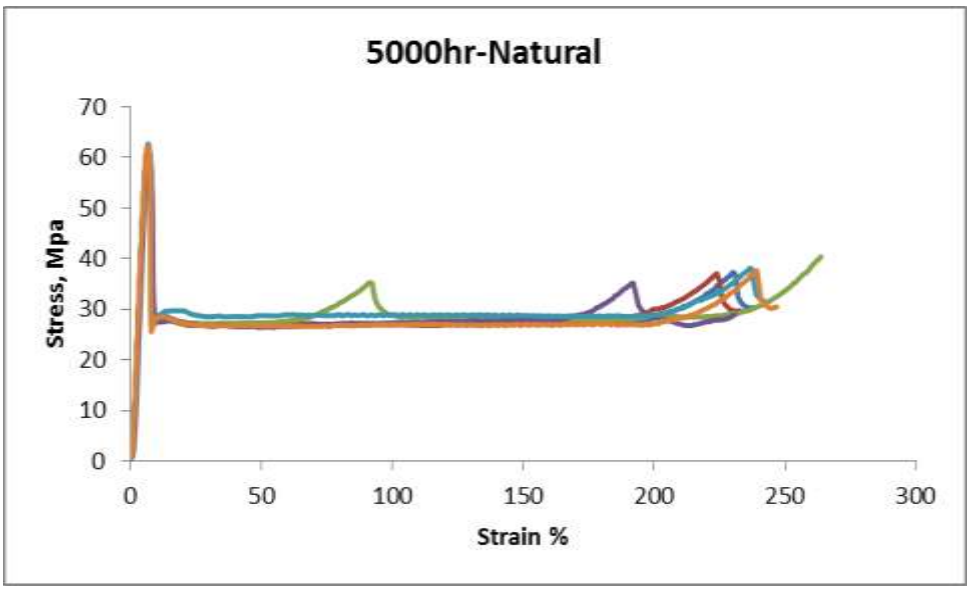

FigureF7: Stress-strain curve for r-PET samples after 5000 hour of UV irradiation under natural weathering.

Table F8: Tensile test data of r-PET specimens after 9000 hour of UV irradiation under natural weathering.

No.	Yield stress	Elong. at yield	Elong. at break	stress at break	True stress at break	Thick	Width	Thick after break	Width after break
	MPa	%	%	MPa	MPa	mm	mm	mm	mm
1	60.40	6.40	292.80	18.32	86.23	4.10	10.12	1.35	6.53
2	61.10	6.00	290.00	32.83	130.71	4.13	10.12	1.45	7.24
3	63.00	6.40	288.00	32.67	132.49	4.11	10.13	1.42	7.23
4	62.20	6.40	296.00	40.34	155.93	4.10	10.11	1.66	6.46
5	62.40	6.40	284.80	32.65	130.65	4.10	10.10	1.47	7.04
6	62.2	6.90	90.40	16.89	77.47	4.10	10.11	1.28	7.06
Avg.	61.88	6.42	257.00	28.95	118.91				
S.d.	0.95	0.29	81.71	9.28	30.39				

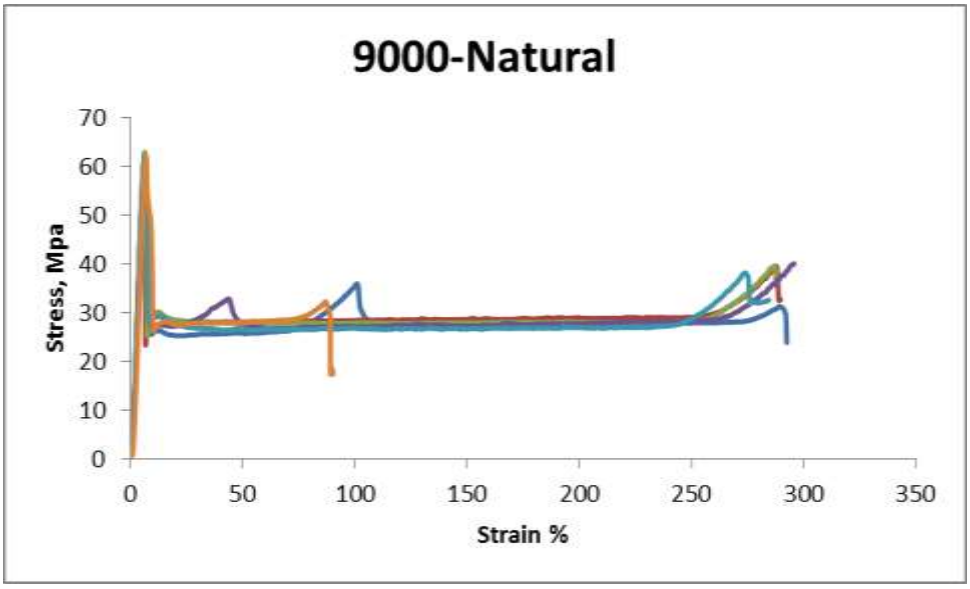

FigureF8: Stress-strain curve for r-PET samples after 9000 hour of UV irradiation under natural weathering.

Table F9: Tensile test data of r-PET specimens after 13000 hour of UV irradiation under natural weathering.

No.	Yield stress	Elong. at yield	Elong. at break	stress at break	True stress at break	Thick	Width	Thick after break	Width after break
	MPa	%	%	MPa	MPa	mm	mm	mm	mm
1	60.90	6.40	303.20	38.15	100.86	4.09	10.10	1.74	8.98
2	62.20	6.40	307.20	34.57	91.01	4.09	10.10	1.65	9.51
3	63.60	7.00	170.00	28.21	105.70	4.09	10.09	1.56	7.06
4	63.80	6.80	296.00	45.11	167.95	4.05	10.05	1.81	6.04
5	63.40	6.25	203.00	33.50	111.03	4.09	10.10	1.64	7.60
6	64.4	6.50	201.00	18.35	71.21	4.10	10.10	1.48	7.21
Avg.	63.05	6.56	246.73	32.98	107.96				
S.d.	1.28	0.28	61.91	9.09	32.56				

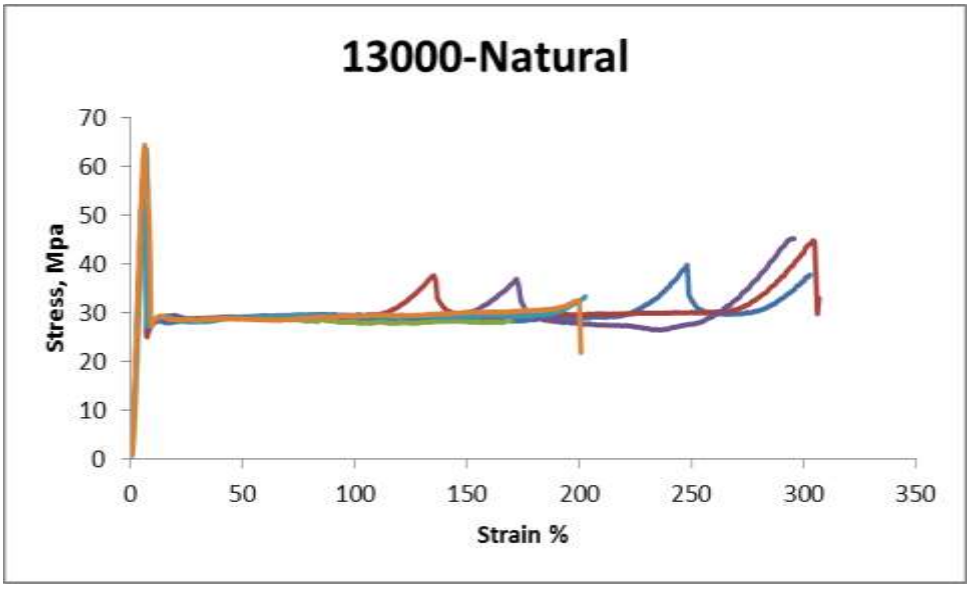

FigureF9: Stress-strain curve for r-PET samples after 13000 hour of UV irradiation under natural weathering.

QUV tensile test results

Table F10: Tensile test data of r-PET specimens after 250 hour of UV irradiation under accelerated weathering.

No.	Yield stress	Elong. at yield	Elong. at break	stress at break	True stress at break	Thick	Width	Thick after break	Width after break
	MPa	%	%	MPa	MPa	mm	mm	mm	mm
1	66.90	7.62	8.00	62.03	121.53	4.11	10.12	2.3	9.23
2	67.30	7.38	7.68	65.20	121.99	4.11	10.12	2.37	9.38
3	68.30	7.35	133.05	32.31	137.19	4.11	10.12	1.43	6.85
4	68.00	7.08	8.95	11.35	57.49	4.11	10.12	1.02	8.05
5	67.60	7.50	69.53	19.71	107.88	4.11	10.12	1.02	7.45
6	68.40	7.30	24.10	7.31	53.95	4.11	10.12	0.93	6.06
Avg.	67.75	7.37	41.89	32.99	100.01				
S.d.	0.59	0.18	50.59	25.24	35.55				

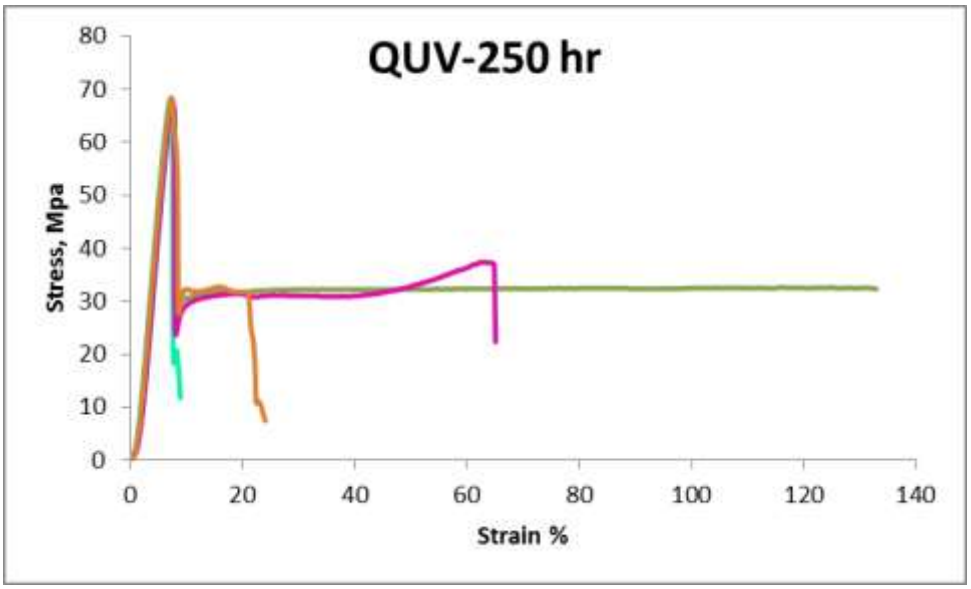

FigureF10: Stress-strain curve for r-PET samples after 250 hour of UV irradiation under accelerated weathering.

Table F11: Tensile test data of r-PET specimens after 500 hour of UV irradiation under accelerated weathering.

No.	Yield stress	Elong. at yield	Elong. at break	stress at break	True stress at break	Thick	Width	Thick after break	Width after break
	MPa	%	%	MPa	MPa	mm	mm	mm	mm
1	72.90	7.64	10.70	17.19	72.94	4.10	10.10	1.31	7.45
2	54.70	5.90	5.90	54.69	54.69	4.12	10.13	4.07	10.11
3	73.50	7.79	12.2	24.20	119.18	4.10	10.12	1.18	7.14
4	68.20	8.02	8.02	68.20	69.01	4.10	10.10	4.06	10.08
5	74.10	7.67	8.06	68.50	103.39	4.09	10.11	2.93	9.35
6	74.50	7.68	21.3	30.60	138.58	4.10	10.11	1.35	6.78
Avg.	69.65	7.45	11.03	43.90	93.10				
S.d.	7.67	0.77	5.50	22.76	32.43				

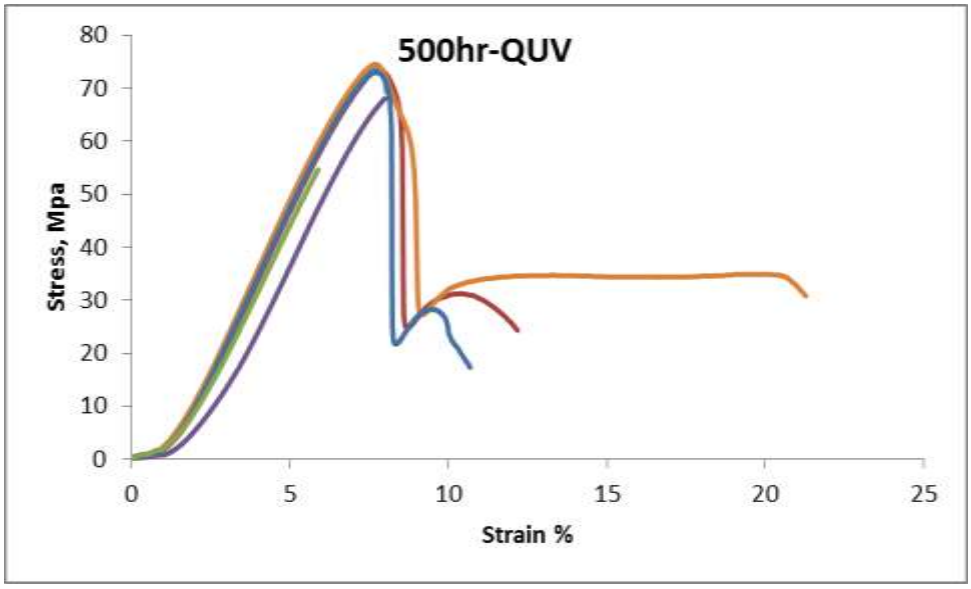

FigureF11: Stress-strain curve for r-PET samples after 500 hour of UV irradiation under accelerated weathering.

Table F12: Tensile test data of r-PET specimens after 750 hour of UV irradiation under accelerated weathering.

No.	Yield stress	Elong. at yield	Elong. at break	stress at break	True stress at break	Thick	Width	Thick after break	Width after break
	MPa	%	%	MPa	MPa	mm	mm	mm	mm
1	69.40	7.28	68.03	11.14	63.48	4.11	10.13	0.99	7.38
2	67.80	7.20	20.20	6.87	58.31	4.14	10.12	0.8	6.17
3	64.10	7.58	7.58	64.06	73.74	4.14	10.12	3.6	10.11
4	68.90	7.18	22.30	7.39	66.18	4.12	10.11	0.76	6.12
5	68.60	7.20	16.70	28.27	126.26	4.11	10.12	1.34	6.95
6	66.10	7.79	11.90	11.20	77.48	4.16	10.13	0.78	7.81
Avg.	67.48	7.37	24.45	21.49	77.58				
S.d.	2.02	0.25	22.02	22.29	24.84				

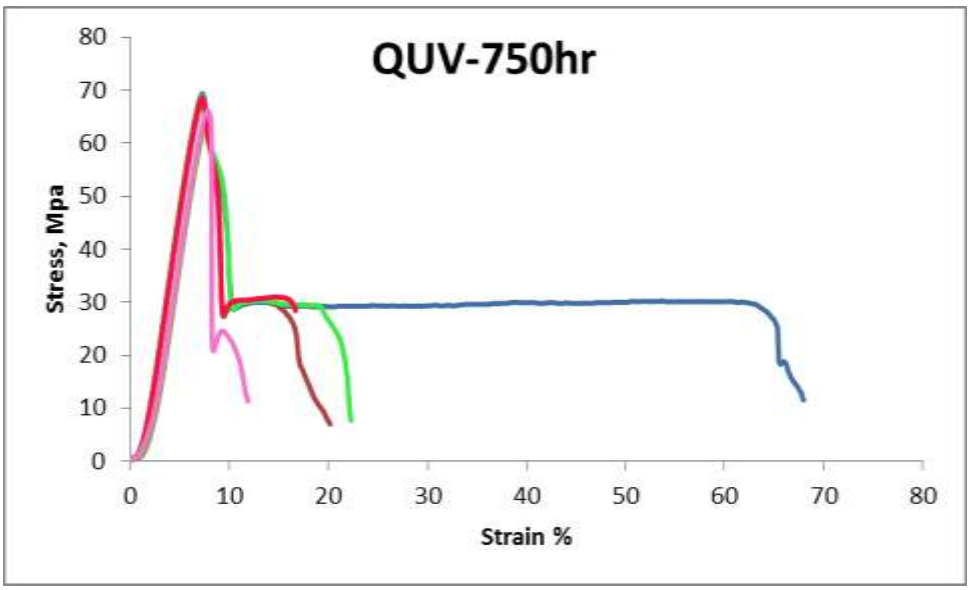

FigureF12: Stress-strain curve for r-PET samples after 750 hour of UV irradiation under accelerated weathering.

Table F13: Tensile test data of r-PET specimens after 1000 hour of UV irradiation under accelerated weathering.

No.	Yield stress	Elong. at yield	Elong. at break	stress at break	True stress at break	Thick	Width	Thick after break	Width after break
	MPa	%	%	MPa	MPa	mm	mm	mm	mm
1	69.70	7.44	13.31	6.86	56.83	4.15	10.12	0.65	7.8
2	69.70	7.72	17.50	7.69	57.78	4.16	10.13	0.82	6.84
3	66.00	7.82	8.06	64.22	101.80	4.13	10.12	2.65	9.95
4	70.20	8.12	17.10	7.18	29.56	4.13	10.12	1.35	7.52
5	69.80	7.53	7.86	67.54	82.02	4.12	10.12	3.43	10.01
6	67.50	7.36	7.56	66.8	76.39	4.12	10.13	3.61	10.11
Avg.	68.82	7.67	11.90	36.72	67.40				
S.d.	1.68	0.28	4.70	32.30	24.96				

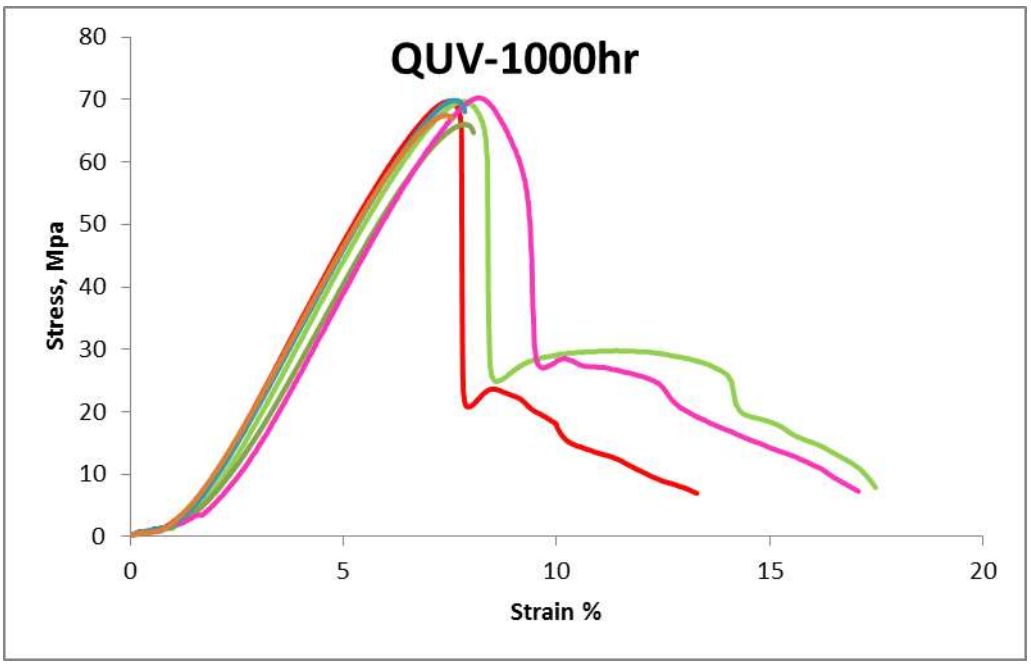

FigureF13: Stress-strain curve for r-PET samples after 1000 hour of UV irradiation under accelerated weathering.

Table F14: Tensile test data of r-PET specimens after 2000 hour of UV irradiation under accelerated weathering.

No.	Yield stress	Elong. at yield	Elong. at break	stress at break	True stress at break	Thick	Width	Thick after break	Width after break
	MPa	%	%	MPa	MPa	mm	mm	mm	mm
1	59.30	6.84	6.84	59.30	59.30	4.11	10.10	4.11	10.10
2	40.40	5.11	5.11	40.40	40.40	4.10	10.10	4.10	10.10
3	28.60	3.83	3.83	28.60	28.60	4.10	10.10	4.10	10.10
4	71.70	8.72	8.95	71.40	71.40	4.11	10.08	4.11	10.08
5	42.30	5.06	5.06	42.30	42.30	4.10	10.09	4.10	10.09
6	58.6	6.00	6.00	58.60	58.60	4.12	10.11	4.12	10.11
Avg.	50.15	5.93	5.97	50.10	50.10				
S.d.	15.75	1.70	1.78	15.67	15.67				

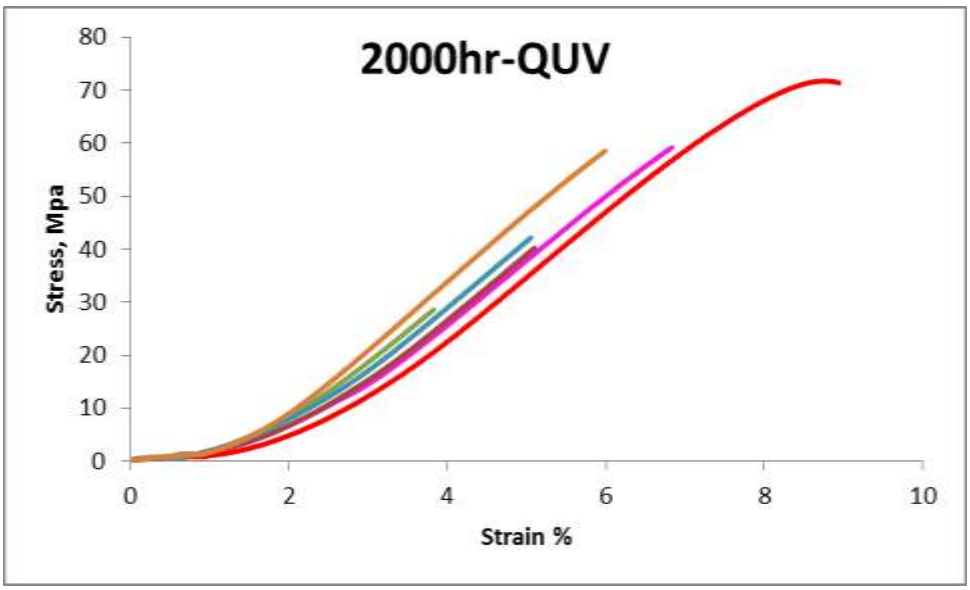

FigureF14: Stress-strain curve for r-PET samples after 2000 hour of UV irradiation under accelerated weathering.

Table F15: Tensile test data of r-PET specimens after 5000 hour of UV irradiation under accelerated weathering.

No.	Yield stress	Elong at yield	Elong at break	stress at break	True stress at break	Thick	Width	Thick after break	Width after break
	MPa	%	%	MPa	MPa	mm	mm	mm	mm
1	33.42	3.848	3.85	33.42	33.42	4.13	10.13	4.13	10.13
2	37.19	4.02	4.02	37.19	37.19	4.16	10.16	4.16	10.16
3	50.56	5.22	5.22	50.56	50.56	4.14	10.14	4.14	10.14
4	25.30	3.37	3.37	25.30	25.30	4.20	10.13	4.20	10.13
5	38.59	4.16	4.16	38.59	38.59	4.11	10.10	4.11	10.10
Avg.	37.01	4.12	4.12	37.01	37.01				
S.d.	9.17	0.68	0.68	9.17	9.17				

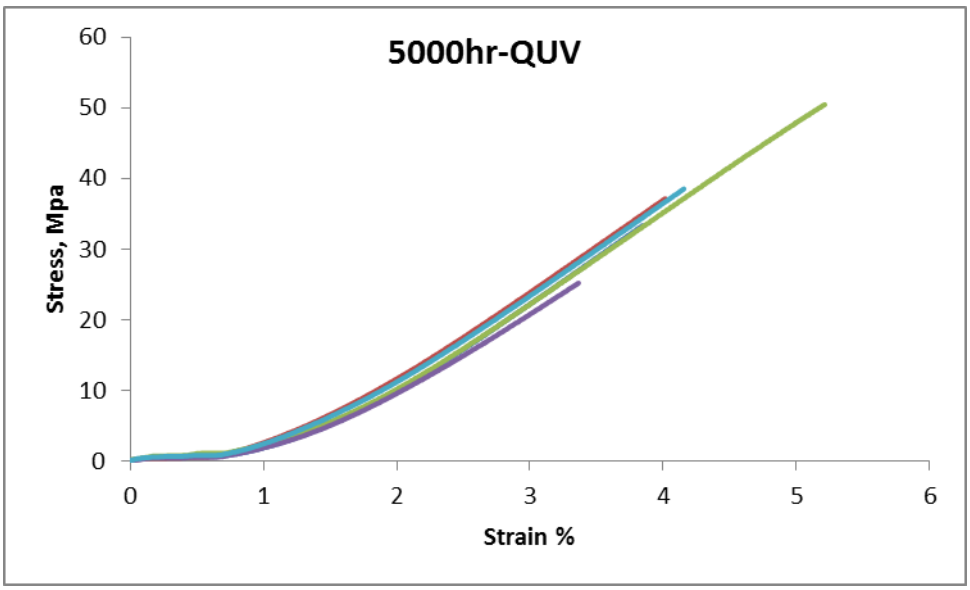

FigureF15: Stress-strain curve for r-PET samples after 5000hr of UV irradiation under accelerated weathering.

Table F16: Tensile test data of r-PET specimens after 9000 hour of UV irradiation under accelerated weathering.

No.	Yield stress	Elong. at yield	Elong. at break	stress at break	True stress at break	Thick	Width	Thick after break	Width after break
	MPa	%	%	MPa	MPa	mm	mm	mm	mm
1	32.31	4.10	4.10	32.31	32.31	4.12	10.12	4.12	10.12
2	29.58	3.62	3.62	29.58	29.58	4.13	10.13	4.13	10.13
3	35.85	4.21	4.21	35.85	35.85	4.13	10.11	4.13	10.11
4	32.99	3.63	3.63	32.99	32.99	4.12	10.11	4.12	10.11
5	30.74	3.90	3.90	30.74	30.74	4.20	10.12	4.20	10.12
6	31.07	3.78	3.78	31.07	31.07	4.12	10.10	4.12	10.10
Avg.	32.09	3.87	3.87	32.09	32.09				
S.d.	2.20	0.24	0.24	2.20	2.20				

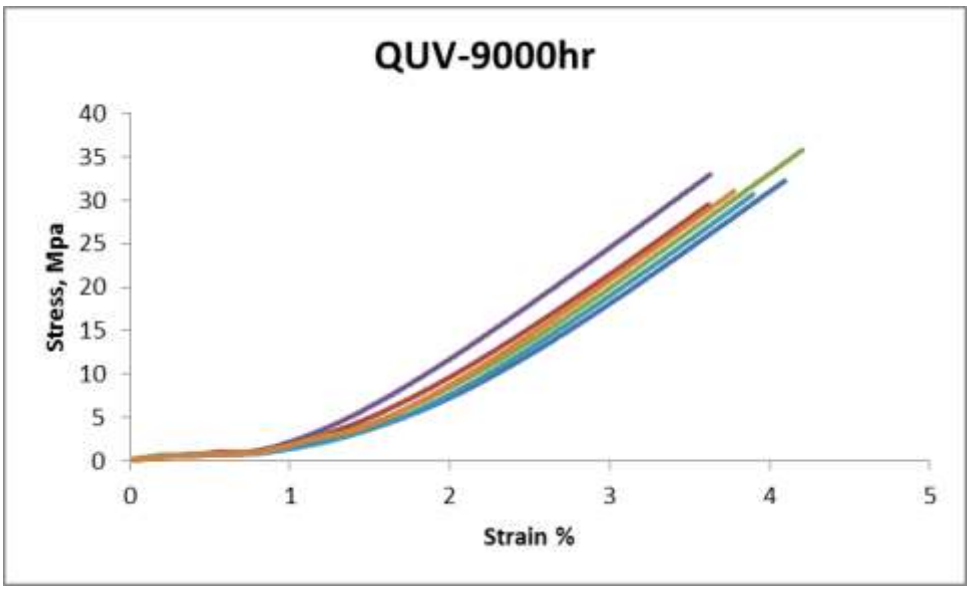

FigureF16: Stress-strain curve for r-PET samples after 9000 hour of UV irradiation under accelerated weathering.

Table F17: Tensile test data of r-PET specimens after 13000 hour of UV irradiation under accelerated weathering.

No.	Yield stress	Elong. at yield	Elong. at break	stress at break	True stress at break	Thick	Width	Thick after break	Width after break
	MPa	%	%	MPa	MPa	mm	mm	mm	mm
1	24.55	3.45	3.45	24.55	24.55	4.12	10.11	4.12	10.11
2	25.80	3.19	3.19	25.80	25.80	4.11	10.09	4.11	10.09
3	22.01	3.17	3.17	22.01	22.01	4.13	10.11	4.13	10.11
4	30.60	3.30	3.30	30.60	30.60	4.10	10.08	4.10	10.08
5	28.25	3.42	3.42	28.25	28.25	4.10	10.08	4.10	10.08
6	25.95	3.29	3.29	25.95	25.95	4.12	10.08	4.12	10.08
Avg.	26.19	3.30	3.30	26.19	26.19				
S.d.	2.97	0.11	0.11	2.97	2.97				

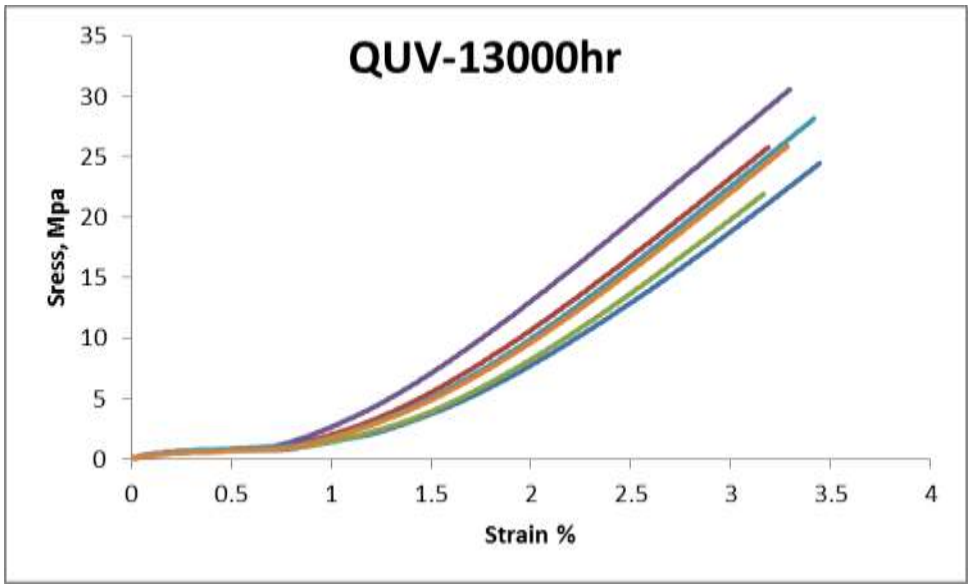

FigureF17: Stress-strain curve for r-PET samples after 13000 hour of UV irradiation under accelerated weathering.

APPENDIX G

CHARPY IMPACT TEST DATA

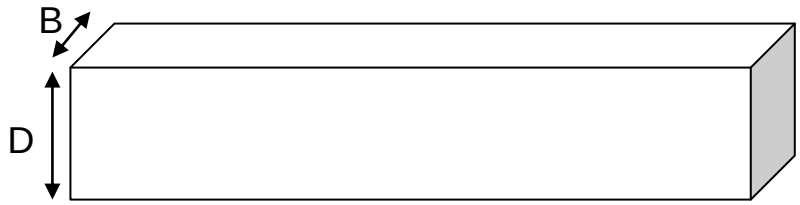

Table G1: Data of Charpy impact strength of r-PET before UV irradiation.

Specimen No.	Width,B (mm)	Thickness, D (mm)	Impact strength (kJ/m²)
1	10.18	4.10	Invalid test
2	10.17	4.10	Invalid test
3	10.18	4.11	Invalid test
4	10.17	4.10	Invalid test
5	10.17	4.10	Invalid test
6	10.17	4.10	Invalid test
7	10.18	4.10	Invalid test
8	10.17	4.11	Invalid test
9	10.17	4.10	Invalid test
10	10.18	4.11	Invalid test
11	10.17	4.11	Invalid test
12	10.17	4.10	Invalid test
13	10.18	4.10	Invalid test
14	10.18	4.10	Invalid test
15	10.16	4.10	Invalid test
16	10.17	4.10	Invalid test
17	10.18	4.11	Invalid test
18	10.17	4.11	Invalid test
19	10.16	4.11	Invalid test
20	10.17	4.10	Invalid test
Average impact strength (KJ/m²)			-
St. Dev.			-

Table G2: Data of Charpy impact strength of r-PET specimens after 250 hour of UV irradiation under accelerated weathering.

Specimen No.	Width,B (mm)	Thickness, D (mm)	Impact strength (kJ/m²)
1	10.19	4.12	45.49
2	10.19	4.12	51.14
3	10.19	4.12	53.91
4	10.18	4.11	45.18
5	10.19	4.12	46.44
6	10.19	4.12	42.95
7	10.19	4.12	44.54
8	10.19	4.12	45.18
9	10.19	4.12	42.31
Average impact strength (KJ/m²)			46.35
St. Dev.			3.79

Table G3: Data of Charpy impact strength of r-PET specimens after 500 hour of UV irradiation under accelerated weathering.

Specimen No.	Width,B (mm)	Thickness, D (mm)	Impact strength (kJ/m²)
1	10.15	4.11	44.01
2	10.16	4.11	44.94
3	10.17	4.13	45.38
4	10.18	4.10	45.38
5	10.18	4.12	45.38
6	10.18	4.12	46.34
7	10.18	4.12	46.66
8	10.17	4.12	46.98
9	10.17	4.11	46.02
10	10.17	4.10	47.3
			49.52
Average impact strength (KJ/m²)			46.17
St. Dev.			1.47

Table G4: Data of Charpy impact strength of r-PET specimens after 750 hour of UV irradiation under accelerated weathering.

Specimen No.	Width, B (mm)	Thickness, D (mm)	Impact strength (kJ/m²)
1	10.18	4.13	47.66
2	10.18	4.13	47.66
3	10.17	4.14	34.44
4			47.97
5	10.18	4.13	49.85
6	10.18	4.13	49.54
Average impact strength (KJ/m²)			46.19
St. Dev.			5.83

Table G5: Data of Charpy impact strength of r-PET specimens after 1000 hour of UV irradiation under accelerated weathering.

Specimen No.	Width, B (mm)	Thickness, D (mm)	Impact strength (kJ/m²)
1	10.17	4.15	40.49
2	10.20	4.13	40.56
3	10.21	4.13	41.52
4	10.17	4.15	40.81
5	10.19	4.12	38.80
6	10.17	4.14	41.55
7	10.18	4.13	39.96
8	10.18	4.15	38.52
9	10.17	4.14	41.23
10	10.18	4.15	38.84
11	10.18	4.15	38.20
Average impact strength (KJ/m²)			40.04
St. Dev.			1.25

Table G6: Data of Charpy impact strength of r-PET specimens after 2000 hour of UV irradiation under accelerated weathering.

Specimen No.	Width, B (mm)	Thickness, D (mm)	Impact strength (kJ/m²)
1	10.18	4.11	42.13
2	10.18	4.11	41.81
3	10.19	4.11	42.45
4	10.18	4.10	41.49
5	10.19	4.11	41.49
6	10.18	4.11	42.13
Average impact strength (KJ/m²)			41.92
St. Dev.			0.39

Table G7: Data of Charpy impact strength of r-PET specimens after 5000 hour of UV irradiation under accelerated weathering.

Specimen No.	Width, B (mm)	Thickness, D (mm)	Impact strength (kJ/m²)
1	10.14	4.10	45.13
2	10.17	4.10	44.85
3	10.16	4.11	44.61
4	10.12	4.14	45.06
5	10.16	4.11	43.97
6	10.18	4.11	44.53
7	10.17	4.11	43.88
8	10.18	4.14	44.59
9	10.16	4.12	44.61
10	10.17	4.13	44.03
11	10.16	4.12	44.61
12	10.19	4.13	44.59
13			23.69
Average impact strength (KJ/m²)			42.93
St. Dev.			5.79

Table G8: Data of Charpy impact strength of r-PET specimens after 9000 hour of UV irradiation under accelerated weathering.

Specimen No.	Width, B (mm)	Thickness, D (mm)	Impact strength (kJ/m²)
1	10.17	4.20	1.984
2	10.17	4.10	2.027
3	10.17	4.11	2.704
4	10.16	4.12	3.042
5	10.14	4.19	1.667
6	10.14	4.11	3.378
7	10.17	4.14	14.13
8	10.13	4.13	1.688
9	10.12	4.13	2.025
10	10.16	4.18	3.347
11	10.14	4.17	3.012
12	10.15	4.14	2.007
13	10.16	4.14	9.416
14	10.12	4.17	2.335
15	10.15	4.16	3.012
16	10.18	4.16	2.001
Average impact strength (KJ/m²)			3.61
St. Dev.			3.35

Table G9: Data of Charpy impact strength of r-PET specimens after 13000 hour of UV irradiation under accelerated weathering.

Specimen No.	Width, B (mm)	Thickness, D (mm)	Impact strength (kJ/m²)
1	10.14	4.13	4.051
2	10.13	4.10	3.375
3	10.16	4.19	2.987
4	10.17	4.15	3.363
5	10.11	4.14	3.037
6	10.17	4.13	4.711
7	10.17	4.15	3.652
8	10.14	4.19	1.991
9	10.17	4.16	3.320
10	10.17	4.12	3.369
11	10.19	4.18	2.987
12	10.18	4.16	2.358
13	10.16	4.16	2.695
14	10.17	4.16	3.369
15	10.18	4.17	2.020
16	10.17	4.13	3.032
17	10.14	4.19	3.707
18	10.17	4.16	4.720
Average impact strength (KJ/m²)			3.260
St. Dev.			0.76

Table G10: Data of Charpy impact strength of r-PET specimens after 250 hour of UV irradiation under natural weathering.

Specimen No.	Width, B (mm)	Thickness,D (mm)	Impact strength (kJ/m²)
1	10.17	4.10	Invalid test
2	10.18	4.10	Invalid test
3	10.20	4.11	Invalid test
4	10.18	4.10	Invalid test
5	10.20	4.12	Invalid test
6	10.18	4.11	Invalid test
7	10.18	4.11	Invalid test
8	10.17	4.10	Invalid test
9	10.19	4.12	Invalid test
10	10.18	4.11	Invalid test
11	10.18	4.11	Invalid test
12	10.18	4.12	Invalid test
13	10.17	4.11	Invalid test
14	10.19	4.11	Invalid test
15	10.20	4.12	Invalid test
16	10.19	4.12	Invalid test
17	10.17	4.11	Invalid test
18	10.19	4.11	Invalid test
19	10.19	4.12	Invalid test
20	10.18	4.11	Invalid test
Average impact strength (KJ/m²)			-
St. Dev.			-

Table G11: Data of Charpy impact strength of r-PET specimens after 500 hour of UV irradiation under natural weathering.

Specimen No.	Width, B (mm)	Thickness,D (mm)	Impact strength (kJ/m²)
1	10.15	4.11	Invalid test
2	10.18	4.11	Invalid test
3	10.17	4.12	Invalid test
4	10.18	4.11	Invalid test
5	10.18	4.11	Invalid test
6	10.18	4.11	Invalid test
7	10.18	4.12	Invalid test
8	10.18	4.12	Invalid test
9	10.18	4.11	Invalid test
10	10.19	4.13	Invalid test
11	10.18	4.11	Invalid test
12	10.18	4.11	Invalid test
13	10.18	4.11	Invalid test
14	10.17	4.11	Invalid test
15	10.18	4.11	Invalid test
16	10.18	4.12	Invalid test
17	10.19	4.11	Invalid test
18	10.17	4.13	Invalid test
19	10.18	4.11	Invalid test
20	10.18	4.11	Invalid test
Average impact strength (KJ/m²)			-
St. Dev.			-

Table G12: Data of Charpy impact strength of r-PET specimens after 750 hour of UV irradiation under natural weathering.

Specimen No.	Width, B (mm)	Thickness, D (mm)	Impact strength (kJ/m²)
1	10.17	4.11	Invalid test
2	10.18	4.11	Invalid test
3	10.17	4.11	Invalid test
4	10.18	4.11	Invalid test
5	10.18	4.11	Invalid test
6	10.18	4.12	Invalid test
7	10.17	4.11	Invalid test
8	10.18	4.12	Invalid test
9	10.17	4.11	Invalid test
10	10.18	4.11	Invalid test
11	10.17	4.11	Invalid test
12	10.18	4.11	Invalid test
13	10.18	4.12	Invalid test
14	10.18	4.11	Invalid test
15	10.18	4.11	Invalid test
16	10.18	4.11	Invalid test
17	10.18	4.11	Invalid test
18	10.18	4.11	Invalid test
19	10.18	4.12	Invalid test
20	10.18	4.11	Invalid test
Average impact strength (KJ/m²)			-
St. Dev.			-

Table G13: Data of Charpy impact strength of r-PET specimens after 1000 hour of UV irradiation under natural weathering.

Specimen No.	Width, B (mm)	Thickness, D (mm)	Impact strength (kJ/m²)
1	10.17	4.11	Invalid test
2	10.17	4.11	Invalid test
3	10.17	4.11	Invalid test
4	10.17	4.11	Invalid test
5	10.18	4.11	Invalid test
6	10.17	4.11	Invalid test
7	10.18	4.11	Invalid test
8	10.17	4.12	Invalid test
9	10.17	4.11	Invalid test
10	10.18	4.11	Invalid test
11	10.18	4.11	Invalid test
12	10.18	4.14	Invalid test
13	10.18	4.13	Invalid test
14	10.18	4.11	Invalid test
15	10.17	4.11	Invalid test
16	10.17	4.11	Invalid test
17	10.17	4.11	Invalid test
18	10.17	4.11	Invalid test
19	10.18	4.11	Invalid test
20	10.18	4.11	Invalid test
Average impact strength (KJ/m²)			-
St. Dev.			-

Table G14: Data of Charpy impact strength of r-PET specimens after 2000 hour of UV irradiation under natural weathering.

Specimen No.	Width, B (mm)	Thickness, D (mm)	Impact strength (kJ/m²)
1	10.18	4.12	Invalid test
2	10.18	4.14	Invalid test
3	10.18	4.11	Invalid test
4	10.19	4.11	Invalid test
5	10.18	4.11	Invalid test
6	10.18	4.12	Invalid test
7	10.18	4.11	Invalid test
8	10.18	4.12	Invalid test
9	10.19	4.11	Invalid test
10	10.19	4.11	Invalid test
11	10.20	4.19	Invalid test
12	10.19	4.12	Invalid test
13	10.18	4.11	Invalid test
14	10.18	4.11	Invalid test
15	10.18	4.13	Invalid test
16	10.18	4.11	Invalid test
17	10.19	4.11	Invalid test
18	10.17	4.11	Invalid test
19	10.18	4.12	Invalid test
20	10.17	4.11	Invalid test
Average impact strength (KJ/m²)			-
St. Dev.			-

Table G15: Data of Charpy impact strength of r-PET specimens after 5000 hour of UV irradiation under natural weathering.

Specimen No.	Width, B (mm)	Thickness, D (mm)	Impact strength (kJ/m²)
1	10.18	4.11	Invalid test
2	10.18	4.11	Invalid test
3	10.17	4.10	Invalid test
4	10.17	4.11	Invalid test
5	10.16	4.11	Invalid test
6	10.16	4.11	Invalid test
7	10.18	4.09	Invalid test
8	10.18	4.09	Invalid test
9	10.18	4.09	Invalid test
10	10.15	4.09	Invalid test
11	10.15	4.11	Invalid test
12	10.17	4.09	Invalid test
13	10.18	4.10	Invalid test
14	10.17	4.09	Invalid test
15	10.17	4.09	Invalid test
16	10.15	4.10	Invalid test
17	10.17	4.10	Invalid test
18	10.17	4.09	Invalid test
19	10.16	4.09	Invalid test
20	10.18	4.09	Invalid test
Average impact strength (KJ/m²)			-
St. Dev.			-

Table G16: Data of Charpy impact strength of r-PET specimens after 9000 hour of UV irradiation under natural weathering.

Specimen No.	Width, B (mm)	Thickness, D (mm)	Impact strength (kJ/m²)
1	10.14	4.09	Invalid test
2	10.15	4.10	Invalid test
3	10.15	4.10	Invalid test
4	10.16	4.11	Invalid test
5	10.17	4.10	Invalid test
6	10.18	4.10	Invalid test
7	10.15	4.10	Invalid test
8	10.16	4.11	Invalid test
9	10.19	4.11	Invalid test
10	10.17	4.10	Invalid test
11	10.19	4.11	Invalid test
12	10.19	4.11	Invalid test
13	10.18	4.11	Invalid test
14	10.18	4.11	Invalid test
15	10.17	4.10	Invalid test
16	10.17	4.11	Invalid test
17	10.18	4.12	Invalid test
18	10.18	4.11	Invalid test
19	10.16	4.10	Invalid test
20	10.18	4.11	Invalid test
Average impact strength (KJ/m²)			-
St. Dev.			-

Table G17: Data of Charpy impact strength of r-PET specimens after 13000 hour of UV irradiation under natural weathering.

Specimen No.	Width, B (mm)	Thickness, D (mm)	Impact strength (kJ/m²)
1	10.14	4.10	Invalid test
2	10.12	4.10	Invalid test
3	10.13	4.10	Invalid test
4	10.13	4.10	Invalid test
5	10.14	4.11	Invalid test
6	10.16	4.11	Invalid test
7	10.15	4.09	Invalid test
8	10.15	4.09	Invalid test
9	10.14	4.12	Invalid test
10	10.15	4.09	Invalid test
11	10.15	4.11	Invalid test
12	10.17	4.09	Invalid test
13	10.18	4.10	Invalid test
14	10.14	4.12	Invalid test
15	10.17	4.09	Invalid test
16	10.15	4.13	Invalid test
17	10.16	4.10	Invalid test
18	10.17	4.09	Invalid test
19	10.16	4.12	Invalid test
20	10.14	4.09	Invalid test
Average impact strength (KJ/m²)			-
St. Dev.			-